4-2016

Development and evaluation of a watershed-scale hybrid hydrologic model

Younghyun Cho
Purdue University

Graduate School Form
30 Updated 12/26/2015

PURDUE UNIVERSITY
GRADUATE SCHOOL
Thesis/Dissertation Acceptance

This is to certify that the thesis/dissertation prepared

By Younghyun Cho

Entitled

DEVELOPMENT AND EVALUATION OF A WATERSHED-SCALE HYBRID HYDROLOGIC MODEL

For the degree of Doctor of Philosophy

Is approved by the final examining committee:

Bernard A. Engel Chair	Rao S. Govindaraju
Dennis C. Flanagan	
Venkatesh M. Merwade	
Margaret Gitau	

To the best of my knowledge and as understood by the student in the Thesis/Dissertation Agreement, Publication Delay, and Certification Disclaimer (Graduate School Form 32), this thesis/dissertation adheres to the provisions of Purdue University's "Policy of Integrity in Research" and the use of copyright material.

Approved by Major Professor(s): Bernard A. Engel

Approved by: Bernard A. Engel 4/12/2016

Head of the Departmental Graduate Program Date

DEVELOPMENT AND EVALUATION OF A WATERSHED-SCALE HYBRID HYDROLOGIC MODEL

A Dissertation

Submitted to the Faculty

of

Purdue University

by

Younghyun Cho

In Partial Fulfillment of the

Requirements for the Degree

of

Doctor of Philosophy

May 2016

Purdue University

West Lafayette, Indiana

To my wife, daughter, and parents

ACKNOWLEDGEMENTS

I would like to express my sincere gratitude and appreciation to my advisor, Dr. Bernard A. Engel, for his immeasurable guidance and encouragement during my graduate studies. I extend many thanks to my dissertation committee members, Dr. Rao S. Govindaraju, Dr. Dennis C. Flanagan, Venkatesh M. Merwade, and Dr. Margaret Gitau, who have provided insights and helpful comments for improving the quality of my research.

I especially wish to thank Larry Theller for his significant assistance in GIS and support for all other works. I would also like to thank all my colleagues and research group friends. I thank Akshay Kochar for recommendations to improve my computer programming works.

I am grateful to the K-water (Korea Water Resources Corporation) for supporting and providing the opportunity to study here at Purdue University; special thanks to Phyll-Sun Hwang, Dr. Kee-Uk Cha, Dr. Young-Ho Shin, and Young-Woo Lee for their faith in me to keep pursuing my work and research. I would also like to thank my M.Sc. degree advisor Dr. Soon-Kuk Kwun, and Dr. Jin-Yong Choi and Dr. Moon Sung Kang at Seoul National University who helped me start my Ph.D. research at Purdue University.

I would like to express my deepest thanks to my wife, Youngju Lee, for her unconditional love, encouragement, understanding, and endless support throughout my journey to achieve a doctorate degree. I would like to acknowledge my lovely, smart, and brilliant daughter, Chaeryung E. Cho, your presence itself has made me have strength and inspiration during the toughest times when I felt down or exhausted. Without my wife and daughter, I could not have finished my Ph.D. works.

I am truly grateful to my mother and father for holding me close to their heart and continuously showing concern about my well-being. I also thank all my family members, especially my parents-in-law. I wish everyone will be happy and healthy forever...

Lastly, I'm trying to engrave the following sentence in my heart with my tiny works: "Real knowledge is to know the extent of one's ignorance." - Confucius

TABLE OF CONTENTS

Page

Page

Page

Page

LIST OF TABLES

Table Page

LIST OF FIGURES

Figure Page

Figure Page

Figure Page

Appendix Figure

ABSTRACT

Cho, Younghyun. Ph.D., Purdue University, May 2016. Development and Evaluation of a Watershed-Scale Hybrid Hydrologic Model. Major Professor: Bernard A. Engel.

A watershed-scale hybrid hydrologic model (Distributed-Clark), which is a lumped conceptual and distributed feature model, was developed to predict spatially distributed short- and long-term rainfall runoff generation and routing using relatively simple methodologies and state-of-the-art spatial data in a GIS environment. In Distributed-Clark, spatially distributed excess rainfall estimated with the SCS curve number method and a GIS-based set of separated unit hydrographs (spatially distributed unit hydrograph) are utilized to calculate a direct runoff flow hydrograph, and time-varied SCS CN values and conditional unit hydrograph approach for different runoff depth-based flow convolution are also used to compute long-term rainfall-runoff flow hydrographs. Spatial data processing and model execution can be performed by Python script tools that were developed in a GIS platform.

Model case studies of short- and long-term hydrologic application for four river watersheds to evaluate performance using spatially distributed (Thiessen polygon and NEXRAD radar-based) precipitation data demonstrate relatively good fit against observed streamflow as well as improved fit in comparison with the outputs of spatially

averaged rainfall data simulations as follows: (1) application with 24 single storm events using Thiessen polygon distributed rainfall provided overall statistical results in E_{NS} of 0.84 and R^2 of 0.86 (improved E_{NS} by 1.8% and R^2 by 2.1% relative to averaged data inputs) for direct runoff, (2) simulation of direct runoff flow for the same storm events using NEXRAD data provided E_{NS} of 0.85 and R^2 of 0.89 (increase of E_{NS} by 3.0% and R^2 by 6.0%), and (3) 6-year long-term daily NEXRAD data provided total simulated streamflow statistics of E_{NS} 0.71 and R^2 0.72 (increased E_{NS} of 42.0% and R^2 of 33.3%). These results also indicate that NEXRAD radar-based data are more appropriate for rainfall-runoff flow predictions than rain gauge observations by capturing spatially distributed rainfall amounts and having fewer missing or erroneous records.

The Distributed-Clark model presented in this research is, therefore, potentially significant to improved implementation of hydrologic simulation, particularly for spatially distributed rainfall-runoff routing using gridded types of quantitative precipitation estimation (QPE) data in a GIS environment, as a relatively simple (few parameter) hydrologic model.

CHAPTER 1. INTRODUCTION

1.1 Problem Statement

Many watershed-scale hydrologic models (i.e., watershed model) to study hydrologic processes primarily attempt to predict watershed rainfall responses; rainfall-runoff flow, peak flow rates, and times to peak have been developed over the years as evident from the proliferation of related hydrologic books and periodicals. The National Research Council (1982) and Singh (1988) noted that these models' approaches are so diverse and hybrid that it is not always possible to distinguish one type of model from another.

Nonetheless, watershed models are typically divided into two groups based on their spatial variation characteristics: lumped models and distributed models (Chow et al., 1988). The former are spatially averaged, or regarded as a single point in space without dimensions; they ignore the internal spatial variation of watershed flow, while the latter consider the hydrologic processes taking place at various points in space and define the model variables as functions of the space dimensions. In addition, the flow routing methods of watershed models are also dominated by this classification; they can be termed lumped flow routing (hydrologic routing; unsteady uniform flow) and distributed flow routing (hydraulic routing; unsteady non-uniform flow) (Chow et al., 1988; Vieux, 2004).

Along with recent increasing availability of spatial data in electronic format (e.g. topography; DEMs, land cover; NLCD, soil; SURRGO/STATSGO, rainfall; NEXRAD and GPM, etc.) and geographic information system (GIS) software to manage, interpret, and prepare spatial data, watershed models for hydrologic application have been enhanced, providing new investigation opportunities and a number of challenges for the inexperienced water resources practitioner (DeVantier and Feldman, 1993; Garbrecht et al., 2001; Martin et al., 2005). Particularly, these improvements have led to more interest in the use of distributed or semi-distributed watershed models than lumped for spatially distributed rainfall-runoff flow simulation. Also, exponential increases in computer capabilities have largely removed historical barriers from the path for development of complex distributed models (Smith et al., 2004).

However, these watershed models have made it difficult to evaluate their simulated results with various parameters and select reasonable values. Many available theoretical watershed models require an extraordinary number of parameters, perhaps more than 100, and they consider all processes and interactions of hydrologic or hydraulic water movements using numerous conceptual or physically-based equations. Thus, parameter estimation (model calibration; optimization) and validation become major tasks in watershed modeling (Koren et al., 2004; Vieux, 2004).

Also, the computation of model outputs (e.g. streamflow) with these parameters by enforcing agreement between observed and simulated data may lead to inconsistencies or incompatibilities among the assumptions of parameters that are incorporated in the model.

Even for the case when estimated parameter values fall within the possible ranges of values, some of them might be overly biased or uncommon cases, compared with other related parameters. Thus, the model performance for different periods of data might be quite poor (Gupta et al., 1999).

Further, the computing time of these watershed models (especially time for automated procedures for model calibration with optimization techniques, not the more time-consuming trial-and-error method) is another issue that makes watershed modeling difficult. Although the speed and capacity of computers have increased, the time consumed running models is still a concern for hydrologic practitioners (Zhang et al., 2009; Razavi et al., 2010; Tsoukalas et al., 2016). Thus, finding available optimization methods which can effectively and efficiently identify good parameter sets is a topic of considerable interest, even more than theoretical hydrologic modeling itself. Thus, decisions based on these available methods might not be optimal because the techniques necessarily disregard some significant hydrologic realities that could not be discounted within computationally tractable analyses. Therefore, to reduce the possible uncertainty in selecting reasonable model parameter values and to avoid time-consuming model calibration (parameter estimation), a watershed model which is relatively simple (few parameters and straightforward computations), but that can utilize state-of-the-art information (e.g. spatially distributed; gridded data), is required.

Hence, in this research, in-depth reviews for finding comparatively simple and popular hydrologic modeling techniques, particularly for runoff estimation and runoff routing

were conducted by referencing published literature and previously developed models. Then, the temporal scales for model simulation (short-term; single event and long-term; discontinuous storm events) were examined. In the big picture, the methodologies focused on in this research for relatively simple watershed-scale hydrologic model (watershed model) development are as follows: (1) runoff estimation (rainfall-runoff prediction); conceptual model, (2) runoff routing (rainfall-runoff flow prediction; watershed rainfall response); lumped conceptual and distributed feature model (hybrid model), (3) temporal scale; both event and continuous streamflow simulation model, and (4) model development and representation; GIS-based spatial data processing and model execution (by Python computer programming language).

1.2 Objectives

The overall goal of this research effort is to develop and evaluate a relatively simple (few parameters and straightforward computations) watershed-scale hydrologic model (watershed model) which can simulate short- and long-term rainfall events in a GIS environment using state-of-the-art spatial data (spatially distributed). The model developed in this study, termed "hybrid hydrologic model," adopted a lumped conceptual and distributed model approach (feature) for runoff routing. More specifically, it was developed based on the combined concept of Clark's unit hydrograph and its spatial decomposition methods. In addition, for runoff estimation, the SCS runoff curve number (CN) method was used with development of a continuous SCS CN method for long-term discontinuous storm events. The specific objectives and each objective's sub-tasks in this study are as follows:

1. Development of a GIS-based spatially distributed Clark's unit hydrograph method (Distributed-Clark) for runoff routing: (1) to develop a spatially distributed Clark's unit hydrograph method (Distributed-Clark), compared with the original and modified Clark's method; through this method, a set of separated (Thiessen polygon, grid cell based, etc.) unit hydrographs are derived, (2) to apply the derived set of separated unit hydrographs to spatially distributed rainfall (in this objective, Thiessen polygon only), and (3) to evaluate the performance of the developed method by making comparisons of simulation results for spatially distributed and averaged (lumped) rainfall data.

2. NEXRAD data (radar-based multi-sensor precipitation estimates) application to runoff routing using Distributed-Clark: (1) to develop a GIS-based NEXRAD precipitation data processing tool, particularly Stage IV composite data, considering its map subset and projection (distortion, scale factor, etc.), (2) to apply the Distributed-Clark model to processed NEXRAD data for spatially distributed rainfall-runoff routing; in this process NEXRAD rainfall estimates need to be verified with gauged data, and (3) to compare and evaluate the performance of simulation results for spatially distributed radar-based rainfall and spatially averaged (lumped) gauged data.

3. Continuous SCS CN method-based long-term hydrologic simulation (runoff routing) using Distributed-Clark: (1) to develop a continuous SCS CN method, compared with previously developed methods, (2) to estimate runoff flow for

spatially distributed long-term discontinuous storm data (NEXRAD radar-based precipitation) using the developed continuous SCS CN method with Distributed-Clark, and (3) to evaluate the performance of the proposed modeling approach by making comparisons between simulation results and observed streamflow for direct runoff following baseflow separation.

1.3 Dissertation Organization

This dissertation consists of five chapters. This chapter is an introduction and overviews research needs for development of a watershed-scale hybrid hydrologic model and specific objectives. Chapters 2 to 4 discuss in detail the methods and results related to the proposed objectives in the previous section. These chapters are presented in a self-contained manner; each chapter has an abstract, introduction, description of study area and data, methodology, results and discussion, and conclusions. However, these chapters are all linked with relatively simple watershed modeling approaches (i.e., hybrid hydrologic model) for short- and long-term applications of spatially distributed rainfall-runoff flow prediction. The overall summary, model characteristics, conclusions, and expected significance synthesizing all chapters and recommendations for future research are presented in Chapter 5.

CHAPTER 2. DEVELOPMENT OF A GIS-BASED SAPTAILLY DISTRIBUTED CLARK'S UNIT HYDROGRAPH METHOD (DISTRIBUTED-CLARK) FOR RUNOFF ROUTING

2.1 Abstract

A GIS-based spatially distributed Clark's unit hydrograph method (Distributed-Clark), a lumped conceptual and distributed feature model (hybrid hydrologic model), was developed based on the combined concept of Clark's unit hydrograph and its spatial decomposition methods to implement hydrologic simulation for spatially distributed rainfall-runoff flow prediction. In Distributed-Clark, the SCS curve number approach (gridded CN) estimated spatially distributed excess rainfall and GIS-derived time-area diagram (isochrones) based on unit hydrographs (a set of separated unit hydrographs) are utilized to calculate a direct runoff hydrograph. Model case studies of single storm event application for four river basins to evaluate the performance of Distributed-Clark using spatially distributed (Thiessen polygon based) rainfall data demonstrate relatively good fit against observed streamflow (direct runoff E_{NS} 0.84, R^2 0.86, and *PBIAS* 0.86%; streamflow E_{NS} 0.91, R^2 0.92, and *PBIAS* 0.32%). The results of spatially distributed precipitation applied cases show better fit in comparison with the outputs of spatially averaged (lumped) rainfall data simulations for Distributed-Clark (E_{NS} of 1.8% and R^2 of 2.1% increase in direct runoff) and HEC-HMS (E_{NS} of 15.5% and R^2 of 14.8% increase in direct runoff) for the same values of model parameters. Thus, Distributed-Clark is a

useful technique to execute spatially distributed rainfall-runoff routing, particularly for storm event flow prediction.

2.2 Introduction

Runoff routing of watershed rainfall response (rainfall-runoff flow prediction) is perhaps the most important part of hydrologic simulation. Numerous theories and computational tools have been developed in the field of engineering hydrology. As one of several hydrologic routing methods available, the unit hydrograph has been a basic tool for rainfall-runoff computation since Sherman (1932) first proposed it in 1932. Sherman initially defined the originally named "unit graph" as representing 1 inch of runoff from a 24-hour (one-day) rainfall. In general though, the unit hydrograph of a watershed is defined as a direct runoff hydrograph resulting from 1 inch (1 cm in SI units) of excess rainfall generated uniformly over the drainage area at a constant rate for an effective duration (Chow et al., 1988). Dooge (1973) pointed out its assumptions, which can be summarized as, "The hydrologic system is linear and time invariant," are not strictly correct for a real catchment system. Nevertheless, he referred to the reasons for clinging to the assumption as follows: linear methods are relatively simple, are by far the best-developed methods, and that the results obtained by using these linear methods are acceptable for engineering purposes.

Through the 1930s to 1950s, many studies on synthetic methods to develop unit hydrographs were conducted. As representative examples, Snyder's (1938), Clark's (1945), and the Soil Conservation Service (SCS)'s (1957, 1972) unit hydrographs have

been most commonly used and remain in use today. The popular hydrologic model HEC-HMS (Hydrologic Modeling System) includes all of these unit hydrograph theories for its hydrograph transformation methods (USACE, 2010).

Among these techniques, Clark's (1945) unit hydrograph method is regarded as the first runoff routing technique based on a time-area diagram (time-area method; Ponce, 1989) which reflects the shape of the drainage area (watershed geomorphology). In this method, Clark not only adopted a time-area concentration curve, which is a graph of incremental drainage area flowing to the outlet within a specific time of travel, but also the concept of the instantaneous unit hydrograph (IUH) whose excess rainfall duration is infinitesimally small. In order to derive a unit hydrograph, Clark first created an IUH by dividing the watershed into isochrones to develop a time-area histogram; it needs to be translated into a time-discharge histogram with instantaneous unit excess rainfall and attenuated by routing through a linear reservoir that has the same storage characteristics as the watershed. Then, the IUH can be converted into a unit hydrograph for any desired period of time by subdividing it into periods of the desired unit length and averaging the ordinates over the preceding periods of time.

As an analogous method, Laurenson (1964) also applied a time-area diagram to a catchment storage model for runoff routing. However, this model did not use the unit hydrograph method; a time-area diagram was only used to determine storage delay time for a series of non-linear storage routing. Similarly, Johnson and Dallmann (1987) and Johnson (1989) used a time-area method as well for flood flow forecasting, introducing a

time-area runoff response function which is a lagged runoff hydrograph from a portion of a watershed (spatial variation is considered) instead of the IUH technique; also it did not account for linear storage routing for its rainfall excess translation.

In the 1990s, the emergence of new technologies such as Geographic Information Systems (GIS) enabled creation of better hydrologic models that can consider the spatial and geomorphologic variation of the watershed. For instance, the time-area histogram can be derived more scientifically and easier than empirical approaches in past applications. Accordingly, there have been considerable attempts to use GIS to construct a unit hydrograph which better reflects spatially distributed flow within watersheds.

Maidment (1993) is one initiator of this GIS-based unit hydrograph modeling; he first presented a grid based methodology for determining a spatially distributed unit hydrograph (SDUH) that reflects the spatially distributed flow characteristics of the watershed. For the SDUH, Maidment adopted a GIS-derived time-area diagram having the assumption of a spatially variable but time-invariant flow velocity field which maintains the same concept of Sherman's (1932) method, and then developed the unit hydrograph as the incremental areas (isochrones-based) of the time-area diagram under assumption of a pure translation process. A more elaborate flow model, which accounts for both translation and storage effects in the watershed, was introduced in another application (Maidment et al., 1996). The watershed response at the outlet point was spatially decomposed into a set of cell-based linear systems whose individual response functions sum to give the watershed response function, and the local velocity function in

each cell was modified by adding the upstream drainage area factor. This model allows subareas within the watershed to be considered as separate units, instead of the conventional assumption that all of the watershed response is spatially lumped.

Muzik (1996) and Ajward et al. (2000) applied Maidment's procedure to flood modeling with a GIS-derived distributed unit hydrograph. However, they used a different approach for a time-area diagram; the overland and channel flow velocity through each grid cell was computed respectively by using the kinematic wave equation and a combined form of Manning's and continuity equation. Also, they tried to calculate each cell's excess rainfall with the SCS runoff curve number method (SCS, 1957, 1972). However, the input rainfall used for deriving the unit hydrograph was spatially averaged. Thus, even though the unit hydrograph was derived in a distributed way, its use was still lumped.

At the same time, there was another trial to consider the spatial variation of runoff routing with radar rainfall data. Peters and Easton (1996) developed a simple quasi-distributed approach (Modified Clark method; ModClark) that applies a linear runoff transform to gridded rainfall excess. It adapted Clark's conceptual runoff model which employs translation and linear storage, but instead of taking the time-area diagram based IUH technique, the SCS time of concentration method (SCS, 1957, 1972) was used for its runoff translation process; each grid cell's rainfall excess is directly lagged to the basin outlet as much as its travel time which is simply proportional to the time of concentration scaled by the ratio of travel length of the cell over the maximum travel length. Kull and Feldman (1998) applied ModClark to non-uniform storm event simulation, using

NEXRAD rainfall data without averaging the rainfall by sub-basin. As a part of application results, they found radar clearly captured the event, whereas the ground gauges completely missed it.

Other attempts to produce GIS-derived SDUH methods based on a more complete mathematical framework were pursued. Olivera and Maidment (1999) proposed a GIS-based spatially distributed runoff routing model using response functions derived from a digital terrain model. In this method, the flow path response function (each cell's IUH), which is the response at the watershed outlet cell to an instantaneous unit input in an upstream watershed cell, was represented as a first-passage-time (statistical) distribution whose flow is modeled with the diffusion wave equation. Thus, the watershed response can be obtained as the sum of the flow path responses to a spatially distributed precipitation excess. De Smedt et al. (2000) also presented a diffusive wave transfer model that enables the calculation of response functions between any start and end point, depending upon slope, flow velocity and dissipation characteristics along the flow lines; all these calculations are performed with standard GIS tools. Liu et al. (2003) enhanced De Smedt's model, especially the average flow velocity for each cell, by combining the maps of hydraulic radius that accounts the flow accumulation, Manning's roughness coefficient, and surface slope. However, these models also used a uniform input precipitation for their case study.

On the other hand, Melesse et al. (2003) and Melesse and Graham (2004) developed a spatially distributed travel time method to generate the direct runoff hydrograph without

relying on unit hydrograph theory. This approach first calculates the average excess rainfall intensity of each cell for the selected storm event, and then computes each cell's cumulative travel time to the watershed outlet by using the same equations Muzik (1996) applied. After that, the volumetric flow rate contributed by that cell (excess rainfall intensity of each cell multiplied by the cell area) at that time was noted. The direct runoff flow was determined by the sum of the volumetric flow rate from all contributing cells at each respective travel time. Because this model used the average excess rainfall intensity for the travel time computation, its variation during the storm cannot be considered. Du et al. (2009) improved this disadvantage by considering travel time field variation due to rainfall variation in time. This, a time variant spatially distributed travel time method, can route spatially-temporally distributed surface runoff (excess rainfall) to the watershed outlet. Therefore, the cumulative travel time for each cell at each time step may be different due to variant surface runoff. However, the method can directly use time variant spatially distributed excess rainfall, but it has critical limitations for its implementation as follows: the storage effects of wetlands, lakes, and depressions are not considered, and the effect of flow accumulation or upslope area is ignored in overland cells (Saghafian and Noroozpour, 2010).

A recently published paper (Buchanan et al., 2012) adapted the methods of Melesse and Graham (2004) and Du et al. (2009) by introducing a four-phase routing scheme also acknowledging the potential limitations. They indicated that even though it has some constraints, it can not only retain a physical basis but also produce acceptable results for operational use (Du et al., 2010). Similar studies on GIS-based spatially distributed unit

hydrograph methods for runoff routing were also conducted with new algorithms for the time-area curve computation based on the knowledge of watershed morphology and of land use (Noto and Loggia, 2007; Gibbs et al., 2010). Also, Chinh et al. (2013) applied a travel time distribution map to the HEC-HMS simulation as input parameters instead of using the unit hydrograph. For this application, they adopted the Thiessen method for considering spatial (aerial) precipitation distributions.

Thus far, major hydrologic runoff routing methods (relatively simple techniques) were reviewed here, particularly for GIS-based spatially distributed hydrologic simulations, which derive resulting unit hydrographs or direct runoff hydrographs. To obtain those results, most methods include the processes of deriving a time-area diagram, translation which transforms an effective storm hyetograph into a runoff hydrograph, and storage attenuation (a linear reservoir routing). Among them, the impulse response function (e.g. IUH) based methods (Maidment et al., 1996; Olivera and Maidment, 1999; Liu et al., 2003) utilize more in-depth theory for spatial decomposition of unit hydrograph. Also, the ModClark method (Peters and Easton, 1996) that targets the spatially varied runoff routing with Clark's approach using gridded rainfall excess did not incorporate a spatially distributed velocity field in computing travel time indices; it was assumed that flow velocity is constant over the watershed. Further, it did not employ the same approach as Clark's unit hydrograph (time-area diagram based IUH technique) but rather used SCS time of concentration. Therefore, the original Clark's unit hydrograph method (Clark, 1945) remained spatially lumped and it can be spatially decomposed with a non-uniform velocity field. Furthermore, even though most studies developed spatially distributed

computational components (unit hydrograph or response function), their applications were still spatially lumped except for Johnson's cases (Johnson and Dallmann, 1987; Johnson, 1989) and HEC-HMS simulations (Peters and Easton, 1996; Kull and Feldman, 1998; Chinh et al., 2013).

In this study, a GIS-based spatially distributed Clark's unit hydrograph method (Distributed-Clark) that can simulate spatially distributed rainfall-runoff flow (runoff routing) was developed based on the combined concept of Clark's (1945) unit hydrograph and Maidment et al.'s (1996) unit hydrograph spatial decomposition methods; it is a lumped conceptual and distributed feature model (hybrid hydrologic model; DeVantier and Feldman, 1993). Also, for its time-area diagram (isochrones) derivation, flow velocity calculation equations for overland (McCuen, 1995) and channel (Muzik, 1996; Melesse and Graham, 2004) were respectively applied with some modification by using GIS. The objectives of this chapter are as follows: (1) to develop a spatially distributed Clark's unit hydrograph method (Distributed-Clark), compared with the original (Clark, 1945) and modified (Peters and Easton, 1996) Clark's method; through this method, a set of separated (Thiessen polygon, grid cell based, etc.) unit hydrographs are derived, (2) to apply the derived set of separated unit hydrographs to spatially distributed rainfall (in this chapter, Thiessen polygon only), and (3) to evaluate the performance of the developed method by making comparisons of simulation results for spatially distributed and averaged (lumped) rainfall data.

2.3 Study Area and Data

2.3.1 Study Area

Four river basins were selected as study areas in this research: Illinois River near Tahlequah, OK; Elk River near Tiff City, MO; Silver Creek near Sellersburg, IN; and Muscatatuck River near Deputy, IN. Two are located near the border of Oklahoma (OK), Arkansas (AR), and Missouri (MO), and two are located in southern Indiana (IN). These watersheds have a data-rich environment (the first two were test basins of DIMP; Distributed Model Inter-comparison Project for NOAA; Smith et al., 2004), as well as limited complications such as upstream diversions, dam operations, snow, or tile drainage (Figure 2.1).

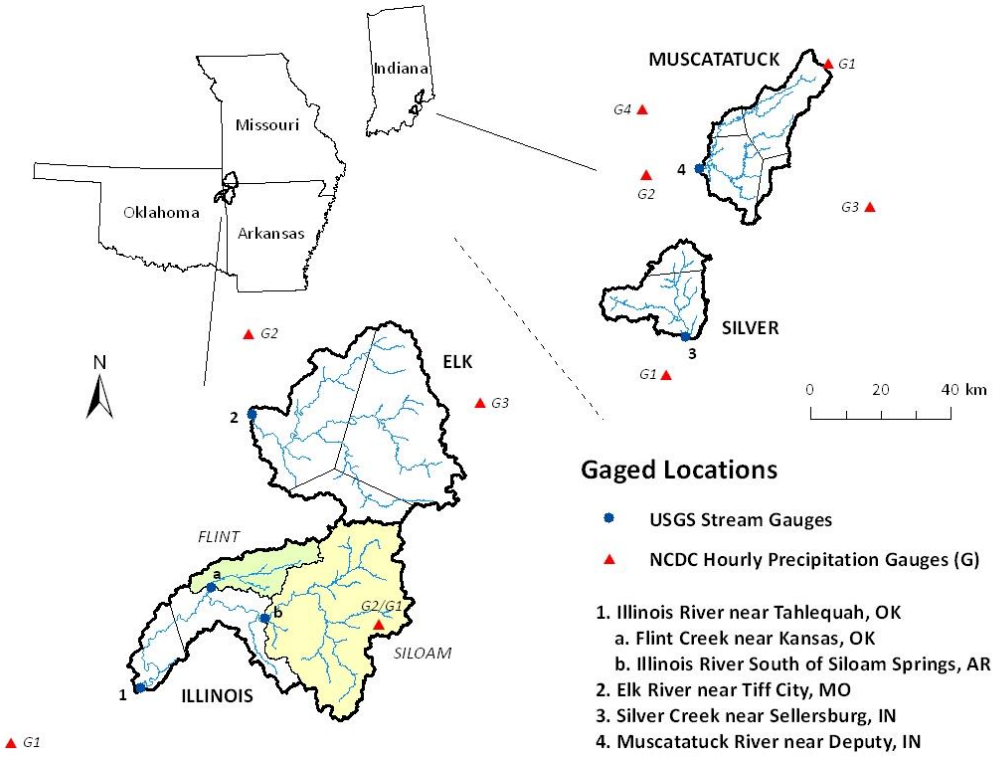

Figure 2.1 Location of study watersheds

The topography of the Illinois River and Elk River watersheds can be characterized as gently rolling to hilly (Smith et al., 2004), while the Silver Creek and Muscatatuck River watersheds are relatively flat (Wilkerson and Merwade, 2010). In the Illinois River basin, which contains two sub-catchments, the elevation above sea level varies from approximately 202 m at the USGS stream gauge to 600 m at the basin edge, while the Elk River basin varies in elevation from 229 m to around 537 m above sea level. The Silver Creek and Muscatatuck River basins rise from elevations of 131 and 165 m to 314 and 309 m, respectively, representing smaller variances of elevation than the first two basins. These areas are also known for their karst landscape that has resulted in the creation of many caves and one of the largest limestone quarry areas in the USA (Veni, 2002), but there is no report of its reflection (influence) for hydrologic simulation as a constraint. Basic topographic and hydrologic characteristics for these watersheds and nested sub-catchments are summarized in Table 2.1, based on USGS stream gauge site information, USGS DEM, etc.

Table 2.1 Basic topographic and hydrologic characteristics of study areas

Watershed	USGS ID	A (km^2)	H (m)	L (km)	S (m/m)	P (mm)
Illinois River near Tahlequah	07196500	2460	202	170.7	0.082	1310
- Flint Creek near Kansas	07196000	300	260	45.8	0.065	1193
- Illinois River South of Siloam Springs	07195430	1489	283	79.2	0.065	1217
Elk River near Tiff City	07189000	2204	229	114.9	0.117	1168
Silver Creek near Sellersburg	03294000	490	131	45.0	0.093	1141
Muscatatuck River near Deputy	03366500	759	165	88.9	0.036	1165

A - drainage area; H - outlet elevation (above NGVD29); L - maximum flow length; S - average slope of watershed; P - average annual precipitation near outlet city (from www.noaa.gov; over 30-year period)

Table 2.2 shows the general information of land use and soil features in the study area basins; the table values are estimated from the USGS NLCD and USDA SSURGO datasets. Most watersheds predominantly include forest (37.4 to 55.8%) followed by agricultural land (33.3 to 48.2%), developed land (up to 14.1%), and water (up to 0.8%); in particular the Silver Creek watershed is occupied by about 56% forest. The dominant land uses are presented with the four hydrologic soil groups (HSG) in Table 2.2. In general, soils in A group have lower runoff potential than the B, C, and D groups; D has the highest runoff potential (USDA NRCS, 2010). For most areas, soil groups B and C are dominant, except in the Illinois River watershed which has a relatively even distribution and the Muscatatuck River that contains a higher percentage (about 75%) of soil group C (typically have clay loams, shallow sandy loam, etc.; see footnote of Table 2.2) than other areas (Figure 2.2).

Table 2.2 Land use and soil types of study areas

Watershed	Land use				Hydrologic Soil Group			
	W (%)	U (%)	F (%)	Ag. (%)	A (%)	B (%)	C (%)	D (%)
Illinois River near Tahlequah	0.3	14.1	37.4	48.2	10.8	35.7	30.5	23.0
- Flint Creek near Kansas	0.6	11.6	34.5	53.3	6.1	26.5	38.1	29.3
- Illinois River South of Siloam Springs	0.3	18.7	28.6	52.4	14.6	36.8	29.4	19.2
Elk River near Tiff City	0.2	8.3	50.5	41.0	14.6	44.0	31.6	9.8
Silver Creek near Sellersburg	0.8	10.0	55.8	33.3	-	45.6	45.6	8.8
Muscatatuck River near Deputy	0.2	4.5	51.4	43.9	-	21.4	74.4	4.2

W - water; U - urban or built-up; F - forest; Ag. - agricultural land

A group (deep sand, deep loess, and aggregated silts); B group (shallow loess and sandy loam); C group (clay loams, shallow sandy loam, soils low in organic content, and soils usually high in clay); D group (soils that swell significantly when wet, heavy plastic clays, and certain saline soils)

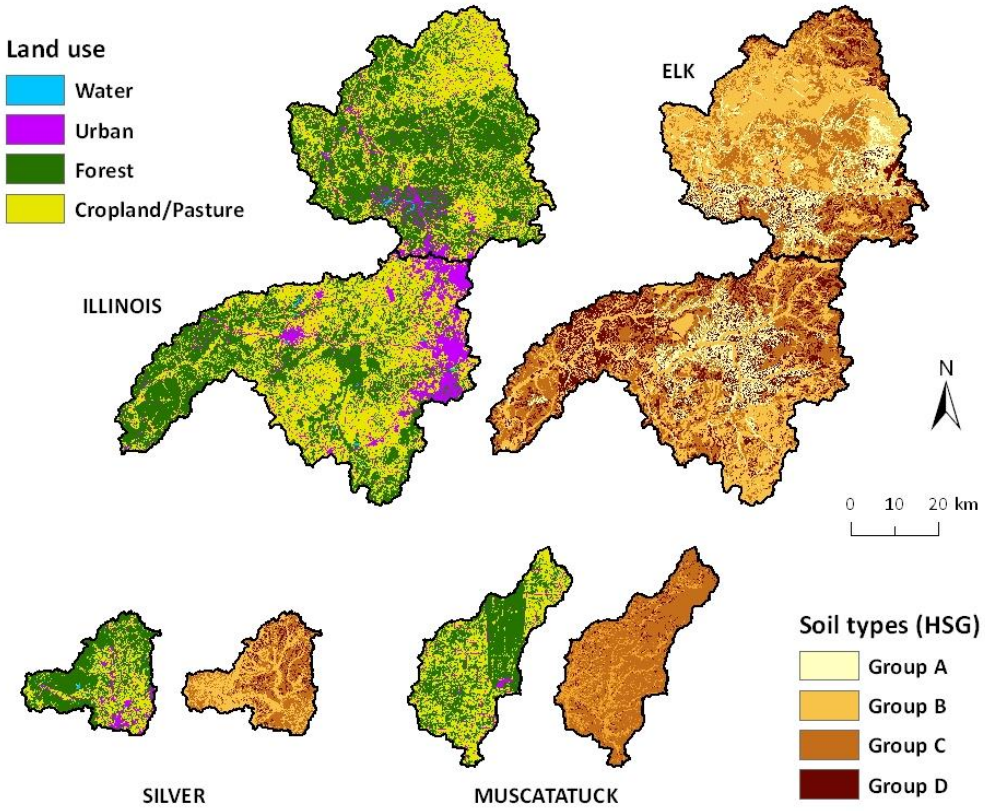

Figure 2.2 Land use and soil types of study areas

2.3.2 Data

The data used in this study include: (1) 1 arc-second (spatial resolution around 30 m) Digital Elevation Model (DEM), National Land Cover Database 2011 (NLCD 2011), and National Hydrography Dataset (NHD) from USGS National Map, (2) Soil Survey Geographic (SURRGO) Database from USDA WSS (Web Soil Survey), and (3) Precipitation Frequency (PF) estimates from NOAA HDSC (Hydro-meteorological Design Studies Center). DEM and NHD data are used for watershed delineation and stream network definition, whereas land use, PF estimates, and soil data are used to

create flow travel time and runoff curve number map. The time-series (hourly) data and gauge information, precipitation (gauged rainfall) from NOAA NCDC (National Climatic Data Center) and streamflow from USGS NWIS (National Water Information System), are used to evaluate the performance of the developed method with several storm event records in the four study watersheds.

2.4 Methodology

2.4.1 Overall Concept of Method

2.4.1.1 Clark's Unit Hydrograph Method

Clark's (1945) method requires two main parameters to calculate a unit hydrograph: a time-area diagram and a storage coefficient, *R*. A time-area diagram defines the incremental area of the watershed (percentages of total area) contributing runoff to the outlet as a function of time. The ordinates of the time-area diagram are converted to volume of runoff per second for unit excess and interpolated to the given time interval. The resulting translation hydrograph is then routed through a linear reservoir to simulate the storage effects of the watershed, and the resulting unit hydrograph for instantaneous excess (IUH) is averaged to produce the hydrograph for unit excess (UH; unit hydrograph) occurring in the given time interval (USACE, 1998). Figure 2.3 shows a conceptual model of this method (Kull and Feldman, 1998). The linear reservoir routing is accomplished using Equation (2.1), which is a modified form of the Muskingum method (Chow et al., 1988):

$$IUH_i = cI_i + (1 - c)IUH_{(i-1)} \tag{2.1a}$$

$$c = \frac{\Delta t}{R + 0.5\Delta t} \tag{2.1b}$$

$$UH_i = \frac{IUH_{(i-1)} + IUH_i}{2} \tag{2.1c}$$

where I_i, IUH_i, and UH_i are the ordinate of the translation hydrograph, instantaneous unit hydrograph, and unit hydrograph at time i [L^2T^{-1}], respectively, c is the routing coefficient, Δt is the computation time interval [T], and R is the storage coefficient [T].

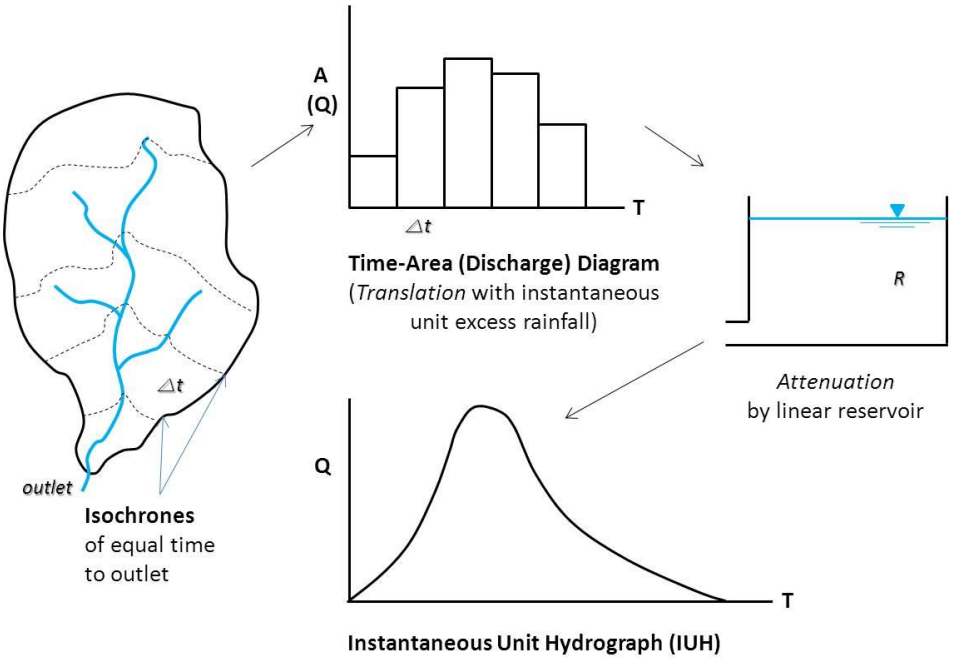

Figure 2.3 Clark's method conceptual model

Clark (1945) provided a means of estimating a storage coefficient, R, by considering a measured hydrograph and calculating it by Equation (2.2):

$$R = -\frac{Q}{dQ/dt} \tag{2.2}$$

where Q [L^3T^{-1}], dQ [L^3T^{-1}], and dt [T] are measured at the inflection point on the recession limb of a hydrograph at the gauge site.

2.4.1.2 ModClark (Modified Clark method)

The Modified Clark method (Peters and Easton, 1996) also requires two watershed parameters to transform rainfall excess to direct runoff hydrograph: a time of concentration, T_c, and a storage coefficient, R (for a linear reservoir). In this method, translation and storage routing are performed on a radar grid cell basis with different approaches. Rainfall excess for each cell is directly lagged to the watershed outlet by using its travel time. The travel time (translation lag) for a grid cell is calculated by Equation (2.3):

$$[travel\ time]_{cell} = T_c \frac{[travel\ length]_{cell}}{\text{maximum of the cell travel lengths}} \tag{2.3}$$

where T_c is the time of concentration for the watershed [T], $[travel\ length]_{cell}$ is the travel length of a grid cell to watershed outlet [L].

Then, the lagged rainfall excess for each cell is routed through a linear reservoir by using Equation (2.4):

$$O_i = \left[\frac{\Delta t}{R + 0.5\Delta t}\right] I_{avg} + \left[1 - \frac{\Delta t}{R + 0.5\Delta t}\right] O_{(i-1)} \quad (2.4)$$

where O_i is the direct runoff at time i [L^3T^{-1}], R is the storage coefficient [T], I_{avg} is the average inflow for the interval i-1 to i [L^3T^{-1}], and Δt is the time interval [T].

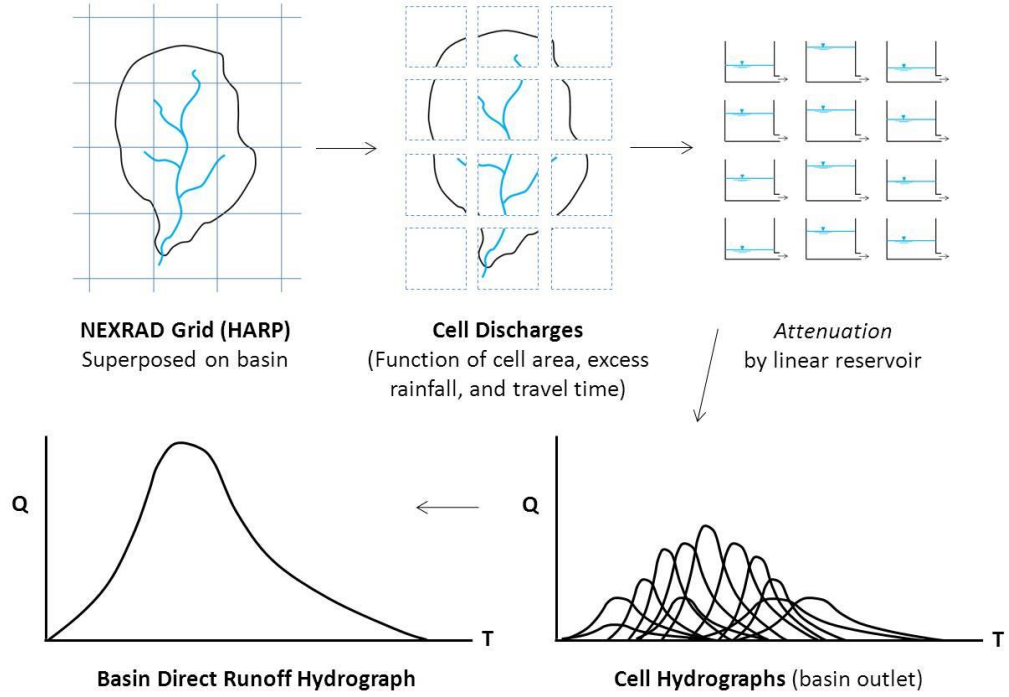

Figure 2.4 ModClark direct runoff conceptual model

Through these processes, ModClark directly obtains each cell's direct runoff hydrograph, instead of using a convolution of unit hydrograph and excess rainfall. Then, these lagged and routed outflows are summed to produce a watershed outlet's direct runoff hydrograph. Thus, its computational approach is clearly different from the original Clark's (1945) method, except for the fact that translation and storage attenuation are adopted. Figure 2.4 represents a conceptual model of ModClark (Kull and Feldman, 1998).

2.4.1.3 Spatial Decomposition of the Unit Hydrograph

In a linear system, the convolution integral of the excess rainfall hyetograph and unit impulse response function for the watershed outlet can be defined as the direct runoff hydrograph (Chow et al., 1988) by Equation (2.5):

$$Q(t) = A\int_0^t I(\tau)u(t-\tau)d\tau \tag{2.5}$$

where $Q(t)$ is the direct runoff hydrograph at time t [L^3T^{-1}], $I(\tau)$ is the rainfall excess function [L], $u(t-\tau)$ is the unit impulse response function [T^{-1}], and A is the watershed area [L^2].

Under the assumption of a spatially varying but time-invariant velocity field, this linear system response at the watershed outlet can be spatially decomposed into a set of cell-based linear systems whose individual response functions sum to give the watershed response function. Maidment et al. (1996) developed the continuous time function as Equation (2.6) that represents the spatial convolution of each ΔA_j watershed subarea's direct runoff responses.

$$Q(t) = \sum_{j=1}^{J}\Delta A_j\int_0^t I_j(\tau)u_j(t-\tau)d\tau \tag{2.6}$$

where ΔA_j is the jth subarea of watershed (j = 1, 2, …, J) [L^2], other factors are the same as in Equation (2.5).

Also, it can be denoted as the discrete time function, Equation (2.7), using the components of unit hydrograph theory. In this equation, the total discharge, Q_n, is found by summing the lagged responses (UH) to all precipitation pulses over all subareas.

$$Q_n = \sum_{i=1}^{n} \sum_{j=1}^{J} \Delta A_j P_{i,j} U_{n-i+1,j} \tag{2.7}$$

where Q_n is the direct runoff hydrograph at the end of nth time interval [L^3T^{-1}], ΔA_j is the jth subarea of watershed [L^2], $P_{i,j}$ is the average excess rainfall in the jth subarea for time interval i [L], and $U_{n-i+1,j}$ is the jth subarea's unit hydrograph at the end of n-i+1th interval [T^{-1}].

From Equation (2.7), any unit hydrograph can be spatially decomposed and applied to non-uniform precipitation data which are obtained from the same subarea's grid cell or compartment for calculating direct runoff hydrograph.

2.4.1.4 Distributed-Clark (GIS-based spatially distributed Clark's unit hydrograph method)

A GIS-based spatially distributed Clark's unit hydrograph method (Distributed-Clark) is a combined technique based on concepts of Clark's (1945) unit hydrograph and its spatial decomposition methods (Maidment et al., 1996). So, to derive its spatially distributed unit hydrograph (a set of separated unit hydrographs), a time-area diagram and the IUH adopted transformation are needed. For this method, the ordinates of the unit hydrograph

(UH) can be obtained by Equation (2.1), and then combining with Equation (2.7) produces Equation (2.8); it can compute a set of separated unit hydrographs, *S*, and the direct runoff, *Q*.

$$S_{i,j} = 0.5\left[\left(\frac{\Delta t}{R + 0.5\Delta t}\right) I_{i,j} + \left(2 - \frac{\Delta t}{R + 0.5\Delta t}\right) IUH_{(i-1),j}\right] \quad (2.8a)$$

$$Q_n = \sum_{i=1}^{n}\sum_{j=1}^{J} P_{i,j} S_{n-i+1,j} \quad (2.8b)$$

where $S_{i,j}$, $I_{i,j}$, and $IUH_{i,j}$ are the *j*th subarea's separated unit hydrograph, translation hydrograph, instantaneous unit hydrograph at the end of *i*th interval [L^2T^{-1}], respectively, and other factors are the same as in Equation (2.7).

It also requires the same parameters as Clark's (1945) unit hydrograph method: a time-area diagram and a storage coefficient, *R*. In this method, a time-area diagram is derived based on GIS applications; multiple Geoprocessing and Python script tools developed in this effort are used (ESRI, 2013). Figure 2.5 shows a conceptual model of the Distributed-Clark approach, and overall procedures for the Distributed-Clark development are represented in Figure 2.6.

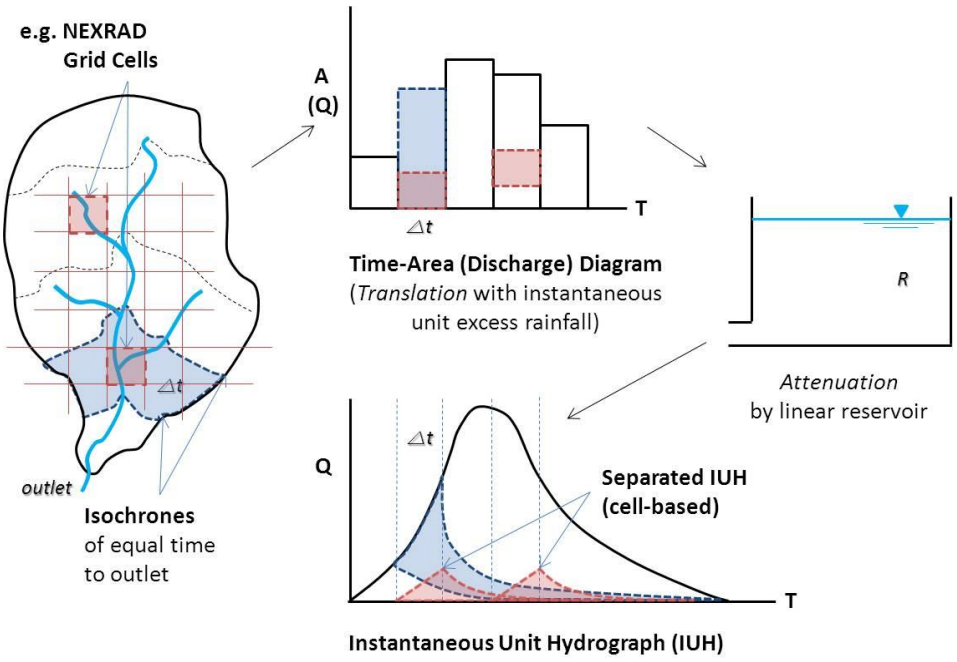

Figure 2.5 Distributed-Clark conceptual model

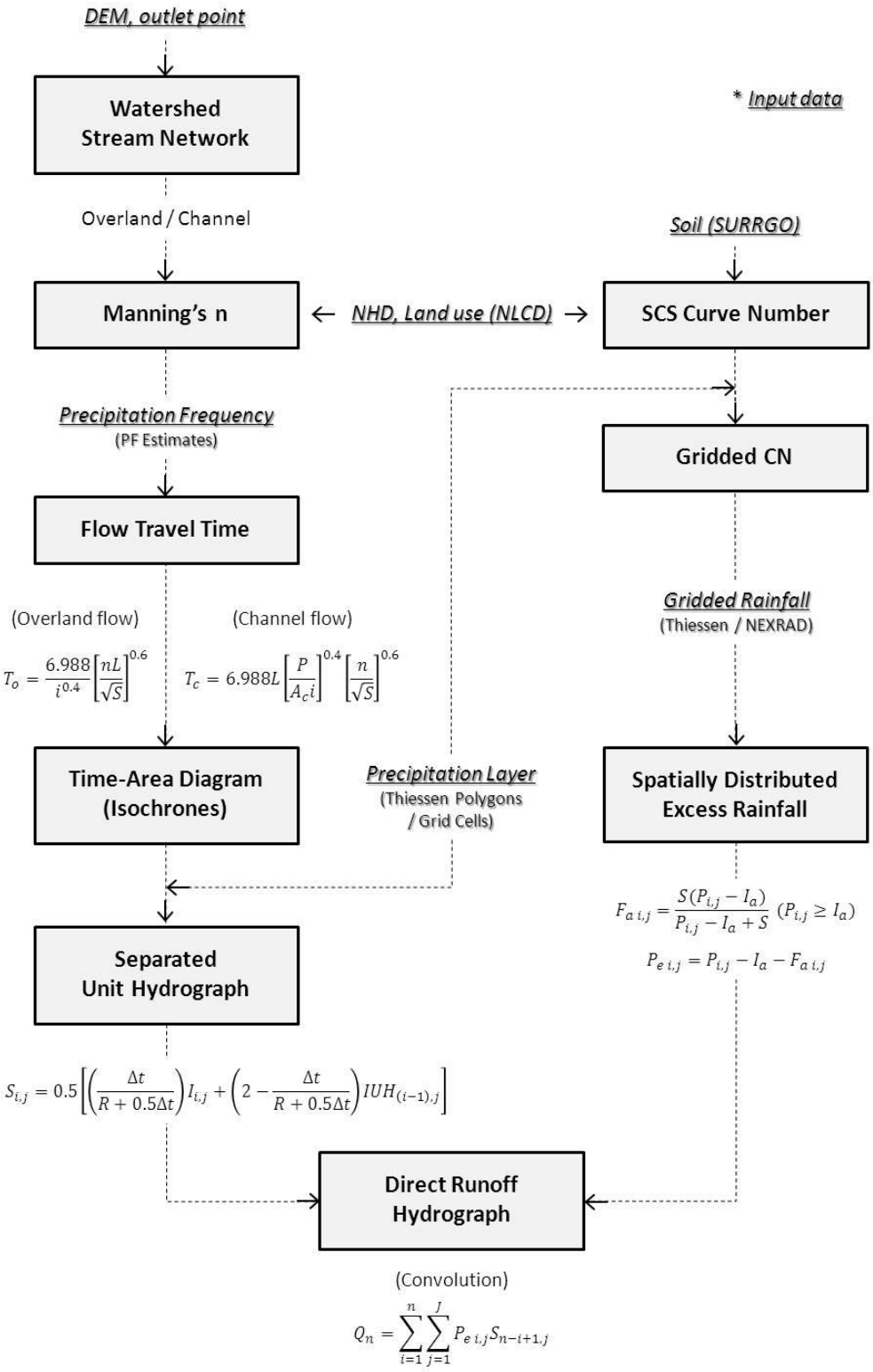

Figure 2.6 Overall procedures of Distributed-Clark development

2.4.2 Distributed-Clark Development

Development of Distributed-Clark model includes four main steps of watershed pre-processing, spatially distributed excess rainfall (runoff) estimation, spatially distributed unit hydrograph derivation, and direct runoff hydrograph convolution. For this implementation, ArcGIS 10.1 (ESRI, 2012) was used as the GIS platform to build and execute the Python script tools (with Spatial Analyst Tools) for each step.

2.4.2.1 Watershed Pre-processing

This step mainly consists of delineating stream network and watershed boundary. Manning's *n* map is created to utilize the kinematic wave and Manning's equations which are needed for computing flow velocity. Also, SCS curve numbers are extracted for computing excess rainfall by using the soil and land used data.

2.4.2.1.1 Watershed and Stream Network

This process uses the standard step-by-step procedure for a DEM to create the following: (1) hydro-DEM after filling sinks, (2) flow direction grid using D8 algorithm (Greenlee, 1987; Mark, 1988; Jenson et al., 1988; Tarboton et al.; 1991), (3) flow accumulation grid, (4) stream network, and (5) watershed boundary for a specified outlet. Getting the stream network from the flow accumulation grid requires the definition of a critical source area threshold, which is the drainage area needed to form a stream. In this case, a stream is defined for areas that receive shallow concentrated flow. According to USDA NRCS (2010), sheet flow (overland flow) occurs for no more than 100 feet (30.48 m) before

transitioning to shallow concentrated flow. Thus, if the flow accumulation value of a cell is greater than or equal to '1' for a 30 m DEM, its flow in the cell is defined as channel flow; this study applied 30 m as the threshold of conceptual stream network definition.

2.4.2.1.2 Manning's Roughness Coefficient

The Manning's roughness coefficient, *n*, values for National Land Cover Database (NLCD) classifications are determined to develop Manning's *n* map for using a given watershed's analysis of flow velocity computation.

Table 2.3 Manning's *n* values for NLCD classifications

NLCD Value	Class	Manning's *n*
11	Open Water	0.030
21	Developed, Open Space	0.015
22	Developed, Low Intensity	0.015
23	Developed, Medium Intensity	0.015
24	Developed High Intensity	0.012
31	Barren Land (Rock/Sand/Clay)	0.020
41	Deciduous Forest	0.120
42	Evergreen Forest	0.120
43	Mixed Forest	0.120
52	Shrub/Scrub	0.075
71	Grassland/Herbaceous	0.035
81	Pasture/Hay	0.040
82	Cultivated Crops	0.035
90	Woody Wetlands	0.085
95	Emergent Herbaceous Wetlands	0.075

Typically, Manning's *n* values can be estimated with guidance from descriptive information and photographs of Barnes' (1967) and Chow's (1986) works (Engman,

1986). Although a number of models refer to different literature (Brater, 1976; Chow et al., 1988; Yen, 1991; Ferguson, 1998; Montes, 1998; McCuen, 2005) values, they are similar to Chow's (1986) values. In this study, all values referenced above were re-considered with recent published values (Vieux, 2004; Kalyanapu et al., 2009; Jung et al., 2013; Dorn et al., 2014) for NLCD classifications, and Table 2.3 shows the final values. These *n* values can be simply applied to GIS to develop a Manning's *n* map with the 'Raster Calculator' tool.

2.4.2.1.3 SCS Curve Number

The SCS CN values are determined to create a CN map based on SURRGO soil and NLCD land use data in GIS. Since the original SCS CN table (SCS, 1957, 1972; USDA NRCS, 2010) was developed from hydrologic soil-cover complexes, a combination of a Hydrologic Soil Group (HSG) and a land use and treatment class (cover) presents different categories from NLCD classifications. Another CN lookup table (Table 2.4) that has values for NLCD classes comparing with the original SCS CN table was developed by referencing previous studies (Mednick, 2010; WRC, 2013; Jeon et. al, 2014; TWRI, 2014). Most values (agricultural lands, forests, and wetlands) in Table 2.4 were directly assigned by referring to analogous cover type, treatment, and hydrologic conditions in the original table, but the values for developed areas are estimated by Equation (2.9) on the basis values of a pervious urban area (assumed equivalent to open space in good hydrologic condition in the original table); 10, 35, 65, and 90% are used as percent

imperviousness for NLCD values of 21, 22, 23, and 24, respectively. Also, in the case of open water, the maximum pervious CN value, 98, is assigned (some papers use 0).

$$CN_c = CN_p + \left(\frac{P_{imp}}{100}\right)(98 - CN_p) \tag{2.9}$$

where CN_c and CN_p are the composite and pervious runoff curve number, respectively, and P_{imp} is the percent imperviousness.

Table 2.4 SCS CN values for NLCD classifications

NLCD Value	Class	Hydrologic Soil Group				Imperviousness (%)
		A	B	C	D	
11	Open Water	98	98	98	98	-
21	Developed, Open Space	45	65	76	82	10
22	Developed, Low Intensity	60	74	82	86	35
23	Developed, Medium Intensity	77	85	90	92	65
24	Developed High Intensity	92	94	96	96	90
31	Barren Land (Rock/Sand/Clay)	77	86	91	94	-
41	Deciduous Forest	36	60	73	79	-
42	Evergreen Forest	30	55	70	77	-
43	Mixed Forest	30	55	70	77	-
52	Shrub/Scrub	35	56	70	77	-
71	Grassland/Herbaceous	30	58	71	78	-
81	Pasture/Hay	49	69	79	84	-
82	Cultivated Crops	62	71	78	81	-
90	Woody Wetlands	45	66	77	83	-
95	Emergent Herbaceous Wetlands	49	69	79	84	-

In addition, to assign CN values for dual HSG of A/D, B/D, and C/D which are introduced for drainage characteristics (the first letter applies to the drained condition and the second to the un-drained condition; USDA NRCS, 2010), it is assumed that 50% (by

area) of these soil types are drained. The Antecedent Runoff Conditions (ARC) are also considered by Equation (2.10) (Chow et al., 1988) for the variability in the CN results from rainfall intensity and duration, total rainfall, soil moisture conditions, cover density, stage of growth, and temperature (USDA NRCS, 2010).

$$CN(I) = \frac{4.2CN(II)}{10 - 0.058CN(II)} \tag{2.10a}$$

$$CN(III) = \frac{23CN(II)}{10 + 0.13CN(II)} \tag{2.10b}$$

where *CN(I)*, *CN(II)*, and *CN(III)* are the dry, average, and wet condition CN, respectively.

2.4.2.2 Spatially Distributed Excess Rainfall

2.4.2.2.1 Runoff Depth

In Distributed-Clark, the SCS runoff curve number (CN) method (SCS, 1957, 1972) is used to estimate runoff depth (excess rainfall) from storm rainfall. For a given rainfall event, each *t* time step's cumulative excess rainfall, $P_{e,t}$, can be calculated by Equation (2.11) (Chow et al., 1988):

$$P_{e,t} = P_t - I_a - F_{a,t} \tag{2.11a}$$

$$F_{a,t} = \frac{S(P_t - I_a)}{P_t - I_a + S} \quad (P_t \geq I_a\,, \qquad \text{if not } F_{a,t} \text{ and } P_{e,t} = 0) \tag{2.11b}$$

$$S = \frac{25400}{CN} - 254 \quad (2.11c)$$

where $P_{e,t}$ and P_t are the cumulative excess rainfall and rainfall depth at the end of time t [L], respectively, I_a is the initial abstraction (λS, λ is the initial abstraction coefficient; 0 to 1, one of calibration parameters for overall results) [L], $F_{a,t}$ is the cumulative abstraction at the end of time t [L], S is the potential maximum retention (mm), and CN is the SCS curve number.

Although this time distribution of SCS abstraction equation (F_a) may not have a strong physical basis for infiltration behavior since the rate of retention of water within the watershed tends to increase as the rainfall intensity increases (Morel-Seytoux and Verdin, 1981), this equation can be used for single storm event runoff application (Chow et al., 1988).

2.4.2.2.2 Gridded CN

The gridded CN which is described as a histogram of CN values corresponding to subarea of interest (in this chapter, Thiessen polygon) is utilized to calculate the spatially distributed rainfall excess with the SCS runoff curve number (CN) method. For this computation in GIS (using Python script tools developed in this effort), a set of gridded CN for given subareas are first derived based on a previously developed CN map. Then, they are applied to each subarea's runoff depth calculation in Equation (2.11), and the resulting average rainfall excess for each subarea is generated. Figure 2.7 shows the process of spatially distributed excess rainfall estimation using graphic representations.

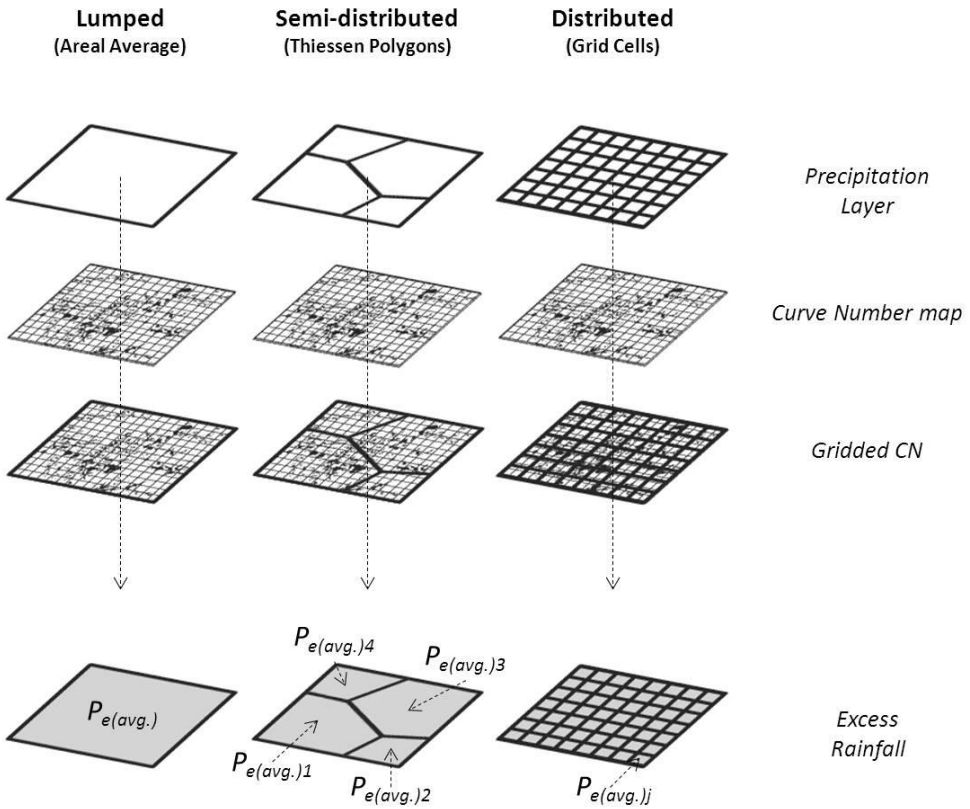

Figure 2.7 Graphical representations of the spatially distributed excess rainfall estimates

2.4.2.3 Spatially Distributed Unit Hydrograph

2.4.2.3.1 Flow Travel Time

In Distributed-Clark, two types of flow (overland flow and channel flow) in a grid cell are considered for a defined stream network's flow. Overland flow (sheet flow) is defined as flow over plane surfaces; it usually occurs in the headwaters of a stream near the ridgeline that defines the watershed boundary (USDA NRCS, 2010). McCuen (1995) indicated the overland flow length must be less than 300 feet (some political jurisdictions believe 300 feet is too long and limit *L* to 100 feet) and presented two kinematic wave

equations for the kinematic time to equilibrium which are used for estimating travel times of overland flow runoff. The first Equation (2.12a) was developed by using the kinematic flow approximation (Overton, 1976), and the other Equation (2.12b) which is a different form of Equation (2.12a) was obtained by rainfall intensity-duration-frequency curve usage (Welle and Woodward, 1986).

$$T_c = \frac{0.93}{i^{0.4}} \left[\frac{nL}{\sqrt{S}}\right]^{0.6} \tag{2.12a}$$

$$T_t = \frac{0.42}{P_2^{0.5}} \left[\frac{nL}{\sqrt{S}}\right]^{0.8} \tag{2.12b}$$

where T_c and T_t are the equilibrium time and travel time (min), i is the rainfall intensity (in./hour), L is the length of sheet flow (ft), n is the Manning's roughness coefficient, S is the slope (ft/ft), and P_2 is 2-year, 24-hour rainfall depth (in.).

In addition, McCuen (2005) also solved the kinematic wave equation for equilibrium time using Manning's equation with the assumption that the hydraulic radius equals the product of the rainfall excess intensity (vertical net incoming flux) and the travel time. Equation (2.13), the adopted equation for this study, represents the velocity and travel time of overland flow with SI unit solutions.

$$V_o = \frac{(iL)^{0.4} S^{0.3}}{419.28 n^{0.6}} \tag{2.13a}$$

$$T_o = \frac{6.988}{i^{0.4}} \left[\frac{nL}{\sqrt{S}}\right]^{0.6} \tag{2.13b}$$

where V_o is the overland flow velocity (m/sec), i is the vertical net incoming flux (mm/hour), L is the length of overland flow (m), S is the slope (m/m), n is the Manning's roughness coefficient, and T_o is the overland flow travel time (min).

The velocity and travel time equations for channel flow are obtained based on the method that Muzik (1996) and Melesse and Graham (2004) applied to their model, whose formula is the combined form of Manning's and continuity equations as Equation (2.14).

$$V = \left[\frac{S^{1/2}}{n}\left(\frac{Q}{B}\right)^{2/3}\right]^{3/5} \tag{2.14}$$

where V is the channel flow velocity (m/sec), n is the Manning's roughness coefficient, S is the slope (m/m), Q is the cumulative discharge (m^3/sec), and B is the channel width (m).

A proposed approach in this study, however, preserves the hydraulic radius, R, as Equation (2.15a), and considers the flow accumulation from the upstream drainage area, A_c, assuming the cumulative discharge equals the product of the upstream drainage area and the vertical net incoming flux as Equation (2.15b). Equation (2.16) is the final derived equation with different units.

$$R = \frac{A}{P} = \frac{Q}{VP} \tag{2.15a}$$

$$Q = A_c i \tag{2.15b}$$

$$V = \frac{1}{n}R^{2/3}S^{1/2} = \frac{S^{0.3}}{n^{0.6}}\left[\frac{Q}{P}\right]^{0.4} = \frac{S^{0.3}}{n^{0.6}}\left[\frac{A_c i}{P}\right]^{0.4} \quad (2.15c)$$

where R is the hydraulic radius (m), A is the cross sectional area of flow (m^2), P is the wetted perimeter (m), A_c is the upstream drainage area (m^2), i is t vertical net incoming flux (m/sec), and other factors are the same as in Equation (2.11).

$$V_c = \frac{S^{0.3}}{419.28n^{0.6}}\left[\frac{A_c i}{P}\right]^{0.4} \quad (2.16a)$$

$$T_c = 6.988L\left[\frac{P}{A_c i}\right]^{0.4}\left[\frac{n}{\sqrt{S}}\right]^{0.6} \quad (2.16b)$$

where V_c and T_c are the channel flow velocity (m/sec) and travel time (min), i is the vertical net incoming flux (mm/hour), L is the length of channel (m), and others are the same as above.

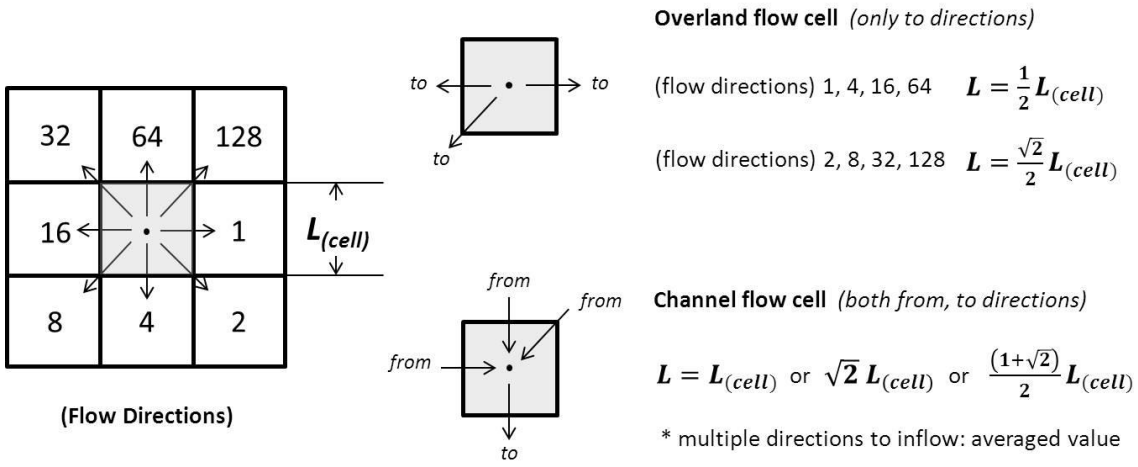

Figure 2.8 Determination of effective flow length, L in the cell

For GIS applications to build a travel time map with these equations, estimation methods for several factors in the above equations are also defined as follows: (1) The effective flow length, *L* in the cell for the overland and channel flow are determined in accordance with flow directions (from, to) as shown in Figure 2.8. In the case of multiple directions to inflow (in channel flow), *L* is assumed to use the averaged value. (2) The wetted perimeter, *P*, is estimated with the NHD (National Hydrography Dataset) flow line, stream order, and satellite imagery. It needs to derive a stream order map which has similar network with the NHD and then assume *P* values on the cells in different stream order lines ('1' m is assigned as a default value for the cells that are not included in these order lines) by using satellite imagery (e.g., ArcGIS base map, ESRI, 2012). (3) The vertical net incoming flux, *i*, is assumed as the average intensity of 2-year, 24-hour rainfall for the given area by default; this factor is later used as one of calibration parameters for overall results. Then the 'Raster Calculator' tool is applied to compute each grid cell's flow travel time with the other factors of equations: slope, *S*, upstream drainage area (obtained by flow accumulation), A_c, and Manning's *n* (in Table 2.3; 0.030 for channel flow).

2.4.2.3.2 Time-Area Diagram (Isochrones)

The time-area diagram establishes a relationship between the travel time and a portion of a basin (watershed) area. To produce a time-area diagram, the cumulative travel time for each cell to the watershed outlet is first calculated by summing the travel times along the respective flow path that follows flow directions; a cumulative travel time map is

obtained. Then, it is divided into subareas by specific travel time interval isochrones (in this study, one hour interval is applied), and the resulting time-area diagram is produced. For this GIS application, Python script tools were developed for cumulative travel time calculation and isochrones derivation are used.

2.4.2.3.3 Separated Unit Hydrograph

Once a time-area diagram is produced, it needs to be translated into a time-discharge diagram (translation hydrograph) with instantaneous unit excess rainfall, and then a set of separated unit hydrographs are calculated by Equation (2.8a). This calculation process can be described as follows: (1) a time-discharge diagram is decomposed into partial fractions (subareas; Thiessen polygons, grid cells, etc.), (2) one (*j*th) subarea's diagram is then routed through a linear reservoir that has a storage coefficient, *R* (one of parameters for overall results calibration); it makes *j*th subarea's IUH (Figure 2.5), and (3) this IUH is averaged to create a *j*th subarea's separated unit hydrograph for desired period (one hour) of time. Through this process, a set of separated unit hydrographs are produced for given subareas of interest (in this chapter, Thiessen polygon is adopted); they can be convoluted with spatially distributed rainfall excess. A Python script tool was also developed for these GIS applications.

2.4.2.4 Direct Runoff Hydrograph

A direct runoff hydrograph is calculated by Equation (2.8b) using previously developed series of spatially distributed excess rainfall and separated unit hydrographs; a set of

distributed direct runoff hydrographs for the watershed outlet point can be calculated, and the sum of all distributed direct runoff hydrographs can be used to create a direct runoff hydrograph using a Python script tool for this convolution calculation.

2.4.3 Model Performance Evaluation

2.4.3.1 Storm Event Selection

Storm events for the four study areas were selected to evaluate the performance of the developed model (Distributed-Clark). For this evaluation of event based runoff simulations, a rainfall storm should be considered an independent (isolated) single event, since the SCS CN method (USDA NRCS, 2010) for runoff depth does not account for infiltration recovery during intervals of no rain; if the model does not consider this recovery, overestimated runoff calculation outcomes will result (Woodward et al., 2002).

The acquisition of recent time-series storm data (hourly records) for rainfall and streamflow from the NOAA NCDC and USGS NWIS web-sites was not a simple process, because the hourly observed streamflow data are only available until the end of September 2007 in the NWIS instantaneous data archive. Furthermore, even though observed streamflow data are available, the required rain gauge data for the study area are alternately missing or have error records, particularly for the periods of appropriate storms to use for model performance evaluation. Consequently, six events (total of 24 events) from 1998 to 2007 data were selected for each study area's model calibration and validation (Table 2.5).

The method for storm event selection was primarily visual inspection of observed streamflow and the corresponding rain gauge data values. Then, to evaluate the model performance over various storm event sizes (flow ranges), different sized (relatively largest, along with moderate size) storms were selected. Also, when possible (under given availabilities of data), rainfall storms were evenly selected throughout the period (1998 to 2007) and from different seasons.

Table 2.5 Storm events for study areas

Watershed	Storm Events (#: Periods)	Precipitation Total (mm)					Streamflow	
		G1	G2	G3	G4	Areal average	Peak flow (m^3/s)	Total (mm)
Illinois River near Tahlequah	1: 2001-02-23~02-28	99.1	71.1	-	-	73.8	719.3	56.4
	2: 2002-04-07~04-12	78.7	91.4	-	-	90.2	560.7	34.1
	3: 2003-05-16~05-20	48.3	*48.3	-	-	48.3	156.6	14.6
	4: 2004-12-05~12-10	35.6	35.6	-	-	35.6	139.3	13.8
	5: 2006-11-29~12-04	96.5	*96.5	-	-	96.5	427.6	24.8
	6: 2007-01-12~01-18	43.2	67.5	-	-	65.1	385.1	33.9
Elk River near Tiff City	1: 2001-02-23~02-28	71.1	68.6	73.7	-	71.5	886.3	54.3
	2: 2001-12-15~12-20	116.8	35.6	73.7	-	65.0	268.7	21.2
	3: 2002-05-17~05-20	38.1	30.5	83.8	-	59.0	937.3	44.0
	4: 2005-01-12~01-16	*61.0	17.8	61.0	-	45.3	566.3	35.7
	5: 2006-05-09~05-14	25.4	22.9	22.9	-	23.2	268.2	22.1
	6: 2007-06-11~06-16	7.6	109.2	40.6	-	61.6	136.8	11.8
Silver Creek near Sellersburg	1: 1998-05-22~05-27	63.5	68.6	-	-	67.5	117.5	30.8
	2: 2000-02-17~02-22	71.1	106.7	-	-	99.3	237.3	79.9
	3: 2002-05-12~05-16	53.3	68.6	-	-	65.4	165.1	55.0
	4: 2004-11-11~11-15	53.3	73.7	-	-	69.5	131.1	37.7
	5: 2005-03-27~03-31	50.8	*50.8	-	-	50.8	150.9	48.2
	6: 2006-10-27~10-30	40.6	50.8	-	-	48.7	85.0	21.1
Muscatatuck River near Deputy	1: 1999-01-22~01-25	50.8	53.3	27.9	50.8	50.2	390.8	55.8
	2: 2002-11-09~11-14	38.1	35.6	71.1	25.4	38.5	112.4	17.5
	3: 2004-01-03~01-07	76.2	71.1	17.8	71.1	69.7	563.5	76.7
	4: 2004-10-18~10-21	*94.0	116.8	*116.8	94.0	104.5	208.1	22.8
	5: 2005-03-27~03-31	*45.7	50.8	*50.8	45.7	48.1	351.1	42.5
	6: 2006-10-27~10-30	*33.0	40.6	*40.6	33.0	36.5	201.9	26.0

G - rain gauge for areal average precipitation (Thiessen polygon weighted); *, used nearest gauged data

Precipitation total is only considered the amount of independent event rainfall (for model simulation period) from the total storm event duration.

2.4.3.2 Baseflow Separation

The baseflows were separated to retrieve direct runoff hydrographs from total streamflow records of selected storm events. For these separation, the straight line method and the recursive digital filter method (Eckhardt, 2005) were first applied. Then after conducting several cases of model calibration with these different baseflow separation methods, the final reasonable baseflow removal method was selected on the basis of calibration results.

Equation (2.17) shows the formula of recursive digital filter which uses two parameters of the recession constant, *a* (0.980 or 0.995), and the maximum value of the baseflow index, BFI_{max} (0.80; for perennial streams with porous aquifers and 0.50; for ephemeral streams with porous aquifers). Also, for the practical uses of this recursive digital filter method, the Web based Hydrograph Analysis Tool (WHAT) system which provides an efficient tool for hydrologic model calibration and validation (Lim et al., 2005) was used.

$$b_k = \frac{(1 - BFI_{max})ab_{k-1} + (1 - a)BFI_{max}y_k}{1 - aBFI_{max}} \tag{2.17}$$

where b_k and b_{k-1} are the filtered base flow at the *k* and *k-1* time step, respectively, and BFI_{max} is the maximum value of long term ratio of base flow to total streamflow, *a* is the filter parameter, and y_k is the total streamflow at the *k* time step.

2.4.3.3 Model Evaluation Criteria

The model performance (including sensitivity analysis, calibration, and validation) was evaluated using four indicators: Nash-Sutcliffe efficiency (E_{NS}); -∞ to 1.0 (perfect fit)

(Nash and Sutcliffe, 1970), coefficient of determination (R^2); 0 (no correlation) to ±1.0 (perfect linear relationship), percent bias (*PBIAS*, %); 0 (optimal value) to ±100 (volume difference tendency against observed counterparts) (Moriasi et al., 2007), and root mean squared error (*RMSE*); 0 (perfect fit) to ∞ (only used for model sensitivity analysis) from Equation (2.18). For all cases of model simulation performance evaluation, the statistics computed for comparisons of observed and simulated streamflow are for the periods of model simulation (for direct runoff), not the total storm event duration.

$$E_{NS} = 1 - \frac{\sum_{i=1}^{n}(O_i - S_i)^2}{\sum_{i=1}^{n}(O_i - \bar{O})^2} \tag{2.18a}$$

$$R^2 = \left[\frac{\sum_{i=1}^{n}(O_i - \bar{O})(S_i - \bar{S})}{\sqrt{\sum_{i=1}^{n}(O_i - \bar{O})^2}\sqrt{\sum_{i=1}^{n}(S_i - \bar{S})^2}}\right]^2 \tag{2.18b}$$

$$PBIAS(\%) = \frac{\sum_{i=1}^{n}(O_i - S_i)}{\sum_{i=1}^{n} O_i} \times 100 \tag{2.18c}$$

$$RMSE = \sqrt{\frac{\sum_{i=1}^{n}(O_i - S_i)^2}{n}} \tag{2.18d}$$

where O_i and S_i are the observed and simulated streamflow, respectively, and $\bar{O}$ and $\bar{S}$ are the averages of observed and simulated streamflow, respectively.

2.4.3.4 Model Comparison

The Distributed-Clark model was compared against the Clark method in HEC-HMS. Distributed-Clark was run by using two rainfall inputs: the first input was spatially

distributed rainfall based on Thiessen polygons and the second was the aerial average rainfall (Thiessen polygon weighted). HEC-HMS also used aerial average of rainfall for all sub-basins to enable fair comparison. Model output from Distributed-Clark that used rainfall from each Thiessen interpolation is designated D1, whereas the output from use of areal average of rainfall is designated D2. The unit hydrographs and SCS CN values applied to each model are summarized in Table 2.6.

Table 2.6 Model input data (rainfall and CN) and unit hydrograph

Model	Distributed-Clark (D1)	Distributed-Clark (D2)	HEC-HMS
Rainfall	Spatially distributed (Thiessen polygon based)	Spatially averaged (Thiessen polygon weighted)	Spatially averaged (Thiessen polygon weighted)
SCS CN	Gridded CN for each subareas	Gridded CN for entire basin area	Sub-basin based averaged CN
Unit hydrograph	A set of separated unit hydrographs	A set of separated unit hydrographs	Sub-basin based lumped UH

Gridded CN - a histogram of CN values corresponding to subarea of interest

2.5 Results and Discussion

2.5.1 Model Development

2.5.1.1 Time-Area Diagram (Isochrones) and Separated Unit Hydrograph

The model development results of the flow travel time (cumulative travel time for each cell to the watershed outlet) map, time-area diagram (isochrones), and separated unit hydrograph for each study area are represented in Figures 2.9 and 2.10. For the given watersheds, the flow travel time map and time-area diagram were obtained from the

vertical net incoming flux, *i* (default value is 2-year, 24-hour rainfall average intensity; calibrated values for four study basins are shown in Table 2.8). In the time-area diagram (Figure 2.10), each subarea's (Thiessen polygon) incremental area contributions (one hour interval) of flow to the outlet (the temporal pattern of subarea response) can be identified. Then, several processes including linear reservoir routing (default storage coefficient, *R*, value is 2 hour), create a set of separated unit hydrographs. These derived unit hydrographs can consider spatially distributed (Thiessen polygon-based) rainfall excess for direct runoff calculation.

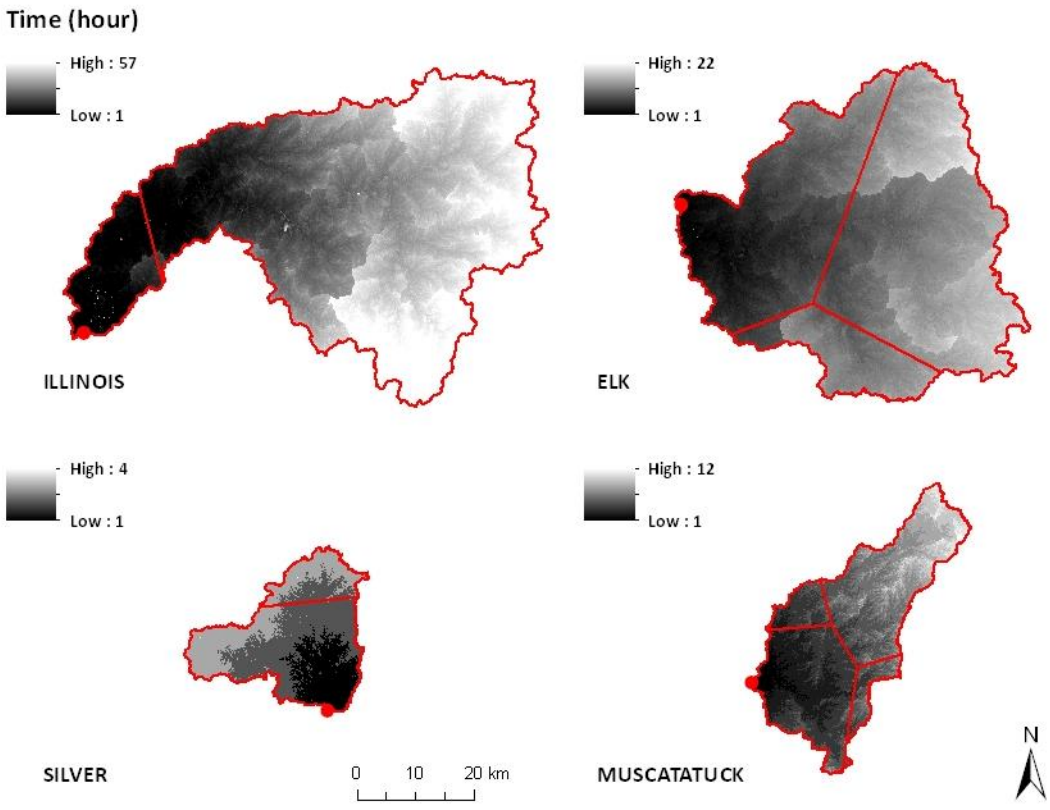

Figure 2.9 Flow travel time map (from calibrated *i*; Table 2.8) for the time-area diagram development

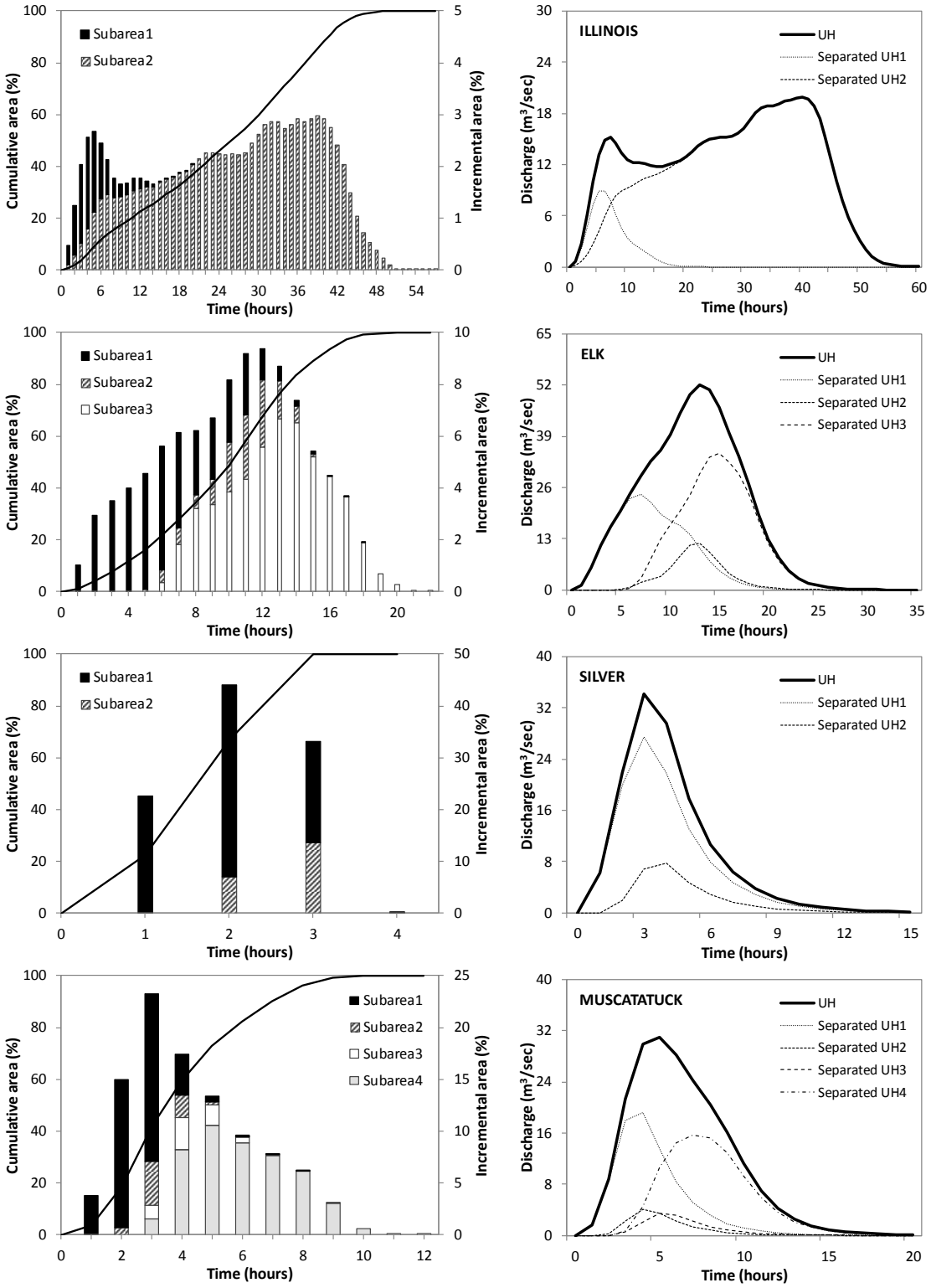

Figure 2.10 Time-area diagram (from calibrated *i*; Table 2.8, left) and separated unit hydrographs (default *R*; 2 hour, right)

2.5.1.2 Gridded CN

The gridded CN maps corresponding to each study watershed's subareas (Thiessen polygons) are shown in Figure 2.11. These gridded CN (histogram of CN values) are initially utilized for each grid cell's rainfall-runoff depth estimation, and then these estimated depths are averaged (counts weighted) with a histogram (gridded CN) of given subarea boundary (Thiessen polygon); this internal process creates the subarea's average runoff depth (spatially distributed excess rainfall).

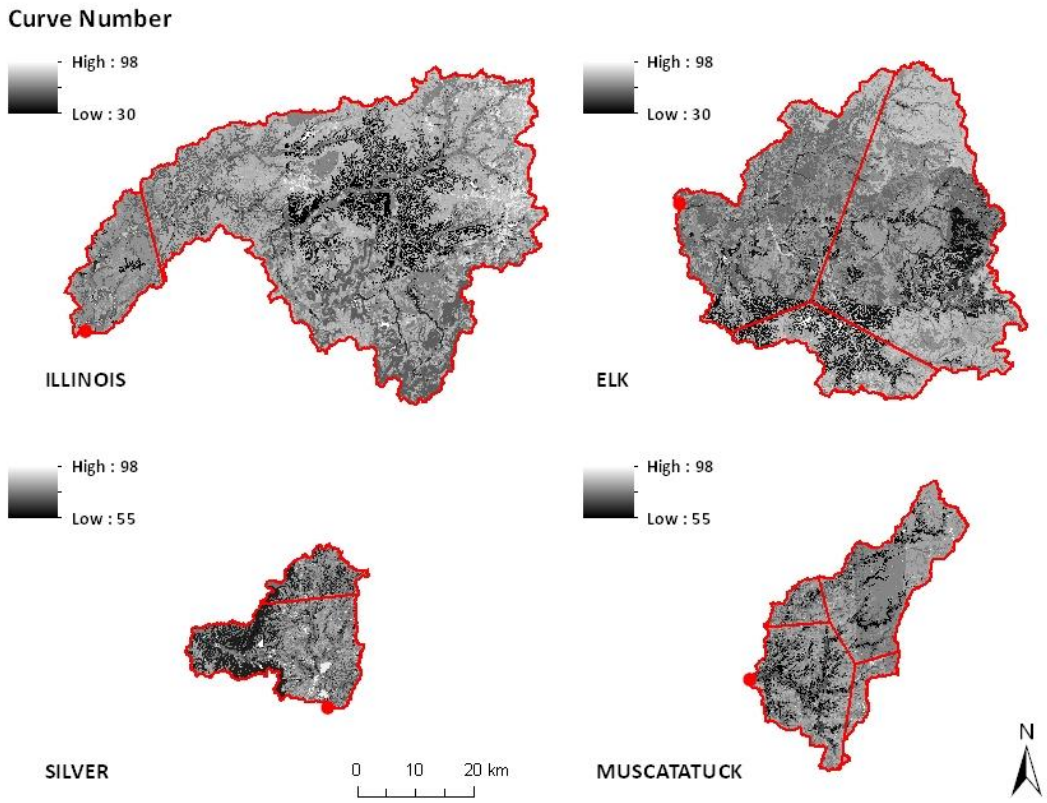

Figure 2.11 Gridded CN map for subarea's (Thiessen polygon) average runoff depth estimation

2.5.2 Model Performance

2.5.2.1 Sensitivity Analysis

Since parameter estimation and sensitivity of the model to estimated values are important to successful model application into unmonitored watersheds (Spruill et al., 2000), a model sensitivity analysis was conducted to provide insight to parameterization of Distributed-Clark. All three parameters, the vertical net incoming flux, *i*, storage coefficient, *R*, and initial abstraction coefficient, λ, were selected and varied to determine model sensitivity in direct runoff flow simulation (each parameter was varied separately). In all cases, storm event #3 for Elk River was considered as the reference input precipitation (it provided the best calibration result). The root mean squared error (*RMSE*) was used to provide variations of model sensitivity against observed flow data (direct runoff flow; baseflow separated observed streamflow) on different parameters. The derived unit hydrograph (a sum of separated unit hydrographs) is also presented to show a graphical view of the effect of parameters (*i* and *R*).

The vertical net incoming flux, *i*, whose default value is assumed as the average intensity of the given area's 2-year, 24-hour rainfall, is mainly used for the flow travel time calculation in a grid cell of a watershed. Because this factor directly affects the distributions of the time-area diagram used to develop the unit hydrograph, it was selected as one of parameters for model simulations. Six *i* values, 1.03, 2.06, 4.13, 6.19, 8.26, and 16.51 mm/hour (25 to 400% change from the default value) were considered to inspect their influence on the direct runoff hydrograph at the outlet, while other

parameters are constant with the calibrated value. As represented in Table 2.7, these changes led to significant variations in the peak flow and time to peak of the simulated direct runoff flow. The peak flow increases (up to 5.6% and 2 hours earlier) and decreases (up to -10.4% and 4 hour delay) as the vertical net incoming flux increases and decreases, respectively. Figure 2.12 shows the effect of vertical net incoming flux on unit hydrograph development (represented only four cases). Of course, their variations (peak flow, time to peak, and sensitivity) are the same as the trends of the simulated direct runoff hydrograph.

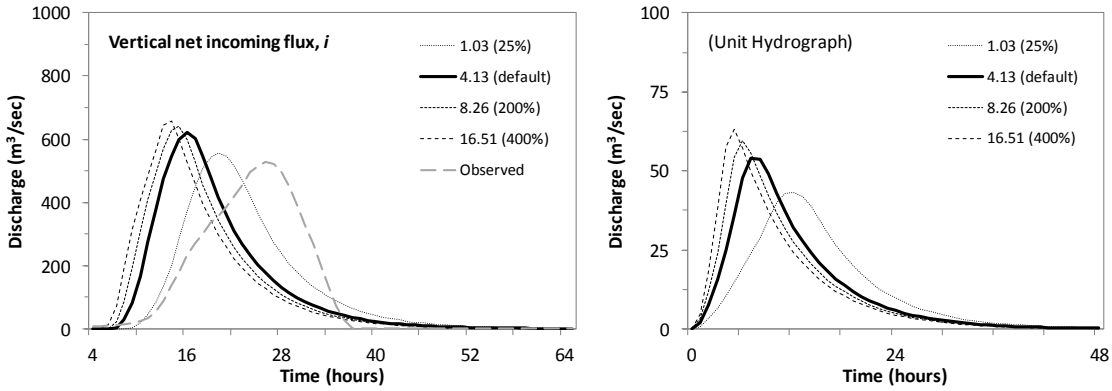

Figure 2.12 Simulated direct runoff hydrograph (left) and calculated unit hydrograph (right) showing the effect of parameter (vertical net incoming flux, *i*)

A second parameter of Distributed-Clark, the storage coefficient, *R*, is used for attenuating the unit hydrograph by routing a time-discharge histogram through a linear reservoir that has the same storage characteristics (parameterized as *R*) as the watershed. The unit hydrographs in Figure 2.13 show the possible change contributions (variations) for the overall model simulation. The simulated direct runoff hydrographs and their variation ranges corresponding to the storage coefficient values of 0.5, 1.0, 2.0, 3.0, 4.0,

and 8.0 are represented in Table 2.7 and Figure 2.13 (only four cases), respectively. In contrast with the previous cases of vertical net incoming flux, the peak flow decreases (up to -34.6%) and shifts (3 hour delay) as the value of storage coefficient increases. Also, these variances in simulated direct runoff flow' peaks (-34.6 to 7.8%) are more than that of *i* parameter (-10.4 to 5.6%), while time to peak varies (up to 3 hour shift) less than *i* parameter's results (up to 4 hour shift). This means the storage coefficient is relatively less sensitive (does not make big changes) in flow time shifting, but it is crucial to adjust the peak of hydrographs.

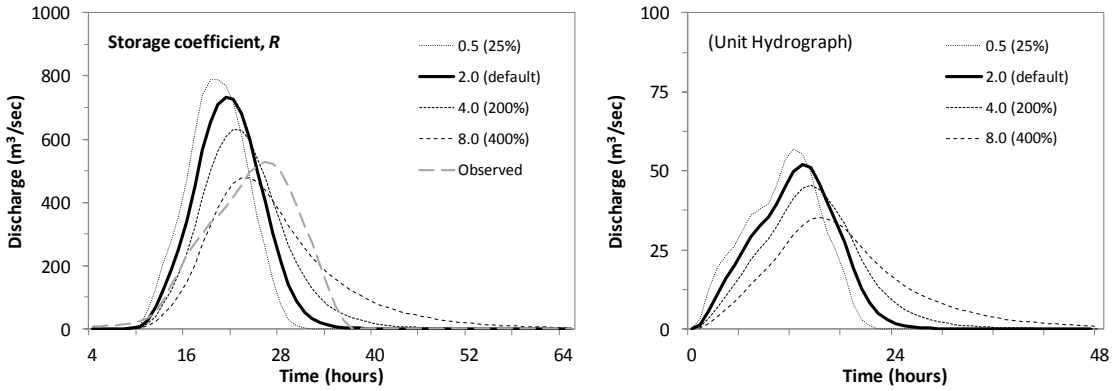

Figure 2.13 Simulated direct runoff hydrograph (left) and calculated unit hydrograph (right) showing the effect of parameter (storage coefficient, *R*)

The model sensitivity for the initial abstraction coefficient, λ, was also studied with varied values (0.05, 0.1, 0.2, 0.3, 0.4, and 0.8). Since this parameter is not related to unit hydrograph creation or the routing process but rather runoff depth (excess rainfall) estimation, it mainly makes changes to the hydrograph's magnitude; there also can be slight time shifts in peak flow. As shown in Table 2.7 and Figure 2.14, peak flow increases (up to 47.1%) and decreases (up to -79.2%) as the λ value varies. It can be

changed from 0 (no initial abstraction) to 1 (loss as the CN's potential maximum retention depth); 0.2 is the default value in the SCS CN method (USDA NRCS, 2010), but it can vary depending on watershed antecedent condition for runoff. The simulation results showing variations for different Antecedent Runoff Conditions (ARC; I dry, II average, and III wetter) are also represented in Figure 2.14.

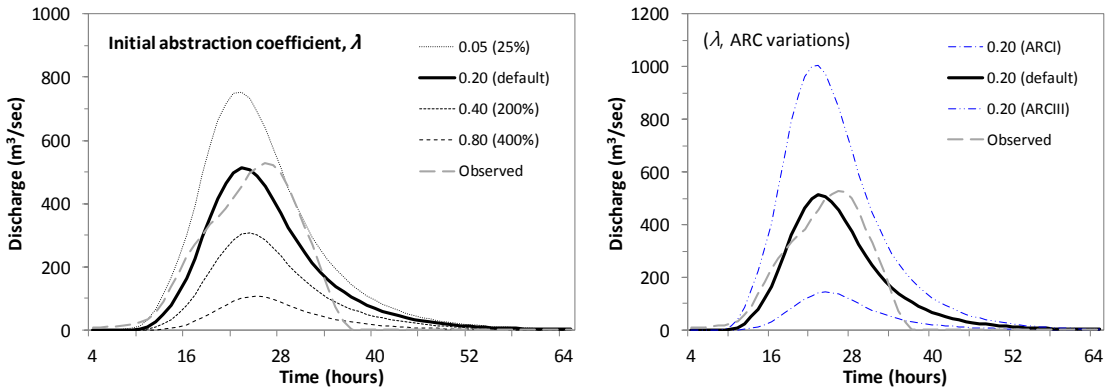

Figure 2.14 Simulated direct runoff hydrograph showing the effect of parameter (initial abstraction coefficient, λ with ARC)

In addition, Table 2.7 and Figure 2.15 present the statistics (*RMSE*) and their variations of model simulations for sensitivity analysis. These variations show similar trends as the simulation results; λ is the most sensitive. Since the *RMSE* is computed on the basis of the difference with observed data, some cases may have different variations. In this analysis, the *RMSE* variations in the λ value for change between 100 and 400% show different trends than the other results.

Table 2.7 Model sensitivity to parameter value changes in direct runoff flow simulation

Parameter			Value changes (%)					
			25	50	default (100)	150	200	400
i (mm/ hour)	Value		1.03	2.06	4.13	6.19	8.26	16.51
	Result (Variations)	Peak flow (m^3/sec, %)	556.8 (-10.4)	590.8 (-5.0)	621.7 (-)	634.9 (2.1)	642.4 (3.3)	656.2 (5.6)
		Time to peak (hour)	20 (4)	18 (2)	16 (-)	15 (-1)	15 (-1)	14 (-2)
		RMSE (m^3/sec, %)	99.5 (-44.0)	145.0 (-18.4)	177.7 (-)	192.0 (8.0)	200.3 (12.7)	215.6 (21.3)
R (hour)	Value		0.5	1.0	2.0	3.0	4.0	8.0
	Result (Variations)	Peak flow (m^3/sec, %)	789.2 (7.8)	776.1 (6.0)	732.2 (-)	683.5 (-6.7)	632.5 (-13.6)	479.0 (-34.6)
		Time to peak (hour)	19 (-1)	19 (-1)	20 (-)	21 (1)	22 (2)	23 (3)
		RMSE (m^3/sec, %)	182.7 (34.5)	168.2 (23.8)	135.9 (-)	105.3 (-22.5)	80.3 (-40.9)	55.7 (-59.0)
λ	Value		0.05	0.10	0.20	0.30	0.40	0.80
	Result (Variations)	Peak flow (m^3/sec, %)	753.5 (47.1)	661.9 (29.2)	512.3 (-)	397.2 (-22.5)	307.2 (-40.0)	106.8 (-79.2)
		Time to peak (hour)	23 (-)	23 (-)	23 (-)	24 (1)	24 (1)	25 (2)
		RMSE (m^3/sec, %)	110.3 (113.3)	77.7 (50.2)	51.7 (-)	73.1 (41.3)	103.3 (99.6)	178.5 (245.0)

Calibrated value: *i* - vertical net incoming flux 0.52; *R* - storage coefficient 7.0; λ - initial abstraction coefficient 0.200; statistics are for the period of model simulation (for direct runoff).

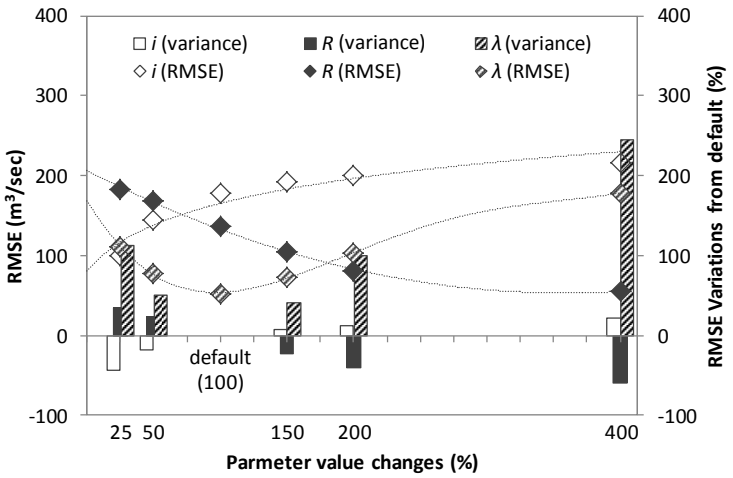

Figure 2.15 *RMSE* variations to parameter value changes in direct runoff flow simulation

2.5.2.2 Calibration and Validation

Model calibration (parameter estimation) and validation are important in hydrologic modeling, as uncertainty in model predictions can be reduced if models are properly calibrated (Engel et al., 2007). In this study, the manual model calibration and validation to find a set of reasonable parameters (*i*, *R*, and λ) which can provide good fit (both graphical and statistical) simulation results against observed data were conducted; in particular, they were made to match the total volume of flow data.

For all four study areas (watersheds), six storm events (total of 24) were applied to estimate direct runoff and streamflow hydrographs with Distributed-Clark; in the case of streamflow, the separated baseflow was added to generate simulated output. The un-calibrated model which has default parameter values (*i*, the average intensity of 2-year, 24-hour rainfall; *R*, 2 hour; λ, 0.20) was calibrated using spatially distributed rainfall data of given storm events; model validation was also performed for three out of six events (randomly selected before calibration). The estimated parameter values following calibration are shown in Table 2.8. While the estimated parameter values of *i* and *R* are the same in each watershed, the initial abstraction coefficient, λ, values differed, considering antecedent runoff conditions in watersheds for each storm event.

In addition, other cases of model calibration for spatially averaged rainfall data using Distributed-Clark and HEC-HMS were also accomplished separately to provide comparisons with spatially distributed rainfall data simulation results; these also matched the total volume of flow with observed data.

Table 2.8 Parameter values of model calibration and validation results for spatially distributed and averaged rainfall data simulations

Watershed	Storm Events (#)	Distributed-Clark									HEC-HMS (Clark transformation; Averaged)						
		Un-calibrated (default)			Distributed simulation			Averaged simulation			Transform		Loss		River channel routing		
		i	*R*	λ (ARC)	*i*	*R*	λ (ARC)	*i*	*R*	λ (ARC)	T_c	*R*	I_a	*Imp.*	*K*	*X*	*N. reaches*
Illinois River near Tahlequah	1	4.23	2.0	0.200 (II)	0.05	15.0	0.004 (III)	0.05	15.0	0.002 (III)	57.0	15.0	-	35.6	7.0	0.5	1
	2	4.23	2.0	0.200 (II)	0.05	15.0	0.247 (II)	0.05	15.0	0.246 (II)	57.0	15.0	19.5	-	7.0	0.5	1
	3	4.23	2.0	0.200 (II)	0.05	15.0	0.064 (I)	0.05	15.0	0.064 (I)	57.0	15.0	21.3	-	7.0	0.5	1
	4	4.23	2.0	0.200 (II)	0.05	15.0	0.104 (II)	0.05	15.0	0.104 (II)	57.0	15.0	6.6	-	7.0	0.5	1
	5	4.23	2.0	0.200 (II)	0.05	15.0	0.068 (I)	0.05	15.0	0.068 (I)	57.0	15.0	34.8	-	7.0	0.5	1
	6	4.23	2.0	0.200 (II)	0.05	15.0	0.271 (III)	0.05	15.0	0.267 (III)	57.0	15.0	-	11.5	7.0	0.5	1
Elk River near Tiff City	1	4.13	2.0	0.200 (II)	0.52	7.0	0.214 (II)	0.52	7.0	0.213 (II)	22.0	7.0	19.7	-	3.0	0.0	1
	2	4.13	2.0	0.200 (II)	0.52	7.0	0.189 (I)	0.52	7.0	0.123 (I)	22.0	7.0	37.2	-	3.0	0.0	1
	3	4.13	2.0	0.200 (II)	0.52	7.0	0.200 (II)	0.52	7.0	0.132 (II)	22.0	7.0	11.7	-	3.0	0.0	1
	4	4.13	2.0	0.200 (II)	0.52	7.0	0.156 (II)	0.52	7.0	0.089 (II)	22.0	7.0	7.3	-	3.0	0.0	1
	5	4.13	2.0	0.200 (II)	0.52	7.0	0.115 (III)	0.52	7.0	0.106 (III)	22.0	7.0	-	6.2	3.0	0.0	1
	6	4.13	2.0	0.200 (II)	0.52	7.0	0.245 (I)	0.52	7.0	0.153 (I)	22.0	7.0	41.8	-	3.0	0.0	1
Silver Creek near Sellersburg	1	3.28	2.0	0.200 (II)	17.5	20.0	0.325 (II)	17.5	20.0	0.356 (II)	4.0	20.0	30.6	-	1.0	0.0	1
	2	3.28	2.0	0.200 (II)	17.5	20.0	0.195 (II)	17.5	20.0	0.067 (I)	4.0	20.0	37.8	-	1.0	0.0	1
	3	3.28	2.0	0.200 (II)	17.5	20.0	0.089 (II)	17.5	20.0	0.184 (II)	4.0	20.0	16.0	-	1.0	0.0	1
	4	3.28	2.0	0.200 (II)	17.5	20.0	0.200 (II)	17.5	20.0	0.334 (II)	4.0	20.0	28.6	-	1.0	0.0	1
	5	3.28	2.0	0.200 (II)	17.5	20.0	0.066 (II)	17.5	20.0	0.066 (II)	4.0	20.0	5.0	-	1.0	0.0	1
	6	3.28	2.0	0.200 (II)	17.5	20.0	0.172 (II)	17.5	20.0	0.242 (II)	4.0	20.0	18.0	-	1.0	0.0	1
Muscatatuck River near Deputy	1	3.25	2.0	0.200 (II)	2.25	7.5	0.045 (III)	2.25	7.5	0.043 (III)	12.0	7.5	-	28.9	1.0	0.0	1
	2	3.25	2.0	0.200 (II)	2.25	7.5	0.095 (II)	2.25	7.5	0.082 (II)	12.0	7.5	6.1	-	1.0	0.0	1
	3	3.25	2.0	0.200 (II)	2.25	7.5	0.160 (III)	2.25	7.5	0.147 (III)	12.0	7.5	-	24.7	1.0	0.0	1
	4	3.25	2.0	0.200 (II)	2.25	7.5	0.281 (I)	2.25	7.5	0.278 (I)	12.0	7.5	66.8	-	1.0	0.0	1
	5	3.25	2.0	0.200 (II)	2.25	7.5	0.213 (III)	2.25	7.5	0.213 (III)	12.0	7.5	-	12.7	1.0	0.0	1
	6	3.25	2.0	0.200 (II)	2.25	7.5	0.205 (III)	2.25	7.5	0.204 (III)	12.0	7.5	-	8.2	1.0	0.0	1

i - vertical net incoming flux (mm/hour); *R* - storage coefficient (hour); λ - initial abstraction coefficient; T_c - time of concentration (hour); I_a - initial abstraction (mm); *Imp.* - impervious (%); *K* - Muskingum K (hour); *X* - Muskingum X; *N. reaches* - number of sub-reaches

T_c, time of concentration is obtained from a calibrated *i* derived time-area diagram for each watershed (HMS model adopts T_c with ratio of sub-basin area)

Whereas the λ value was only adjusted for Distributed-Clark as well (it can be different for the shape of applied unit hydrograph and its gauged rainfall), HEC-HMS that adopted the Clark transformation method (it uses same concept parameters for unit hydrograph derivation and runoff depth estimation as Distributed-Clark) required additional parameter adjustment for river channel routing since its model structure is different. Typically, HEC-HMS first computes sub-basin based unit hydrographs, then conducts river channel routing to get the watershed outlet's hydrograph. Table 2.8 also includes these calibrated values.

As shown in Table 2.8, the Illinois and Elk River models (Distributed-Clark), which are developed on relatively large watersheds, need smaller *i* values than the Silver Creek and Muscatatuck River models for creating good fit calibration results because they have more flow accumulation effects on calculating channel flow travel time; Distributed-Clark theoretically considers upstream flow area for computing channel flow grid cell's flow travel time. These can be interpreted as that even though the same amount of excess rainfall intensity (vertical net incoming flux) is adopted, the average watershed response flow (i.e., unit hydrograph) at the outlet would be different according to watershed area and its characteristics (e.g. shape, slope, etc.). Thus, the unit hydrograph used for excess rainfall convolution to develop direct runoff flow can be varied in different models with different *i* values. For instance, the Elk River model can demonstrate good performance when it uses the unit hydrograph which is derived from the input vertical net incoming flux, *i*, value of 0.52 mm/hour (calibration result); it would be linearly convoluted with different intensities of excess rainfall for a given time step though.

In addition, the process of flow attenuation using the storage coefficient, *R*, is also required to calibrate the simulation results with observed streamflow because *i* parameter is mainly used to shift the time of the simulated flow hydrograph. Hence, the estimation of reasonable *R* values for study areas were simultaneously conducted with reference to *i* values; estimated *R* values for each study area are 15.0, 7.0, 20.0, and 7.5 hours, respectively. Among the results, the Silver Creek model needed relatively long storage routing hours; however, this was required to match simulation results with noticeably delayed observed streamflow hydrographs (Figure 2.18).

Figures 2.16 to 2.19 show each model's graphical results of model calibration and validation, the estimated and observed flow hydrographs (total streamflow and direct runoff) are plotted in the same diagram to show the model's goodness-of-fit and output differences in spatially distributed and averaged rainfall simulations. In most cases, the calibrated model enables creation of similar simulation results with observed data but some cases produce gaps from observed flow, particularly in direct runoff hydrographs; uncertainty arises when estimating observed direct runoff flow, according to baseflow separation procedure chosen. Also, this may indicate the imperfection of using just one representative set of calibrated parameters to estimate direct runoff flow for various storm events, since the rainfall patterns (amount and duration; intensity) and watershed storage conditions can differ; these related the model parameter of *i* and *R* to derive unit hydrographs. Thus, if the *i* or *R* parameter is determined differently for each event or event group of similar rainfall pattern, it can produce better model performance results against observed flow hydrograph.

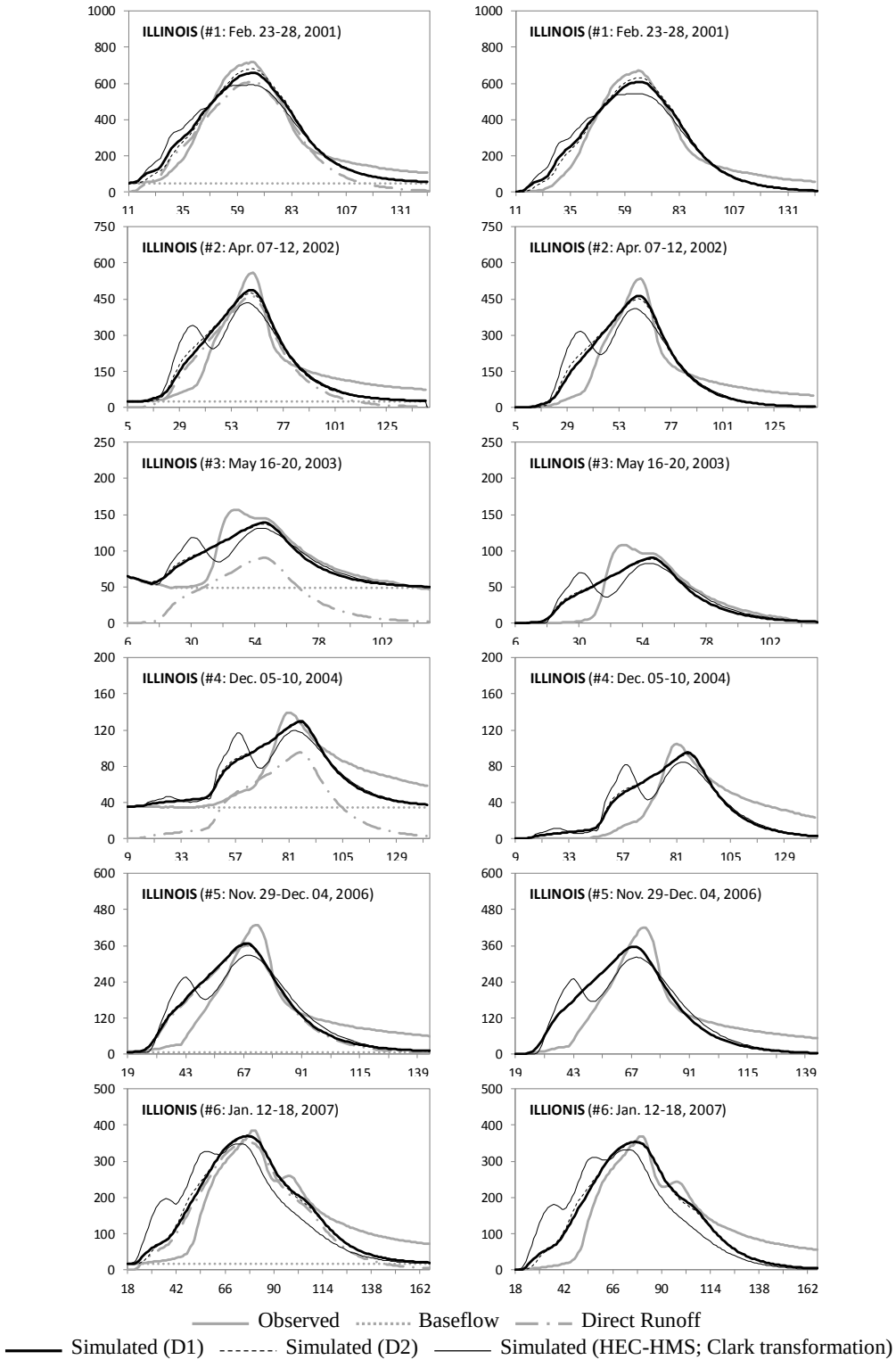

Figure 2.16 Graphical results (total streamflow; left and direct runoff; right) for model calibration and validation (Illinois River)

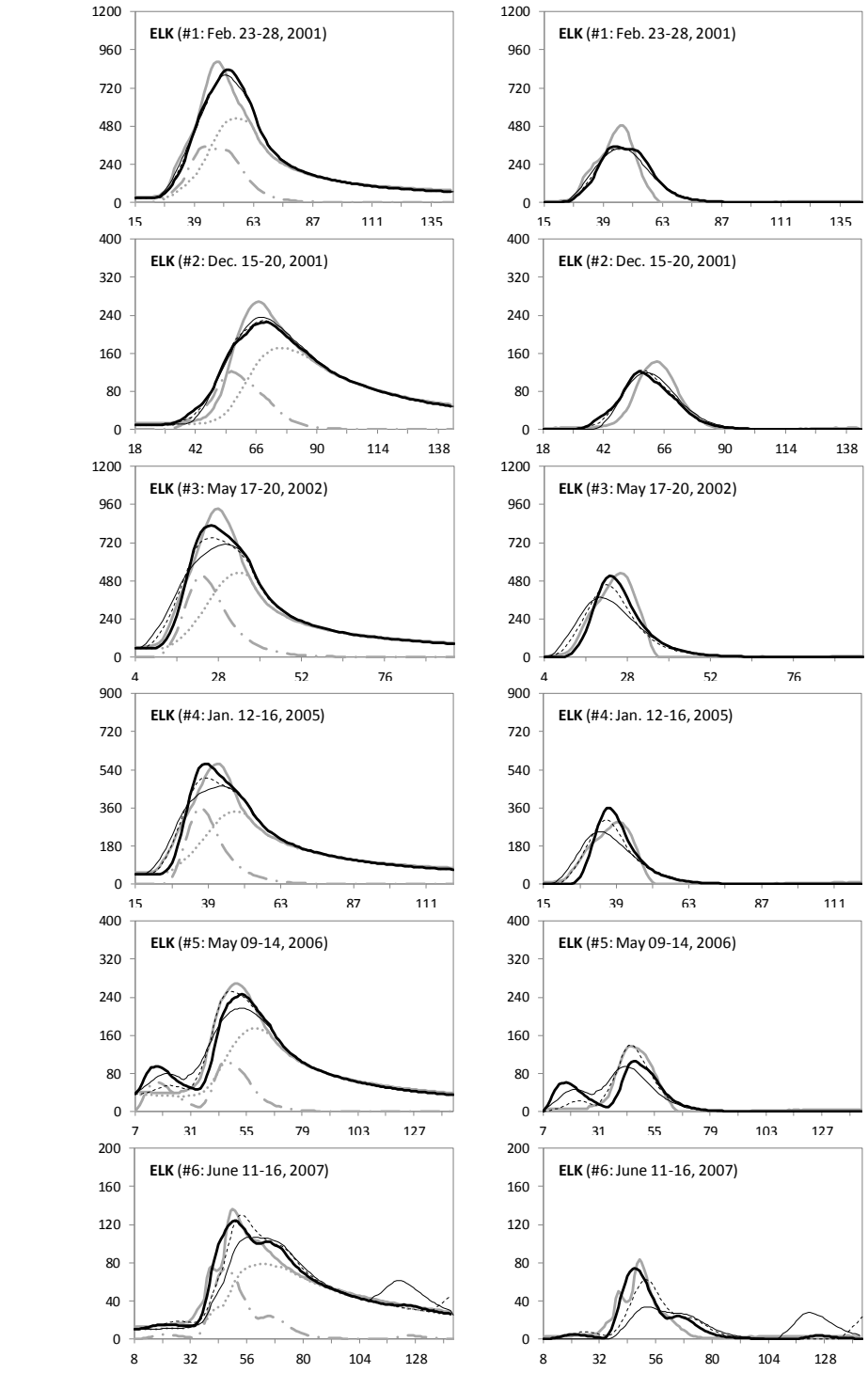

Baseflow separation: recursive digital filter method (*a* 0.995, BFI_{max} 0.80)
X-axis represents simulation time (hours) and Y-axis represents discharge (m^3/sec)

Figure 2.17 Graphical results (total streamflow; left and direct runoff; right) for model calibration and validation (Elk River)

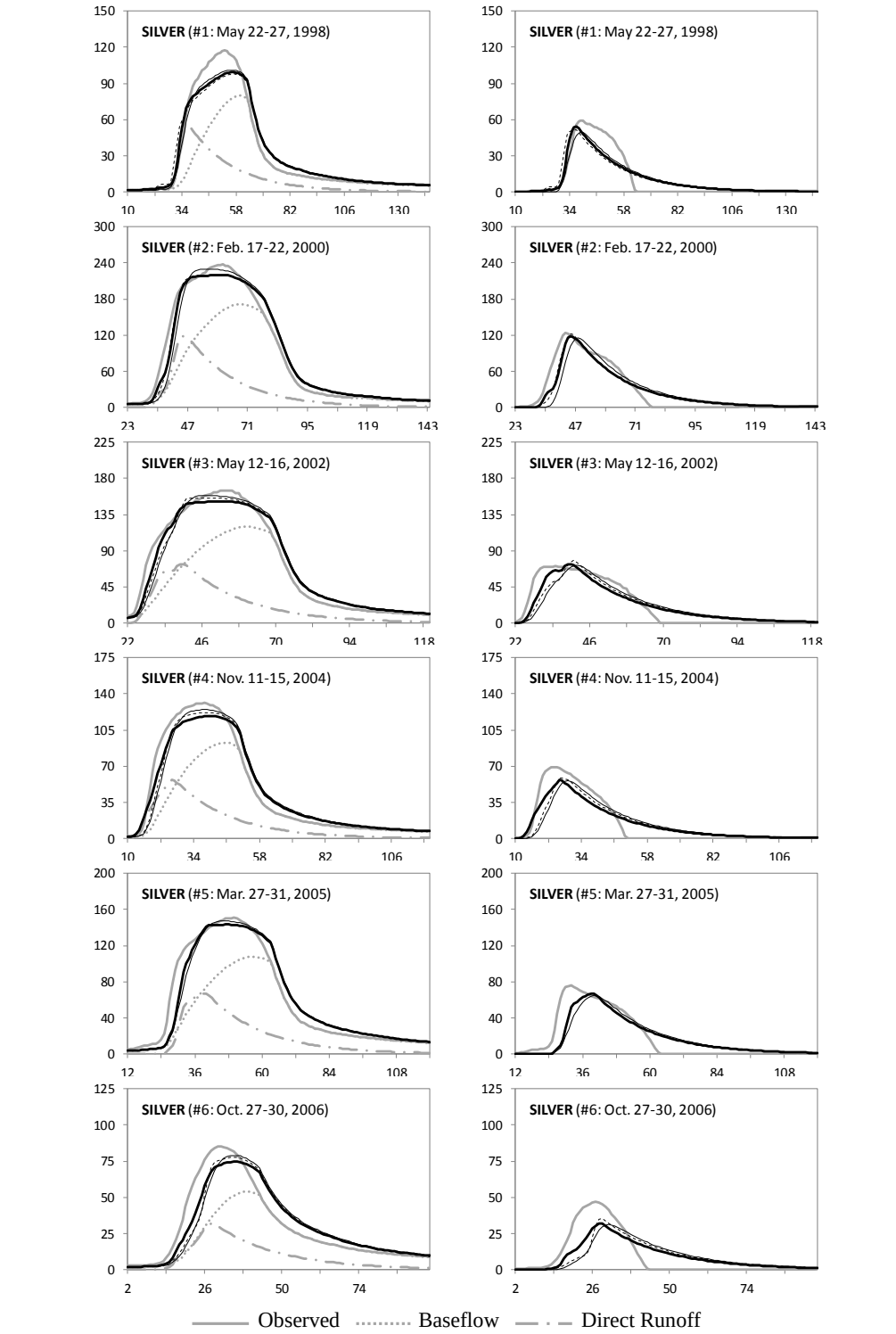

Baseflow separation: recursive digital filter method (*a* 0.980, BFI_{max} 0.80)
X-axis represents simulation time (hours) and Y-axis represents discharge (m^3/sec)

Figure 2.18 Graphical results (total streamflow; left and direct runoff; right) for model calibration and validation (Silver Creek)

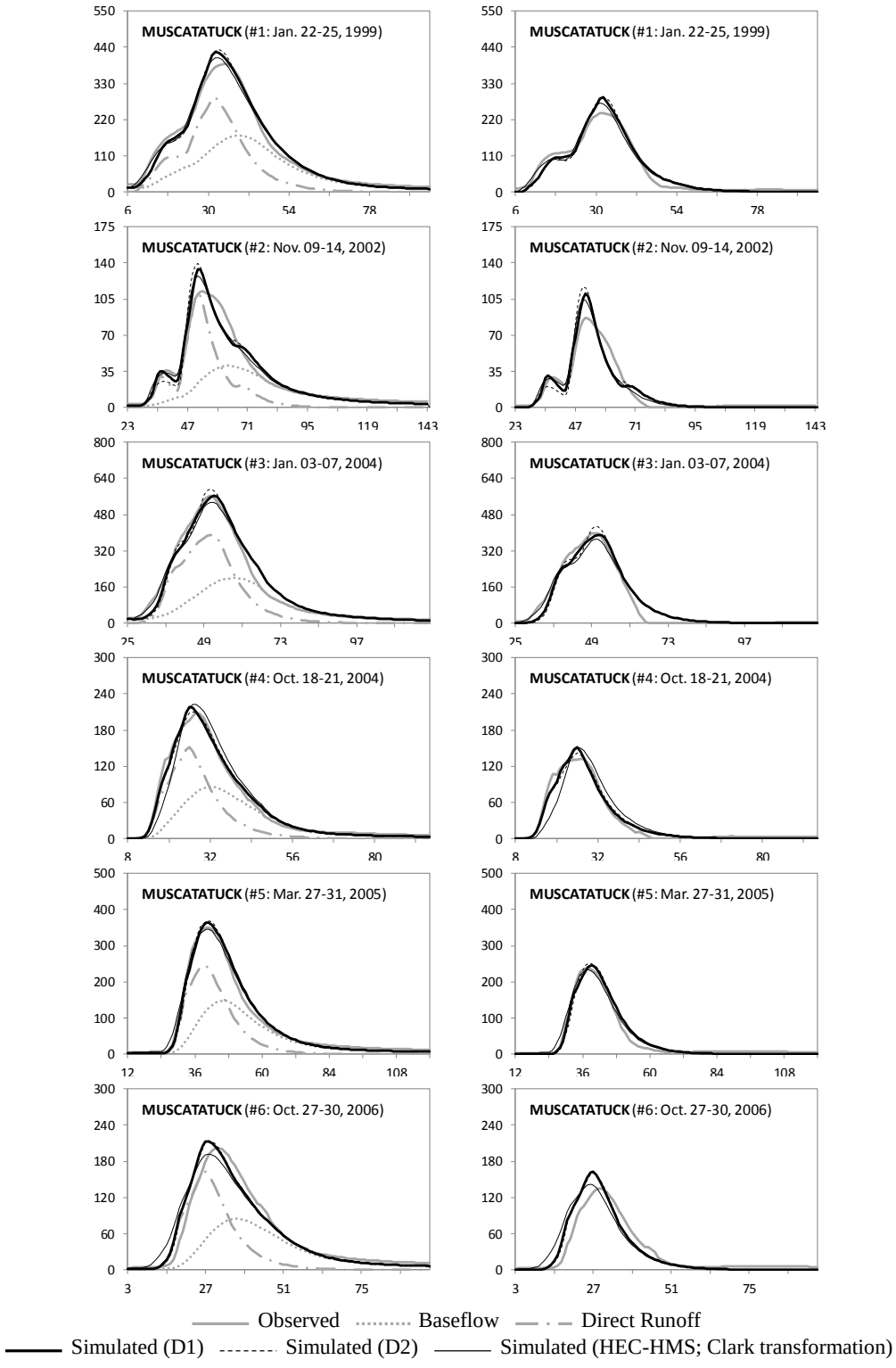

Baseflow separation: recursive digital filter method (*a* 0.980, BFI_{max} 0.50)
X-axis represents simulation time (hours) and Y-axis represents discharge (m^3/sec)

Figure 2.19 Graphical results (total streamflow; left and direct runoff; right) for model calibration and validation (Muscatatuck River)

The statistical results (average) for direct runoff and streamflow are shown in Table 2.9. The overall statistical results of model (Distributed-Clark; both spatially distributed and averaged rainfall data simulation cases) calibration and validation demonstrate relatively good model performance (direct runoff E_{NS} 0.83, R^2 0.85, and *PBIAS* 0.86%; streamflow E_{NS} 0.90, R^2 0.91, and *PBIAS* 0.33%) compared with observed data for all four study watersheds; this also outperforms HEC-HMS model results (direct runoff E_{NS} 0.73, R^2 0.75, and *PBIAS* 0.72%; streamflow E_{NS} 0.84, R^2 0.85, and *PBIAS* 0.30%).

Table 2.9 Statistical results (average) of model calibration and validation for study areas

Watershed	Model	Rainfall Data	Direct Runoff			Streamflow		
			E_{NS}	R^2	*PBIAS* (%)	E_{NS}	R^2	*PBIAS* (%)
Illinois River near Tahlequah	D1	Distributed	0.77	0.79	0.06	0.77	0.79	0.04
	D2	Averaged	0.75	0.78	0.08	0.75	0.78	0.05
	HEC-HMS	Averaged	0.56	0.61	0.18	0.56	0.60	0.15
Elk River near Tiff City	D1	Distributed	0.83	0.84	1.48	0.94	0.95	0.36
	D2	Averaged	0.85	0.86	1.49	0.95	0.95	0.36
	HEC-HMS	Averaged	0.73	0.74	1.14	0.91	0.92	0.28
Silver Creek near Sellersburg	D1	Distributed	0.81	0.84	0.49	0.95	0.95	0.15
	D2	Averaged	0.75	0.76	0.42	0.93	0.93	0.13
	HEC-HMS	Averaged	0.69	0.70	0.25	0.92	0.92	0.08
Muscatatuck River near Deputy	D1	Distributed	0.94	0.95	1.41	0.97	0.98	0.74
	D2	Averaged	0.94	0.95	1.48	0.97	0.97	0.78
	HEC-HMS	Averaged	0.92	0.93	1.30	0.96	0.96	0.69
Average	D1	Distributed	0.84	0.86	0.86	0.91	0.92	0.32
	D2	Averaged	0.82	0.84	0.87	0.90	0.91	0.33
	HEC-HMS	Averaged	0.73	0.75	0.72	0.84	0.85	0.30
	Total		0.83	0.85	0.86	0.90	0.91	0.33

D1 and D2 - Distributed-Clark; E_{NS} and R^2 - arithmetic mean; *PBIAS* - arithmetic mean of absolute value

Total does not include HEC-HMS results

The use of spatially distributed and averaged (lumped) rainfall data in Distributed-Clark did not make a big difference (slightly better fit in distributed rainfall data simulations for direct runoff; increases in E_{NS} of 1.8% and in R^2 of 2.1%). This is likely because the Thiessen method created only two to four polygons (few available rain gauges for hourly data) to provide spatial distributions; this is insufficient to fully evaluate model output differences in spatially distributed and averaged rainfall data simulations.

More detailed (each case) comparison results of the two simulations that are represented in Tables A 1 to A 4, however, show some differences. For instance, results of storm event #2 simulations for the Muscatatuck River watershed show inequalities in both graphical (Figure 2.19) and statistical (better fit in distributed rainfall simulation for direct runoff; E_{NS} 5.1%, R^2 2.1%, and *PBIAS* 19.8% are increased) results. More specifically, the shape of four separated unit hydrographs (Figure 2.10) and gauged rainfall amount on their dominant area enabled the model to create different outputs from the results of the average rainfall data simulation which applied a lumped unit hydrograph (or separated unit hydrographs). The dominant areas and applied rainfall amount for the separated unit hydrographs were 46.6, 39.0, 7.0, and 7.4% and 38.1, 35.6, 71.1, and 25.4 mm, respectively, while the average rainfall amount was 38.5 mm. On the other hand, the case of event #4 simulations for the Elk River show poorer fit (E_{NS} 4.9%, R^2 2.2%, and *PBIAS* 5.2% are decreased) in distributed rainfall simulation for direct runoff; the gauged precipitation values for three separated unit hydrographs are also different from the 45.3 mm of average rainfall as 61.0 (11.9%), 17.8 (36.3%), and 61.0

(51.8%) mm. However, most Distributed-Clark applications represent slightly better performance using distributed rainfall simulation for direct runoff.

As another Distributed-Clark distributed rainfall simulation performance comparison target, HEC-HMS application outputs for spatially averaged rainfall data are also presented in Figures 2.16 to 2.19 and Tables 2.8 to 2.9 (and Table A 1 to A 4). Except for the Illinois River and Elk River cases, the estimated parameters and comparison results of two models (Distributed-Clark and HEC-HMS) did not significantly differ. This is because HEC-HMS models for smaller watershed areas (Silver Creek and Muscatatuck River cases) were sufficient to simulate similar results as Distributed-Clark without river channel routing (set as input parameters value of K 1.0 hour and X 0.0), while the larger basin area models were needed to use the river routing for calibration. However, even though the larger catchment models used these parameters, it was hard to get good fit simulated hydrographs, particularly in the Illinois River since only one set of calibrated parameters were applied for all sub-basins. This study did not consider each sub-basin level's parameter estimation to maintain a simple Distributed-Clark approach. Hence, better performance also can be found in distributed rainfall data simulations (E_{NS} of 15.5% and in R^2 of 14.8% increase in direct runoff); Distributed-Clark used fewer calibration parameters but better fit results were obtained.

2.6 Summary and Conclusions

A lumped conceptual and distributed feature model (hybrid hydrologic model), Distributed-Clark, was developed. In Distributed-Clark, a simple approach using spatially decomposed GIS-based Clark's unit hydrograph (separated unit hydrograph) targets the implementation of spatially distributed rainfall-runoff flow prediction with CN technique estimated excess rainfall; spatial data processing and model execution can be performed by Python script tools that were developed in a GIS platform. The model has relatively few parameters compared with other physically-based distributed (PBD) models that also can simulate spatially distributed runoff routing. Instead, Distributed-Clark only focuses on flow simulations for a watershed outlet point rather than fully consider flow interactions between specified subareas (within the watershed).

The calibrated models for four study river watersheds using all three parameters for unit hydrograph derivation (vertical net incoming flux, i, and storage coefficient, R) and runoff depth calculation (initial abstraction coefficient, λ) show relatively good performance in single storm event simulations with spatially distributed rainfall data (direct runoff E_{NS} 0.84, R^2 0.86, and *PBIAS* 0.86%; streamflow E_{NS} 0.91, R^2 0.92, and *PBIAS* 0.32%). Thus, Distributed-Clark can be a useful technique to execute spatially distributed rainfall-runoff routing particularly for short-term storm event flow prediction.

In this study, Thiessen polygon distributed rainfall data applications which can create only a few polygons given available rainfall gages did not provide sufficient spatial distributions to fully evaluate the developed model with Distributed-Clark's averaged

rainfall simulations; slightly better statistical results (E_{NS} of 1.8% and R^2 of 2.1% increase in direct runoff) were produced for distributed rainfall simulations. Therefore, Distributed-Clark applications using more spatially distributed rainfall data (e.g. NEXRAD radar, TRMM or GPM satellite-based precipitation estimates; hourly data are also available) are needed to further investigate model performance.

In addition, to apply the developed approach for long-term (multiple discontinuous storm events) hydrologic simulations, the variable unit hydrograph (derived from different excess rainfall intensities or storage coefficients) adoption for different rainfall patterns and continuously applicable SCS CN values (time-varied soil moisture index method) should be developed since the original CN approach is only effective for event based rainfall-runoff depth estimation; the calculated direct runoff does not contain any expression for time.

On the other hand, it can be also applicable for time variant unit hydrographs which are derived from different excess rainfall intensities using the same approach of GIS-derived time-area diagram (isochrones) based unit hydrograph development, so they can be convoluted with different intensity based excess rainfall; but it would be effective only for averaged (lumped) rainfall case simulation. This approach may create better fit simulated direct runoff hydrograph with observed data.

CHAPTER 3. NEXRAD DATA (RADAR-BASED MULTI-SENSOR PRECIPITATION ESTIMATES) APPLICATION TO RUNOFF ROUTING USING DISTRIBUTED-CLARK

3.1 Abstract

The applicability of NEXRAD data (radar-based multi-sensor precipitation estimates; MPEs) in a hydrologic model for runoff generation and routing were explored. A GIS-based tool was first developed for automation of NEXRAD data processing to generate spatiotemporally varied rainfall inputs for hydrological modeling. It includes three steps: map projection transformation, modeling extent and NEXRAD grid subsetting, and raster and time-series data generation. Distributed-Clark, a lumped conceptual and distributed feature model (hybrid hydrologic model) which adopts a relatively simple approach with few parameters compared to physically-based distributed (PBD) models, was introduced for use with NEXRAD data to simulate runoff flow. Case studies for single storm event application for four river basins were conducted including NEXRAD rainfall product validation against available rain gauge observations and performance evaluation with model simulation result comparisons for inputs of spatially distributed radar-based rainfall and spatially averaged gauged data. Results show significant differences in radar-based and gauged rainfall amounts (NEXRAD data are 7.6 and 11.3% overestimated and 2.2 and 15.1% underestimated in the four study watersheds) along with spatial variability. These differences affect model performance in hydrologic simulations. Flow predictions

using NEXRAD data demonstrate relatively good fit (direct runoff E_{NS} 0.85, R^2 0.89, and *PBIAS* 3.92%; streamflow E_{NS} 0.91, R^2 0.93, and *PBIAS* 1.87%) against observed flow as well as better fit (E_{NS} of 3.0% and R^2 of 6.0% increase in direct runoff) than spatially averaged rainfall data for the same model calibration approach, enabling improved prediction of flow volumes and peak rates which can be discounted in hydrologic simulations for spatially averaged rainfall.

3.2 Introduction

Precipitation is one of the primary inputs for hydrological modeling and related fields of work, especially by the National Weather Service (NWS), as it is used by meteorological forecasters for the issuance of flash flood forecasts and is crucial to the hydrologic forecaster preparing main stem river forecasts (Shedd and Smith, 1991). As a grand effort to improve precipitation estimation procedures, the NWS deployed a nationwide network of Weather Surveillance Rader-1988 Doppler (WSR-88D) radars (over 160) under the Next-Generation Weather Radar (NEXRAD) program. The first radars were installed in 1991 and the last ones in 1997 (Hudlow and Smith, 1989; Crum and Alberty, 1993; Fulton et al., 1998). The reflectivity data which is collected by WSR-88D radar is used to generate a number of value-added products. Among them, precipitation estimates are produced for various time periods by the Precipitation Processing System (PPS) that is one of the radar product generators (Shedd and Fulton, 1993). These radar-based rainfall data targets used at the modernization of NWS's river and flood program (Fread et al., 1995), particularly as valuable data in areas where localized storms completely miss rain

gauges, and operational guidance in hydrologic forecasts and warnings (Reed and Maidment, 1999; Young et al., 2000).

Fulton et al. (1998) described the real-time processing steps (three Stages) of the algorithm of PPS that produces rainfall products, including multi-sensor precipitation estimates (Seo, 1998) that are combined with gauge data. In the processing, Stage I generates Hourly Digital Precipitation (HDP, now labeled Digital Precipitation Array; DPA) accumulations from WSR-88D radar reflectivity data, performing quality control with only limited amount of rain gauge data incorporation. Stage II uses additional rain gauge data as well as satellite data to produce individual multi-sensor precipitation estimates, and the NWS River Forecast Centers (RFCs) makes Stage III products (regional multi-sensor precipitation estimates; MPEs) which are mosaicked from Stage II data in a RFC area of responsibility (Shedd and Fulton, 1993). In addition, in late 2001 the NWS's National Centers for Environmental Prediction (NCEP) began to routinely generate "NCEP Stage IV", mosaicked from the 12 RFCs regional multi-sensor data covering the entire Continental United States (CONUS) (Lin and Mitchell, 2005).

As graphical products, rainfall estimates from WSR-88D radar are first recorded on a 2 km rectilinear grid (geographic coordinate system) with 16 data levels, then all Stage products are defined on the Hydrologic Rainfall Analysis Project (HRAP) grid (projected coordinate system) that is a rectangular grid of approximately 4 km by 4 km and defined in a polar stereographic map projection using a spherical earth datum (Reed and Maidment, 1995, 1999).

NEXRAD multi-sensor precipitation products have been used by scientists and engineers for various purposes, including GIS-based hydrological modeling due to their spatial variability features. However, to be used in conjunction with other geospatial products, the HRAP grid based data have to be translated into other coordinate systems. As a practical attempt, in 1995 the U.S. Army Corps of Engineers (USACE) Hydrologic Engineering Center (HEC) proposed the use of a Standard Hydrologic Grid (SHG) whose map system is the Albers equal-area projection; a series of utility programs were also developed (e.g. HEC-DSSVue, HEC-GridUtil, etc.) (USACE, 2009, 2011, 2013), but are only applicable in HEC software. Nelson et al. (2003) developed a data browser in a GIS platform instead as a processing tool for radar rainfall data, using a cylindrical equidistant project as a map projection. Similarly, Xie et al. (2005) introduced automated NEXRAD Stage III precipitation data processing approaches for GIS-based data integration and visualization with the Universal Transverse Mercator (UTM) coordinate system. On the other hand, Hardegree et al. (2008) modified NWS source code to produce decoding and geo-referencing tools for backward coordinate transformations of non-HRAP grid based gauge rainfall data into the HRAP grid. Zhang and Srinivasan (2010) also developed GIS software for NEXRAD data processing, taking into account NEXRAD data's validation and calibration using rain gauge data, and its processing automation for hydrologic and ecological model applications.

Returning back to the issue of NEXRAD applications to GIS-based hydrologic modeling, there have also been considerable works whose programs can be termed distributed watershed models (Garbrecht et al., 2001; Ogden et al., 2001). The proliferation of GIS

data sets and ever-increasing capabilities of computer systems have continued to push distributed modeling (Smith et al., 2004). Johnson and Dallmann (1987) and Johnson (1989) are possibly the starters for radar-rainfall data application to hydrological modeling. They developed a digital map-based hydrologic modeling system, called MAPHYD, which pursued the use of time-area relations integrated with high-resolution radar sensing of rainfall and applied it to urban watersheds. CASC2D, a two-dimensional physically-based distributed parameter hydrologic model, also used radar rainfall for runoff model sensitivity to radar precipitation data resolution issues (Ogden and Julien, 1994) and hydrologic analyses of flash floods which are caused by intense thunderstorms moving across partial areas of a watershed (Julien et al., 1995; Ogden et al., 2000). ModClark (Modified Clark method) in HEC-HMS, which is an adapted Clark's (1945) conceptual runoff model; it employs translation and linear storage process with the SCS time of concentration method, used radar rainfall estimates as well for pilot applications of runoff forecasting, implementing its data on the SHG plane (USACE, 1996a, 1996b, 1996c). Neary et al. (2004) and Paudel et al (2009) also applied it to examine improvement of HEC-HMS predictions for rainfall spatial variability. In addition, the GSSHA (Gridded Surface Subsurface Hydrologic Analysis) model (Ogden et al., 2003) that is a physically-based, distributed-parameter, structured grid, hydrologic model and a significant reformulation and enhancement of CASC2D, utilized NEXRAD products for their case studies of an extreme flood simulation (Sharif et al., 2010) and comparison of the model results with gauge and satellite precipitation data (Chintalapudi et al., 2012).

The NWS formulated and initiated the Distributed Model Inter-comparison Project (DMIP) to improve river and flash flood forecasting with distributed models which utilized information from high resolution radar rainfall estimates and GIS data sets (Reed et al., 2004; Smith et al., 2012). In this project, the NWS provided required data for hydrologic modeling, including the use of NEXRAD radar-based rainfall estimates; 12 (DMIP Phase 1) and 16 (DMIP Phase 2) continuous models followed it and showed the model performance against radar-based precipitation data applications. Representative models are as follows:

- HL-RMS (Hydrology Laboratory Research Modeling System; NWS's operational hydrologic model) which employs SAC-SMA (Sacramento Soil Moisture Accounting Model) water balance model (lumped) and the kinematic wave for hill-slope-channel routing; it is a physically-based conceptual model (Koren et al., 2004).

- SWAT (Soil and Water Assessment Tool) that adopts various soil moisture accounting models and channel routing techniques; it is a conceptual semi-distributed model (Luzio et al., 2004; Arnold and Fohrer, 2005).

- HRCDHM (Hydrologic Research Center Distributed Hydrologic Model) whose method is similar to HL-RMS; it is a catchment-based distributed model (Carpenter et al, 2001, 2004).

- tRIBS (TIN-based Real-time Integrated Basin Simulator) that simulates the soil-moisture profile with topographically driven, lateral, element to element interaction as well as kinematic wave routing; it is a physically-based fully-distributed model (Ivanov et al, 2004).

- TOPNET which uses the physically based variable contributing area for the soil moisture deficit calculation with kinematic wave routing; it is a distributed version of TOPMODEL (semi-distributed model) (Beven and Kirkby, 1979; Bandaragoda et al., 2004).

- HSPF (Hydrologic Simulation Program-Fortran) that uses soil moisture storage concepts and Muskingum channel routing; it is a conceptual semi-distributed model (Ryu, 2009).

In the case of HL-RMS, it evolved into HL-RDHM (Hydrology Laboratory Research Distributed Hydrologic Model) with modifications of the gridded SAC-SMA component (e.g. soil moisture temperature, snow, etc.). SWAT was also further applied using NEXRAD rainfall products to demonstrate the potential of the SWAT model for application in flood analysis and prediction (Jayakrishnan et al., 2005), and to estimate streamflow in a watershed containing no rain gauges (Sexton et al., 2010). In general, all models above performed well using NEXRAD data (radar-based rainfall estimates); their performance is not perfect but is acceptable in engineering hydrology. In the particular cases of DMIP, the lumped model (distributed model features) outperformed distributed models in more cases (Reed et al., 2004); but it was not possible to determine which model has better overall performance.

The question is often raised about the effect of radar-rainfall estimation errors and how good the estimates are (Krajewski and Smith, 2002) for NEXRAD products in hydrologic applications. Recently, several comparisons for radar and gauge rainfall data found some overestimation of results in Stage III data; Jayakrishnan et al. (2004) identified overestimation trends during 1998-1999 over the Texas-Gulf basin, Xie et al. (2006) reported overestimated (up to 28.2%) or underestimated of rainfall values (up to 11.9%) over central New Mexico from 1995-2001, Wang et al. (2008) found overestimated values (20%) in 2001 in the Hill Country of central Texas, and Hardegree et al. (2008) also looked at values during 2002-2004 in southwestern Idaho that were overestimated (20-40%). However, these results differ from underestimation trends of early reports for central and eastern U.S. study sites (Smith et al., 1996; Klazura et al., 1999; Johnson et

al., 1999). These differences might be rooted in improvements of precipitation processing algorithms (Seo et al., 1999; Steiner et al., 1999; Fulton et al., 2003; Istok et al., 2003; etc.), but it is certain that the efforts to enhance the quality of NEXRAD products are still underway. For this reason, the practical application of radar-rainfall estimates should include validation against available rain gauge observations (Garbrecht et al., 2001) and necessary correction (e.g. Zhang and Srinivasan, 2010; Xie et al., 2011). Furthermore, Smith et al. (2012) mentioned that hydrologic modeling experiments are needed to understand the impacts of hydrologic, model structure, and parametric uncertainty on model performance. Of course a number of uncertainty analyses have been conducted for the radar-estimated rainfall based hydrologic modeling. For instance, Winchell et al. (1998), Carpenter et al. (2001, 2003), and Habib et al. (2008) investigated how the temporal (e.g. storm-to-storm) and spatial (e.g. pixel-to-pixel) variability of radar-estimated precipitation data affects runoff simulations and showed significant dependencies on both.

In this study, a GIS-based spatially distributed Clark's unit hydrograph method (Distributed-Clark) is introduced for use with NEXRAD radar-based multi-sensor precipitation estimates for runoff routing. Distributed-Clark is a lumped conceptual and distributed feature model (hybrid hydrologic model; DeVantier and Feldman, 1993) which combines the concept of Clark's (1945) unit hydrograph (time-area diagram based hydrologic runoff routing method) and its spatial decomposition methods (Maidment et al., 1996); it can consider spatially distributed rainfall as model inputs. Differing from other aforementioned physically-based distributed (PBD) watershed models, Distributed-

Clark (conceptual) has relatively few parameters (only three parameters are needed for rainfall event simulation). Also, if pre-processing is completed, it can perform rapid computations for obtaining hydrographs at watershed outlets. The objectives of this chapter are as follows: (1) to develop a GIS-based NEXRAD precipitation data processing tool, particularly Stage IV composite data, considering its map subset and projection (distortion, scale factor, etc.), (2) to apply the Distributed-Clark model to processed NEXRAD data (grid cell based spatially distributed rainfall) for runoff routing; in this process NEXRAD rainfall estimates need to be verified with gauged data, and (3) to compare and evaluate the performance of simulation results for spatially distributed radar-based rainfall and spatially averaged (lumped) gauged data.

3.3 Study Area and Data

3.3.1 Study Area

Four river basins were selected as study areas in this research: Illinois River near Tahlequah, OK; Elk River near Tiff City, MO; Silver Creek near Sellersburg, IN; and Muscatatuck River near Deputy, IN. The study areas were the same watersheds as for a previous chapter in order to continue model (Distributed-Clark) application for spatially distributed rainfall inputs from Thiessen polygon to NEXRAD based data (Figure 3.1).

3.3.2 Data

The data used in this study include: (1) 1 arc-second (spatial resolution around 30 m) Digital Elevation Model (DEM), National Land Cover Database 2011 (NLCD 2011), and National Hydrography Dataset (NHD) from USGS National Map, (2) Soil Survey

Geographic (SURRGO) Database from USDA WSS (Web Soil Survey), and (3) Precipitation Frequency (PF) estimates from NOAA HDSC (Hydro-meteorological Design Studies Center). DEM and NHD data are used for watershed delineation and stream network definition, whereas land use, PF estimates, and soil data are used to create flow travel time and runoff curve number map. The time-series (hourly) data and gauge information, precipitation (gauged rainfall) from NOAA NCDC (National Climatic Data Center) and streamflow from USGS NWIS (National Water Information System), are used to evaluate the performance of simulation results for spatially distributed radar-based rainfall and spatially averaged (lumped) gauged data.

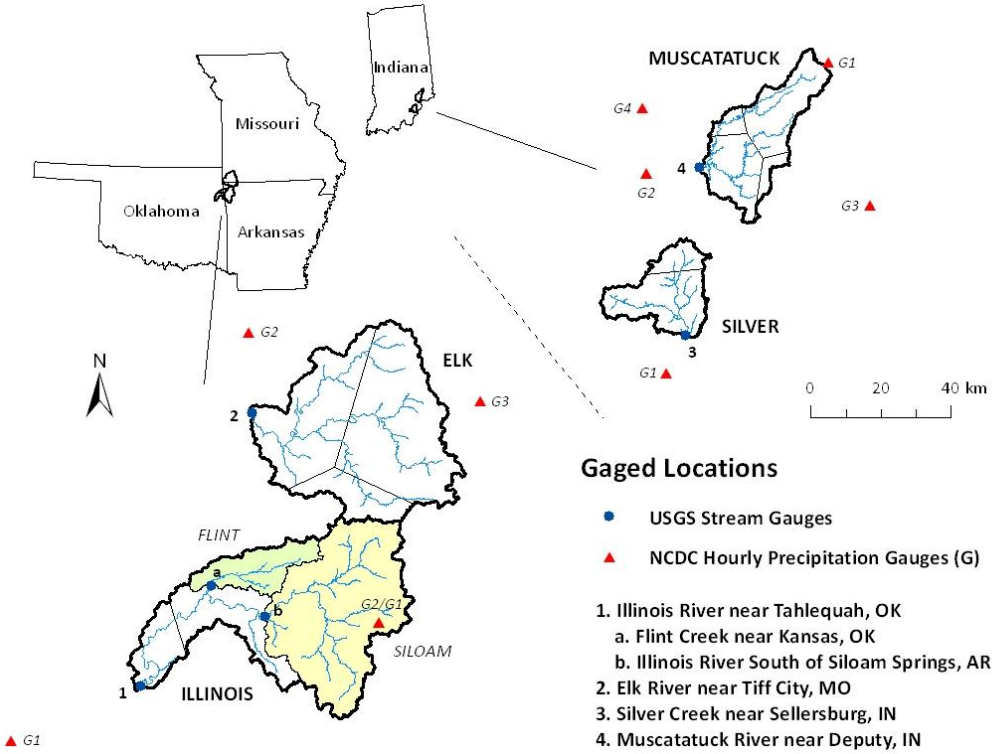

Figure 3.1 Location of study watersheds

3.3.3 NEXRAD Data

NEXRAD data, "NCEP Stage IV" products, which are mosaicked from the 12 RFCs regional hourly/6-hourly multi-sensor precipitation estimates or estimator (Stage III products or MPEs; manual quality-controlled data) in CONUS by NCEP (Lin and Mitchell, 2005), are available through the NOAA Advanced Hydrologic Prediction Service (APS) and National Center for Atmospheric Research (NCAR) web-accessible archives. In this study, the hourly NEXRAD Stage IV data (GRIB; Gridded Binary format) were used as model (Distributed-Clark) input of spatiotemporally varied radar-based rainfall with data processing to subset and generate required datasets, appropriately matching its extent with study areas. Figure 3.2 shows the locations of individual NEXRAD radar sites and their coverage (umbrella radius; 230 km) for study watersheds. All study areas are well inside at least one radar umbrella.

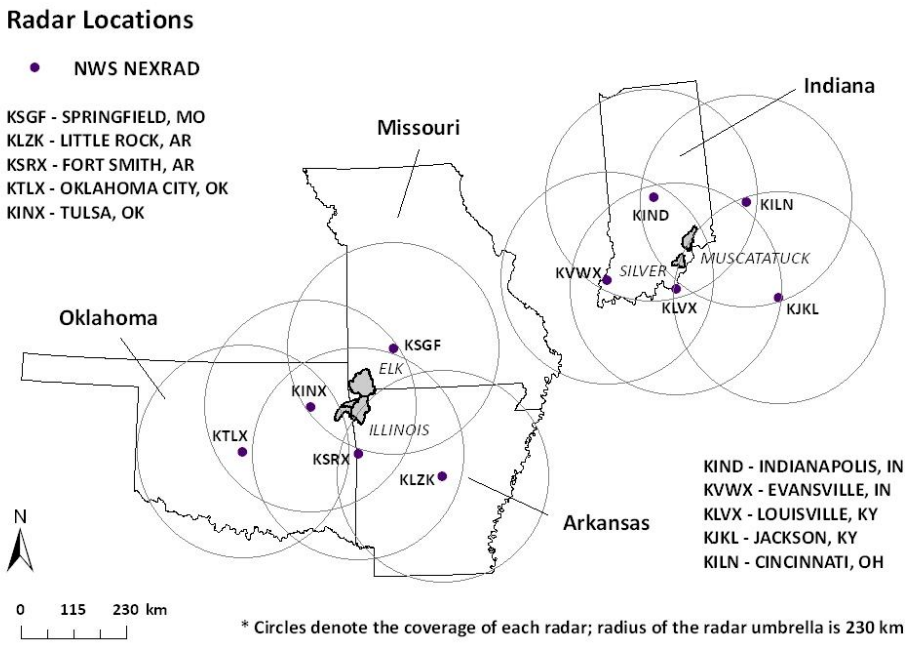

Figure 3.2 Location of NEXRAD radar sites and coverage for study area

3.4 Methodology

3.4.1 NEXRAD Data Map System (HRAP grid)

The Hydrologic Rainfall Analysis Project (HRAP) grid (projected map system) is used for precipitation estimation from the WSR-88D radars. The grid is based on a polar stereographic map plane (spherical earth datum) with a standard latitude of 60° North and standard longitude of 105° West. The mesh length at 60° North latitude is 4.7625 km (Fulton, 1998). As shown in Figure 3.3, the grid is positioned such that coordinates (401, 1601) are at the pole, resulting in all positive coordinate within the United States. Also, HRAP coordinates (hrapx, hrapy) can be written in terms of polar stereographic coordinates (with x and y in kilometers) under the assumption of fixed mesh length (4.7625 km) (Reed and Maidment, 1995, 1999).

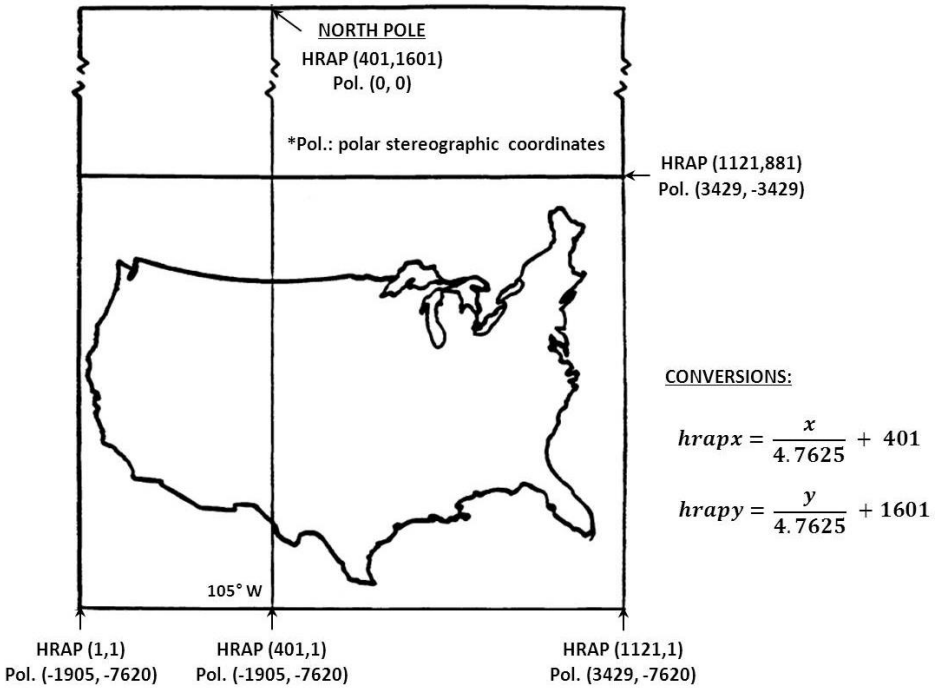

Figure 3.3 HRAP coordinate system and conversions

3.4.2 NEXRAD Data Processing

NEXRAD radar-based rainfall can be interpreted and processed in a GIS environment. In this study, a GIS-based tool was developed for automation of required NEXRAD precipitation data (particularly for Stage IV composite products) processing to generate spatiotemporally varied radar-based rainfall (model input). Figure 3.4 shows overall procedures for NEXRAD data processing using the developed GIS-based (Python script) tools; it includes three steps of map projection (coordinate system) transformation, modeling extent and NEXRAD grid subsetting, and raster and time-series data generation.

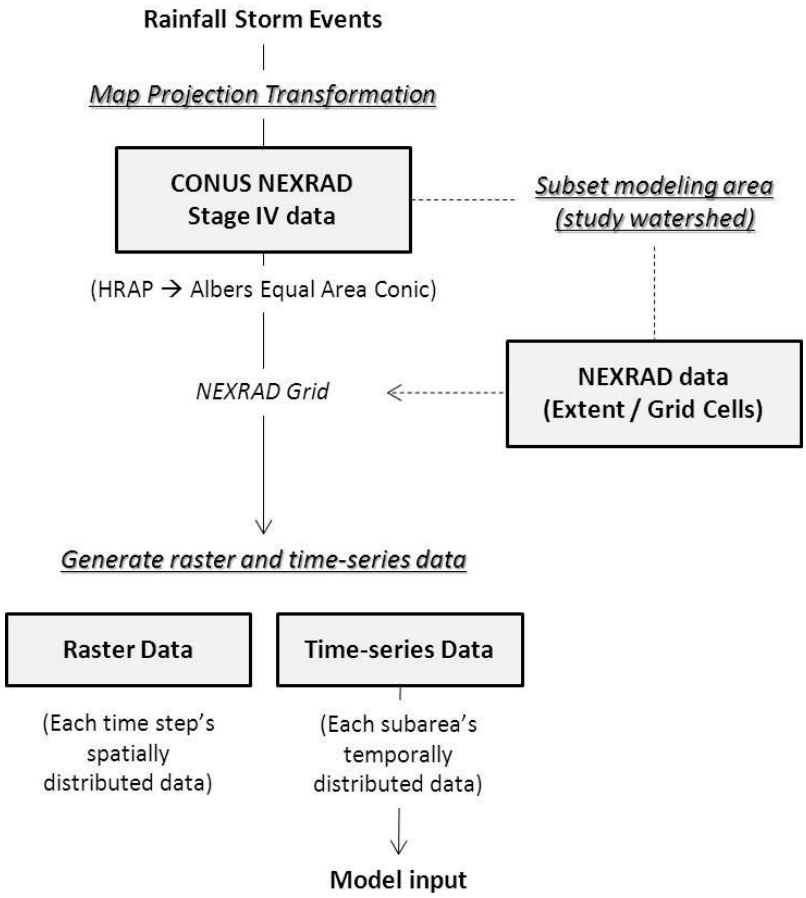

Figure 3.4 Overall procedures for NEXRAD data processing

3.4.2.1 Map Projection Transformation

Use of the HRAP grid-based NEXRAD precipitation data in hydrologic applications requires transformation of data to a regular grid, which uses an appropriate map projection system, thereby allowing integration with a watershed's geospatial data. Because the earth area that HRAP grids represent varies significantly with latitude, these grid cells are ill-suited for hydrologic modeling (Reed and Maidment, 1999). In this study, a USA Contiguous Albers Equal Area Conic USGS map system (ESRI, 2012) with the parameters listed in Table 3.1 was chosen as the standard map projection. This projection is commonly used for maps of the conterminous United States at scales of 1:2,500,000 and smaller; the scale error will be slightly less than 1 percent at the center of the US with a maximum scale error of 1.25 percent at the northern and southern borders (Snyder, 1987). The USACE HEC and NOAA APS also use these same parameters for mapping NEXRAD radar-based rainfall. An equal-area projection seems appropriate to use for hydrologic modeling, since the drainage area is preserved and the rainfall depth-volume relationships are also preserved (Reed and Maidment, 1995).

The GRIB format NEXRAD rainfall can be used as raster data without a conversion process (e.g. binary to ASCII, ASCII to raster, etc.) in a GIS platform, and thus it only needs to be changed from the HRAP to Albers Equal Area Conic map projection. However, due to the geographic map system difference between the geocentric (spherical earth datum) and geodetic (ellipsoidal datum) coordinates, it needs to be correctly registered when transforming data map projections; the "true" transformation (in Figure 3.5) is required (Reed and Maidment, 1995). Figure 3.5 shows a conceptual diagram of

procedures to transform coordinates from a sphere-based map into an ellipsoidal-based map projection; in this figure, the “matching” transformation can also be used, but an approximately 18.5 km (10') shift on the earth’s surface can be seen (Reed and Maidment, 1995). In this study, therefore, the “true” transformation was used; it may have possible errors as well in backward transformation from the HRAP to a sphere due to the assumption of fixed grid size (4.7625 km) when HRAP forward mapping (0.25 to 1.13 km mesh length differences exist in 50 to 25° North latitude) (Reed and Maidment, 1999).

Table 3.1 Parameters of map projections (HRAP, Sphere, and Albers Equal Area Conic)

Parameters	HRAP (Polar Stereographic)	Sphere	Albers Equal Area Conic
Geographic Coordinate System (GCS)			
- Datum	-	-	NAD 83
- Spheroid	Spherical (6371.2 km)	Spherical (6371.2 km)	GRS 80 (6378.137 km)
Projected Coordinate System (PCS)			
- Longitude of central meridian	105° W	-	96° W
- Latitude of the projection origin	-	-	23° N
- First standard parallel	60° N	-	29.5° N
- Second standard parallel	-	-	45.5° N
- False Easting	0.0	-	0.0
- False Northing	0.0	-	0.0

NAD 83, North American Datum of 1983; GRS 80, Geodetic Reference System of 1980 (ellipsoidal)

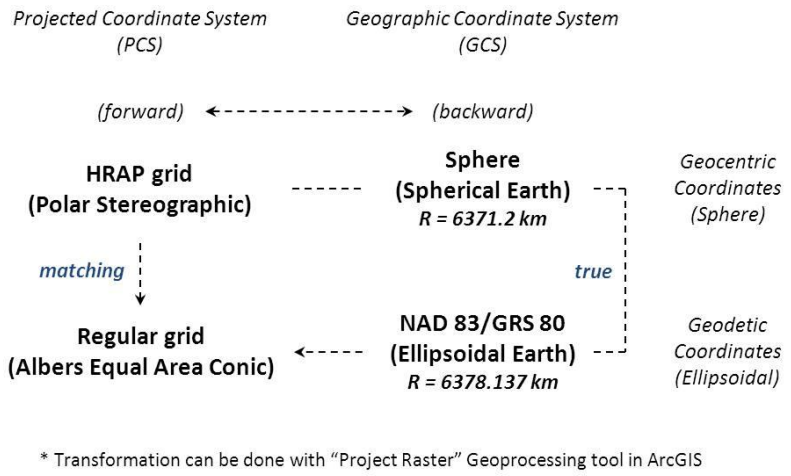

Figure 3.5 Conceptual diagram of procedures for map projection transformation (HRAP to Albers Equal Area Conic)

3.4.2.2 Modeling Extent and NEXRAD Grid

The application extent of NEXRAD radar-based precipitation data for the modeling area was specified by subsetting the study watershed area from the CONUS NEXRAD Stage IV data. Then, the NEXRAD grid which is a layer of spatially distributed rainfall was obtained. These processes also require matching the map projection system between NEXRAD data and the study watersheds; watershed layers need to be transformed into Albers Equal Area Conic for subsetting. For these GIS applications, multiple Geoprocessing tools (ESRI, 2013) that include 'Project Raster', 'Clip', 'Create Fishnet', 'Make Feature Layer', and 'Raster Calculator' are used by Python script tools.

3.4.2.3 Raster and Time-series Data Generation

For the selected rainfall storm events (CONUS NEXRAD Stage IV data; GRIB format), the model input (spatially distributed radar-based rainfall) of time-series data and other

required datasets (raster images for total storm duration and each time step) on the NEXRAD grid were generated using Python script tools which were developed in this effort and Geoprocessing tools (i.e., 'Is Null', 'Con', 'Raster to Point', 'Spatial Join', etc.) in ArcGIS (ESRI, 2013). The raster data can represent the total or each time step's spatial distribution of precipitation amounts, and the time-series data, which are directly utilized for the Distributed-Clark model input to compute spatially distributed rainfall-runoff flow, can provide each subarea's temporally distributed rainfall amounts. On the other hand, since the CONUS NEXRAD Stage IV data are produced based on the Coordinated Universal Time (UTC) zone, time difference with other observed data (gaged rainfall, streamflow, etc.) must be considered. In this study, all other observed data in the watershed used local time (e.g. EDT, EST, CDT, and CST; 4 to 6 hours later than UTC).

3.4.3 Distributed-Clark

Distributed-Clark, a GIS-based spatially distributed Clark's unit hydrograph method, adopts a runoff routing technique based on the combined concept of Clark's (1945) unit hydrograph and its spatial decomposition methods (Maidment et al., 1996); it is a lumped conceptual and distributed feature model (hybrid hydrologic model; DeVantier and Feldman, 1993). Differing from the conventional Clark's lumped unit hydrograph method, Distributed-Clark utilizes a set of separated unit hydrographs which are derived for partitioned subareas of a watershed; therefore, it can take spatially distributed rainfall (e.g. NEXRAD radar-based precipitation) for implementing hydrologic simulation (spatially distributed rainfall-runoff routing). In Distributed-Clark, the SCS curve number approach estimated spatially distributed excess rainfall and GIS-derived time-area diagram

(isochrones) based on a set of unit hydrographs (i.e., spatially distributed unit hydrograph) are utilized to calculate a direct runoff hydrograph. The Distributed-Clark model has relatively few parameters compared with other PBD models which also can simulate spatially distributed runoff routing. Instead, it only focuses on flow simulations for a watershed outlet point rather than fully considering flow interactions between specified grid cells (within the watershed).

3.4.3.1 Spatially Distributed Excess Rainfall

The SCS runoff curve number (CN) method (SCS, 1957, 1972) is utilized to estimate runoff depth (excess rainfall) from storm rainfall. For a given rainfall event, each *t* time step's cumulative excess rainfall, $P_{e,t}$, can be calculated by Equation (3.1) (Chow et al., 1988):

$$P_{e,t} = P_t - I_a - F_{a,t} \tag{3.1a}$$

$$F_{a,t} = \frac{S(P_t - I_a)}{P_t - I_a + S} \quad (P_t \geq I_a\,, \qquad \text{if not } F_{a,t} \text{ and } P_{e,t} = 0) \tag{3.1b}$$

$$S = \frac{25400}{CN} - 254 \tag{3.1c}$$

where $P_{e,t}$ and P_t are the cumulative excess rainfall and rainfall depth at the end of time *t* [L], respectively, I_a is the initial abstraction (λS, λ is the initial abstraction coefficient; 0 to 1, one of calibration parameters for overall results) [L], $F_{a,t}$ is the cumulative abstraction at the end of time *t* [L], *S* is the potential maximum retention (mm), and *CN* is the SCS curve number.

To calculate the spatially distributed rainfall excess with the SCS curve number method, a set of gridded CN (i.e., histogram of CN values corresponding to subarea of interest) for given subareas (e.g. NEXRAD grid cells) are first derived based on a CN map. Then, they are applied to each subarea's runoff depth calculation in Equation (3.1), and the resulting average rainfall excess for each subarea is generated. Figure 3.6 shows the process of spatially distributed excess rainfall estimation using graphic representations.

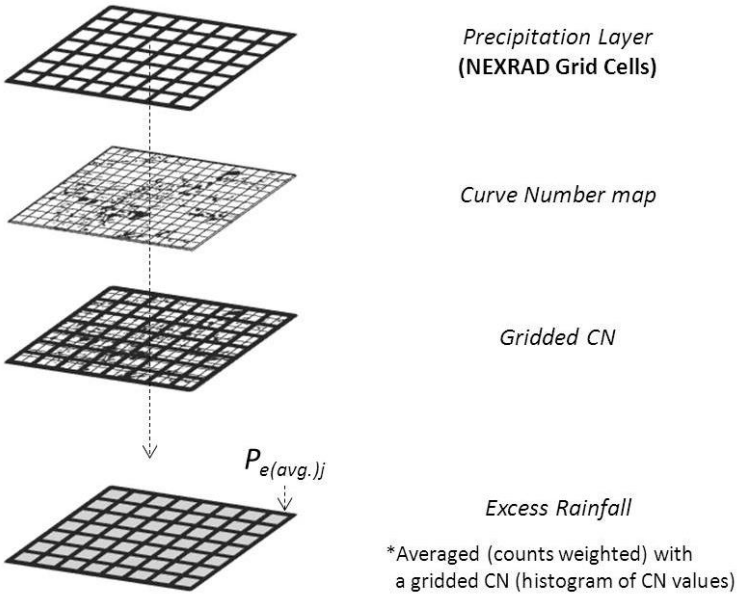

Figure 3.6 Graphical representations of the spatially distributed excess rainfall estimates

3.4.3.2 Spatially Distributed Unit Hydrograph

For the spatially distributed unit hydrograph development, a time-area diagram (isochrones, GIS-derived; in Distributed-Clark, grid cell-based flow velocity calculation using McCuen's (1995), Muzik's (1996), and Melesse and Graham's (2004) approaches are applied with some modification) and the instantaneous unit hydrograph (IUH) utilized

transformation, which includes the instantaneous unit excess rainfall applied time-area diagram translation and its linear reservoir attenuation, are required. Figure 3.7 shows a conceptual model of the Distributed-Clark approach, particularly for obtaining NEXRAD grid cell-based separated unit hydrographs. In this method, the ordinates of the separated unit hydrograph, $S_{i,j}$, can be obtained by Equation (3.2) and their summation results in the spatially distributed unit hydrograph.

$$S_{i,j} = 0.5\left[\left(\frac{\Delta t}{R + 0.5\Delta t}\right) I_{i,j} + \left(2 - \frac{\Delta t}{R + 0.5\Delta t}\right) IUH_{(i-1),j}\right] \tag{3.2}$$

where $S_{i,j}$, $I_{i,j}$, and $IUH_{i,j}$ are the jth subarea's separated unit hydrograph, translation hydrograph, instantaneous unit hydrograph at the end of ith interval [L^2T^{-1}], respectively, Δt is the computation time interval [T], and R is the storage coefficient [T].

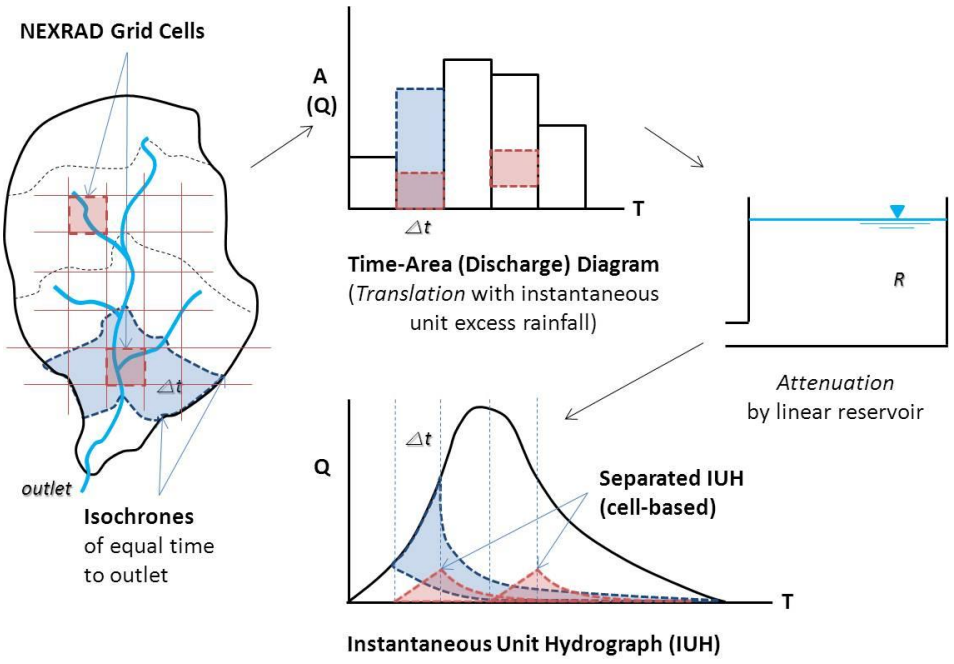

Figure 3.7 Distributed-Clark conceptual model

3.4.3.3 Direct Runoff Hydrograph

A direct runoff hydrograph is calculated by Equation (3.3) using previously developed series of spatially distributed excess rainfall and separated unit hydrographs. In this calculation, a set of distributed direct runoff hydrographs for the watershed outlet point are calculated, and the sum of all distributed direct runoff hydrographs makes a direct runoff hydrograph.

$$Q_n = \sum_{i=1}^{n} \sum_{j=1}^{J} P_{i,j} S_{n-i+1,j} \tag{3.3}$$

where Q_n is the direct runoff hydrograph at the end of nth time interval [L^3T^{-1}], $P_{i,j}$ is the average excess rainfall in the jth subarea for time interval i [L], and $S_{i,j}$ is the jth subarea's separated unit hydrograph at the end of the ith interval [L^2T^{-1}].

3.4.3.4 Model Parameters and Development

In Distributed-Clark application, all three parameters of the vertical net incoming flux, i, storage coefficient, R, and initial abstraction coefficient, λ, are used to calibrate the model simulation results; other possible but pre-fixed (during model development) factors were not parameterized. The first two parameters affect the shape of the spatially distributed unit hydrograph; they are utilized for flow travel time calculation and time-discharge diagram attenuation, respectively, and the last one was used for adjusting the amount of spatially distributed excess rainfall. Model development including watershed pre-processing (i.e., watershed and stream network definition; Manning's n and SCS CN map

creation), spatially distributed excess rainfall estimation, spatially distributed unit hydrograph derivation, and direct runoff hydrograph convolution can be implemented using Python script tools which were developed in a GIS platform. Further details of the Distributed-Clark model parameters, specific equations, and development procedures are described in a previous chapter (Chapter 2).

3.4.4 Model Performance Evaluation

3.4.4.1 Storm Event Selection

Storm events for the four study areas were selected to compare and evaluate the performance of simulation results for spatially distributed radar-based rainfall and spatially averaged (lumped) gauged data in the Distributed-Clark model. For this application of event based runoff simulations, an independent (isolated) single storm event should be considered because the SCS CN method (USDA NRCS, 2010) for runoff depth does not account for infiltration recovery during intervals of no rain.

Hence, isolated single events of NEXRAD rainfall estimates were chosen for each study area to conduct initial validation against gauged data (NEXRAD precipitation data may have both over and under estimations) and model (Distributed-Clark) calibration. In this case, due to the data (hourly) availability of the NEXRAD Stage IV precipitation products (generated from January 1997), rain gauge observations (many missing or erroneous records), and streamflow (until September 2007), a total of 24 events (six events for each watershed) from 1998 to 2007 were selected (Table 3.2).

Table 3.2 Storm events for study areas

Watershed	Storm Events (#: Periods)	Precipitation Total (mm)									Streamflow	
		NEXRAD radar-based data (spatially distributed)				Gauged data (spatially averaged; lumped)						
		Min.	Max.	Skew.	Areal average	G1	G2	G3	G4	Areal average	Peak flow (m^3/s)	Total (mm)
Illinois River near Tahlequah	1: 2001-02-23~02-28	51.1	105.2	0.24	80.4	99.1	71.1	-	-	73.8	719.3	56.4
	2: 2002-04-07~04-12	34.4	165.8	-0.46	105.5	78.7	91.4	-	-	90.2	560.7	34.1
	3: 2003-05-16~05-20	19.7	71.3	-1.02	50.9	48.3	*48.3	-	-	48.3	156.6	14.6
	4: 2004-12-05~12-10	22.2	44.5	0.14	34.1	35.6	35.6	-	-	35.6	139.3	13.8
	5: 2006-11-29~12-04	62.7	127.0	0.42	94.6	96.5	*96.5	-	-	96.5	427.6	24.8
	6: 2007-01-12~01-18	58.6	104.4	1.09	74.9	43.2	67.5	-	-	65.1	385.1	33.9
Elk River near Tiff City	1: 2001-02-23~02-28	44.3	87.8	-0.05	64.4	71.1	68.6	73.7	-	71.5	886.3	54.3
	2: 2001-12-15~12-20	42.3	76.9	-0.33	59.2	116.8	35.6	73.7	-	65.0	268.7	21.2
	3: 2002-05-17~05-20	30.9	121.8	0.31	74.9	38.1	30.5	83.8	-	59.0	937.3	44.0
	4: 2005-01-12~01-16	29.1	73.7	-0.10	51.4	*61.0	17.8	61.0	-	45.3	566.3	35.7
	5: 2006-05-09~05-14	29.3	92.7	-	58.5	25.4	22.9	22.9	-	23.2	268.2	22.1
	6: 2007-06-11~06-16	13.3	117.2	1.01	46.7	7.6	109.2	40.6	-	61.6	136.8	11.8
Silver Creek near Sellersburg	1: 1998-05-22~05-27	50.4	74.2	1.13	58.9	63.5	68.6	-	-	67.5	117.5	30.8
	2: 2000-02-17~02-22	91.3	136.1	3.25	100.1	71.1	106.7	-	-	99.3	237.3	79.9
	3: 2002-05-12~05-16	35.0	46.9	-0.10	41.9	53.3	68.6	-	-	65.4	165.1	55.0
	4: 2004-11-11~11-15	33.7	62.3	-0.07	48.0	53.3	73.7	-	-	69.5	131.1	37.7
	5: 2005-03-27~03-31	49.8	72.0	-0.02	60.1	50.8	*50.8	-	-	50.8	150.9	48.2
	6: 2006-10-27~10-30	25.8	38.2	-0.04	32.0	40.6	50.8	-	-	48.7	85.0	21.1
Muscatatuck River near Deputy	1: 1999-01-22~01-25	22.9	53.0	0.51	34.8	50.8	53.3	27.9	50.8	50.2	390.8	55.8
	2: 2002-11-09~11-14	34.8	48.0	0.27	40.7	38.1	35.6	71.1	25.4	38.5	112.4	17.5
	3: 2004-01-03~01-07	28.4	57.7	-0.26	44.5	76.2	71.1	17.8	71.1	69.7	563.5	76.7
	4: 2004-10-18~10-21	52.4	111.9	-0.76	90.9	*94.0	116.8	*116.8	94.0	104.5	208.1	22.8
	5: 2005-03-27~03-31	49.2	68.9	0.09	59.2	*45.7	50.8	*50.8	45.7	48.1	351.1	42.5
	6: 2006-10-27~10-30	22.2	45.7	-0.84	37.8	*33.0	40.6	*40.6	33.0	36.5	201.9	26.0

Skew. - skewness; G - rain gauge for areal average precipitation (Thiessen polygon weighted); * used nearest gauged data

Precipitation total is only considered the amount of independent event rainfall (for model simulation period) from the total storm event duration.

The specific method for storm event selection was primarily visual inspection of observed streamflow and the corresponding rain gauge data values. Then, to evaluate the model performance over various storm event sizes (flow ranges), different sized (relatively largest, along with moderate size) storms were selected throughout the period (1998 to 2007; given availabilities of data) and from different seasons. Since NEXRAD precipitation data can differ (over or under estimated) compared with gauged data, their corrections for matching the amount of gauged rainfall may need to be considered in some cases. In this study, however, due to insufficient gauged data (hourly) for spatial interpolation to create good reference, it was applied without correction.

For the selected storm events (streamflow records), the baseflows were separated to retrieve direct runoff hydrographs. For this separation, the same approaches used in previous chapter, the straight line method and the recursive digital filter method (Eckhardt, 2005), were applied. The final selected baseflow removal method for each study area is also the same as previous ones.

3.4.4.2 Model Evaluation Criteria

The model performance in calibration and validation phases was evaluated using three indicators: Nash-Sutcliffe efficiency (E_{NS}); -∞ to 1.0 (perfect fit) (Nash and Sutcliffe, 1970), coefficient of determination (R^2); 0 (no correlation) to ±1.0 (perfect linear relationship), and percent bias (*PBIAS*, %); 0 (optimal value) to ±100 (volume difference tendency against observed counterparts) (Moriasi et al., 2007); same as Equations (2.18a

to 2.18c) from Chapter 2. For all cases of model simulation performance evaluation, the statistics computed for comparisons of observed and simulated streamflow are for the periods of model simulation (for direct runoff), not the total storm event duration.

3.4.4.3 Model Comparison

Model simulation results for spatially distributed NEXRAD radar-based rainfall and spatially averaged gauged data were compared. To investigate model performances for NEXRAD data's spatial variability as well, model outputs from the areal average of NEXRAD precipitation are also presented. The rainfall inputs, unit hydrographs, and SCS CN values applied to each model are summarized in Table 3.3. For reference, model output from use of rainfall for each NEXRAD grid cell interpolation is designated D1, the areal average using NEXRAD grid cell is designated D1a, and the areal average of gauge observation based on the Thiessen method is designated D2.

Table 3.3 Model input data (rainfall and CN) and unit hydrograph

Model	Distributed-Clark (D1)	Distributed-Clark (D1a)	Distributed-Clark (D2)
Rainfall	Spatially distributed (NEXRAD; grid cell based)	Spatially averaged (NEXRAD; grid cell weighted)	Spatially averaged (Gauged; Thiessen polygon weighted)
SCS CN	Gridded CN for each NEXRAD grid cell	Gridded CN for entire basin area	Gridded CN for entire basin area
Unit hydrograph	A set of separated unit hydrographs	A set of separated unit hydrographs	A set of separated unit hydrographs

Gridded CN - a histogram of CN values corresponding to subarea of interest

3.5 Results and Discussion

3.5.1 NEXRAD Data

3.5.1.1 Validation

All selected storm event data, NEXRAD radar-based hourly precipitation estimates, for model application were validated against rain gauge observations. In this validation, the average value of NEXRAD rainfall estimates for each study area's extent were compared with watershed areal average rainfall from gauges (by Thiessen method) due to most available rain gauges being located outside watershed boundaries; grid cell values of NEXRAD data could not be directly compared with rain gauge point values.

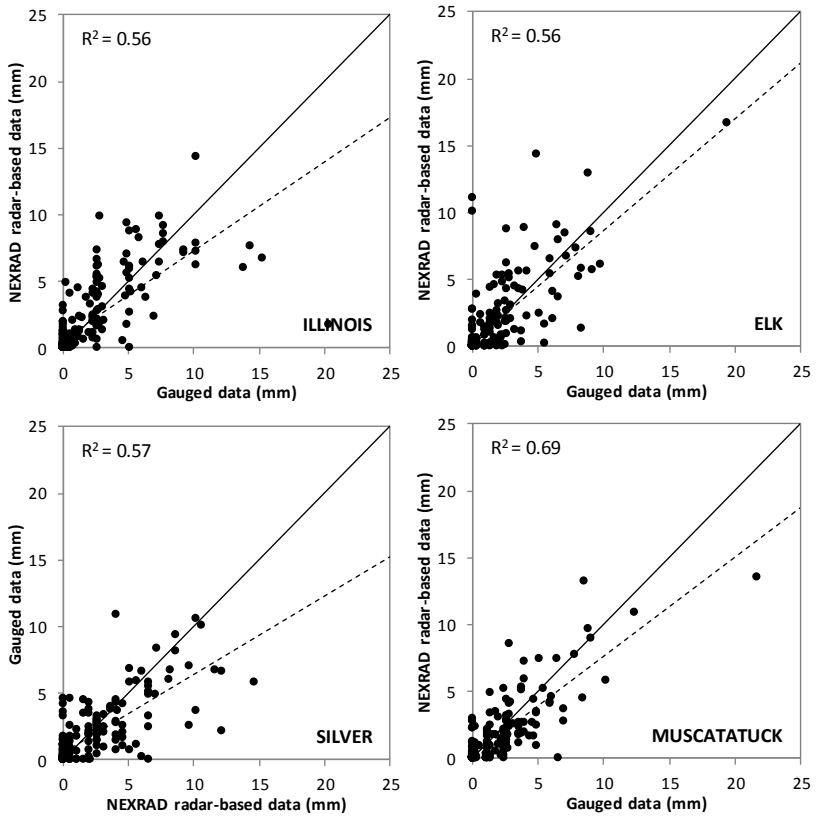

Figure 3.8 Scatter plots comparing radar-based and gauged data (areal average)

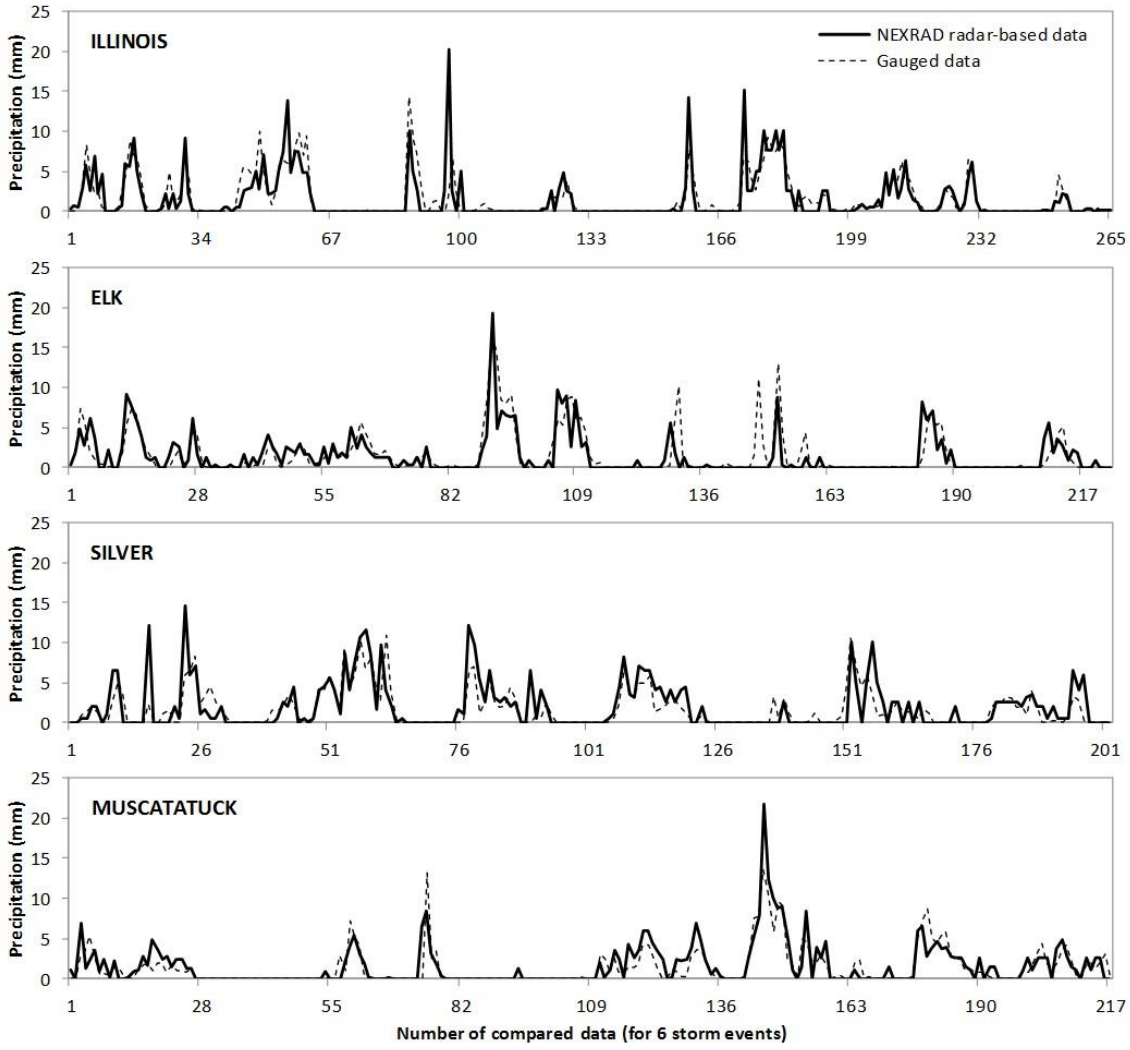

Figure 3.9 Time-series plots comparing radar-based and gauged data (areal average)

As shown in scatter plots (Figure 3.8), both rainfall estimates have significant correlations for amounts. The data for the Muscatatuck River basin show the highest correlation (R^2 0.69) in contrast to the lowest correlation for Silver Creek (R^2 0.56). Underestimation trends also can be seen for larger values of NEXRAD radar-based precipitation. The total NEXRAD rainfall amounts are overestimated by 7.6 and 11.3% in the Illinois and Elk Rivers, respectively, while underestimated by 2.2 and 15.1% in Silver

Creek and Muscatatuck River, respectively. Time-series plots showing temporal variations of these two data sets are also presented in Figure 3.9.

3.5.1.2 Spatial Variability

For each watershed's selected storm events, the spatial variability of cumulative precipitation depth was examined. Figure 3.10 to 3.12 show the 2 km by 2 km regular grid based NEXRAD precipitation data which were resampled from the original approximately 4 km by 4 km HRAP grid; they adopt the Albers Equal Area Conic map projection system.

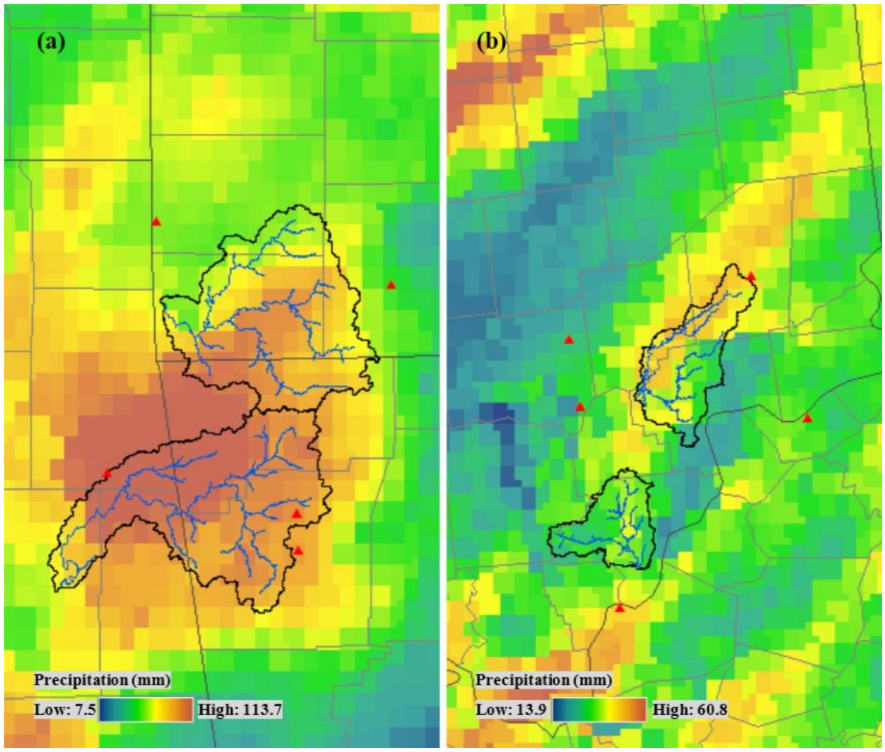

Figure 3.10 Spatial variability of cumulative precipitation depth (mm) for study areas for common storm events of (a) 23-28 Feb 2001 and (b) 27-30 Oct 2006, as obtained by NCEP Stage IV products

The significant spatial distributions can be seen with each event's gridded rainfall amounts. For instance, differences of 782% (13.3 to 117.2 mm) occurred in event #6 for the Elk River (second largest basin) with a skewness value of 1.01 (in Table 3.2), whereas only differences were 85% (33.7 to 62.3 mm, skewness -0.10) in event #3 for the Silver Creek basin. These spatially distributed rainfall data can be used as model (Distributed-Clark) inputs after excess runoff depth estimation to convolute a direct runoff flow hydrograph with a set of separated unit hydrographs.

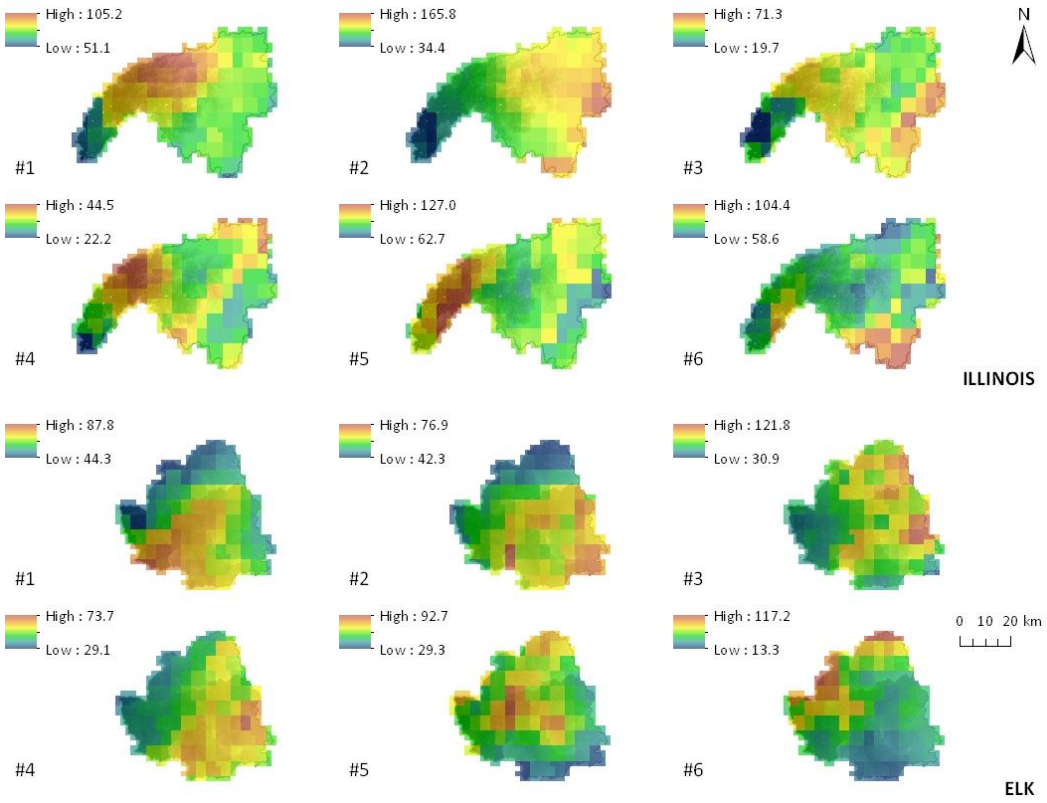

Figure 3.11 Spatially distributed NEXAD radar based precipitation (Illinois and Elk River)

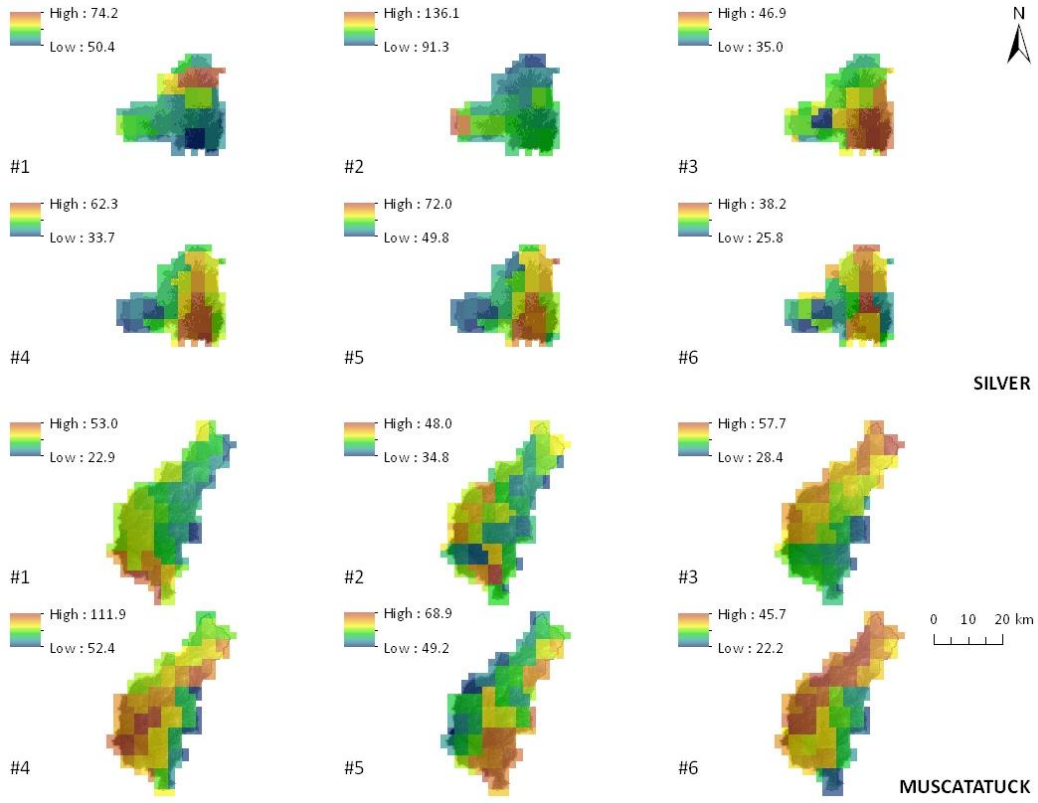

Figure 3.12 Spatially distributed NEXAD radar based precipitation (Silver Creek and Muscatatuck River)

3.5.2 Model Development

3.5.2.1 Time-Area Diagram (Isochrones) and Separated Unit Hydrograph

The model development results of the flow travel time map, time-area diagram (isochrones), and separated unit hydrographs for each study watershed are represented in Figures 3.13 and 3.14. In the time-area diagram and unit hydrograph (Figure 3.14), the selected areas' (S1 and S2; NEXRAD grid cells) results, which represent the portion of incremental area contributions (one hour interval) of flow to the outlet and separated unit hydrographs can be identified. These grid cell separated unit hydrographs can consider

NEXRAD data based on spatially distributed excess rainfall, which are estimated using the SCS curve number approach (gridded CN), to obtain a watershed outlet's direct runoff flow hydrograph.

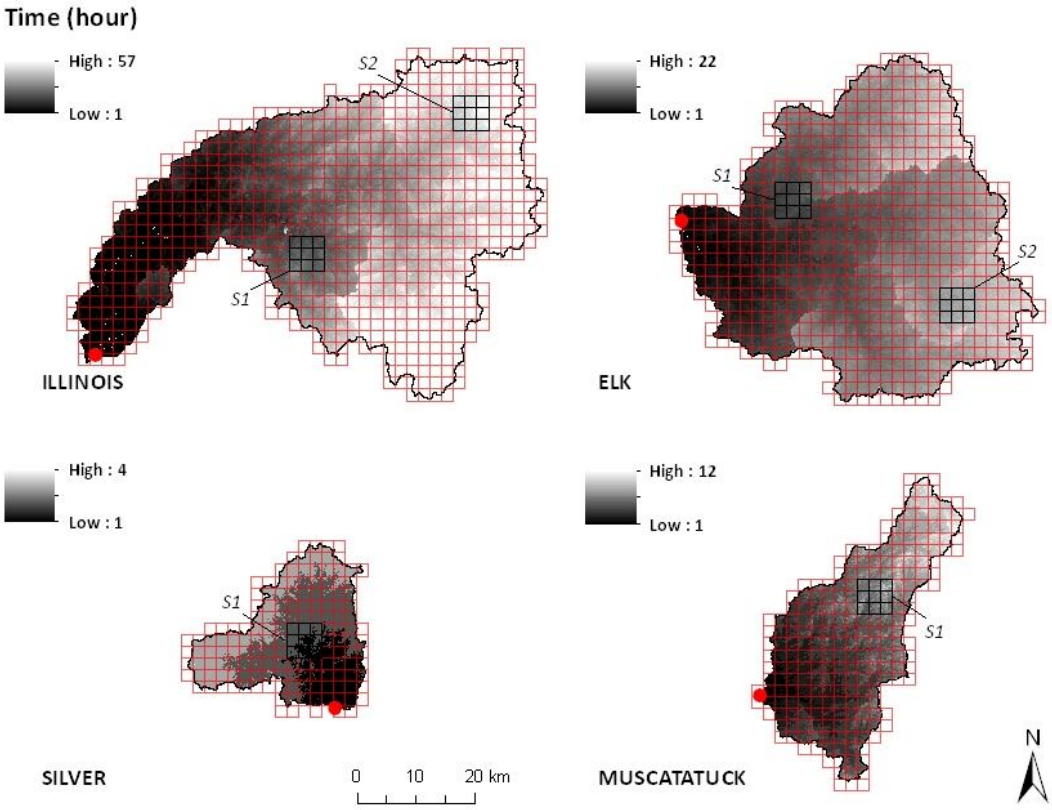

Figure 3.13 Flow travel time map (from calibrated *i*; Table 3.4) for the time-area diagram development

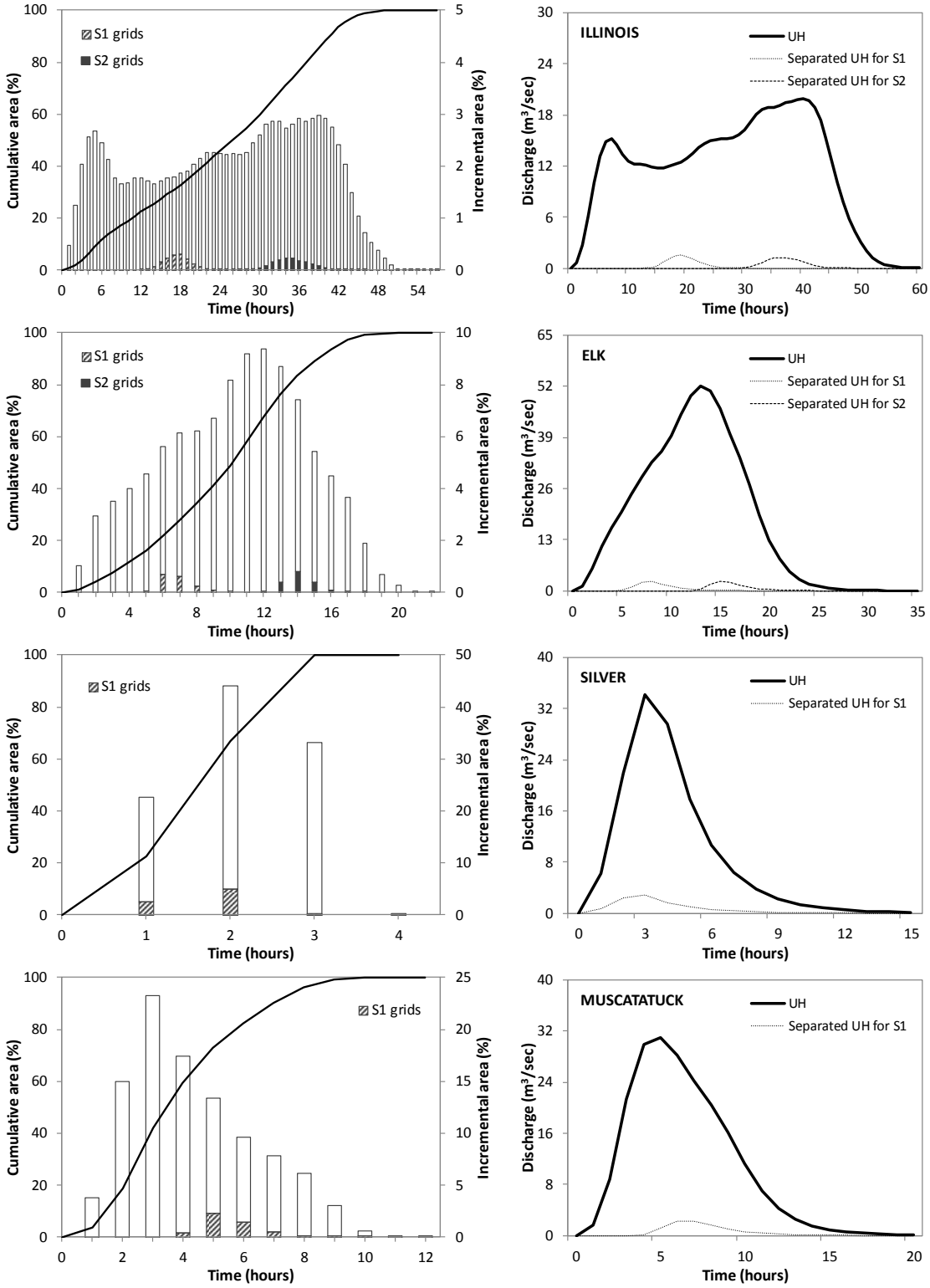

Figure 3.14 Time-area diagram (from calibrated *i*; Table 3.4, left) and separated unit hydrograph (default *R*; 2 hour, right)

3.5.2.2 Gridded CN

The gridded CN maps corresponding to each study watershed's subareas (NEXRAD grid cells) are shown in Figure 3.15. These gridded CN (histogram of CN values) are initially utilized for each grid cell's rainfall-runoff depth estimation, and then these estimated depths are averaged (counts weighted) with a histogram (gridded CN) of given subarea boundary (NEXRAD grid); this internal process creates the subarea's average runoff depth (spatially distributed excess rainfall; NEXRAD precipitation estimated).

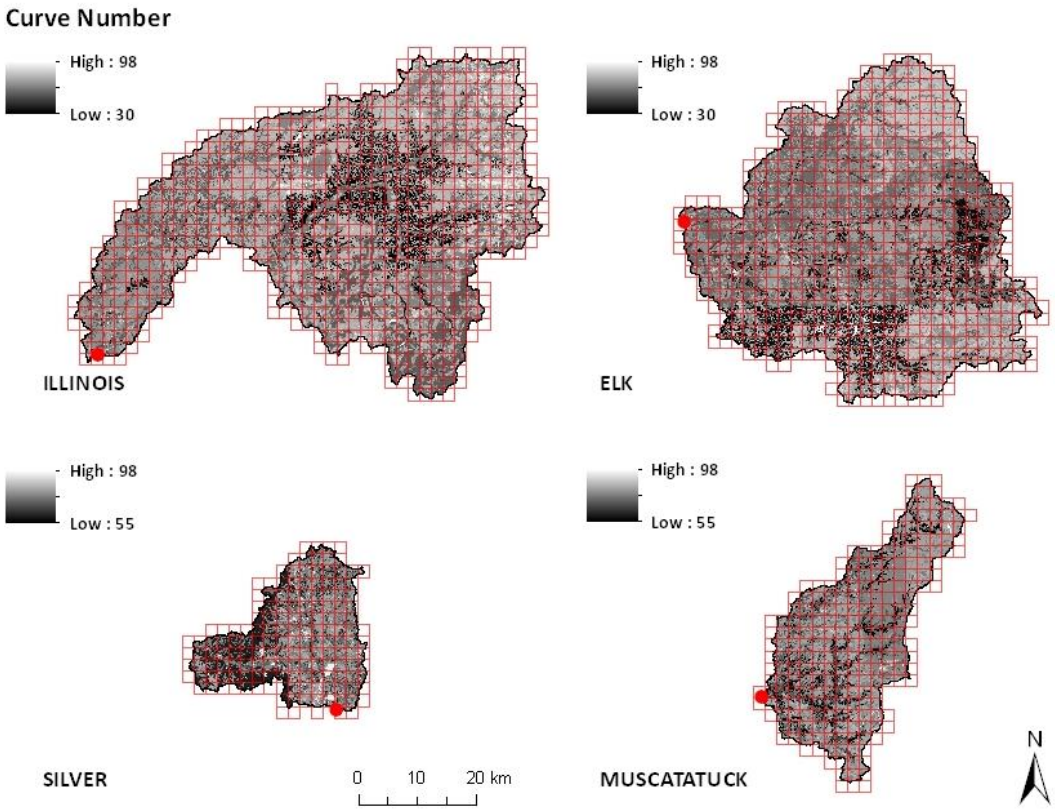

Figure 3.15 Gridded CN map for subarea's (NEXRAD radar-based grid cell) average runoff depth estimation

3.5.3 Model Performance

3.5.3.1 Calibration and Validation

Model calibration and validation to improve fit of simulation hydrographs against observed streamflow were conducted for all four study watersheds using six storm events for each area (total of 24). The default Distributed-Clark model using parameter values of the average intensity of 2-year, 24-hour rainfall; 2 hour; and 0.20 for *i*; *R*; and λ, respectively, was calibrated using rainfall inputs for spatially distributed NEXRAD precipitation and spatially averaged gauged data; model validation was also performed for three out of six events (randomly selected before calibration). The estimated parameter values following calibration are shown in Table 3.4. While the estimated parameter values of *i* and *R* are the same in each watershed, the initial abstraction coefficient, λ values, which are used to adjust for antecedent runoff conditions in watersheds for each storm event, differed since the model calibration and validation were made to match the total volume of observed flow data.

The simulated and observed flow hydrographs for total streamflow and direct runoff are represented in Figures 3.16 to 3.19 to show the graphical goodness-of-fit of each model's calibration and validation; for streamflow, the separated baseflow was added to create simulation outputs. In most cases, the calibrated model generated similar hydrographs with observed flows, but some cases produced gaps, particularly from observed direct runoff hydrographs. This indicates the imperfection of using just one representative calibrated *i* and *R* parameter value to create outputs for various storm events, since their

average rainfall intensity and watershed storage conditions can differ from those of the calibrated unit hydrograph. Nevertheless, the overall statistical results (Distributed-Clark) for both spatially distributed and averaged rainfall data simulation cases demonstrate relatively good performance (direct runoff E_{NS} 0.84, R^2 0.86, and *PBIAS* 2.39%; streamflow E_{NS} 0.91, R^2 0.92, and *PBIAS* 0.33%) compared with observed data for all four study watersheds as shown in Table 3.5.

Table 3.4 Parameter values of model calibration and validation results for spatially distributed and averaged rainfall data simulations

Watershed	Storm Events (#)	Un-calibrated parameters			Resulted parameters			
		i	*R*	λ (ARC)	*i*	*R*	NEXRAD data (D1; D1a)	Gauged data (D2*)
							λ (ARC)	λ (ARC)
Illinois River near Tahlequah	1	4.23	2.0	0.200 (II)	0.05	15.0	0.169 (III)	0.002 (III)
	2	4.23	2.0	0.200 (II)	0.05	15.0	0.070 (I)	0.246 (II)
	3	4.23	2.0	0.200 (II)	0.05	15.0	0.085 (I)	0.064 (I)
	4	4.23	2.0	0.200 (II)	0.05	15.0	0.091 (II)	0.104 (II)
	5	4.23	2.0	0.200 (II)	0.05	15.0	0.061 (I)	0.068 (I)
	6	4.23	2.0	0.200 (II)	0.05	15.0	0.049 (II)	0.267 (III)
Elk River near Tiff City	1	4.13	2.0	0.200 (II)	0.52	7.0	0.142 (II)	0.213 (II)
	2	4.13	2.0	0.200 (II)	0.52	7.0	0.095 (I)	0.123 (I)
	3	4.13	2.0	0.200 (II)	0.52	7.0	0.340 (II)	0.132 (II)
	4	4.13	2.0	0.200 (II)	0.52	7.0	0.167 (II)	0.089 (II)
	5	4.13	2.0	0.200 (II)	0.52	7.0	0.105 (I)	0.106 (III)
	6	4.13	2.0	0.200 (II)	0.52	7.0	0.127 (I)	0.153 (I)
Silver Creek near Sellersburg	1	3.28	2.0	0.200 (II)	17.5	20.0	0.264 (II)	0.356 (II)
	2	3.28	2.0	0.200 (II)	17.5	20.0	0.069 (I)	0.067 (I)
	3	3.28	2.0	0.200 (II)	17.5	20.0	0.155 (III)	0.184 (II)
	4	3.28	2.0	0.200 (II)	17.5	20.0	0.133 (II)	0.334 (II)
	5	3.28	2.0	0.200 (II)	17.5	20.0	0.182 (II)	0.066 (II)
	6	3.28	2.0	0.200 (II)	17.5	20.0	0.051 (II)	0.242 (II)
Muscatatuck River near Deputy	1	3.25	2.0	0.200 (II)	2.25	7.5	0.000 (III)	0.043 (III)
	2	3.25	2.0	0.200 (II)	2.25	7.5	0.112 (II)	0.082 (II)
	3	3.25	2.0	0.200 (II)	2.25	7.5	0.000 (III)	0.147 (III)
	4	3.25	2.0	0.200 (II)	2.25	7.5	0.213 (I)	0.278 (I)
	5	3.25	2.0	0.200 (II)	2.25	7.5	0.068 (II)	0.213 (III)
	6	3.25	2.0	0.200 (II)	2.25	7.5	0.261 (III)	0.204 (III)

i - vertical net incoming flux (mm/hour); *R* - storage coefficient (hour); λ - initial abstraction coefficient

* Averaged data simulation (D2) has the same *i* and *R* values with distributed data simulation (D1; D1a)

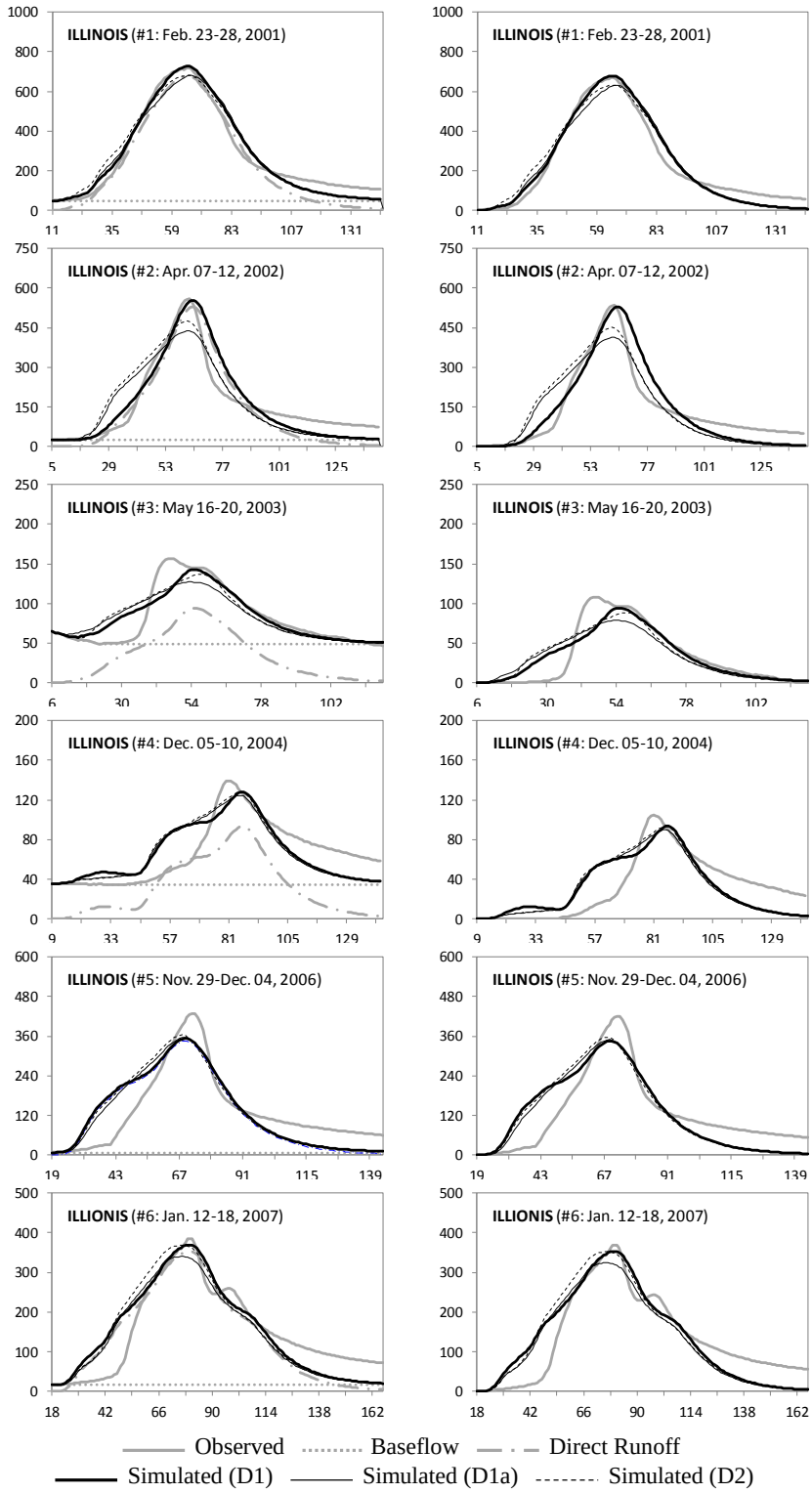

Baseflow separation: straight line method
X-axis represents simulation time (hours) and Y-axis represents discharge (m^3/sec)

Figure 3.16 Graphical results (total streamflow; left and direct runoff; right) for model calibration and validation (Illinois River)

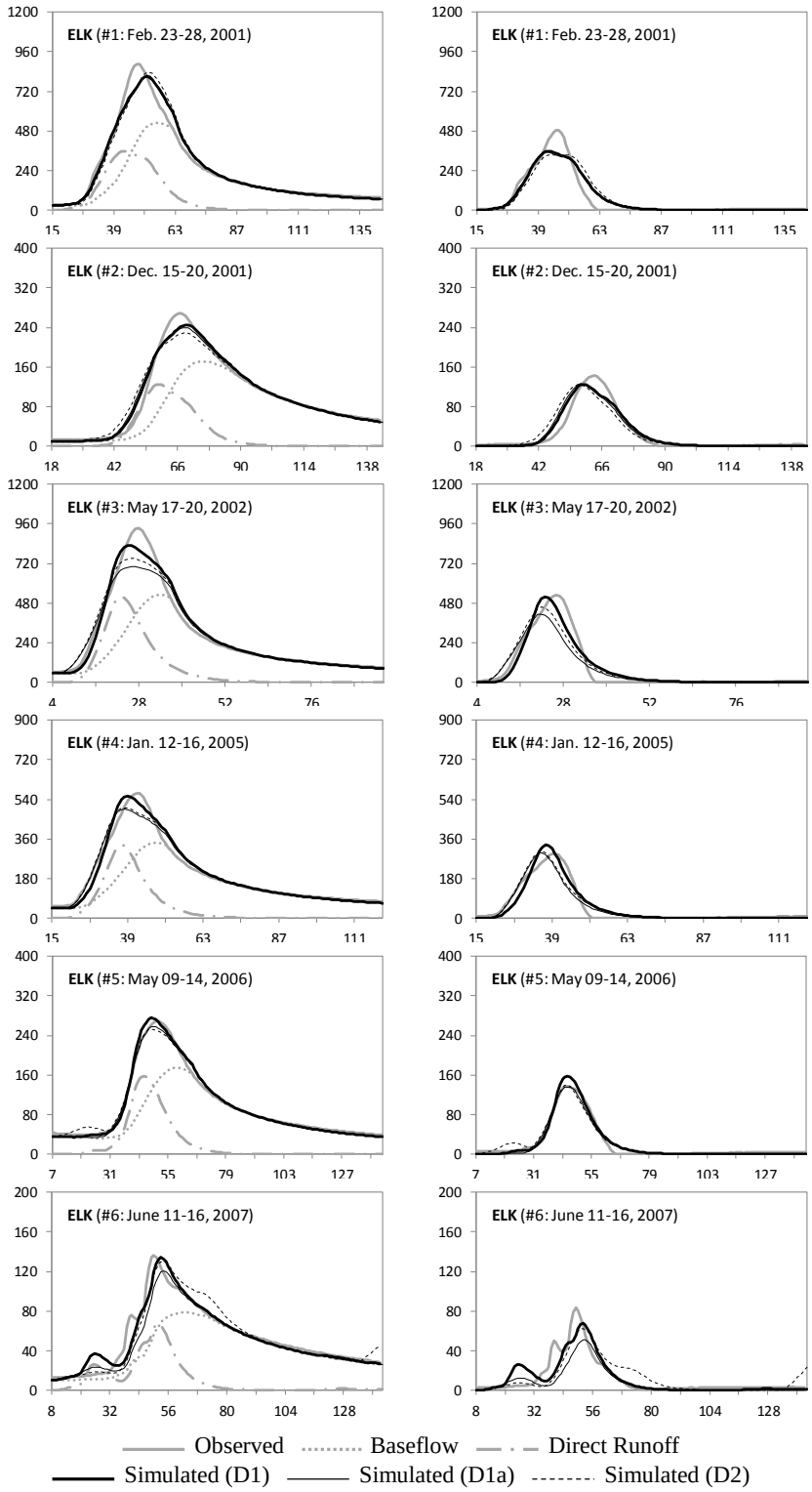

Baseflow separation: recursive digital filter method (*a* 0.995, BFI_{max} 0.80)
X-axis represents simulation time (hours) and Y-axis represents discharge (m^3/sec)

Figure 3.17 Graphical results (total streamflow; left and direct runoff; right) for model calibration and validation (Elk River)

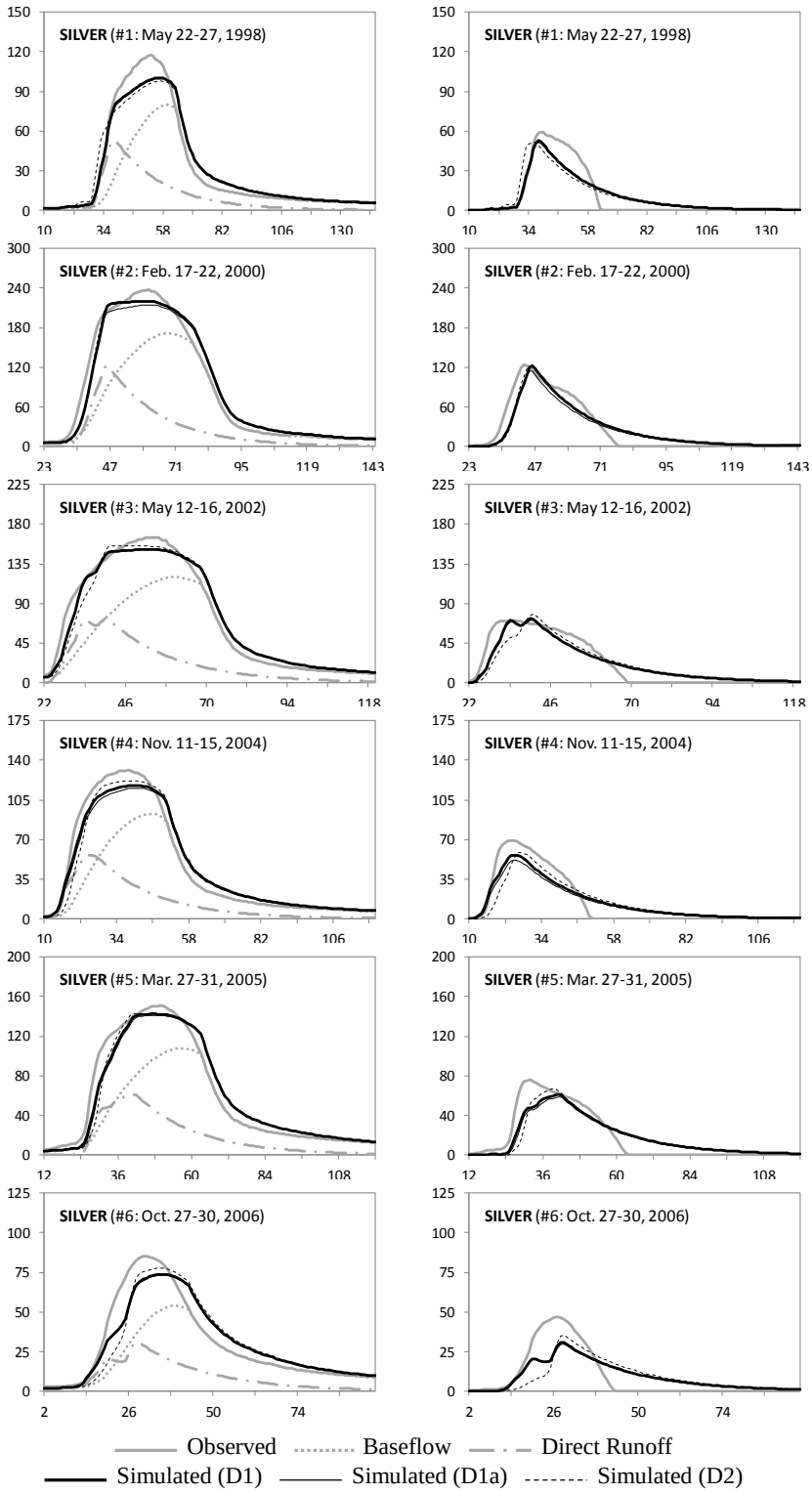

Baseflow separation: recursive digital filter method (*a* 0.980, BFI_{max} 0.80)
X-axis represents simulation time (hours) and Y-axis represents discharge (m^3/sec)

Figure 3.18 Graphical results (total streamflow; left and direct runoff; right) for model calibration and validation (Silver Creek)

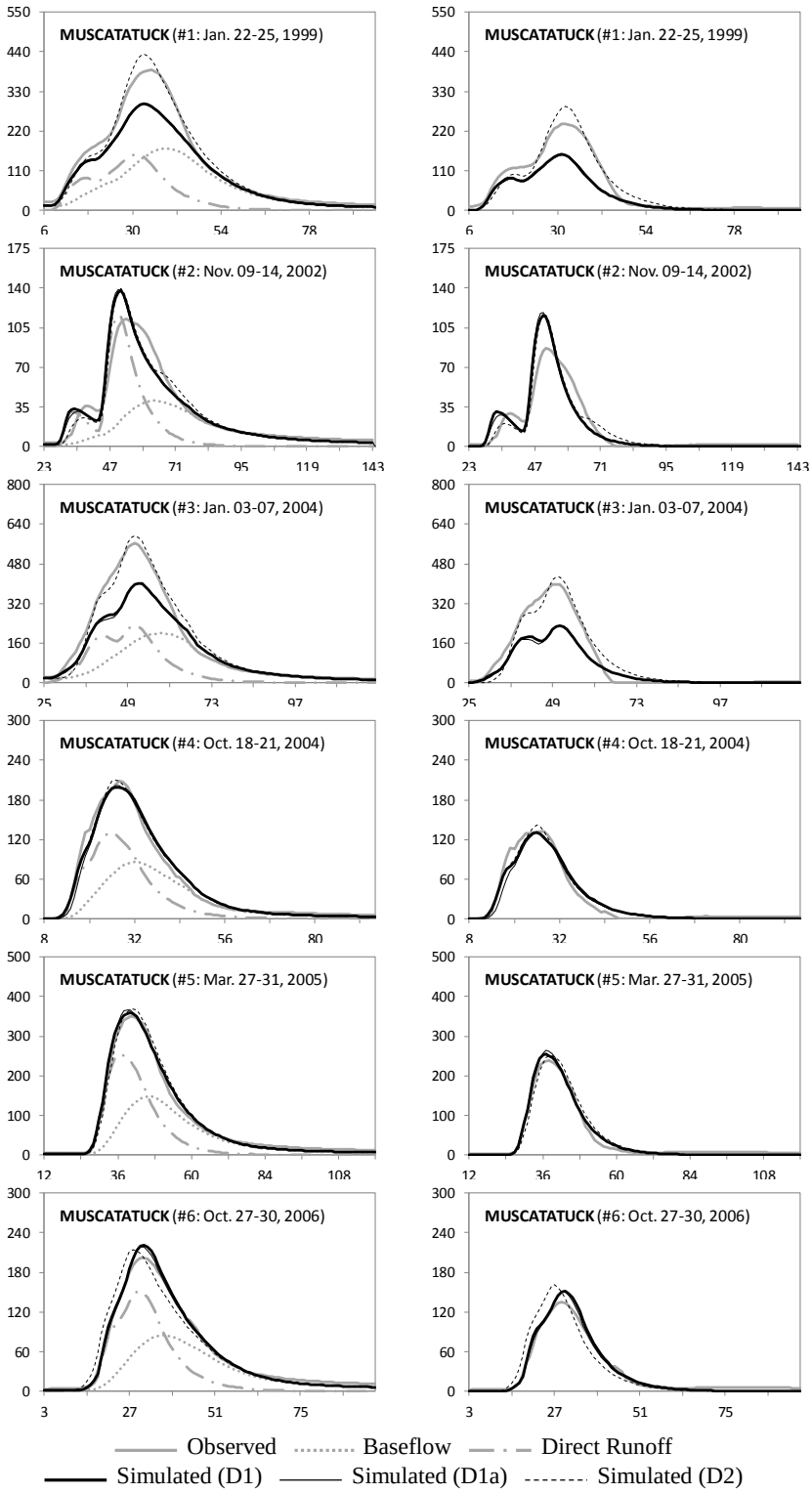

Baseflow separation: recursive digital filter method (*a* 0.980, BFI_{max} 0.50)
X-axis represents simulation time (hours) and Y-axis represents discharge (m^3/sec)

Figure 3.19 Graphical results (total streamflow; left and direct runoff; right) for model calibration and validation (Muscatatuck River)

Table 3.5 Statistical results (average) of model calibration and validation for study areas

Watershed	Model	Rainfall Data	Direct Runoff			Streamflow		
			E_{NS}	R^2	*PBIAS* (%)	E_{NS}	R^2	*PBIAS* (%)
Illinois River near Tahlequah	D1	Distributed	0.79	0.81	0.08	0.79	0.81	0.07
	D2	Averaged	0.75	0.78	0.08	0.75	0.78	0.05
Elk River near Tiff City	D1	Distributed	0.91	0.91	2.06	0.97	0.97	0.49
	D2	Averaged	0.85	0.86	1.49	0.95	0.95	0.36
Silver Creek near Sellersburg	D1	Distributed	0.82	0.87	0.72	0.95	0.96	0.22
	D2	Averaged	0.75	0.76	0.42	0.93	0.93	0.13
Muscatatuck River near Deputy	D1	Distributed	0.87	0.96	12.82	0.94	0.97	6.68
	D2	Averaged	0.94	0.95	1.48	0.97	0.97	0.78
Average	D1	Distributed	0.85	0.89	3.92	0.91	0.93	1.87
	D2	Averaged	0.82	0.84	0.87	0.90	0.91	0.33
	Total		0.84	0.86	2.39	0.91	0.92	1.10

E_{NS} and R^2 arithmetic mean; *PBIAS* arithmetic mean of absolute value

3.5.3.2 Comparisons

Table 3.5 compares averaged results of model simulations for spatially distributed NEXRAD radar-based and spatially averaged gauged rainfall inputs. Overall, the use of NEXRAD precipitation products in Distributed-Clark (D1) did not result in large differences from outputs of gauged data application (D2); it shows slightly better fit with improved statistical values for E_{NS} of 3.0% (0.82 to 0.85) and R^2 of 6.0% (0.84 to 0.89) in direct runoff relative to results from spatially averaged rainfall simulations.

However, each case of storm event simulation comparison results for two models (D1 and D2) that are represented in Tables B 1 to B 4 and Figures 3.16 to 3.19 show some significant differences. For instance, simulation results of storm event #2 for the Illinois River, #6 for the Elk River, and #6 for the Muscatatuck River watershed present

differences in both graphical and statistical results. In these cases, better statistical values occurred for spatially distributed rainfall data simulations; for direct runoff, E_{NS} increases of 6.8, 12.4, and 9.7% and R^2 increases of 8.8, 12.4, and 7.0% occurred, respectively. These differences are likely because of the amount of input rainfall and the rainfall spatial variability; relatively larger skewness values of NEXRAD precipitation amount, -0.46, 1.01, and -0.84, are found in these storm events, respectively, and they differed from gauged average rainfall. Thus, these rainfall inputs and each dominant area's (NEXRAD grid cell) separated unit hydrographs enabled the model to create different outputs. Comparison of most other cases also show good fit results in distributed rainfall simulation. This may indicate the model results from NEXRAD precipitation inputs are more appropriate to simulate rainfall-runoff flow predictions than gauged data for the same model calibration approach.

Since data quality issues can exist with NEXRAD rainfall estimates, simulation results may not be always appropriate. For the Muscatatuck River basin cases, NEXRAD precipitation underestimation of 31.4% (event #1) and 36.2% (event #3) affected the model performance in hydrologic simulations; the model output hydrographs for event #1 and #3 could not be matched with observed flows, even though they were simulated with potential maximum parameter values for their runoff depth (0 and ARC III for λ). Thus, these results are poor compared with other cases, and only the Muscatatuck River watershed's distributed rainfall simulations have poorer performance than gauged data simulations for averaged E_{NS} and *PBIAS* values.

Another case of model results comparison (D1 and D1a; Distributed-Clark) to examine model performances for NEXRAD data's spatial variability are also presented in Tables B 1 to B 4 and Figures 3.16 to 3.19. In this case, the D1a model which used the areal average of NEXRAD precipitation as input data was not calibrated from the D1 model which conducted distributed rainfall simulation using spatially distributed NEXRAD data, since the intention of this comparison is only to distinguish the volume changes between distributed and averaged NEXRAD data simulation results for the same parameters value calibrated models. For the results, the larger differences in each NEXRAD grid cell's precipitation can result in output gaps between distributed (D1) and averaged (D1a) models for each selected storm event; but, gaps are not significant for the storm events having small amounts of rainfall. This aspect should not be disregarded when predicting storm event flows using hydrologic models because the results can be underestimated or overestimated according to the type of rainfall inputs.

The Distributed-Clark model examined the effect of NEXRAD data's spatial variability in rainfall-runoff flow simulations. In most cases of this study's selected storm events, the runoff flow simulation results for spatially averaged NEXRAD data resulted in decreased flow volumes from that of distributed NEXRAD data simulation. This is because the amount of each NEXRAD grid cell's excess rainfall are reduced after they are averaged from spatially distributed rainfall values; typically, the CN method estimates larger depths of rainfall excess for larger input depths of rainfall (Chow et al., 1988). In other words, the averaged values of precipitation in grid cells, which were previously larger amounts, resulted in a smaller depth of excess rainfall than their possible excess

depth for distributed data simulations; these decreased runoff amounts affected the overall volumes of simulated flow. Each study watershed's results for this comparison in Tables B 1 to B 4 present flow volume differences for distributed and averaged NEXRAD data simulation, which differed up to 1.8 (6.0%), 1.4 (10.9%), 1.7 (7.2%), and 0.8 mm (6.8%) for the Illinois River, Elk River, Silver Creek, and Muscatatuck River watershed, respectively; these volumes also changed the rate and time for peak flow of streamflow hydrographs up to 115.8 (2), 126.7 (1), 5.6 (2), and 7.6 m^3/s (1 hour) for each watershed.

In addition, these results were also affected by the skewness of precipitation amount distributions. More specifically, storm event cases of NEXRAD data that have high skewness values or wide amount ranges (Table 3.2) made more gaps in model flow simulations; as these cases, storm event #2 (skewness -0.46; range 131.4 mm) and #6 (-1.09; 45.8 mm) for the Illinois River, #3 (0.31; 90.9 mm) and #6 (1.01; 103.9 mm) for the Elk River, #2 (3.25; 44.8 mm) for the Silver Creek, and #4 (-0.76; 59.3 mm) for the Muscatatuck River watershed show larger flow volume or peak flow differences than other events (Tables B 1 to B 4). However, since these gaps for compared models (D1 and D1a) can result from other modeling components as well (e.g. the shape of separated unit hydrographs and CN values for each NEXRAD grid cell; for four study watersheds, the numbers of 717, 624, 159, and 239 grid cells are defined, respectively), it is hard to generalize the above trends from precipitation data distributions as the main explanation for the model simulation result differences.

3.6 Summary and Conclusions

This study examined the applicability of NEXRAD data (spatiotemporally varied gridded precipitation; NCEP Stage IV composite products) for rainfall-runoff flow prediction using a hybrid hydrologic model, Distributed-Clark, including development of a GIS-based automation tool for NEXRAD data processing. The SCS CN approach estimated spatially distributed excess rainfall obtained from NEXRAD data and a set of separated unit hydrographs that are derived using GIS-based time-area diagram (isochrones) are utilized to convolute a direct runoff hydrograph; NEXRAD and required spatial data processing for hydrological modeling framework and model execution for flow simulation were implemented by Python script tools in a GIS platform.

Results of NEXRAD data validation with gauged rainfall show correlations (0.56 to 0.69) and underestimation trends for larger values in NEXRAD precipitation, and significant differences (NEXRAD data are 7.6 and 11.3% overestimated in two watersheds; 2.2 and 15.1% underestimated in two watersheds) between the amounts of spatially distributed radar-based rainfall and spatially averaged gauged data for four study watersheds were also found; these differences and NEXRAD data's spatial variability (skewness ranges -1.02 to 3.25 for total of 24 storm events) affected model performance for single storm event flow prediction. From two cases of model application results comparison for the same calibration approach, it can be identified following model performances of Distributed-Clark in rainfall-runoff flow simulations for the use of spatially distributed NEXRAD precipitation data.

1. The comparison of model simulation results with input of spatially averaged gauged rainfall showed slightly improved flow prediction outputs in most NEXRAD data simulations (overall, E_{NS} of 3.0% and R^2 of 6.0% increase in direct runoff for evaluations with observed flow). This suggests that NEXRAD data application is more appropriate to predict storm event runoff flows than gauged rainfall (for flood predictability). However, NEXRAD precipitation product quality issues may result in poor model performance; in this study, two cases of inadequate simulation results for flow volumes compared with observed flows were caused due to significantly underestimated precipitation amounts.

2. The second case compared model simulation results from the same NEXRAD data; but, in this case, the outputs of the NEXRAD grid cell-based areal average rainfall input model were utilized as comparison targets. The results identified differences in flow volume amount and peak flow rate for these different types of rainfall input simulations; spatially distributed rainfall cases showed more increased flow volumes and peak rates than spatially averaged cases, and more gaps occurred for the storm events having significant spatial variability with high skewness values. Thus, it can be noted that the hydrologic model simulation using spatially averaged precipitation may produce underestimated results compared to spatially distributed cases for the use of the same parameter values in calibrated models.

These results indicate that spatially distributed NEXRAD radar-based precipitation estimates provided better results in hydrologic application of rainfall-runoff flow predictions than spatially averaged gauge rainfall, enabling improved predictions of flow volumes and peak rates which can be disregarded in hydrologic simulations for spatially averaged rainfall.

Furthermore, since many gridded types of quantitative precipitation estimation (QPE) have been developing in the research fields of earth and space science with intensive quality control (e.g. Multi-Radar Multi-Sensor; MRMS QPE, which is beyond NEXRAD, GPM satellite-based QPE, etc.), these types of gridded precipitation would be more reliable data for hydrological modeling. Therefore, it can be expected that this study's simple approaches would support the improved implementation of hydrologic simulation, particularly for spatially distributed rainfall-runoff flow prediction in a GIS environment.

CHAPTER 4. CONTINUOUS SCS CN METHOD-BASED LONG-TERM HYDROLOGIC SIMULATION USING DISTRIBUTED-CLARK

4.1 Abstract

A continuous SCS CN method which can consider continuously variable SCS CN values for estimation of long-term discontinuous storm runoff depth was developed based on the original SCS CN method with a revised soil moisture accounting approach, and it was applied to hydrologic simulation for spatially distributed long-term rainfall-runoff flow prediction using Distributed-Clark, incorporating conditional unit hydrograph adoption for different runoff precipitation depth-based flow convolution. Case studies of long-term (total of 6 years) Distributed-Clark simulation for four river basins using spatially distributed NEXRAD radar-based daily precipitation demonstrate overall performances of E_{NS} 0.62, R^2 0.64, and *PBIAS* 0.33% in direct runoff and E_{NS} 0.71, R^2 0.72, and *PBIAS* 0.15% in total streamflow for model result comparison against observed flow, and these show better fit (improved E_{NS} of 42.0% and R^2 of 33.3% in total streamflow) than the same model applications using spatially averaged rainfall data. Also, logic for conditional initial abstraction in a continuous SCS CN method, which can accommodate amounts of initial abstraction in accordance with previous rainfall, slightly enhances model simulation performance; both E_{NS} and R^2 increased by 1.4% for total streamflow in a 4-year calibration period. Thus, a continuous SCS CN method-based Distributed-Clark is a useful technique for spatially distributed long-term rainfall-runoff flow prediction.

4.2 Introduction

The SCS runoff curve number (CN) method that was developed in the 1950s by the Soil Conservation Service (SCS; now NRCS, Natural Resources Conservation Service) (SCS, 1957, 1972; USDA NRCS, 2010) is a popular, ubiquitous, and enduring means of estimating storm runoff from rainfall events (Hawkins et al., 2009). This method of rainfall excess estimation from rainfall depth is widely used in applied hydrology. Hjelmfelt (1980) and Ponce et al. (1996) mentioned that its advantages of convenience, simplicity, and responsiveness to readily identified catchment properties (soil type, land use/treatment, surface condition, antecedent condition, etc.) are the grounds to maintain its popularity. Furthermore, Geographic Information System (GIS), introduced in the 1990s, also enables this method to be easily adopted in hydrologic models, particularly for its parametric data (soil, land use, etc.) processing. A number of water resource models (now GIS-based) including AGNPS/AnnAGNPS (Young et al., 1986; Cronshey and Theurer, 1998), CREAMS/GLEAMS (Knisel, 1980, 1993; Leonard et al., 1987), SWAT (Arnold et al., 1993, 1998), and L-THIA (Harbor, 1994; Bhaduri, 2000; Engel, 2001), employ the SCS CN method as their basic equation for runoff depth calculation.

However, this method has limitations when it is applied to some hydrologic modeling applications (e.g. infiltration behavior, long-term continuous simulation, etc.) because it originated as an empirical, event-based procedure for flood hydrology (Garen and Moore, 2005). Woodward et al. (2002) indicated that the SCS CN method equation (USDA NRCS, 2010) that calculates direct runoff does not contain any expression for time, and it estimates runoff from single storms. However, they additionally noted that the total

runoff from storms of long duration (in the case of a continuous storm with no breaks in the rainfall) can be calculated as the sum of daily increments, and the amounts of daily excess rainfall are often used to represent a runoff time series. Chow et al. (1988) also presented an equation for time distribution of SCS abstraction which computes the cumulative abstraction for a given time; it can express the time increments of excess rainfall as well, and it can be used for single storm event runoff application. While this equation considers time, it may not have a strong physical basis for infiltration behavior for the following reasons: (1) the rate of retention of water within the watershed tends to increase as the rainfall intensity increases (Morel-Seytoux and Verdin, 1981), (2) if rainfall rate varies within storm, infiltration rates are predicted to respond accordingly to maintain the unrealistic assumption of proportionality of excess to rainfall (Smith, 1976), and (3) the infiltration rate will approach zero during storms of long duration instead of a constant terminal infiltration rate (Hjelmfelt, 1980).

In the case of runoff estimation from a long-term discontinuous storm which has intervals (exceeding an hour) of no rain, the recovery of infiltration rates during the intervals should be considered (Woodward et al., 2002). If the model does not consider this recovery, abnormal (overestimated) runoff calculation outcomes will result due to the increased cumulative rainfall depth. For the same reason, the SCS CN method should not consider intermittent events as whole storm inputs for runoff calculation without a term for infiltration rates (Hjelmfelt, 1980). Thus, to use this method for discontinuous storm (sporadic or several single events) runoff simulations, the amount of water retention (i.e., soil moisture) should be continuously accounted for at every time step over the storm

duration considering infiltration rates. In addition, the initial abstraction, which consists mainly of interception, infiltration during early parts of the storm, and surface depression storage (USDA NRCS, 2010) also needs to be re-considered according to the duration of intervals of no rainfall.

In the SCS CN method, generally three classes of Antecedent Runoff Condition (ARC; I dry, II average, and III wetter) which result from variability of rainfall intensity and duration, total rainfall, soil moisture conditions, cover density, stage of growth, and temperature (USDA NRCS, 2010) are recognized as the average watershed runoff conditions for single storm event runoff estimation. In order to estimate runoff from long-term discontinuous storm events, a different technique that can consider continuously varied watershed runoff conditions (especially soil moisture) is needed. For this effort, most continuous models with the SCS CN method use adjusted CN values. Hawkins et al. (2009) described the general method of continuous models as follows: (1) the CN values and storage indices for ARC I and ARC III condition are established from the initial values that are assumed to be ARC II; the CN (from soil moisture budget) varies between these indices, (2) daily direct runoff is generated from daily rainfall and daily CN, (3) site soil moisture is estimated based on total losses to runoff (infiltration amounts) and losses of evapotranspiration, drainage, percolation, etc., and (4) the next day CN is calculated from the residual soil moisture content. Van Mullem et al. (2002) also stated that most models assume ARC I and ARC III are equivalent to wilting point and field capacity of the soil, respectively; this allows estimation of the appropriate daily CN.

Among current existing SCS CN method based continuous models, the pioneering work by Williams and LaSeur (1976) is typically the basis of these models (Hawkins et al., 2009); they developed a water yield model (soil moisture index accounting technique) using the SCS CN method to predict daily, monthly, and annual runoff. Because CN varies continuously with soil moisture in reality, it has many values instead of only three cases. Williams and LaSeur (1976) introduced a soil moisture index to consider variable CN and computed it with conceptual components of evapotranspiration (observed average monthly lake evaporation is used) and deep seepage depletions as well as infiltration restoration; the model has one parameter (soil moisture index, calibrated with depletion coefficient), uses a one-day time interval, and outputs runoff volume. However, Hawkins (1977) remarked that this model should include initial abstraction as an element of the total retention to provide a more meaningful physical interpretation and presented a similar concept for varying site moisture based CN values (Hawkins, 1978); in this method, conceptual loss and gain terms consider evapotranspiration and infiltration (rainfall losses to runoff).

Knisel (1980) further indicated that although the above soil moisture accounting model was found to be superior to the ARC method, it did not contain a percolation component or a physically based water balance. He linked this CN technique with evapotranspiration and percolation models to form a model capable of maintaining a physically based continuous water balance (CREAMS; Chemicals, Runoff, and Erosion from Agricultural Management Systems). This water balance approach is also utilized in other models or has been adapted for use in other models. For example, GLEAMS (Groundwater Loading

Effects of Agricultural Management Systems) (Leonard et al., 1987; Knisel, 1993), which estimates pesticide ground water loadings, and EPIC (Erosion Productivity Impact Calculator) (Williams et al., 1984), which simulates the impact of erosion on crop production, were developed from CREAMS. The SWRRB (Simulator for Water Resources in Rural Basins) (Williams et al., 1985) model was also established by modifying CREAMS to simulate weather, return flow, crop growth, transmission losses, pond and reservoir storage, and sediment movement, allowing simultaneous computations on several sub-basins. The CREAMS, GLEAMS, EPIC, and SWRRB models also significantly contributed to the development of AnnAGNPS (Annualized Agricultural Nonpoint Source model) (Cronshey and Theurer, 1998) and SWAT (Soil and Water Assessment Tool) (Arnold et al., 1993, 1998).

Choi et al. (2002) proposed a similar concept using a water balance equation (CN technique based cell-by-cell soil moisture balance approach) for daily streamflow modeling. CELTHYM, a cell-based long-term hydrological model, which can compute direct runoff, base flow, soil moisture, and evapotranspiration, is however comprised of a simple concept rather than a physically based water balance; they indicated the complexity and demands of detailed field data are still barriers for use of the model.

Even simpler conceptual models re-appeared for long-term storm events runoff simulation. Mishra and Singh (2003, 2004) used the methods of Williams and LaSeur (1976) and Hawkins (1978), which are non-water balance based techniques. They pointed out that Hawkins' (1978) remarks regarding initial abstraction do not play a part in the

infiltration process since the cumulative abstraction (infiltration; F_a) does not include the initial abstraction, I_a (in SCS CN method, $F_a = P - Q - I_a$, where P and Q are rainfall and runoff), and presented a modified SCS-CN model (Mishra and Singh, 2003, 2004), incorporating more sophisticated infiltration (dynamic/static) components and an evapotranspiration formula (Schaake et al., 1996). Kannan et al. (2008) also proposed a one-parameter evapotranspiration and precipitation based continuous soil moisture accounting procedure which uses a modified retention parameter of the APEX (Agricultural Policy/Environmental eXtender) model (Williams et al., 2000); it originally came from Williams and LaSeur's (1976) method, but it adopts two evapotranspiration (Hargreaves and Penman-Monteith) equations. Most recently, Kannan et al.'s (2008) equation was changed with addition of two parameters (SCS CN index coefficient and upper limit of retention) for efficient calibration (Williams et al., 2012).

Several recent studies also consider the soil moisture accounting (SMA) procedure in SCS CN method including Durbude et al. (2011) and Jain et al. (2012) who created and applied a long-term hydrologic simulation advanced soil moisture accounting (LTHS ASMA) model. However, its runoff calculation is implemented based on Michel et al.'s (2005) concept of the SCS CN formula; it incorporates an intrinsic parameter "S_a" which consists of the initial abstraction, I_a, and the initial soil moisture storage level, V_0, and considers the case of $I_a < 0$, in which case some flow is occurring from the soil moisture reservoir at the beginning of the event; it can be added to the runoff. Despite its consistency of theory with other SCS CN based models, this model needs to define other sub-formulas for estimating the terms S_a and V_0.

Among the reviewed continuous models using the SCS CN method, the present in-depth study to improve long-term storm events runoff simulation with the SCS CN was developed based on Mishra and Singh's (2003, 2004) model because it is relatively simple and preserves the original SCS CN method's (USDA NRCS, 2010) concept and formula; these are advantages of the SCS CN method. However, the modified SCS-CN model (Mishra and Singh, 2003, 2004) requires refinement in its equation development with respect to soil moisture index, retention, and initial abstraction. In addition, as previously mentioned, initial abstraction should also be re-considered according to duration of intervals without rain (it does not need to be subtracted every time step, but needs to be considered for recovery) with different ratios (e.g. original method 0.2). Hawkins et al. (2002) indicated an initial abstraction ratio value of about 0.05 gives a better fit to the data and would be more appropriate for use in runoff calculation.

In this study, a continuous SCS CN method is proposed to estimate long-term discontinuous storm runoff, incorporating time-varied potential maximum retention (i.e., soil moisture index), conditional initial abstraction, static (constant terminal) infiltration, and parameter generalization for an evapotranspiration equation based on the formula of the original SCS CN method (USDA NRCS, 2010) with the revised concepts of Hawkins' (1978) and Mishra and Singh's (2003, 2004) models for time-varied soil moisture computation. Then, this runoff depth computation method is combined with the GIS-based spatially distributed Clark's unit hydrograph method (Distributed-Clark) for long-term hydrologic simulation (runoff routing) by using NEXRAD radar-based multi-sensor rainfall estimates. Distributed-Clark, a lumped conceptual and distributed feature model

(hybrid hydrologic model; DeVantier and Feldman, 1993), can consider spatially distributed rainfall as model inputs. The objectives of this chapter are as follows: (1) to develop a continuous SCS CN method, compared with previously developed methods particularly Hawkins' (1978) and Mishra and Singh's (2003, 2004) equations, (2) to estimate runoff flow for spatially distributed long-term discontinuous storm data (NEXRAD radar-based precipitation) using the developed continuous SCS CN method with Distributed-Clark, and (3) to evaluate the performance of the proposed modeling approach by making comparisons between simulation results and observed streamflow for direct runoff following baseflow separation.

4.3 Study Area and Data

4.3.1 Study Area

Four river basins were selected as study areas in this research: Illinois River near Tahlequah, OK; Elk River near Tiff City, MO; Silver Creek near Sellersburg, IN; and Muscatatuck River near Deputy, IN. The study areas were the same watersheds as for previous chapters in order to continue model (Distributed-Clark) application for spatially distributed rainfall inputs from short-term single storm event to long-term discontinuous storm events (Figure 4.1).

4.3.2 Data

The data used in this study include: (1) 1 arc-second (spatial resolution around 30 m) Digital Elevation Model (DEM), National Land Cover Database 2011 (NLCD 2011), and National Hydrography Dataset (NHD) from USGS National Map, (2) Soil Survey

Geographic (SURRGO) Database from USDA WSS (Web Soil Survey), and (3) Precipitation Frequency (PF) estimates from NOAA HDSC (Hydro-meteorological Design Studies Center). DEM and NHD data are used for watershed delineation and stream network definition, whereas land use, PF estimates, and soil data are used to create flow travel time and runoff curve number map. The time-series (daily) data and gauge information for precipitation (gauged rainfall) and temperature from NOAA NCDC (National Climatic Data Center), and streamflow from USGS NWIS (National Water Information System), are used to validate NEXRAD rainfall estimates, calculate evapotranspiration, and evaluate the performance simulation results, respectively.

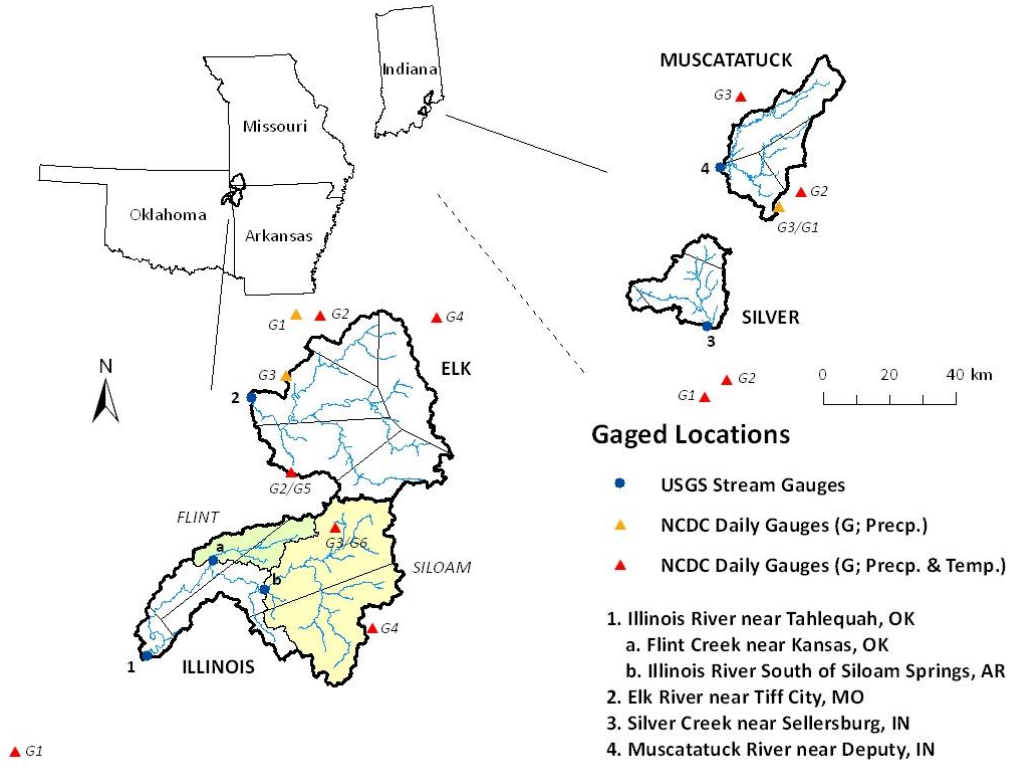

Figure 4.1 Location of study watersheds

4.3.3 NEXRAD Data

NEXRAD data, "NCEP Stage IV" products, which are mosaicked from the 12 RFCs regional hourly/6-hourly multi-sensor precipitation estimates or estimator (Stage III products or MPEs; manual quality-controlled data) in CONUS by NCEP (Lin and Mitchell, 2005), are available through the NOAA Advanced Hydrologic Prediction Service (APS) and National Center for Atmospheric Research (NCAR) web-accessible archives. In this study, the hourly NEXRAD Stage IV data (GRIB; Gridded Binary format) were used for obtaining model (Distributed-Clark) input of daily based spatially distributed precipitation with data processing to subset and generate required datasets, appropriately matching its extent with study areas. Figure 4.2 shows the locations of individual NEXRAD radar sites and their coverage (umbrella radius; 230 km) for study watersheds. All study areas are well inside at least one radar umbrella.

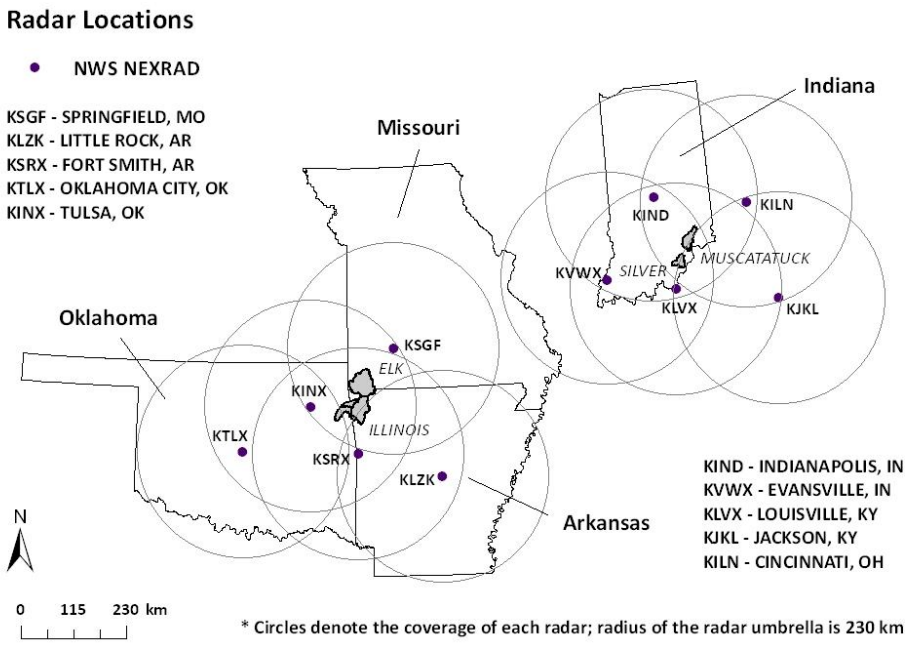

Figure 4.2 Location of NEXRAD radar sites and coverage for study area

4.4 Methodology

4.4.1 Continuous SCS CN Method

4.4.1.1 Hawkins' Model Refinement

Hawkins (1978) assumed the total water storage available on the site is 1.2*S* (*S* is the potential maximum retention), considering the initial abstraction as an element of the total retention; it can be represented as Equation (4.1) which is derived from the original SCS CN method.

$$P - Q = S\left(1.2 - \frac{S}{P + 0.8S}\right) \quad (P \geq 0.2S = I_a, \quad \text{as } P \to \infty, P - Q \to 1.2S) \tag{4.1}$$

where *P* and *Q* are the cumulative rainfall and excess rainfall depth [L], respectively, *S* is the potential maximum retention [L], and I_a is the initial abstraction (0.2*S*) [L].

Then, Hawkins provided Equation (4.2) to calculate varying site moisture with CN values, taking into account evapotranspiration and infiltration terms.

$$CN_t = \frac{1200}{\left(\frac{1200}{CN_{t-1}}\right) + [ET - (P - Q)]_t} \tag{4.2}$$

where CN_t is the SCS curve number value at time *t*, ET_t and $(P\text{-}Q)_t$ are the cumulative depth (inch) of evapotranspiration losses and infiltration (rainfall losses to runoff) in time interval *t-1* to *t*, respectively.

However, Mishra and Singh (2003, 2004) pointed out that the initial abstraction in Hawkins' model does not play a part in the infiltration process since the cumulative abstraction (F_a) does not include the initial abstraction, I_a (in SCS CN method, $F_a = P - Q - I_a$, where P and Q are rainfall and runoff). So, Equation (4.1) needs to be changed to Equation (4.3).

$$F = S\left(1 - \frac{S}{P + 0.8S}\right) \quad (P \geq 0.2S = I_a, \quad \text{as } P \to \infty, F = P - Q - I_a \to S) \tag{4.3}$$

where F is the cumulative abstraction (infiltration) depth [L] and others are the same as above.

In addition, Equation (4.2) also needs modification by substitution of 1000 for 1200 as below in Equation (4.4); all factors are the same as above in Equation (4.2).

$$CN_t = \frac{1000}{\left(\frac{1000}{CN_{t-1}}\right) + [ET - (P - Q)]_t} \tag{4.4}$$

However, this equation also ignores the initial abstraction, I_a, term for the denominator; it should be included as a calculation component of the infiltration process ($F = P - Q - I_a$). Thus, the equation of varying site moisture with CN values has to be modified as Equation (4.5). Also, it needs to account for the case of $P < I_a$, since all equations above are presented for the case of $P \geq I_a$.

(for $P \geq I_a$)

$$F = S\left(1 - \frac{S}{P + 0.8S}\right) \quad (\text{as } P \to \infty, \quad F = P - Q - I_a \to S)$$

$$CN_t = \frac{1000}{\left(\frac{1000}{CN_{t-1}}\right) + [ET - (P - Q - I_a)]_t} \tag{4.5a}$$

(for $P < I_a$)

$$F = 0, \qquad CN_t = \frac{1000}{\left(\frac{1000}{CN_{t-1}}\right) + [ET]_t} \tag{4.5b}$$

where all factors are the same as for equations above.

In addition, because the initial abstraction, I_a, consists mainly of interception, infiltration during early parts of the storm, and surface depression storage (USDA NRCS, 2010), it does not need to be subtracted at every time step for continuous rainfall-runoff simulation; it should be re-considered according to the duration of intervals of no rainfall. For instance, if the I_a is reset ($I_a = 0.2S$) when no rainfall occurs in the previous time step, it can be written for time *t* as:

$$[P_{cum}]_t = P_t + [P_{cum}]_{t-1} \quad (\text{if } P_t = 0, \quad [P_{cum}]_t = 0)$$
$$(\text{for } 0.2S_{t-1} \geq [P_{cum}]_{t-1}) \quad [I_a]_t = 0.2S_{t-1} - [P_{cum}]_{t-1}$$
$$(\text{for } 0.2S_{t-1} < [P_{cum}]_{t-1}) \quad [I_a]_t = 0 \tag{4.6}$$

where $[P_{cum}]_t$ is the total cumulative rainfall [L] at time *t*, S_t and $[I_a]_t$ are the potential maximum retention and initial abstraction depth [L] at time *t*, respectively, and P_t is the cumulative rainfall depth [L] in time interval *t-1* to *t*.

4.4.1.2 Mishra and Singh's Model Refinement

Mishra and Singh (2003, 2004) presented the modified SCS-CN model based on the original SCS CN method as Equation (4.7) by introducing static and dynamic infiltration components, F_c and F_d ($F_c + F_d$ is the same as F_a of the original SCS CN formula), and the soil moisture index, M, which is the antecedent moisture amount, prior to the beginning of the storm.

$$\begin{aligned}
&(\text{for } P_{(t,t+\Delta t)} \geq I_{a(t)} + F_{c(t,t+\Delta t)}) \\
&RO_{(t,t+\Delta t)} = \frac{(P_{(t,t+\Delta t)} - I_{a(t)} - F_{c(t,t+\Delta t)})(P_{(t,t+\Delta t)} - I_{a(t)} - F_{c(t,t+\Delta t)} + M_t)}{P_{(t,t+\Delta t)} - I_{a(t)} - F_{c(t,t+\Delta t)} + M_t + S_t} \\
&(\text{for } P_{(t,t+\Delta t)} < I_{a(t)} + F_{c(t,t+\Delta t)}) \quad RO_{(t,t+\Delta t)} = 0 \\
&if \;\; P_{(t,t+\Delta t)} \leq I_{a(t)} + F_{c(t,t+\Delta t)}, \quad \text{then} \quad F_{c(t,t+\Delta t)} = P_{(t,t+\Delta t)} - I_{a(t)} \\
&if \;\; P_{(t,t+\Delta t)} \leq I_{a(t)}, \quad \text{then} \quad F_{c(t,t+\Delta t)} = 0 \quad \text{and} \quad RO_{(t,t+\Delta t)} = 0
\end{aligned} \tag{4.7a}$$

$$\begin{aligned}
&F_{d(t,t+\Delta t)} = P_{(t,t+\Delta t)} - I_{a(t)} - F_{c(t,t+\Delta t)} - RO_{(t,t+\Delta t)} \;\; (\text{for } RO_{(t,t+\Delta t)} \geq 0) \\
&F_{d(t,t+\Delta t)} = 0 \;\; (\text{for } RO_{(t,t+\Delta t)} < 0)
\end{aligned} \tag{4.7b}$$

$$M_{(t,t+\Delta t)} = F_{d(t,t+\Delta t)} + M_t - ET_{(t,t+\Delta t)}, \quad S_{(t,t+\Delta t)} = S_t - F_{d(t,t+\Delta t)} + ET_{(t,t+\Delta t)} \tag{4.7c}$$

where $RO_{(t,t+\Delta t)}$, $P_{(t,t+\Delta t)}$, $F_{c(t,t+\Delta t)}$, $F_{d(t,t+\Delta t)}$, and $ET_{(t,t+\Delta t)}$ are the cumulative runoff, rainfall, static infiltration, dynamic infiltration, and evapotranspiration [L] in time interval Δt, respectively, M_t, $M_{(t,t+\Delta t)}$, S_t, and $S_{(t,t+\Delta t)}$ are the soil moisture index ($M = S_{abs} - S$, S_{abs} is the absolute potential maximum retention) and potential maximum retention [L] at time t and $t+\Delta t$, respectively, and I_a is the initial abstraction [L] at time t.

However, in Equation (4.7a), there is no reason to include the soil moisture index term, *M*, because the potential maximum retention term, *S*, already exists in the equation; they are related to each other as $S = S_{abs} - M$. Also, the runoff, *Q*, can be represented with only *S* or $S_{abs} - M$ as Equation (4.8), separately; this is the original SCS CN method's assumption.

$$\frac{Q}{P - I_a - F_c} = \frac{F_d}{S} = \frac{F_d}{S_{abs} - M} \tag{4.8}$$

where S_{abs} is the absolute potential maximum retention [L] and others are the same as above.

4.4.1.3 Continuous SCS CN method

The continuous SCS CN method is developed based on the original SCS CN equation (USDA NRCS, 2010) with the revised concepts of Hawkins' (1978) and Mishra and Singh's (2003, 2004) models for time-varied soil moisture (potential maximum retention; curve number) computation to estimate long-term discontinuous storm runoff depth. In this method, both the cumulative abstraction (infiltration), F_a, which is divided into the static (constant terminal) infiltration, F_c, and dynamic infiltration, F_d, components, and the *ET*, evapotranspiration, term are employed in the equations of the developed model. In addition, the time varying initial abstraction, $I_{a,t}$, is also introduced by using Equation (4.6).

Hence, for a given long-term rainfall event, the direct runoff depth (excess rainfall), dynamic infiltration, and potential maximum retention at time t (Q_t, $F_{d,t}$, and S_t; CN_t) can be calculated by Equation (4.9); it preserves the form of the original SCS CN equation despite the use of additional terms.

$$\text{(for } P_t \geq I_{a,t} + F_c\text{)}$$

$$Q_t = \frac{\left(P_t - I_{a,t} - F_c\right)^2}{P_t - I_{a,t} - F_c + S_{t-1}}, \quad F_{d,t} = \frac{S_{t-1}\left(P_t - I_{a,t} - F_c\right)}{P_t - I_{a,t} - F_c + S_{t-1}} = P_t - I_{a,t} - F_c - Q_t \tag{4.9a}$$

$$\text{(for } P_t < I_{a,t} + F_c\text{)} \quad Q_t = 0, \quad F_{d,t} = 0$$

$$\text{(for } \lambda S_{t-1} \geq P_{cum,t-1}\text{)} \quad I_{a,t} = \lambda S_{t-1} - P_{cum,t-1}$$
$$\text{(for } \lambda S_{t-1} < P_{cum,t-1}\text{)} \quad I_{a,t} = 0 \tag{4.9b}$$
$$\lambda = \frac{I_a}{S}, \quad P_{cum,t} = P_t + P_{cum,t-1} \quad (\text{if } P_t = 0, \quad P_{cum,t} = 0)$$

$$S_t = S_{t-1} + ET_t - F_{d,t} \quad \left(S_{t-1} \leq S_{0,\,\mathrm{I}} = \frac{1000}{CN_{0,\,\mathrm{I}}} - 10\right), \quad CN_t = \frac{1000}{S_t + 10} \tag{4.9c}$$

where P_t, Q_t, F_c, $F_{d,t}$, and ET_t are the cumulative rainfall, direct runoff (excess rainfall), static and dynamic infiltration, and evapotranspiration depth [L] in time interval *t-1* to *t*, respectively, $P_{cum,t}$ is the total cumulative rainfall [L] at time *t*, $I_{a,t}$ is the initial abstraction [L] at time *t*, λ is the initial abstraction coefficient (0 to 1), S_t is the potential maximum retention (inch) at time *t* ($S_{0,I}$; maximum retention storage from $CN_{0,I}$), and CN_t is the SCS curve number value at time *t*.

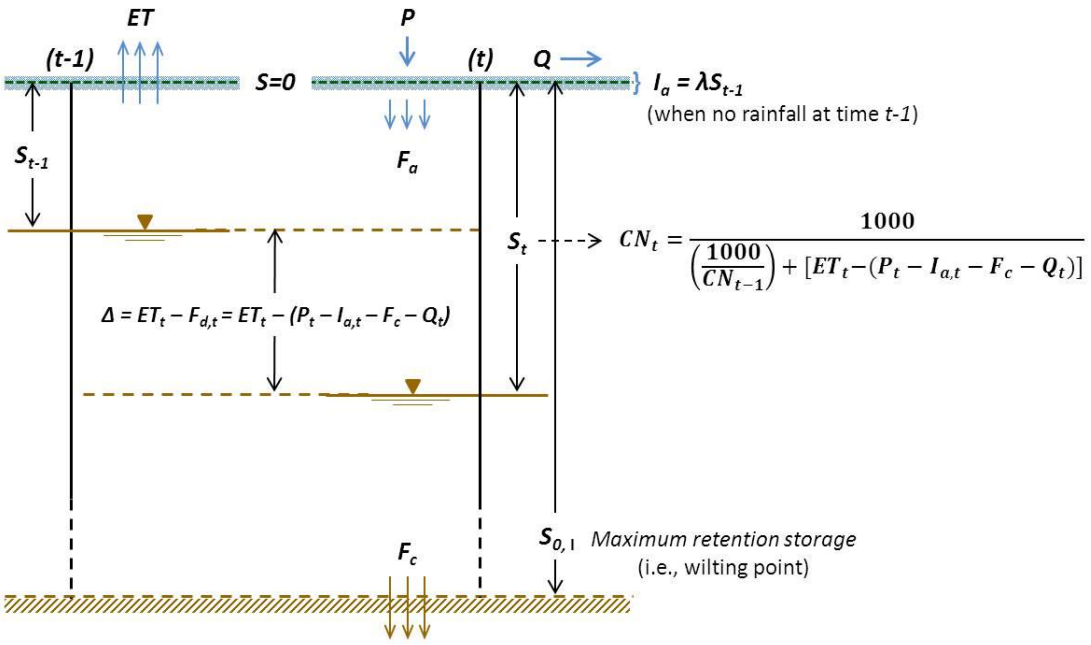

Figure 4.3 Schematic of time-varied CN computation in continuous SCS CN method

Figure 4.3 shows the diagrammatic approach of the continuous SCS CN method, particularly for the time-varied CN computation. In this method, the static infiltration, F_c, which is the same concept factor of Horton's (1939) constant terminal infiltration rate, f_c, is later used as one of the calibration parameters. Also, the time varying initial abstraction, $I_{a,t}$, is reset ($I_{a,t} = \lambda S_{t-1}$) when no rainfall occurs in the previous time (daily) step.

For estimation of the evapotranspiration, ET_t, in Equation (4.9c), Schaake et al.'s (1996) formula, which was applied to Mishra and Singh's (2003, 2004) model, was also used with the assumption that the ratio of moisture deficits for both upper and lower soil layers is equal to each other; the upper soil layer water which is intercepted by leaves, stored in surface depressions or top soil evaporates locally at rates governed by the ability of the

atmosphere to accept, and the lower soil layer water is directly lost by evaporation from the soil and evapotranspiration through vegetation as Equation (4.10).

$$ET_t = PET_t \left[1 - \left(\frac{S_{u,t}}{S_{u,max}}\right)\left(\frac{S_{b,t}}{S_{b,max}}\right)\right] = PET_t \left[1 - \left(\frac{S_t}{S_{0,\,\mathrm{I}}}\right)^2\right] \quad (4.10)$$

where PET_t is the total amount of potential evapotranspiration [L] in time interval *t-1* to *t*, $S_{u,t}$, and $S_{b,t}$ are the moisture deficits for both upper and lower soil layers at time *t*, $S_{u,max}$ and $S_{b,max}$ are the maximum moisture deficits, respectively, and others are the same as above.

Then, to calculate the potential evapotranspiration, PET_t, Hargreaves method (Hargreaves and Samani, 1985), which is a relatively simple temperature-based approach but widely used in many regions of the U.S. (Xu and Singh, 2001; Hargreaves and Allen, 2003; Lu et al., 2005; Kannan et al., 2008), was chosen. As shown in Equation (4.11), they considered extraterrestrial radiation, R_a, for estimating solar radiation at the Earth's surface, since these data are frequently not available. Thus, it only requires measured values of temperatures.

$$PET = ET_0 = 0.00023\, R_a\, TR^{0.50}\, (TC + 17.8) \quad (4.11)$$

where *PET* is the potential evapotranspiration or reference crop evapotranspiration (mm/day), R_a is the water equivalent of extraterrestrial radiation (mm/day), *TR* is the daily temperature range (difference between the mean daily maximum temperature; T_{max}

and mean daily minimum temperature; T_{min} for a given month) (°C), and *TC* is the temperature of (T_{max} + T_{min})/2 (°C) (in present study, all temperature data for *TR* and *TC* calculation were considered as daily maximum and minimum measured values).

Also, for a given latitude and day, R_a can be calculated by Equation (4.12) (Maidment, 1993).

$$R_a = 15.392\, d_r\, (\omega_s \sin\varphi \sin\delta + \cos\varphi \cos\delta \sin\omega_s) \quad (4.12a)$$

$$d_r = 1 + 0.033\, \cos\left(\frac{2\pi}{365}J\right) \quad (4.12b)$$

$$\delta = 0.4093\, \sin\left(\frac{2\pi}{365}J - 1.405\right) \quad (4.12c)$$

$$\omega_s = \arccos\left(-\tan\varphi \tan\delta\right) \quad (4.13d)$$

where d_r is the relative distance between the Earth and the sun on day *J*, *J* is Julian day, δ is the solar declination on day *J* (radians), φ is the latitude of the site (positive for the Northern hemisphere, negative for the Southern hemisphere) (degrees), and ω_s is the sunset hour angle (radians) and others are the same as above (for example, the extraterrestrial solar radiation value at latitude 30°N on April 15 (*J* = 105) is 15.0 mm/day).

4.4.2 Distributed-Clark

Distributed-Clark, a GIS-based spatially distributed Clark's unit hydrograph method, adopts a runoff routing technique based on the combined concept of Clark's (1945) unit

hydrograph and its spatial decomposition methods (Maidment et al., 1996); it is a lumped conceptual and distributed feature model (hybrid hydrologic model; DeVantier and Feldman, 1993). Differing from the conventional Clark's lumped unit hydrograph method, Distributed-Clark utilizes a set of separated unit hydrographs which are derived for partitioned subareas of a watershed; therefore, it can take spatially distributed rainfall (e.g. NEXRAD radar-based precipitation) for implementing hydrologic simulation (spatially distributed rainfall-runoff routing).

4.4.2.1 Spatially Distributed Excess Rainfall

For long-term hydrologic simulation with Distributed-Clark, the continuous SCS CN method presented in this chapter is used to estimate long-term excess rainfall. For given long-term storm events, the direct runoff depth (excess rainfall) at time *t*, Q_t, can be calculated by Equation (4.9a). In this case, for estimating each subarea's initial retention storage, S_0, which is assumed as the same amount of initial CN (ARC II condition; $CN_{0,II}$) values' potential maximum retention, a set of gridded CN (i.e., histogram of CN values corresponding to subarea of interest) for given subareas (e.g. NEXRAD grid cells) are first derived based on a CN map. Then, they are applied to each subarea's initial retention storage calculation in Equation (4.9c), and the results of the first time step's average excess rainfall (direct runoff, Q_1) for each subarea are generated. From these results, the time-varied potential maximum retention, S_t and SCS curve number, CN_t, can be calculated by Equation (4.9). Figure 4.4 shows the process of spatially distributed long-term excess rainfall estimation using graphic representations.

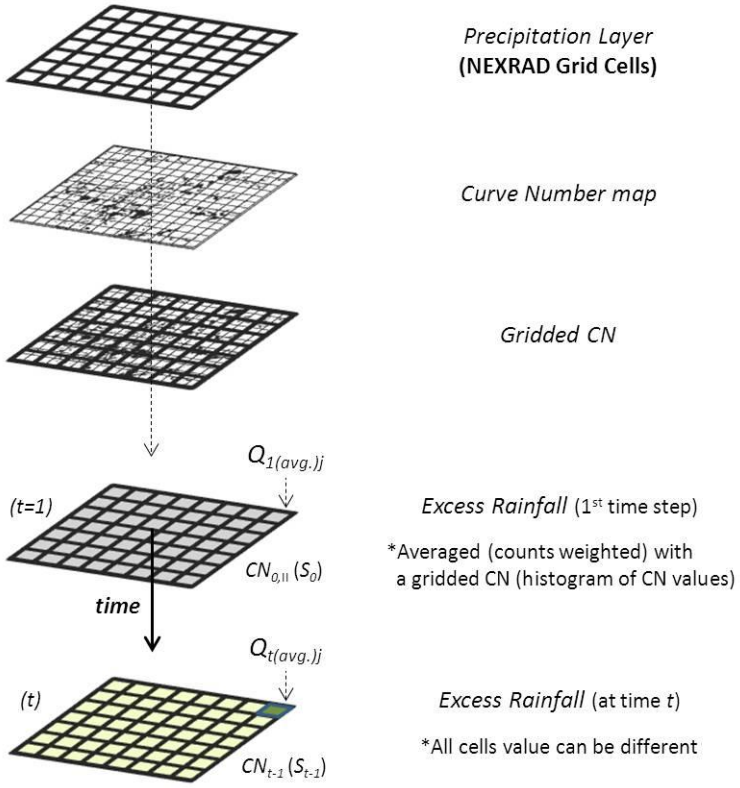

Figure 4.4 Graphical representations of the spatially distributed long-term excess rainfall estimates

4.4.2.2 Spatially Distributed Unit Hydrograph

For the spatially distributed unit hydrograph development, a time-area diagram (isochrones, GIS-derived; in Distributed-Clark, grid cell-based flow velocity calculation using McCuen's (1995), Muzik's (1996), and Melesse and Graham's (2004) approaches are applied with some modification) and the instantaneous unit hydrograph (IUH) utilized transformation, which includes the instantaneous unit excess rainfall applied time-area diagram translation and its linear reservoir attenuation, are required. Figure 4.5 shows a conceptual model of the Distributed-Clark approach, particularly for obtaining NEXRAD

grid cell-based separated unit hydrographs. In this method, the ordinates of the separated unit hydrograph, $S_{i,j}$, can be obtained by Equation (4.14), and their summation results in the spatially distributed unit hydrograph.

$$S_{i,j} = 0.5\left[\left(\frac{\Delta t}{R + 0.5\Delta t}\right) I_{i,j} + \left(2 - \frac{\Delta t}{R + 0.5\Delta t}\right) IUH_{(i-1),j}\right] \tag{4.14}$$

where $S_{i,j}$, $I_{i,j}$, and $IUH_{i,j}$ are the jth subarea's separated unit hydrograph, translation hydrograph, instantaneous unit hydrograph at the end of ith interval [L^2T^{-1}], respectively, Δt is the computation time interval [T], and R is the storage coefficient [T].

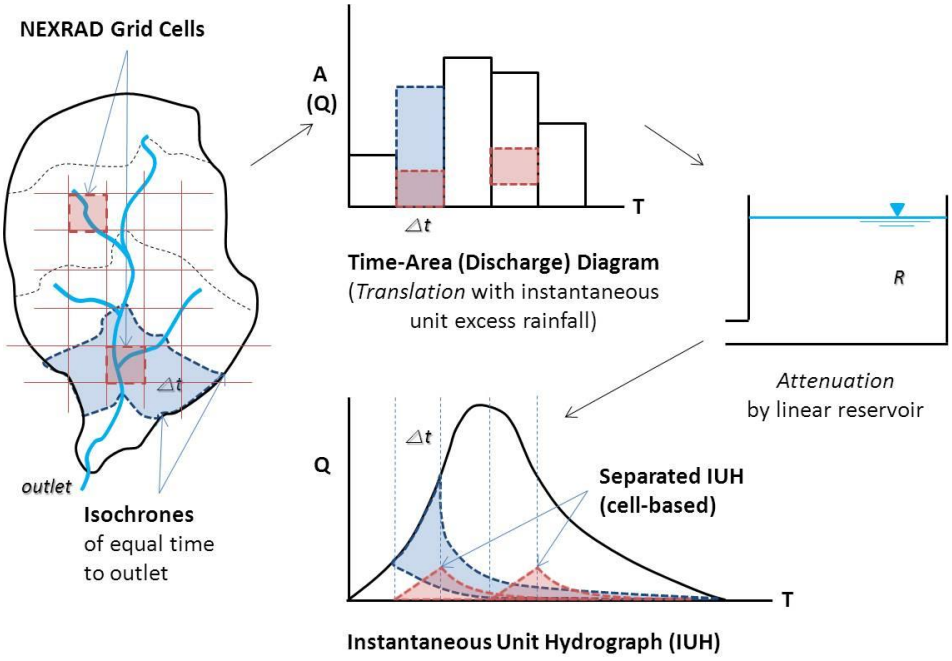

Figure 4.5 Distributed-Clark conceptual model

4.4.2.3 Unit Hydrograph Conversion

Since the one-hour interval (Δt) applied time-area diagram (isochrones) was used to derive a set of separated unit hydrographs, these unit hydrographs need to be converted into a different duration (24-hour) for long-term (daily time interval) hydrologic simulation, particularly with daily direct runoff (excess rainfall). Theoretically, when a unit hydrograph of a given excess rainfall duration is available, the unit hydrographs of other durations can be derived (Chow et al., 1988). For this conversion, the S-hydrograph, which results from a continuous excess rainfall at a constant rate of 1 cm/hour (or 1 inch/hour) for an indefinite period, should be first prepared. Then, the difference between the ordinates of the original S-hydrograph, $g_j(t)$, and the Δt (24-hour) lagged S-hydrograph, $g_j(t-\Delta t)$, divided by Δt (24-hour), creates the Δt (24-hour) duration unit hydrograph, $h_j(t)$, by Equation (4.15).

$$h_j(t) = \frac{1}{\Delta t}\left[g_j(t) - g_j(t - \Delta t)\right] \tag{4.15}$$

where $h_j(t)$ is the Δt-hour duration unit hydrograph and $g_j(t)$ is S-hydrograph for the jth subarea.

This 24-hour (excess rainfall) duration unit hydrograph consists of one-hour time step interval ordinates. So, after convolution with long-term (daily) excess rainfall, it needs to be averaged as daily flow for comparison purposes with observed daily flow data.

4.4.2.4 Direct Runoff Hydrograph

A direct runoff hydrograph is calculated by Equation (4.16) using previously developed series of spatially distributed long-term excess rainfall and separated unit hydrographs. In this calculation, a set of distributed direct runoff hydrographs for the watershed outlet point are calculated, and the sum of all distributed direct runoff hydrographs makes a direct runoff hydrograph.

$$Q_n = \sum_{i=1}^{n} \sum_{j=1}^{J} P_{i,j} S_{n-i+1,j} \tag{4.16}$$

where Q_n is the direct runoff hydrograph at the end of nth time interval [L^3T^{-1}], $P_{i,j}$ is the average excess rainfall in the jth subarea for time interval i [L], and $S_{i,j}$ is the jth subarea's separated unit hydrograph at the end of the ith interval [L^2T^{-1}].

4.4.2.5 Model Parameters and Development

In Distributed-Clark application for event based simulation, all three parameters of the vertical net incoming flux, i, storage coefficient, R, and initial abstraction coefficient, λ, are used to calibrate the model simulation results; other possible but pre-fixed (during model development) factors were not parameterized. The first two parameters affect the shape of the spatially distributed unit hydrograph; they are utilized for flow travel time calculation and time-discharge diagram attenuation, respectively, and the last one is used for adjusting the amount of spatially distributed excess rainfall. However, in the case of runoff routing for long-term discontinuous events, the parameter of static infiltration, F_c

(i.e., f_c: the constant rate of static infiltration [L/T]), is added to consider time-varied soil moisture calculation with evapotranspiration, *ET*, term (this is not a model parameter). Model development including watershed pre-processing (i.e., watershed and stream network definition; Manning's *n* and SCS CN map creation), spatially distributed long-term excess rainfall estimation, spatially distributed unit hydrograph derivation, and direct runoff hydrograph convolution can be implemented using Python script tools which were developed in a GIS platform. Further details of the Distributed-Clark model parameters, specific equations, and development procedures are described in a previous chapter (Chapter 2).

4.4.3 NEXRAD Data Processing

NEXRAD radar-based rainfall can be interpreted and processed in a GIS environment. In this study, a GIS-based tool was developed for automation of required NEXRAD precipitation data (particularly for Stage IV composite products; GRIB format) processing to generate daily long-term spatially distributed radar-based rainfall (model input). Figure 4.6 shows overall procedures for NEXRAD data (daily) processing using the developed GIS-based (Python script) tools; it includes four steps of map projection (coordinate system) transformation, modeling extent and NEXRAD grid subsetting, hourly to daily data stack, and raster (each daily time step's spatially distributed) and time-series (each subarea's temporally distributed) precipitation data generation. Further details of the NEXRAD data map system (HRAP grid), projection parameters, and transformation process are described in a previous chapter (Chapter 3).

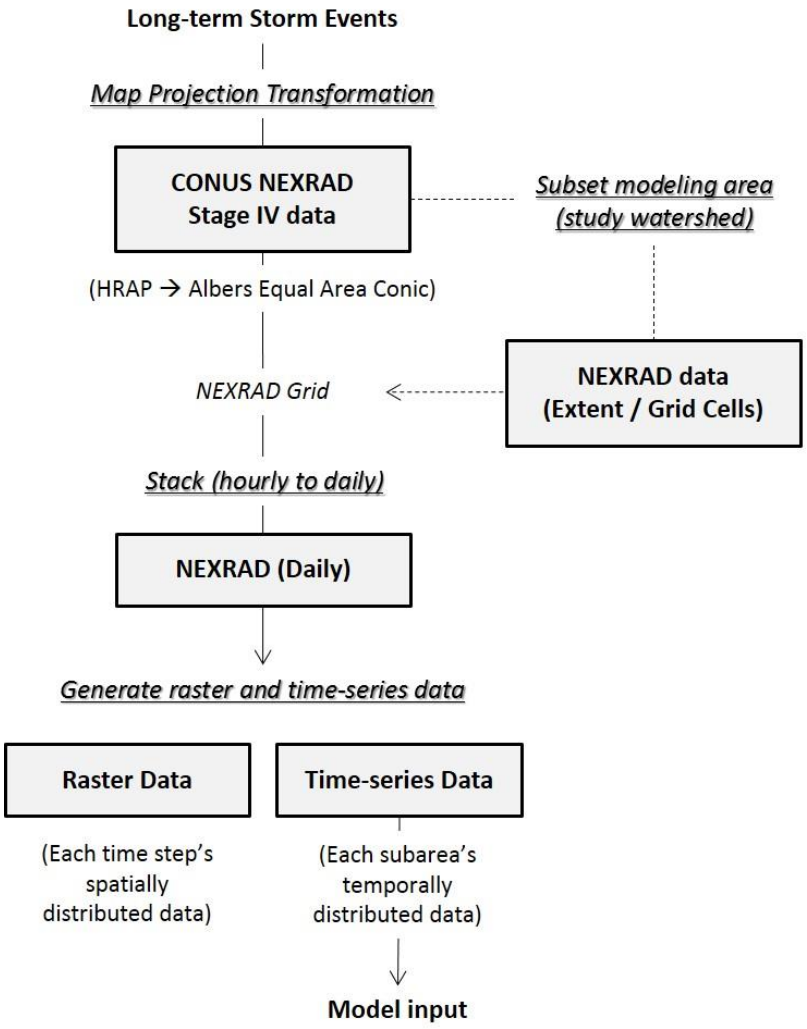

Figure 4.6 Overall procedures for daily NEXRAD data processing

On the other hand, since the CONUS NEXRAD Stage IV data are produced based on the Coordinated Universal Time (UTC) zone, time difference with other observed data (gaged rainfall, streamflow, etc.) must be considered. In this study, all other observed data in the watershed used local time (e.g. EDT, EST, CDT, and CST; 4 to 6 hours later than UTC). Thus, daily data (01 to 24 hour) for EDT/EST and CDT/CST were stacked from UTC (05 to 04)/(06 to 05) and UTC (06 to 05)/(07 to 06) hourly data, respectively.

4.4.4 Model Performance Evaluation

4.4.4.1 Long-Term Storm Events Selection

Long-term storm events for four study areas were selected to compare and evaluate the performance of the developed continuous SCS CN method with the Distributed-Clark model for spatially distributed radar-based rainfall and spatially averaged (lumped) gauged data simulations. A total of 6 years (2009 to 2014) were considered as the model simulation period. Table 4.1 presents the period of rainfall events (data length) used in model setup (warm-up test), calibration, and validation for each study watershed.

Table 4.1 Data length for long-term storm events for model setup, calibration, and validation

Watershed	Period of rainfall events (data length)		
	Setup (warm-up test)	Calibration	Validation
Illinois River near Tahlequah Elk River near Tiff City Silver Creek near Sellersburg Muscatatuck River near Deputy	2009-01~2010-06 (tested for different starting dates)	2009-01~2012-12 (4 years)	2013-01~2014-12 (2 years)

Quality controlled NEXRAD Stage IV (GRIB format) data are available from 2002 in NCAR archives.

For the selected long-term streamflows, the baseflows were separated to retrieve direct runoff hydrographs. For this separation, the same approach used in previous chapters, the recursive digital filter method (Eckhardt, 2005), was applied. The final selected baseflow removal method for each study area is the same as previous ones, except for the Illinois River which used the straight line method for storm event applications; for long-term application, it is not reasonable to describe continuously varied baseflows.

4.4.4.2 Model Evaluation Criteria

The model performance (model setup, calibration, validation, etc.) was evaluated using four indicators: Nash-Sutcliffe efficiency (E_{NS}); -∞ to 1.0 (perfect fit) (Nash and Sutcliffe, 1970), coefficient of determination (R^2); 0 (no correlation) to ±1.0 (perfect linear relationship), percent bias (*PBIAS*, %); 0 (optimal value) to ±100 (volume difference tendency against observed counterparts) (Moriasi et al., 2007), and root mean squared error (*RMSE*); 0 (perfect fit) to ∞; same as Equations (2.18a to 2.18d) from Chapter 2.

4.4.4.3 Model Comparison

Model simulation results for long-term spatially distributed NEXRAD radar-based rainfall and spatially averaged gauged data were compared. In the case of distributed data input, outputs from model simulation with and without conditional initial abstraction, I_a, logic were also compared. The rainfall inputs, unit hydrographs, and SCS CN values applied to each model are summarized in Table 4.2.

Table 4.2 Model input data (rainfall and CN) and unit hydrograph

Model	Distributed-Clark (Distributed)	Distributed-Clark (Averaged)
Rainfall	Spatially distributed (NEXRAD; grid cell based)	Spatially averaged (Gauged; Thiessen polygon weighted)
SCS CN	Gridded CN for each NEXRAD grid cell (time-varied)	Gridded CN for entire basin area (time-varied)
Unit hydrograph	A set of separated unit hydrographs	A set of separated unit hydrographs

Gridded CN - a histogram of CN values corresponding to subarea of interest

4.5 Results and Discussion

4.5.1 NEXRAD data

4.5.1.1 Validation

For the 6 years (2009 to 2014) of long-term storm event data, the average value of NEXRAD radar-based daily precipitation estimates for each study area's extent were validated against watershed areal average rainfall from rain gauge observations. In particular, 4, 6, 3, and 3 gauges for each study area (Figure 4.1) were utilized to develop Thiessen polygon weighted average precipitation.

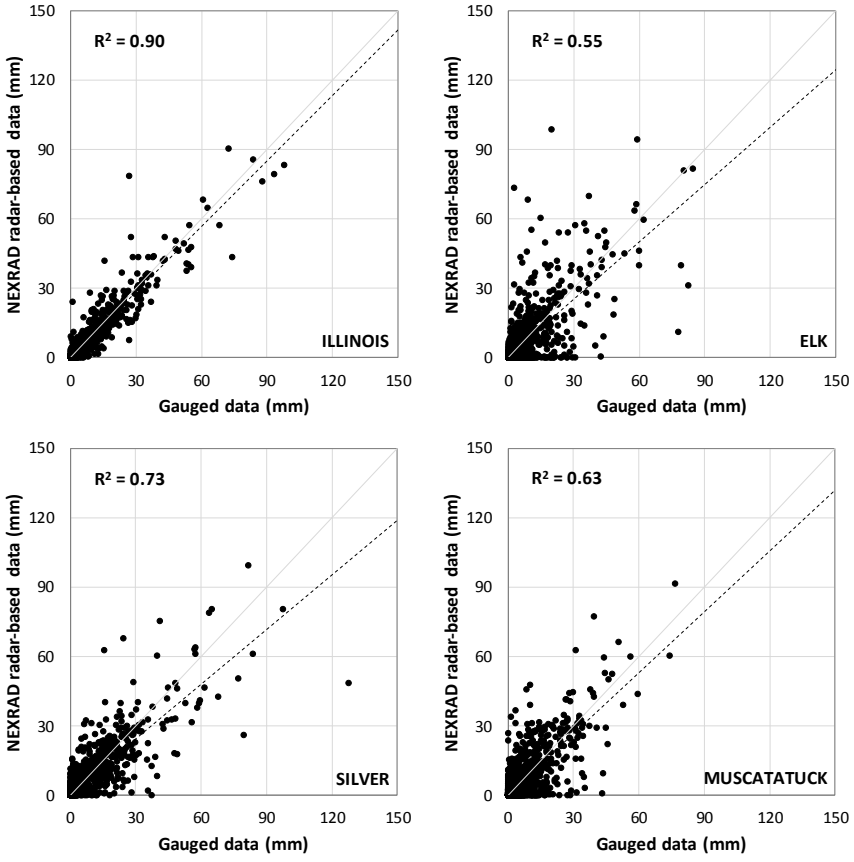

Figure 4.7 Scatter plots comparing radar-based and gauged data (areal average)

As shown in scatter plots (Figure 4.7), both rainfall estimates have significant correlations for amounts. The data for the Illinois River basin show the highest correlation (R^2 0.90) in contrast to the lowest correlation for Elk River (R^2 0.55). Underestimation trends also can be seen for larger values of NEXRAD data; these are the same trends as hourly data validation results for storm event application in a previous chapter (Chapter 3).

On the other hand, a better correlation (R^2 0.74) can be found in a scatter plot (Figure 4.8) for a different gauge in the Elk River which showed the lowest correlation (R^2 0.55). In this case, since only one rain gauge (G6; Figure 4.1), which was used for the Illinois River's Thiessen polygon creation as well with relatively high weights (G3, 49.6%), resulted in more significant correlation, it can be inferred that specific gauge data were commonly utilized for quality control (calibration or data correction) of NEXRAD radar-based precipitation products.

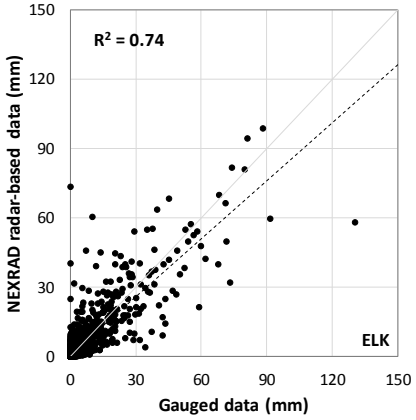

Figure 4.8 Scatter plot showing enhanced correlation value for different rainfall gauges compared with NEXRAD data in the Elk River

The amount of total precipitation is almost the same for both NEXRAD and gauged data; NEXRAD rainfall are slightly overestimated by 1.0 and 1.3% in the Elk and Muscatatuck Rivers, and underestimated by 0.3 and 2.6% in Illinois River and Silver Creek, respectively (in Table 4.3).

Table 4.3 Total precipitation (long-term storm events) for study areas

Watershed	Precipitation Total (mm)										
	NEXRAD radar-based data (spatially distributed)				Gauged data (spatially averaged; lumped)						
	Min.	Max.	Skew.	Avg.*	G1	G2	G3	G4	G5	G6	Avg.
Illinois River near Tahlequah	5920	7362	0.27	6516 (0.31↓)	6114	6906	6398	6724	-	-	6536
Elk River near Tiff City	6105	7500	-0.06	6873 (0.95↑)	7012	7387	6949	7025	6906	6398	6809
Silver Creek near Sellersburg	7515	8557	0.23	7624 (2.64↓)	7702	7825	7911	-	-	-	7831
Muscatatuck River near Deputy	6923	8367	0.07	7441 (1.32↑)	7907	7877	6862	-	-	-	7344

Skew. - skewness; Avg.*- areal average, values in parenthesis refer to over or underestimated % from gauged data; G - rain gauge for areal average precipitation (Thiessen polygon weighted)

4.5.1.2 Spatial Variability

The spatial variability of total cumulative NEXRAD precipitation depth for each watershed's selected long-term (6 years) storm events are shown in Figure 4.9; the original approximately 4 km by 4 km HRAP grid based NEXRAD precipitation data were resampled as 2 km by 2 km regular grid data adopting Albers Equal Area Conic map projection system. As expected, there are significant differences in the spatial patterns with each long-term events' gridded rainfall amounts. For each of the four watersheds, the total precipitation amounts in each grid cell differed about 20%;

differences of 24% (1442 mm) occurred in the Illinois River (largest watershed) with a skewness value of 0.27, whereas 14% differences (1042 mm, skewness 0.23) occurred in Silver Creek (smallest basin). However, these total precipitation differences do not describe the spatial distribution of input rainfall amounts for the actual hydrological modeling, since the estimation of spatially distributed excess rainfall (runoff depth) to convolute a direct runoff flow hydrograph with a set of separated unit hydrographs is conducted on a daily basis; each day's spatially distributed precipitation data are used as model (Distributed-Clark) inputs.

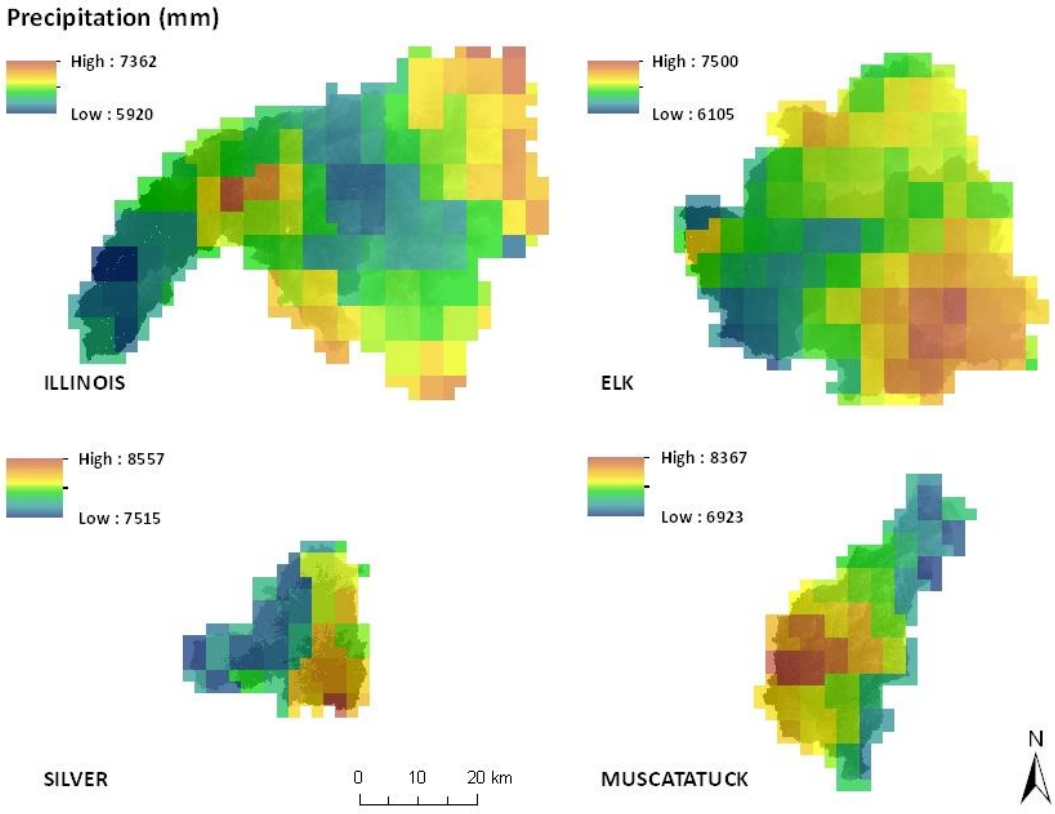

Figure 4.9 Spatial variability of total cumulative precipitation depth (mm) for four study areas, as obtained by NCEP Stage IV products

4.5.2 Model Development

4.5.2.1 Time-Area Diagram (Isochrones) and Separated Unit Hydrograph

The model development results of the flow travel time map, time-area diagram (isochrones), and separated unit hydrographs for each study watershed are represented in Figures 4.10 and 4.11.

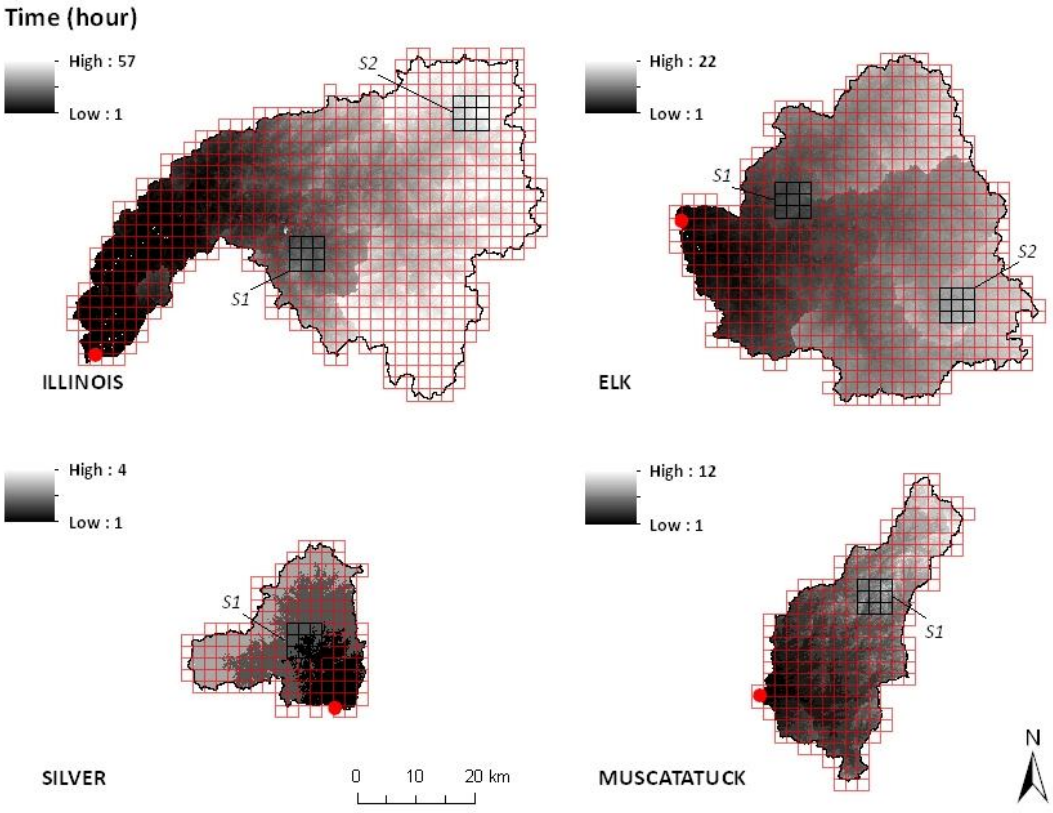

Figure 4.10 Flow travel time map (from calibrated *i*; Table 4.4) for the time-area diagram development

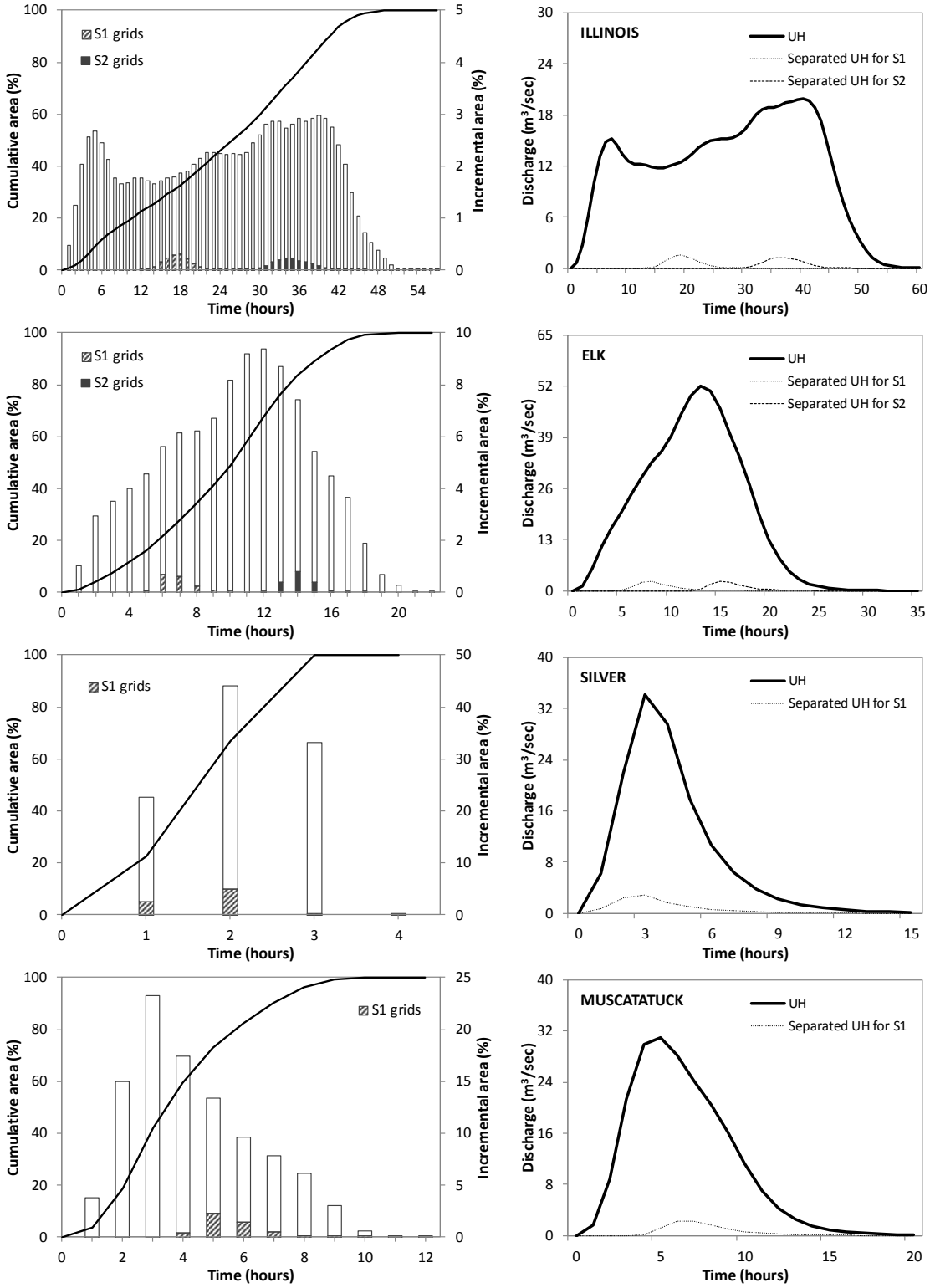

Figure 4.11 Time-area diagram (from calibrated *i*; Table 4.4, left) and separated unit hydrograph (default *R*; 2 hour, right)

In the time-area diagram and unit hydrograph (Figure 4.11), the selected areas' (S1 and S2; NEXRAD grid cells) results, which represent the portion of incremental area contributions (one hour interval) of flow to the outlet and separated unit hydrographs can be identified. These grid cell separated unit hydrographs can consider NEXRAD data based on spatially distributed long-term excess rainfall, which are estimated using the continuous SCS CN method (time-varied gridded CN) presented in this chapter, to obtain a watershed outlet's long-term direct runoff flow hydrograph.

4.5.2.2 Time-Varied Gridded CN

The initial gridded CN maps corresponding to each study watershed's subareas (NEXRAD grid cells) are shown in Figure 4.12. In the continuous SCS CN method, these gridded CN (histogram of CN values) are first utilized for estimating each grid cell's initial retention storage (S_0) and rainfall-runoff depth (Q_1), and then these estimated values are averaged (counts weighted) with a histogram (gridded CN) of given subarea boundary (NEXRAD grid); this internal process creates the subarea's average initial retention storage ($S_{0(avg.)j}$) and runoff depth ($Q_{1(avg.)j}$) as shown in Figure 4.4 (spatially distributed excess rainfall; NEXRAD precipitation estimated).

Then, corresponding to the time-varied potential maximum retention (S_t) and SCS curve number (CN_t,) which can be calculated by Equation (4.9), the CN values of gridded CN can be updated. In this case, however, the histogram of gridded CN is the same as initial

cell count weights since the distributions of CN values for given subareas (NEXRAD grid cells) are not changed.

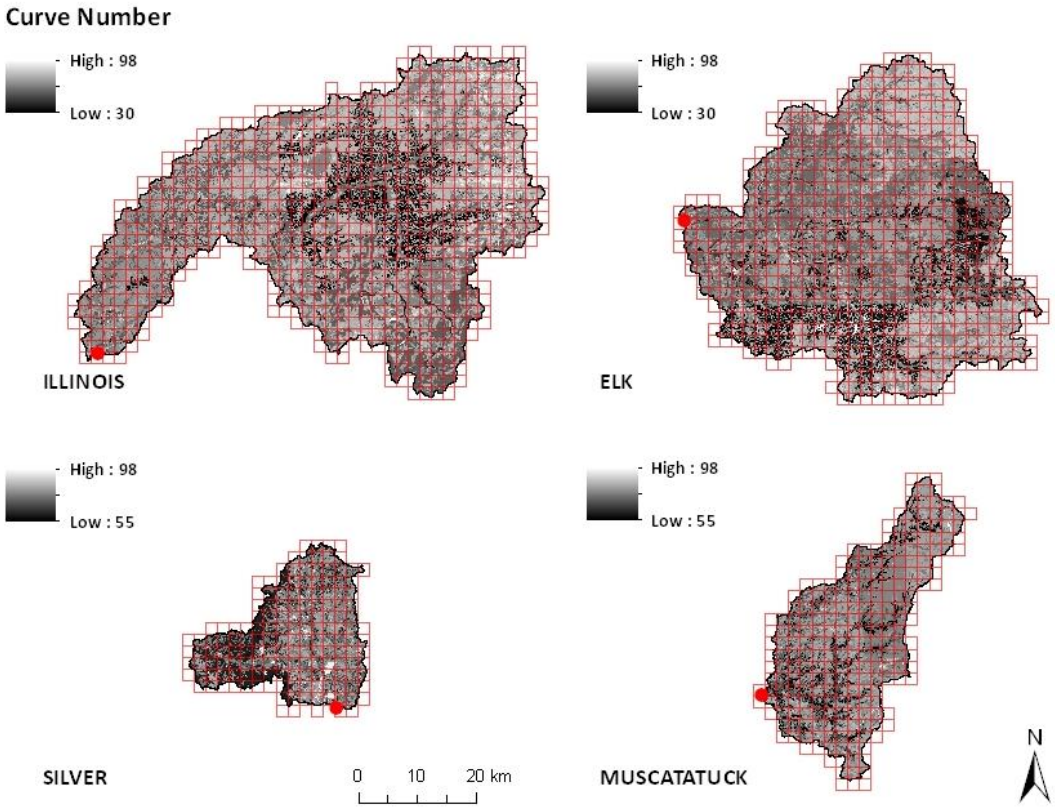

Figure 4.12 Initial gridded CN map for subarea's (NEXRAD radar-based grid cell) average runoff depth (at first time step) estimation

4.5.3 Model Performance

4.5.3.1 Model Setup

A model setup test was performed to examine the necessity of a warm-up period for the application of Distributed-Clark model's spatially distributed long-term rainfall-runoff flow simulation using the continuous SCS CN method. For the models of Illinois River and Silver Creek (the largest and smallest areas), one and a half years (from January 2009 to June 2010) of simulation results from three cases of different starting points (the first day of January and July 2009 and January 2010) were investigated. In this simulation, the model parameter values of i (0.05 and 17.50 mm/hour) and R (15.0 and 20.0 hour) were acquired from previously calibrated ones for storm event applications, and λ and F_c were assumed as default values of 0.05 and 2.5 mm/day, respectively.

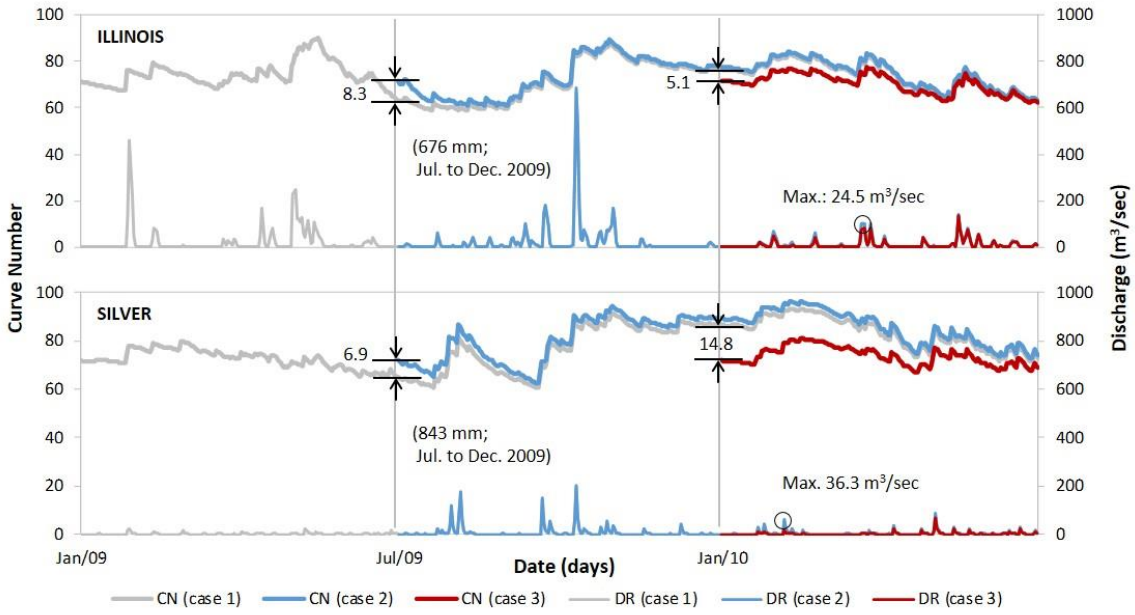

Figure 4.13 Curve number (averaged) and direct runoff flow variations showing differences of model simulation results for the different starting points

Judging from differences for simulation results of average CN and direct runoff (DR) flow variations shown in Figure 4.13, two common simulation periods (from July 2009 and January 2010 to June 2010) can be considered as a possible warm-up period for each watershed model. Whereas a six-month period is required to narrow the gap between each cases' simulation results for the Illinois River model, at least one year is needed for the Silver Creek model to obtain similar amounts of CN and flow discharge.

The warm-up periods were related to the initial average CN value gap and associated storm events during these simulation periods, regardless of watershed size. For instance, the Silver Creek model shows a larger difference for initial CN (in case 3) and storm events, which can delay CN gap decreases for a large gap in CN values (in case 2), than the Illinois River model for their simulations (Figure 4.13); so, the Silver Creek model requires a more extended period to warm-up. However, this warm-up effect for direct runoff flow is not critical to evaluate model performance, particularly in using statistics (i.e., E_{NS}, R^2, *PBIAS*, and *RMSE* values). Hence, a warm-up period for long-term model simulation was ignored for the following cases of calibration and validation.

4.5.3.2 Calibration and Validation

With respect to the continuous SCS CN method-based long-term hydrologic simulation model (Distributed-Clark) for all four study watersheds, calibration and validation to improve fit of simulation hydrographs against observed streamflow were conducted. A 4-year calibration (from 2009 to 2012) and a 2-year validation (from 2013 to 2014) were

performed for a total simulation period of 6 years; this followed a split-sample test (Klemes, 1986) which splits a total period into two consecutive non-overlapping phases of calibration and validation. The default long-term Distributed-Clark model utilizing parameter values of the average intensity of 2-year, 24-hour rainfall; 2 hour; 0.05 (fixed); 2.50 mm/day for i; R; λ; and F_c, respectively, was calibrated using rainfall inputs for spatially distributed NEXRAD precipitation and spatially averaged gauged data for a given period (4 years; no warm-up); in particular, this was mainly made to match the total volume of observed flow data. A 2-year validation was also accomplished with the same parameter values for model calibration, except for the F_c parameter which is needed for adjusting the volume of simulated hydrographs to match with observed streamflow. These estimated parameter values are shown in Table 4.4.

Among the estimated parameter values, while the vertical net incoming flux, i, and storage coefficient, R values are the same as previously studied ones (except the Illinois River case; 15 to 5 hours) for storm event flow prediction which considers high flow cases of model calibration, the initial abstraction coefficient, λ, values are determined differently from previous applications; a value of 0.05 is fixed for all calibration. This is because the developed continuous SCS CN method computes updated watershed runoff conditions using the time-varied soil moisture equation with infiltration, F_a, and evapotranspiration, ET, terms in Equation (4.9). Thus, the λ does not need to be assumed with different values for each time step of excess rainfall computation; but conditional initial abstraction, $I_{a,t}$, was applied for this study's continuous excess rainfall estimation. Instead, the static infiltration, F_c, which also can play a role in runoff depth adjustment,

was used to match with observed flows, assuming a constant value that can be regarded as an average permanent infiltration (i.e., percolation) throughout the simulation period in each watershed.

In this study's application of long-term rainfall-runoff flow prediction, however, there is a limitation to calibrate the model with observed hydrographs using only one flow phase of unit hydrograph (e.g. high flow case for storm event simulation) for the entire duration of discontinuous storms, since most rainfall-runoff depths are not equally routed; even for the same depth of excess rainfall, a routed (convoluted) direct runoff hydrograph can be different according to selection of unit hydrograph. Thus, in order to enhance model simulation performance, the unit hydrograph for low flow cases, which can be applied to runoff routing for small events or model calibration for delayed flows from previous events, was introduced. For this unit hydrograph derivation, the *R* parameter value was changed from the calibrated unit hydrograph for high flow cases. The *i* value can be used as well for this calibration, but it is less sensitive than the *R* parameter to create attenuated and delayed flows; rather, it can be utilized to shift the peak of unit hydrographs. For reference, these calibrated *R* parameters for high and low flows were represented as R_{high} and R_{low} in Table 4.4.

As the last consideration for long-term Distributed-Clark model calibration, a threshold of storm amounts (excess rainfall) for dividing high and low flow phase unit hydrographs was adopted. Hence, the conditional unit hydrograph adoption for different amounts of daily runoff precipitation to convolute direct runoff hydrographs could also be performed

in model calibration. These calibrated thresholds and different phase's *R* values in each study watershed's model are represented in Table 4.4 as well. In addition, the results of intensive calibration to find reasonable and best matched simulated hydrographs using many cases of low flow unit hydrographs (having different R_{low} values) are also listed in Appendix C (Tables C 1 to C 8).

Table 4.4 Parameter values of model calibration and validation results for spatially distributed and averaged rainfall data simulations

Watershed	Parameters	Un-calibrated value	Resulted value	
			NEXRAD data	Gauged data
Illinois River near Tahlequah	i	4.23	0.05	0.05
	R_{high}	2.0	5.0	5.0
	R_{low}	2.0	42.0	30.0
	(Threshold)	(-)	(10 mm)	(20 mm)
	λ (ARC)	0.050 (II)	0.050 (II)	0.050 (II)
	F_c (cali./vali.)*	2.50	4.82/6.95	5.10/6.46
Elk River near Tiff City	i	4.13	0.52	0.05
	R_{high}	2.0	7.0	7.0
	R_{low}	2.0	42.0	30.0
	(Threshold)	(-)	(20 mm)	(30 mm)
	λ (ARC)	0.050 (II)	0.050 (II)	0.050 (II)
	F_c (cali./vali.)*	2.50	2.30/4.45	3.51/2.29
Silver Creek near Sellersburg	i	3.28	17.5	17.5
	R_{high}	2.0	20.0	20.0
	R_{low}	2.0	20.0	24.0
	(Threshold)	(-)	(-)	(40 mm)
	λ (ARC)	0.050 (II)	0.050 (II)	0.050 (II)
	F_c (cali./vali.)*	2.50	2.06/4.31	3.41/4.61
Muscatatuck River near Deputy	i	3.25	2.25	2.25
	R_{high}	2.0	7.5	7.5
	R_{low}	2.0	24.0	24.0
	(Threshold)	(-)	(50 mm)	(50 mm)
	λ (ARC)	0.050 (II)	0.050 (II)	0.050 (II)
	F_c (cali./vali.)*	2.50	1.53/1.97	2.10/2.18

i - vertical net incoming flux (mm/hour); $R_{high/low}$ - storage coefficient (hour) for high/low flows; λ - initial abstraction coefficient; F_c - static infiltration (mm/day)

* F_c for calibration (cali.) and validation (vali) are differently estimated

In summary, the suggested step-by-step procedures of manual calibration for long-term simulation in Distributed-Clark are as follows:

- (step 1) Adjust the F_c parameter value (λ value is fixed with 0.05) for matching the overall volume between simulated flow and observed streamflow; it estimates runoff depths for a given simulation period (with the continuous SCS CN method).
- (step 2) Calibrate the R parameter (R_{high}) to obtain a unit hydrograph for high flow cases; it is recommended to use the same R value for storm event application (if applicable) or find new ones (i and R) which can fit the peak of big storm events (needed several calibration targets).
- (step 3) Calibrate the R parameter (R_{low}) to obtain a unit hydrograph for low flow cases; it should match with shapes of low flow hydrographs for small events or delayed flows from the previous events.
- (step 4) Set a threshold of storm runoff precipitation depth which divides high and low flow phases for application of different unit hydrographs daily direct runoff convolution; this step should be simultaneously conducted with step 3; an intensive calibration is required using many cases of low flow unit hydrographs (having different R_{low} values).

The simulated and observed long-term flow hydrographs for total streamflow are represented in Figure 4.14 to show graphical goodness-of-fit of each model's calibration (4 years) and validation (2 years); the separated baseflow was added to create simulation outputs. In most simulation periods, model results for both inputs of spatially distributed NEXRAD precipitation and spatially averaged gauged rainfall data showed similar variations with their observed daily flows, but some cases of extremely large storm events and several of mid-sized flows, particularly in the Muscatatuck River model, showed significant differences. This may indicate the limitations of the model that generates runoff using a simple soil moisture accounting method and routes runoff only applying two high and low phases of unit hydrograph for various daily storm events.

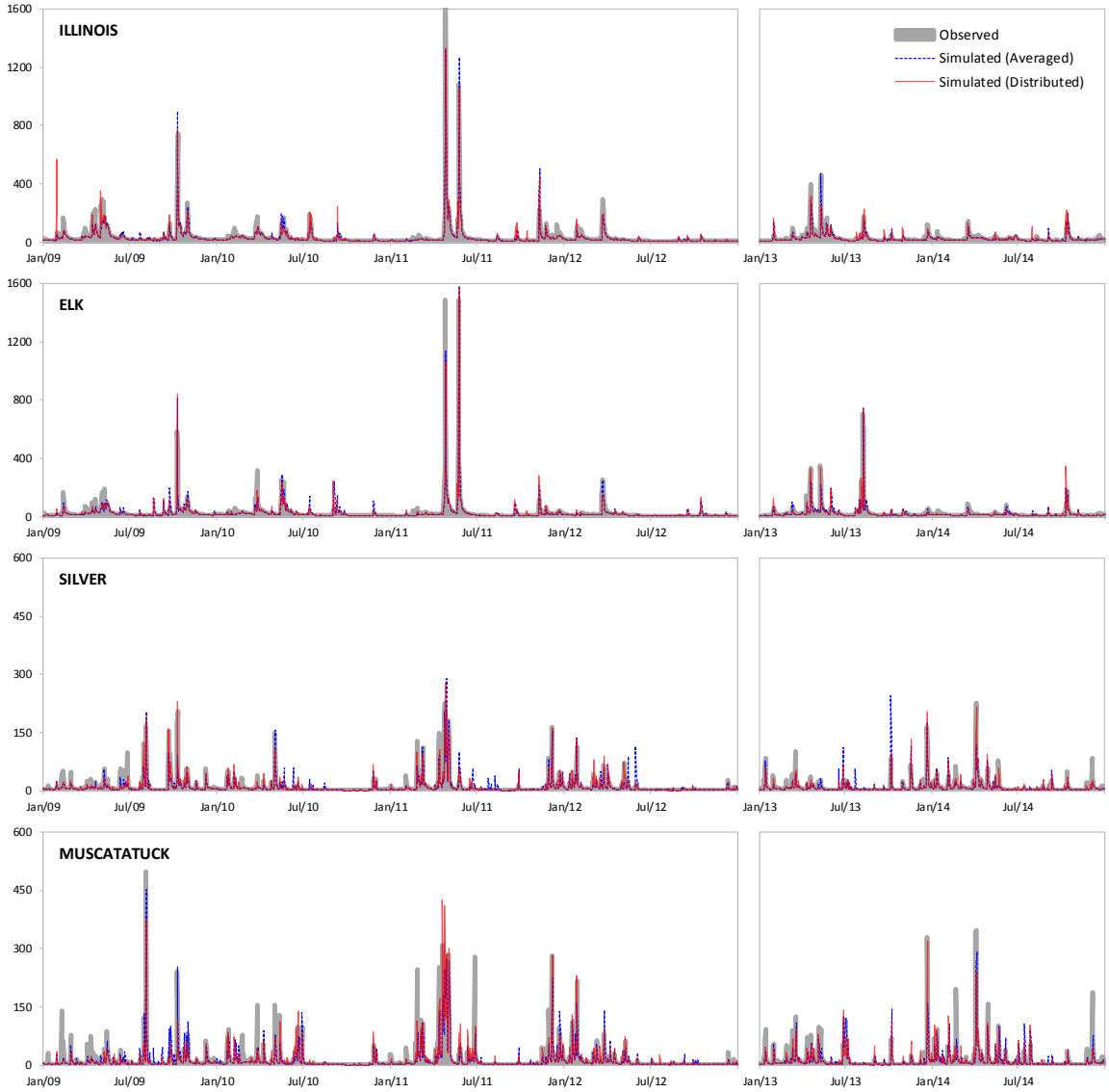

X-axis represents simulation date (days) and Y-axis represents discharge (m^3/sec)

Baseflow separation (recursive digital filter method): Illinois River and Silver Creek (*a* 0.980, BFI_{max} 0.80), Elk River (*a* 0.995, BFI_{max} 0.80), and Muscatatuck River (*a* 0.980, BFI_{max} 0.50)

Figure 4.14 Graphical results (observed and simulated streamflow hydrographs) of model calibration (4 years; left) and validation (2 years; right) for four study areas

So, if more variable unit hydrographs (derived from various excess rainfall intensities or storage coefficients) are adopted for different rainfall patterns in the flow calibration process, better fit of simulated results against observed flow hydrographs may result.

The statistical results of model calibration and validation for direct runoff and streamflow of four study watersheds are shown in Table 4.5. The overall model performance (average statistics) for total streamflow E_{NS}, R^2, and *PBIAS*, which compare both distributed and averaged rainfall data simulation results against observed data, are 0.66, 0.68, and 0.08% for calibration, and 0.55, 0.58, and 0.19% for validation, respectively. However, these results differ depending on study watersheds. In particular, whereas the Muscatatuck River model showed poorer performances (streamflow E_{NS} 0.39, R^2 0.44, and *PBIAS* 0.94%), the Illinois River model had relatively good statistical results (streamflow E_{NS} 0.76, R^2 0.77, and *PBIAS* 0.06%); these may be caused by differences in data quality or watershed scale which can affect simulated flow.

Table 4.5 Statistical results of model calibration and validation for four study areas

Watershed	Statistics	Distributed (NEXRAD data)		Averaged (Gauged data)	
		Direct Runoff	Streamflow	Direct Runoff	Streamflow
Illinois River near Tahlequah	E_{NS}	0.75 (0.51)	0.83 (0.69)	0.78 (0.46)	0.85 (0.66)
	R^2	0.75 (0.55)	0.83 (0.70)	0.78 (0.55)	0.85 (0.69)
	PBIAS (%)	-0.24 (0.22)	-0.09 (0.07)	-0.16 (-0.01)	-0.06 (-0.00)
	RMSE (m^3/sec)		36.44 (17.60)		34.17 (18.42)
Elk River near Tiff City	E_{NS}	0.80 (0.81)	0.82 (0.83)	0.37 (0.37)	0.44 (0.45)
	R^2	0.80 (0.82)	0.82 (0.84)	0.43 (0.42)	0.48 (0.49)
	PBIAS (%)	0.02 (0.89)	0.01 (0.46)	-0.16 (-0.13)	-0.08 (-0.07)
	RMSE (m^3/sec)		32.21 (17.87)		57.04 (32.13)
Silver Creek near Sellersburg	E_{NS}	0.64 (0.55)	0.76 (0.68)	0.42 (0.15)	0.61 (0.40)
	R^2	0.65 (0.59)	0.76 (0.70)	0.47 (0.35)	0.63 (0.48)
	PBIAS (%)	-0.11 (-0.24)	-0.06 (-0.13)	-0.03 (-0.15)	-0.02 (-0.08)
	RMSE (m^3/sec)		10.28 (10.01)		13.01 (13.80)
Muscatatuck River near Deputy	E_{NS}	0.47 (0.42)	0.53 (0.47)	0.31 (0.08)	0.39 (0.16)
	R^2	0.51 (0.44)	0.57 (0.49)	0.38 (0.21)	0.43 (0.26)
	PBIAS (%)	-0.08 (-0.41)	-0.06 (-0.30)	-0.24 (-0.54)	-0.18 (-0.40)
	RMSE (m^3/sec)		23.00 (21.12)		26.31 (26.44)
Average	E_{NS}	0.67 (0.57)	0.74 (0.67)	0.47 (0.27)	0.57 (0.42)
	R^2	0.68 (0.60)	0.75 (0.68)	0.52 (0.38)	0.60 (0.48)
	PBIAS (%)	0.11 (0.44)	0.06 (0.24)	0.15 (0.21)	0.09 (0.14)

Average - E_{NS} and R^2 arithmetic mean, *PBIAS* arithmetic mean of absolute value; Values in parenthesis refer to validation results

4.5.3.3 Comparisons

The average statistical values of model simulation results for long-term spatially distributed NEXRAD radar-based and spatially averaged gauged rainfall inputs are compared in Table 4.5. In this comparison, the Distributed-Clark model using NEXRAD precipitation products shows better performance (direct runoff 0.62, 0.64, and 0.33%; streamflow 0.71, 0.72, and 0.15% for E_{NS}, R^2, and *PBIAS* values, respectively) than the same model with gauged data (direct runoff 0.37, 0.45, and 0.18%; streamflow 0.50, 0.54, and 0.12%); this shows substantial differences for E_{NS} of 42.0% (0.50 to 0.71) and R^2 of 33.3% (0.54 to 0.72) in total streamflow.

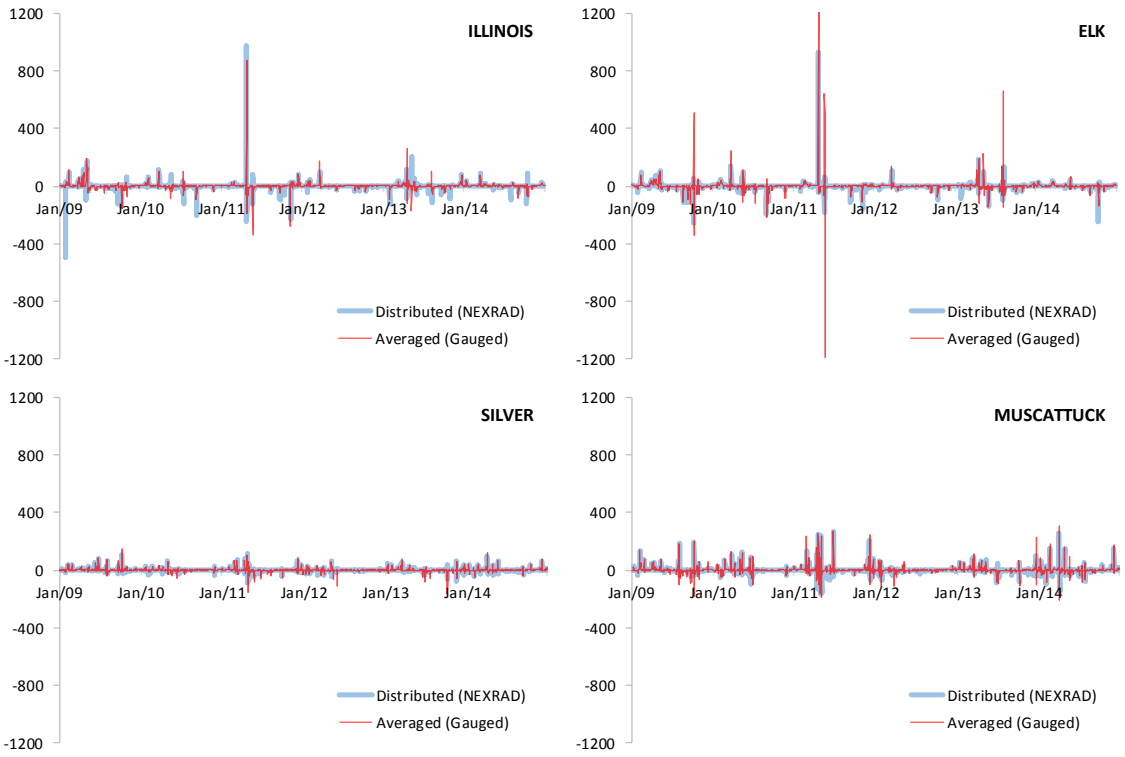

X-axis represents simulation date (days) and Y-axis represents discharge differences (m^3/sec)

Figure 4.15 Differences between observed and simulated streamflow hydrographs for four study areas

Additional specific differences also can be found in Figure 4.15, which represents each watershed model's simulated flow gaps from observed streamflow hydrographs; the root mean squared error, *RMSE*, values are 31.43, 28.24, 10.19, and 22.39 m^3/sec in each distributed data input model (for the Illinois and Elk Rivers, Silver Creek, and Muscatatuck River, respectively) and 29.85, 50.12, 13.28, and 26.35 m^3/sec in averaged rainfall input models. Among these, the Elk River case shows the most considerable *RMSE* differences including many outliers, which can cause poor performances for model evaluation, particularly in averaged gauged data simulation. Also, it can be noticed that these substantial gaps come from input rainfall data, since the validation results of precipitation between NEXRAD and gauge observations in the previous paragraphs provided the lowest correlation (R^2 0.55) in the Elk River. The Illinois River case also supports this rainfall data dependency in model simulation with the highest correlation (R^2 0.90), presenting similar *RMSE* values in both inputs and even better performance for gauged data input. The other cases for Silver Creek and Muscatatuck River also show some differences for rainfall values and simulation results, with better performances for spatially distributed precipitation input.

These potentially suggest NEXRAD radar-based precipitation are more reliable than gauged data for use in long-term rainfall-runoff flow simulation. Even though these radar reflectivity-based quantitative precipitation estimation (QPE) values are indirectly produced by QPE algorithms and validated (quality controlled) using gauge observations, they can capture spatially distributed amounts in watersheds, which cannot be obtained from the several surrounding gauge observations based on watershed average rainfall (e.g.

Thiessen method). Of course NEXRAD data can be underestimated or overestimated relative to actual amounts in particular storm events with pre-determined algorithms, but data quality issues for gauged rainfall data are also prevalent with more missing or error records than continuously available gridded NEXRAD data. Also, another possible data constraint for watershed flow prediction can be in streamflow observations which are typically estimated by indirect regression methods using water gage height; one of the reasons for the poorer performance in the Muscatatuck River model's distributed and averaged data simulation (Figures 4.14 and 4.15) may be caused from this uncertainty.

Figure 4.16 shows watershed model results of average curve number variations for spatially distributed and averaged rainfall data simulations. The initial average CN values of 71.5, 67.5, 71.7, and 75.5 for the Illinois and Elk Rivers, Silver Creek, and Muscatatuck River, respectively, were changed corresponding to different input types of precipitation, having different variation in each watershed. These are likely because of the amount and spatial variability of input rainfall and the associated CN values for each subarea. In cases of spatially distributed precipitation input models, in particular, the numbers of 717, 624, 159, and 239 different rainfall amounts and gridded CN values were used for each respective simulation; the highest and lowest CN variations also can be seen in Figure 4.16, whereas only one average value of rainfall and CN are utilized for each averaged rainfall data input model simulation. These time-varied CN were used for estimating daily excess rainfall and updating daily potential maximum retention. On the other hand, since these estimated time-varied CN values may not describe actual

watershed conditions for accurate runoff calculation, it may be another possible explanation (error) for disagreement of simulated and observed streamflow hydrographs.

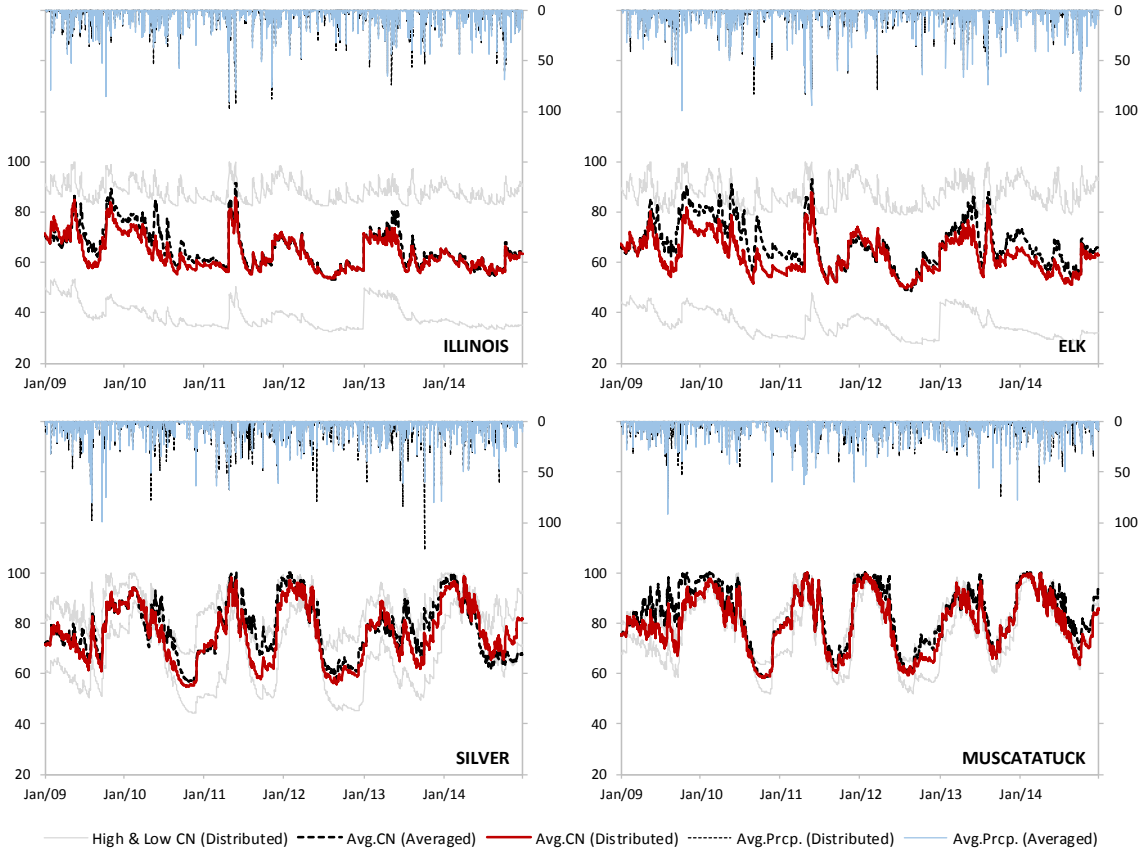

X-axis, Primary Y-axis, and Secondary Y-axis represent simulation date (days), Curve number, and Precipitation (mm), respectively

Figure 4.16 Average curve number variations for spatially distributed and averaged rainfall data simulations for four study areas

Another comparison of model simulation results using NEXRAD data for a 4-year calibration period to evaluate logic for conditional initial abstraction, I_a, in a continuous SCS CN method is presented in Figure 4.17 and Table 4.6 with result differences and statistical values, respectively. Since the conditional I_a logic considers the amounts of

initial abstraction according to previous precipitation and does not subtract the full amount of initial abstraction (λS) at every time step for continuous rainfall-runoff simulation, it can affect the volume of simulated runoff flow. In this comparison, thus, because each total volume of simulated flows (with and without the conditional I_a logic) was matched with observed total flow volume in model calibration, daily volume gaps which occurred along with daily rainfall in simulated flows can be compared as conditional I_a logic effects. Figure 4.17 represents these daily flow volume differences between model simulation results in each watershed.

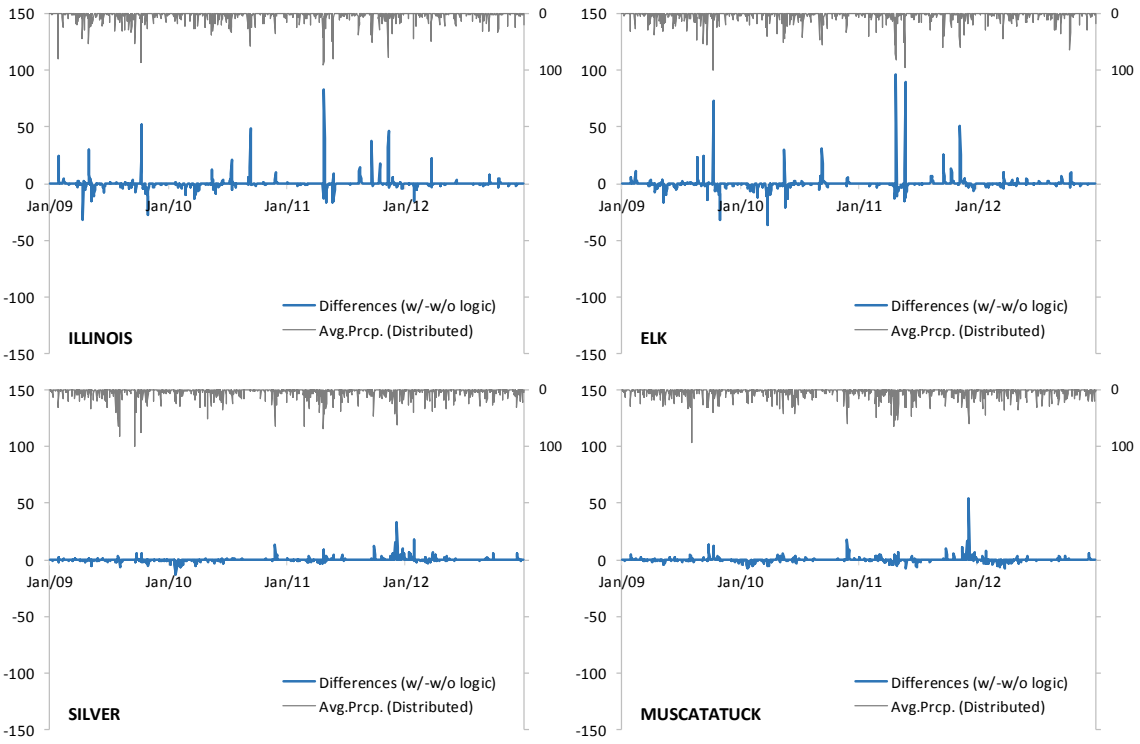

X-axis, Primary Y-axis, and Secondary Y-axis represent simulation date (days), discharge differences (m^3/sec), and Precipitation (mm), respectively

Figure 4.17 Flow differences between model simulation results with and without conditional I_a logic for four study areas

However, these differences did not have much effect on overall model performances. The *RMSE* values only differed 0.05 to 1.30 m^3/sec. This is because even though the initial abstraction formula (λS) considers the retention parameter S, the proportion of λ was fixed with a relatively small 0.05 value for overall model calibration. Nevertheless, the four study watershed average statistics for model performance evaluation against observed streamflow data were slightly enhanced for E_{NS} of 1.4% (0.73 to 0.74) and R^2 of 1.4% (0.74 to 0.75) in total streamflow simulations of the conditional I_a logic models.

Table 4.6 Statistical results (model calibration period) for spatially distributed data simulations (with and without conditional I_a logic)

Watershed	Statistics	With conditional I_a logic		Without conditional I_a logic	
		Direct Runoff	Streamflow	Direct Runoff	Streamflow
Illinois River near Tahlequah	E_{NS}	0.75	0.83	0.73 (0.02↓)	0.81 (0.02↓)
	R^2	0.75	0.83	0.74 (0.01↓)	0.82 (0.01↓)
	PBIAS (%)	-0.24	-0.09	-0.01 (0.23↑)	-0.00 (0.09↑)
	RMSE (m^3/sec)		36.44		37.74 (1.30↑)
Elk River near Tiff City	E_{NS}	0.80	0.82	0.78 (0.02↓)	0.81 (0.01↓)
	R^2	0.80	0.82	0.79 (0.01↓)	0.82 (-)
	PBIAS (%)	0.02	0.01	-0.04 (0.06↓)	-0.02 (0.03↓)
	RMSE (m^3/sec)		32.21		33.45 (1.24↑)
Silver Creek near Sellersburg	E_{NS}	0.64	0.76	0.64 (-)	0.76 (-)
	R^2	0.65	0.76	0.65 (-)	0.77 (0.01↑)
	PBIAS (%)	-0.11	-0.06	-0.09 (0.02↑)	-0.05 (0.01↑)
	RMSE (m^3/sec)		10.28		10.15 (0.13↓)
Muscatatuck River near Deputy	E_{NS}	0.47	0.53	0.47 (-)	0.53 (-)
	R^2	0.51	0.57	0.50 (0.01↓)	0.56 (0.01↓)
	PBIAS (%)	-0.08	-0.06	-0.05 (0.03↑)	-0.04 (0.02↑)
	RMSE (m^3/sec)		23.00		23.05 (0.05↑)
Average	E_{NS}	0.67	0.74	0.66 (0.01↓)	0.73 (0.01↓)
	R^2	0.68	0.75	0.67 (0.01↓)	0.74 (0.01↓)
	PBIAS (%)	0.11	0.06	0.05 (0.06↓)	0.03 (0.03↓)

Average - E_{NS} and R^2 arithmetic mean, *PBIAS* arithmetic mean of absolute value; Values in parenthesis refer to results differences

4.6 Summary and Conclusions

A continuous SCS CN method which can consider time-varied SCS CN values was developed based on the original SCS CN method with a revised soil moisture accounting approach to estimate long-term runoff depth for discontinuous storm events. Then, this method was combined with the GIS-based spatially distributed Clark's unit hydrograph method, Distributed-Clark (hybrid hydrologic model), for spatially distributed long-term rainfall-runoff flow prediction, introducing conditional unit hydrograph adoption which can perform runoff precipitation depth-based flow convolution. In order to implement this long-term hydrologic application, Python script tools including NEXRAD and required spatial data processing, long-term spatially distributed excess rainfall estimation, and conditional unit hydrograph adoption-applied direct runoff hydrograph convolution were developed in a GIS platform. Case studies of Distributed-Clark application to long-term rainfall-runoff routing (flow prediction) for four river basins using 6-years of daily inputs of spatially distributed NEXRAD radar-based precipitation provided the following results and model performances.

1. NEXRAD data (watershed areal average rainfall) validation results relative to gauged rainfall showed various correlations (R^2 0.55 to 0.90) and underestimated trends in larger values of NEXRAD radar-based precipitation with almost the same total amounts for each watershed; because model simulations were conducted on a daily basis, these different correlations and spatial variability of daily NEXRAD data which can be inferred from that of total cumulative

precipitation (skewness ranges -0.06 to 0.27) affected model performance for overall long-term discontinuous storm event flow prediction.

2. Model output comparison with observed flow data in NEXRAD data application demonstrated overall performances of E_{NS} 0.62, R^2 0.64, and *PBIAS* 0.33% in direct runoff and E_{NS} 0.71, R^2 0.72, and *PBIAS* 0.15% in total streamflow with *RMSE* values of 10.19 to 31.43 m^3/sec (the smallest to largest watersheds, respectively). These also showed better fit (E_{NS} of 42.0% and R^2 of 33.3% increase in total streamflow) than results from the same models which used spatially averaged gauged rainfall data.

These application results and model performances indicate that a continuous SCS CN method can be a useful technique to estimate spatially distributed long-term rainfall-runoff generation and routing, particularly in combination with Distributed-Clark; this combined modeling approach required relatively few parameters as well. Model simulation results (i.e., performance against observed data) were dependent on input rainfall data, and NEXRAD precipitation inputs were more appropriate for long-term continuous simulations than gauge observations due to fewer issues with data quality and acquisition.

On the other hand, model simulation results for a 4-year calibration period to evaluate a conditional initial abstraction, I_a, logic in a continuous SCS CN method did not result in significant differences; the average statistics for performance of all four study models

against observed flow were slightly enhanced (1.4 % of both E_{NS} and R^2 increase in total streamflow) in the models that adopted a conditional initial abstraction logic.

Future research might include the following topics: (1) improvement of the conditional unit hydrograph adoption using not only two phase of unit hydrographs (high and low flows) but also other multiple cases of unit hydrographs (e.g. time variant unit hydrographs) and (2) baseflow computation that assumes the calibrated value of static infiltration, F_c, as baseflow portion (percolation), adding other geological parametric components (e.g. hydraulic conductivity, etc.) for soil moisture behavior in groundwater flows can be applicable.

CHAPTER 5. SYNTHESIS

5.1 Summary

This research was conducted to develop, describe, and evaluate methodologies for relatively simple watershed-scale hydrological modeling (hybrid hydrologic model), particularly for spatially distributed short- and long-term rainfall-runoff generation and runoff routing using state-of-the-art spatial data in a GIS environment. The specific objectives of the dissertation were to:

1. Develop and evaluate a GIS-based spatially distributed Clark's unit hydrograph method (Distributed-Clark) for spatially distributed rainfall-runoff routing.
2. Develop a NEXRAD data processing tool for spatiotemporally varied precipitation data generation and apply Distributed-Clark to NEXRAD data-based spatially distributed rainfall-runoff routing.
3. Present a continuous SCS CN method to estimate long-term discontinuous storm runoff depth and combine and evaluate Distributed-Clark for spatially distributed long-term rainfall-runoff routing (flow prediction).

A GIS-based spatially distributed Clark's unit hydrograph method (Distributed-Clark), a lumped conceptual and distributed feature model (hybrid hydrologic model), was

developed and evaluated under the first objective. In Distributed-Clark, a simple approach using spatially decomposed GIS-based Clark's unit hydrograph (separated unit hydrograph) was utilized for the implementation of spatially distributed rainfall-runoff routing with CN technique estimated excess rainfall. The calibrated models for four study river watersheds using all three parameters for unit hydrograph derivation (vertical net incoming flux, *i*, and storage coefficient, *R*) and runoff depth calculation (initial abstraction coefficient, λ) showed relatively good fit against observed streamflow in single storm event simulations (total of 24 events) with Thiessen polygon-based spatially distributed rainfall data (direct runoff E_{NS} 0.84, R^2 0.86, and *PBIAS* 0.86%; streamflow E_{NS} 0.91, R^2 0.92, and *PBIAS* 0.32%) as well as slightly better fit (E_{NS} of 1.8% and R^2 of 2.1% increase in direct runoff) in comparison with the outputs of spatially averaged rainfall data simulations. In this application, however, the Thiessen polygon approach using limited rain gauges did not provide sufficient spatial distributions to fully evaluate the developed model.

In the second objective, the Distributed-Clark model's single storm event application was continued using more spatially distributed NEXRAD data (radar-based multi-sensor precipitation estimates), including development of a GIS-based automation tool for three steps of NEXRAD data processing (map projection transformation, modeling extent and NEXRAD grid subsetting, and raster and time-series data generation). As expected, model simulation results of case studies for four river basins also demonstrated relatively good performance (direct runoff E_{NS} 0.85, R^2 0.89, and *PBIAS* 3.92%; streamflow E_{NS} 0.91, R^2 0.93, and *PBIAS* 1.87%) for matching with observed flow. However, these did

not show a larger improvement compared with the results of spatially averaged rainfall simulations due to two cases of significantly underestimated (31.4 and 36.2%) NEXRAD precipitation amounts; E_{NS} of 3.0% and R^2 of 6.0% increase in direct runoff (E_{NS} of 1.2% and R^2 of 3.9% were increased from outputs of Thiessen polygon-based spatially distributed rainfall simulations). This indicated NEXRAD product quality issues may result in poor model performance. Nonetheless, spatially distributed NEXRAD radar-based precipitation estimates show better results in hydrologic application of rainfall-runoff flow predictions than other input data cases simulation, enabling improved predictions of flow volumes and peak rates which can be disregarded in hydrologic simulations for spatially averaged rainfall.

In order to continue model (Distributed-Clark) application for spatially distributed NEXRAD precipitation inputs from short-term single storm event to long-term discontinuous storm events, the last objective created a continuous SCS CN method which can consider time-varied SCS CN values to estimate long-term discontinuous storm runoff depth (the parameter of static infiltration, F_c, was added). Then, Distributed-Clark was combined with this method for spatially distributed long-term rainfall-runoff routing, introducing conditional unit hydrograph adoption which can perform runoff precipitation depth-based flow convolution. Case studies of long-term (total of 6 years) Distributed-Clark simulation for four river basins using spatially distributed NEXRAD radar-based daily precipitation demonstrated overall performances of E_{NS} 0.62, R^2 0.64, and *PBIAS* 0.33% in direct runoff and E_{NS} 0.71, R^2 0.72, and *PBIAS* 0.15% in total streamflow for model result comparison against observed flow, and these showed better

fit (E_{NS} of 42.0% and R^2 of 33.3% increase in total streamflow) than the same model applications using spatially averaged rainfall data. This indicated model simulation results were dependent on input rainfall data, and NEXRAD precipitation inputs were more appropriate for long-term continuous simulations than gauge observations by capturing spatially distributed rainfall amounts and having fewer missing or erroneous records.

For all of the above described GIS-based spatial data processing and model execution, Python script tools (ArcGIS based Python Toolbox) of DistributedClark_10.1 (storm event ver.) and DistributedClark_10.1 (continuous ver.) were developed in the ArcGIS 10.1 (ESRI, 2012) platform (Figures D 1 and D 2).

5.2 Model Characteristics

Since the Distributed-Clark model adopts a relatively simple runoff routing calculation procedure using the unit hydrograph method, this model has similar characteristics with the unit hydrograph approach. In simple terms, the unit hydrograph method can be described as a linear and time invariant hydrologic system approach. Therefore, unit hydrographs are applicable only when channel conditions remain unchanged and watersheds do not have appreciable storage. This condition is violated when the drainage area contains many reservoirs, or when the flow overflows into the flood plain, thereby producing considerable storage (Chow et al., 1988). In the same vein, the Distributed-Clark approach, which uses excess rainfall intensity (vertical net incoming flux, i) based time-area diagram (isochrones) and storage coefficient, R, to develop the unit hydrograph,

also cannot fully consider watershed conditions that are constantly changed by different flows, because Distributed-Clark takes only one representative case of these parameters (*i* and *R*) to calibrate an average watershed response flow generating and invariable unit hydrograph. To compensate for this feature of the unit hydrograph approach, the developed model adopted a spatial decomposition method which can derive a set of grid cell-based unit hydrographs (separated unit hydrographs). Also, for the long-term simulation Distributed-Clark model, two cases of unit hydrographs that can consider high and low flow phases were used, introducing conditional unit hydrograph adoption to perform runoff precipitation depth-based flow convolution.

In addition, the unit hydrograph method assumes that excess rainfall is uniformly distributed throughout the whole drainage area. Concerning this assumption, the unit hydrograph may become inapplicable when the drainage area is too large to be covered by a nearly uniform distribution of rainfall (Chow et al., 1988). Distributed-Clark, which can divide a watershed area into subareas and use spatially distributed rainfall inputs for each subarea, permits violation of this assumption; Distributed-Clark can be applied to large drainage areas which have a streamflow gauged outlet point. However, in such cases, it would have a relatively small *i* value as a calibrated input for creating good fit outputs (e.g. Illinois River model in case studies of Chapters 2 and 3) because Distributed-Clark theoretically considers upstream flow accumulation area which is required to be multiplied with *i* value for computing channel flow grid cell's flow travel time in Equation (2.16).

As for model input of DEM grid size, because Distributed-Clark assumes that the overland flow is effective up to 30 m length (USDA NRCS, 2010), the following stream network definition for model development uses one grid cell size threshold (flow accumulation value '1') of 30 m grid DEM by default. Thus, the use of another grid size DEM may not transfer the assumed model calculations of flow travel time for both flow regimes (overland and channel). For instance, a coarse grid DEM (e.g. 100 m or 1000 m spatial resolution) cannot preserve the 30 m length for overland flow characteristic with a one grid cell size threshold; this coarse grid may create rather delayed unit hydrographs because it can increase the total effective length of overland flow. The use of a fine grid DEM (e.g. under 1 m) also requires caution, because these gridded areas may not hold flow under actual situations. Since different grid sizes can change the ratio of channel flow network as well as overland flow or may not represent the actual flow network, this Distributed-Clark modeling approach should use 30 m grid DEM for unit hydrograph (i.e., time-area diagram; isochrones) development.

Also, Distributed-Clark cannot fully consider grid cell-based (spatially distributed subareas; e.g. Thiessen polygon, NEXRAD, etc.) flow interactions (computations), because it simply calculates each DEM grid cell's flow travel time to the watershed outlet point. Therefore, if it needs to calculate flow for a specific point of a watershed, a different unit hydrograph for a target watershed's outlet point should be developed using the same approach to produce a unit hydrograph; it may need a gauged hydrograph for calibration or comparison. This might be a limitation in Distributed-Clark application, particularly for obtaining detailed cell based flow routing results. Typically, this kind of

flow routing can be executed using distributed hydrologic models that consider hydrologic processes taking place at various points in space and define the model variables as functions of the space dimensions (Chow et al., 1988; Vieux, 2004). However, even though distributed models can calculate cell based flow interactions, it would not be useful if it does not have observed gauge points to calibrate simulation results within the watershed, as compared to its complexity to arrange model inputs. In this respect, Distributed-Clark (hybrid hydrologic model) is more practical because it targets flow simulation for watersheds with gauged data using a simple approach.

In Distributed-Clark, three (i, R, and λ) and four parameters (i, R, λ, and F_c) are used for the model calibration of event based and continuous hydrologic simulations, respectively. For these parameters, the model initially uses default values of 2-year, 24-hour rainfall intensity (for i), 2.0 hour (for R), 0.20 and 0.05 (for λ), and 2.5 mm/day (for F_c), but these parameter values should be appropriately changed to calibrate the model along with the observed flows. In these cases, the ranges of i and R which are used for unit hydrograph derivation are dependent on watershed areas; if model application area is larger, the use of relatively smaller i and larger R values than their default values are recommended. However, since the application of the Distributed-Clark model is typically needed to match its runoff volume with observed flows using λ and F_c values, there are no recommendations for these values in calibration; the trial-and-error method is required for estimation of these parameter values.

5.3 Conclusions and Expected Significance

Throughout this research to develop and evaluate a watershed-scale hybrid hydrologic model (Distributed-Clark), spatially distributed rainfall-runoff flow prediction, which may be considered as rather complex and tedious procedures, was achieved by relatively simple approaches using state-of-the-art spatial data. The Distributed-Clark model was implemented for flow simulations of storm events (first and second objectives) and long-term discontinuous storm events (third objective), and all of these results showed appropriate model performances. Therefore, Distributed-Clark is expected to contribute to the following as a useful hydrologic model.

Few watershed models that can be used for both event and continuous streamflow simulation to manage watersheds are currently available since the intended use of watershed model simulation results (modeling purpose) are different. Single storm event simulation results are used for analyzing severe actual or design storms for structural practices, while the results of multiple events simulation provide long-term effects of hydrological changes and watershed management practices (Borah and Bera, 2004). The work outlined in this research is, therefore, potentially significant to enhancements in the hydrologic model implementation for various purposes because the model created can be applied to both temporal scale simulations.

The developed model has relatively few parameters compared with other physically-based distributed (PBD) hydrologic models; only three or four parameters are needed. Further, if model input data pre-processing is completed, it can perform rapid

computations for obtaining hydrographs at watershed outlets. Thus, the hydrologic modeling work for this developed model will be easier and have more efficient capabilities than other PBD models. More specifically, execution time of Python script tools for watershed spatial data processing to obtain curve number maps, excess rainfall, and isochrones-based unit hydrographs typically do not exceed five minutes; however, NEXRAD data associated work may take more time due to grid cell-based (spatially distributed subareas) computations. In addition, these operation times vary according to data length (short- or long-term).

Since many gridded types of airborne and spaceborne quantitative precipitation estimation (QPE) have been developing in the research fields of earth and space science with intensive quality control (e.g. Multi-Radar Multi-Sensor; MRMS QPE, Global Precipitation Measurement; GPM satellite-based QPE, etc.), these types of gridded precipitation may be more reliable data for hydrological modeling. Therefore, this study's approaches are potentially significant in supporting these gridded types of QPE uses for runoff generation and routing.

In addition, based on the hydrological analysis, the model developed in this research can be extended to water quality issues (typically, watershed models can be applied to analyze non-point source pollution problems; Borah and Bera, 2003), and it is also expected that the model can be applied for assessing the environmental conditions of a watershed, evaluating best management practices (BMPs), TMDL development and implementation.

5.4 Recommendations for Future Research

While this dissertation culminated in significant results and contributions, it also identified knowledge gaps that can be addressed in future studies. The following are opportunities for future model enhancement:

1. Since Distributed-Clark only focuses on a direct runoff flow calculation and adds the separated baseflow to generate streamflow, a baseflow estimation module to simulate total streamflow is required; in this case, the calibrated value of static infiltration, F_c, can potentially be used to estimate baseflow (percolation), adding other geological parametric components (e.g. hydraulic conductivity, etc.) for soil moisture behavior in groundwater flows. In addition, a backward calculation approach from the recursive filter model may also be applicable.

2. For improvement of calibration performance for Distributed-Clark, development of different types of unit hydrographs may be needed. For instance, time variant unit hydrographs which are derived from different excess rainfall intensities can be used for a spatially averaged case of storm event application; and multiple flow phases of unit hydrographs can be applied to the conditional unit hydrograph adoption for long-term rainfall-runoff flow prediction. Also, for more efficient model calibration, automated procedures using various optimization techniques (e.g. shuffled complex evolution algorithm, SCE-UA; genetic algorithm, GA; etc.) can be integrated with Distributed-Clark.

3. Multiple watershed-based simulations conducted in tandem or parallel may need to be tested for more complicated and systematic hydrologic application; in this case, river networks and a river flow routing method for the attenuation and delay of flows from upstream watersheds, diversions, or dam operations should be defined and included, respectively.

LIST OF REFERENCES

LIST OF REFERENCES

Ajward, M.H., Muzik, I., 2000. A spatially varied unit hydrograph model. Journal of Environmental Hydrology 8, 1-8.

Arnold, J.G., Allen, P.M., Bernhardt, G., 1993. A comprehensive surface-groundwater flow model. Journal of Hydrology 142, 47-69.

Arnold, G., Srinavasan, R., Muttiah, R.S., Williams, J.R., 1998. Large Area Hydrologic Modeling and Assessment. Part I. Model Development. Journal of the American Water Resources Association 34 (1), 73-89.

Arnold, J.G., Fohrer, N., 2005. SWAT2000: current capabilities and research opportunities in applied watershed modeling. Hydrological Processes 19, 563-572.

Bandaragoda, C., Traboton, D.G., Woods, R., 2004. Application of TOPNET in the distributed model intercomparison project. Journal of Hydrology 298, 178-201.

Barnes, Jr., H.H., 1967. Roughness characteristics of natural channels. U.S. Geological Survey Water Supply Paper 1849, USGS, Washington, D.C.

Beven, K.J., Kirkby, M.J., 1979. A physically based, variable contributing area model of basin hydrology. Hydrological Sciences Bulletin 24 (1), 43-69.

Bhaduri, B., Harbor, J., Engel, B., Grove, M., 2000. Assessing watershed-scale, long-term hydrologic impacts of land-use change using a GIS-NPS model. Environmental Management 26 (6), 643-658.

Borah, D.K., Bera, M., 2003. Watershed-scale hydrologic and nonpoint-source pollution models: review of mathematical bases. Transactions of the American Society of Agricultural Engineers 46 (6), 1553-1566.

Borah, D.K., Bera, M., 2004. Watershed-scale hydrologic and nonpoint-source pollution models: review of applications. Transactions of the American Society of Agricultural Engineers 47 (3), 789-803.

Brater, E.F., King, H.W., 1976. Handbook of hydraulics for the solution of hydraulic engineering problems. McGraw-Hill Inc., New York, NY., 7-22.

Buchanan, B., Easton, Z.E., Schneider, R., Walter, M.T., 2012. Incorporating variable source area hydrology into a spatially distributed direct runoff model. Journal of the American Water Resources Association, 48 (1), 43-60.

Carpenter, T.M., Georgakakos, K.P., Sperfslagea, J.A., 2001. On the parametric and NEXRAD-radar sensitivities of a distributed hydrologic model suitable for operational use. Journal of Hydrology 253, 169-193.

Carpenter, T.M., Georgakakos, K.P., 2004. Continuous streamflow simulation with the HRCDHM distributed hydrologic model. Journal of Hydrology 298, 61-79.

Chinh, L., Iseri, H., Hiramatsu, K., 2013. Simulation of rainfall runoff and pollutant load for Chikugo River basin in Japan using a GIS-based distributed parameter model. Paddy and Water Environment 11 (1-4), 97-112.

Chintalapudi, S., Sharif, H.O., Yeggina, S., Elahassan, A., 2012. Physically based, hydrologic model results based on three precipitation products. Journal of the American Water Resources Association 48 (6), 1191-1203.

Choi, J.-Y., Engel, B.A., Chung, H.W., 2002. Daily streamflow modelling and assessment based on the curve-number technique. Hydrological Processes 16, 3131-3150.

Chow, V.T., 1986. Open-channel hydraulics. McGraw-Hill Inc., New York, NY., 110-113.

Chow, V.T., Maidment, D.R., Mays, L.W., 1988. Applied hydrology. McGraw-Hill Inc., New York, NY.

Clark, C.O., 1945. Storage and the unit hydrograph. Transactions of the American Society of Civil Engineers 110, 1419-1446.

Cronshey, R.G., Theurer, F.D., 1998. AnnAGNPS - Non-point pollutant loading model. In: Subcommittee on Hydrology of the Interagency Advisory Committee on Water Data. Proceedings of the First Federal Interagency Hydrologic Modeling Conference, Las Vegas, Nevada, Vol. 1, 9-16.

Crum, T., Alberty, R., 1993. The WSR-88D and the WSR-88D operational support facility. Bulletin of the American Meteorological Society 74 (9), 1669-1687.

De Smedt, F., Liu, Y.B., Gebremeskel, S., 2000. Hydrologic modelling on a catchment scale using GIS and remote sensed land use information. in Risk Analysis Ⅱ, WTI press, Southampton, Boston. 259-304.

DeVantier, A.B., Feldman, A.D., 1993. Review of GIS applications in hydrologic modeling. Journal of Water Resources Planning and Management 119 (2), 246-261.

Dooge, J.C.I., 1973. Linear theory of hydrologic systems. Technical Bulletin No. 1468, Agricultural Research Service, U.S. Department of Agriculture, Washington, D.C.

Dorn, H., Vetter, M., Hofle, B., 2014. GIS-based roughness derivation for flood simulations: a comparison of orthophotos, LiDAR and crowdsourced geodata. Remote Sensing 6, 1739-1759.

Du, J., Xie, H., Hu, Y., Xu, Y., Xu, C., 2009. Development and testing of a new storm runoff routing approach based on time variant spatially distributed travel time method. Journal of Hydrology 369, 44-45.

Du, J., Xie, H., Hu, Y., Xu, Y., Xu, C., 2010. Reply to comment on "Development and testing of a new storm runoff routing approach based on time variant spatially distributed travel time method" by Du et al. [Journal of Hydrology 369 (2009) 44-45]. Journal of Hydrology 381, 374-376.

Durbude, D.G., Jain, M.K., Mishra, S.K., 2011. Long-term hydrological simulation using SCS-CN-based improved soil moisture accounting procedure. Hydrological Processes 25 (4), 561-579.

Eckhardt, K., 2005. How to construct recursive digital filters for baseflow separation. Hydrological Processes 19 (2), 509-515.

Engel, B.A., 2001. L-THIA NPS long-term hydrologic impact assessment and nonpoint source pollution model, Version 2.1. Purdue University and USEPA.

Engel, B.A., Storm, D., White, M., Arnold, J., Arabi, M., 2007. A hydrologic/water quality model application protocol. Journal of the American Water Resources Association 43 (5), 1223-1236.

Engman, E.T., 1986. Roughness coefficients for routing surface runoff. Journal of Irrigation and Drainage Engineering 112 (1), 39-53.

Environmental System Research Institute (ESRI), 2012. ESRI ArcGIS 10.1. Redlands, CA.

Environmental System Research Institute (ESRI), 2013. Virtual Campus Training: Basics of Python (for ArcGIS 10), and Python Scripting for Geoprocessing Workflows (for ArcGIS 10). Redlands, CA.

Ferguson, B.K., 1998. Introduction to stormwater; concept, purpose, and design, Wiley, NY., 110-113.

Fread, D.L., Shedd, R.C., Smith, G.F., Farnsworth, R., Hoffeditz, C.N., Wenzel, L.A., Wiele, S.M., Smith, J.A., Day, G.N., 1995. Modernization in the National Weather Service river and flood program. Weather and Forecasting 10, 477-484.

Fulton, R.A., 1998. WSR-88D polar-to-HRAP mapping. Tech. Memo., Hydrology Research Laboratory, Office of Hydrology, National Weather Service, Silver Spring, MD, 1-33.

Fulton, R.A., Breidenbach, J.P., Seo, D.-J., Miller, D.A., 1998. The WSR-88D Rainfall Algorithm. Weather and Forecasting 13, 377-395.

Fulton, R.A., Ding, F., Miller, D.A., 2003. Truncation errors in historical WSR-88D rainfall products. In: Proceedings of the 31st Conference on Radar Meteorology, Seattle, WA, Boston, MA, American Meteorological Society, 270-273.

Garbrecht, J., Ogden, F.L., Debarry, P.A., Maidment, D.R., 2001. GIS and distributed watershed models. I: data coverages and sources. Journal of Hydrologic Engineering 6 (6), 506-514.

Garen, C.G., Moore, D.S., 2005. Curve number hydrology in water quality modeling: uses, abuses, and future directions, Journal of the American Water Resources Association 41 (2), 377-388.

Gibbs, M.S., Dandy, G.C., Maier, H.R., 2010. Evaluation of parameter setting for two GIS based unit hydrograph models. Journal of Hydrology 393, 197-205.

Greenlee, D.D., 1987. Raster and vector processing for scanned linework. Photogrammetric Engineering and Remote Sensing 53 (10), 1383-1387.

Gupta, H.V., Sorooshian, S., Yapo, P.O., 1999. Status of automatic calibration for hydrologic models: comparison with multilevel expert calibration. Journal of Hydrologic Engineering 4 (2), 135-143.

Habib, E., Aduvala, A.V., Meselhe, E.A., 2008. Analysis of radar-rainfall error characteristics and implications for streamflow simulation uncertainty. Hydrologic Science Journal 53 (3), 568-587.

Harbor, J., 1994. A practical method for estimating the impact of land use change on surface runoff, groundwater recharge and wetland hydrology. Journal of the American Planning Association 60 (1), 95-108.

Hardegree, S.P., Van Vactor, S.S., Levinson, D.H., Winstral, A.H., 2008. Evaluation of NEXRAD radar precipitation products for natural resource applications. Rangeland Ecology and Management 61, 346-353.

Hargreaves, G.H., Samani, Z.A., 1985. Reference crop evapotranspiration from temperature. Applied Engineering in Agriculture 1 (2), 96-99.

Hargreaves, G.H., Allen, R.G., 2003. History and evaluation of Hargreaves evapotranspiration equation. Journal of Irrigation and Drainage Engineering 129, 53-63.

Hawkins, R.H., 1977. Discussion of water yield model using SCS curve numbers, by Williams, J. R., and W. V. LaSeur. Journal of the hydraulics division 103 (HY8), 933-936.

Hawkins, R.H., 1978. Runoff curve numbers with varying site moisture. Journal of the irrigation and drainage division, 104 (IR4), 389-398.

Hawkins, R.H., Jiang, R., Woodward, D.E., Hjelmfelt, A.T., Van Mullem, J.A., 2002. Runoff curve number method: examination of the initial abstraction ratio. In: Hydrologic Modeling for the 21st Century. 2nd Federal Interagency Hydrologic Modeling Conference, July 28 to August 1, Las Vegas, Nevada.

Hawkins, R.H., Ward, T.J., Woodward, D.E., Van Mullem, J.A., 2009. Curve Number Hydrology, American Society of Civil Engineers (ASCE), Reston, Virginia.

Hjelmfelt, A.T., 1980. Curve-number procedure as infiltration method. Journal of Hydraulics Division 106 (HY6), 1107-1110.

Horton, R.E., 1939. Analysis of runoff plat experiments with varying infiltration capacity, Transactions American Geophysical Union 20 (4), 693-711.

Hudlow, M.D., Smith, J.A., 1989. NEXRAD-new era in hydrometeorology in the United States. Preprints, International Symposium on Hydrologic Applications of Weather Radar, Salford, England, Paper B-1.

Istok, M.J., Elvander, R., Saffle, R., Roe, J., 2003. NEXRAD product improvement-implementing new science. In: Proceedings of the 31st Conference on Radar Meteorology, Seattle, WA, Boston, MA, American Meteorological Society, 850-853.

Ivanov, V.Y., Vivoni, E.R., Bras, R.L., Entekhabi, D., 2004. Preserving high-resolution surface and rainfall data in operational-scale basin hydrology: a fully-distributed physically-based approach. Journal of Hydrology 298, 80-111.

Jain, M.K., Durbude, D.G., Mishra, S.K., 2012. Improved CN-based long-term hydrologic simulation model. Journal of hydrological Engineering 17 (11), 1204-1220.

Jayakrishnan, R., Srinivasan, R., Arnold, J.G., 2004. Comparison of raingage and WSR-88D Stage III precipitation data over the Texas-Gulf basin. Journal of Hydrology 292, 135-152.

Jayakrishnan, R., Srinivasan, R., Santhi, C., Arnold, J.G., 2005. Advances in the application of the SWAT model for water resources management. Hydrological Processes 19, 749-762.

Jenson, S.K., Domingue, J.O., 1988. Extracting topographic structure from digital elevation data for geographic information system analysis. Photogrammetric Engineering and Remote Sensing 54 (11), 1593-1600.

Jeon, J.-H., Lim, K.-J., Engel, B.A., 2014. Regional calibration of SCS-CN L-THIA model: application for ungauged basins. Water 6, 1339-1359.

Johnson, D., Smith, M., Koren, V., Finnerty, B., 1999. Comparison mean areal precipitation estimates from NEXRAD and rain gauge networks. Journal of Hydrologic Engineering 4 (2), 117-124.

Johnson, L.E., Dallmann, J.L., 1987. Flood flow forecasting using microcomputer graphics and radar imagery. Microcomputers in Civil Engineering 2, 85-99.

Johnson, L.E., 1989. MAPHYD - a digital map-based hydrologic modeling system. Photogrammetric Engineering and Remote Sensing 55 (6), 911-917.

Julien, P.Y., Saghafian, B., Ogden, F.L., 1995. Raster-based hydrologic modeling of spatially-varied surface runoff. Water Resources Bulletin 31 (3), 523-536.

Jung, Y., Merwade, V., Yeo, K., Shin, Y., Lee, S.O., 2013. An approach using a 1D hydraulic model, landsat imaging and generalized likelihood uncertainty estimation for an approximation of flood discharge. Water 5, 1598-1621.

Kannan, N., Santhi, C., Williams, J.R., Arnold, J.G., 2008. Development of a continuous soil moisture accounting procedure for curve number methodology and its behaviour with different evapotranspiration methods. Hydrological Processes 22, 2114-2121.

Kalyanapu, A.J., Burian, S.J., McPherson, T.N., 2009. Effect of land use-based surface roughness on hydrologic model output. Journal of Spatial Hydrology 9 (2), 51-71.

Klazura, G.E., Thomale, J.M., Kelly, D.S., Jendrowski, P., 1999. A comparison of NEXRAD WSR-88D radar estimates of rain accumulation with gauge measurements for high- and low-reflectivity horizontal gradient precipitation events. Journal of Atmospheric and Oceanic Technology 16, 1842-1850.

Klemes, V., 1986. Operational testing of hydrological simulation models. Hydrological Sciences Journal 31 (1), 13-24.

Knisel, W.G., 1980. CREAMES: A field scale model for chemicals, runoff, and erosion from agricultural management systems (Conservation Report No. 26), USDA ARS, Washington, D.C.

Knisel. W.G., 1993. GLEAMS Groundwater loading effects of agricultural management systems, Version 2.10. (Dept. Publication No. 5), Biological & Agricultural Engineering Department, University of Georgia-Coastal Plain Experiment Station, Tifton, GA.

Koren, V., Reed, S., Smith, M., Zhang, Z., Seo, D.-J., 2004. Hydrology laboratory research modeling system (HL-RMS) of the US national weather service. Journal of Hydrology 291, 297-318.

Krajewski, W.F., Smith, J.A., 2002. Radar hydrology: rainfall estimation. Advance in Water Resources 25, 1387-1394.

Kull, D.W., Feldman, A.D., 1998. Evolution of Clark's unit graph method to spatially distributed runoff. Journal of Hydrologic Engineering 3 (1), 9-19.

Laurenson, E.M., 1964. A catchment storage model for runoff routing. Journal of Hydrology 2, 141-163.

Leonard, R.A., Knisel, W.G., Still, D.A., 1987. GLEAMS: Groundwater loading effects of agricultural management systems. Transactions of the American Society of Agricultural Engineers 30 (5), 1403-1418.

Lim, K.J., Engel, B.A. Tang, Z., Choi, J., 2005. Automated web GIS based hydrograph analysis tool, WHAT. Journal of the American Water Resources Association 41 (6), 1407-1416.

Lin, Y., Mitchell, K.E., 2005. The NCEP Stage II/IV hourly precipitation analyses: development and applications. Preprints, 19th Conference on Hydrology, American Meteorological Society, San Diego, CA, Paper 1.2.

Liu, Y.B., Gebremeskel, S., De Smedt, F., Hoffmann, L., Pfister, L., 2003. A diffusive transport approach for flow routing in GIS-based flood modeling. Journal of Hydrology 283, 91-106.

Lu, J., Sun, G., McNulty, S.G., Amatya, D.M., 2005. A comparison of six potential evapotranspiration methods for regional use in the southeastern United States. Journal of the American Water Resources Association 41 (3), 621-633.

Luzio, M.D., Arnold, J.G., 2004. Formulation of a hybrid calibration approach for a physically based distributed model with NEXRAD data input. Journal of Hydrology 298, 136-154.

Maidment, D. R., 1993. Handbook of hydrology. McGraw-Hill Inc., New York, NY.

Maidment, D.R., 1993. Developing a spatially distributed unit hydrograph by using GIS. In: Kovar, K. and Nachtnebel, H.P. (Eds.), Application of Geographic Information Systems in Hydrology and Water Resources Management. IAHS Publication No. 211, 181-192.

Maidment, D.R., Olivera, J.F., Calver, A., Eatherall, A., Fraczek, W., 1996. Unit hydrograph derived from a spatially distributed velocity filed. Hydrological Processes 10, 831-844.

Maidment, D.R., 2002. Arc Hydro GIS for water resources. ESRI Press, Redlands, CA.

Mark, D.M., 1988. Network models in geomorphology in Modeling Geomorphological Systems, ed. Anderson, M.G., New York: John Wiley, 73-97.

Martin, P.H., LeBoeuf, E.J., Dobbins, J.P., Daniel, E.B., Abkowitz, M.D., 2005. Interfacing GIS with water resource model: a state-of-the-art review. Journal of the American Water Resources Association 41 (6), 1471-1487.

McCuen, R.H., Spiess, J.M., 1995. Assessment of kinematic wave time of concentration. Journal of Hydraulic Engineering 121 (3), 256-266.

McCuen, R.H., 2005. Hydrologic analysis and design (3rd edition), Prentice-Hall Inc., Upper Saddle River, NJ.

Mednick, A.C., 2010. Does soil data resolution matter? state soil geographic database versus soil survey geographic database in rainfall-runoff modeling across Wisconsin. Journal of Soil and Water Conservation 65 (3), 190-199.

Melesse, A.M., Graham, W.D. Jordan, J.D., 2003. Spatially distributed watershed mapping and modeling: GIS-based storm runoff response and hydrograph analysis: Part 2. Journal of Spatial Hydrology 3 (2), 1-28.

Melesse, A.M., Graham, W.D., 2004. Storm runoff prediction based on a spatially distributed travel time method utilizing remote sensing and GIS. Journal of the American Water Resources Association 40 (4), 863-879.

Michel, C., Vazken, A., Perrin, C., 2005. Soil conservation service curve number model: how to mend a wrong soil moisture accounting procedure. Water Resources Research 41 (2), 1-6.

Mishra, S.K., Singh, V.P., 2003. Soil conservation service curve number (SCS-CN) methodology. Kluwer Academic Publishers, Dordrecht, The Netherlands.

Mishra, S.K., Singh, V.P., 2004. Long-term hydrological simulation based on the soil conservation service curve number. Hydrological Processes 18, 1291-1313.

Montes, S., 1998. Hydraulics of open channel flow. ASCE Press, Reston, VA., 103-104.

Morel-Seytoux, H.J., Verdin, J.P., 1981. Extension of the Soil Conservation Service rainfall runoff methodology for ungaged watersheds (FHWA/RD-81/060). Federal Highway Administration, Washington, D.C.

Moriasi, D.N., Arnold, J.G., Van Liew, M.W., Bingner, R.L., Harmel, R.D., Veith, T.L., 2007. Model evaluation guidelines for systematic quantification of accuracy in watershed simulations. Transactions of the American Society of Agricultural Engineers, 50 (3), 885-900.

Muzik, I., 1996. A GIS-derived distributed unit hydrograph. In: Kovar, K. and Nachtnebel, H.P. (Eds.), Application of Geographic Information Systems in Hydrology and Water Resources Management. IAHS Publication No. 235, 453-460.

Muzik, I., 1996. Flood modeling with GIS-derived distributed unit hydrographs. Hydrological Processes 10, 1401-1409.

Nash, J.E., Sutcliffe, J.V., 1970. River flow forecasting through conceptual models part I – a discussion of principles. Journal of Hydrology 10, 282-290.

National Research Council, 1982. Scientific basis of water resource management. National Academy Press, Washington, D.C., 3-13.

Neary, V.S., Habib, E., Fleming, M., 2004. Hydrologic modeling with NEXRAD precipitation in middle Tennessee. Journal of Hydrologic Engineering 9 (5), 339-349.

Nelson, B.R., Krajewski, W.F., Kruger, A., Smith, J.A., Baeck, M.L., 2003. Archival precipitation data set for the Mississippi River Basin: development of a GIS-based data browser. Computers and Geosciences 29, 595-604.

Noto, L.V., Loggia, G.L., 2007. Derivation of a distributed unit hydrograph integrating GIS and remote sensing. Journal of Hydrologic Engineering 12 (6), 639-650.

Ogden, F.L., Julien, P.Y., 1994. Runoff model sensitivity to radar rainfall resolution. Journal of Hydrology 158, 1-18.

Ogden, F.L., Sharif, H.O., Senarath, S.U.S., Smith, J.A., Baeck, M.L., Richardson, J.R., 2000. Hydrologic analysis of the Fort Collins, Colorado, flash flood of 1997. Journal of Hydrology 228, 82-100.

Ogden, F.L., Garbrecht, J., DeBarry, P.A., Johnson, L.E., 2001. GIS and distributed watershed models. II: module, interfaces, and models. Journal of Hydrologic Engineering 6 (6), 515-523.

Ogden, F.L., Downer, C.W., Meselhe, E., 2003. U.S. Army Corps of Engineers Gridded Surface/ Subsurface Hydrologic Analysis (GSSHA) model: distributed-parameter, physically based watershed simulations. In: P. Bizier and P. DeBarry (Eds.), World Water & Environmental Resources Congress 2003, Philadelphia, PA, EWRI, 23-26.

Olivera, F., Maidment, D., 1999. Geographic information systems (GIS)-based spatially distributed model for runoff routing. Water Resources Research 35 (4), 1155-1164.

Overton, D.E., Meadows, M.E., 1976. Stormwater modeling. Academic Press, New York, NY.

Paudel, M., Nelson, E.J., Scharffenberg, W., 2009. Comparison of lumped and quasi-distributed Clark runoff models using the SCS curve number equation. Journal of Hydrologic Engineering 14 (10), 1098-1106.

Peters J.C., Easton, D.J., 1996. Runoff simulation using radar rainfall data. Water Resources Bulletin 32 (4), 753-760.

Ponce, V.M., 1989. Engineering Hydrology Principles and Practices. Prentice-Hall, New Jersey.

Ponce, V.M., Hawkins, R.H., 1996. Runoff curve number: has it reached maturity? Journal of Hydrologic Engineering 1 (1), 11-19.

Razavi, S., Tolson, B.A., Matott, L.S., Thomson, N.R., MacLean, A., Seglenieks, F.R., 2010. Reducing the computational cost of automatic calibration through model preemption. Water Resources Research 46 (11), W11523.

Reed, S.M., Maidment, D.R., 1995. A GIS procedure for merging NEXRAD precipitation data and digital elevation models to determine rainfall-runoff modeling parameters. Center for Research in Water Resources (CRWR), University of Texas at Austin Online Report 95-3.

Reed, S.M., Maidment, D.R., 1999. Coordinate transformations for using NEXRAD data in GIS-based hydrologic modeling. Journal of Hydrologic Engineering 4 (2), 174-182.

Reed, S., Koren, V., Smith, M., Zhang, Z., Moreda, F., Seo, D.-J., DMIP Participants, 2004. Overall distributed model intercomparison project results. Journal of Hydrology 298, 27-60.

Ryu, J.H., 2009. Application of HSPF to the distributed model intercomparison project: case study. Journal of Hydrologic Engineering 14 (8), 847-857.

Saghafian, B., Noroozpour, S., 2010. Comment on "Development and testing of a new storm runoff routing approach based on time variant spatially distributed travel time method" by Jinkang Du, Hua Xie, Yujun Hu, Youpeng Xu, Chong-Yu Xu. Journal of Hydrology 381, 372-373.

Schaake, J.C., Koren, V.I., Duan, Q.-Y., 1996. Simple water balance model for estimating runoff at different spatial and temporal scales. Journal of Geophysical Research 101 (D3), 7461-7475.

Seo, D.-J., 1998. Real-time estimation of rainfall fields using radar rainfall and rain gage data. Journal of Hydrology 208, 37-52.

Seo, D.-J., Breidenbach, J.P., Johnson, E.R., 1999. Real-time estimation of rainfall fields bias in radar rainfall data. Journal of Hydrology 223, 131-147.

Sexton, A.M., Sadeghi, A.M., Zhang, X., Srinivasan, R., Shirmohammadi, A., 2010. Using NEXRAD and rain gauge precipitation data for hydrologic calibration of SWAT in a northwestern watershed. Transactions of the American Society of Agricultural Engineers 53 (5), 1501-1510.

Sharif, H.O., Hassan, A.A., Bin-Shafique, S., Xie, H., Zeitler, J., 2010. Hydrologic modeling of an extreme flood in the Guadalupe River in Texas. Journal of the American Water Resources Association 46 (5), 881-891.

Shedd, R.C., Smith, J., 1991. Interactive Precipitation processing for the modernized National Weather Service. Preprints, Seventh International Conference on Interactive Information and Processing System for Meteorology, Hydrology, and Oceanography, New Orleans, LA, American Meteorological Society, 320-323.

Shedd, R.C., Fulton, R.A., 1993. WSR-88D precipitation processing and its use in National Weather Service hydrologic forecasting. Proceedings of the ASCE International Symposium on Engineering Hydrology, San Francisco, CA, ASCE, 16-21.

Sherman, L.K., 1932. Streamflow from rainfall by unit-graph method. Engineering News-Record 108, 501-505.

Singh, V.P., 1988. Hydrologic systems, volume 1, rainfall-runoff modeling. Prentice Hall, Englewood Cliffs, NJ., 1-6.

Smith, J.A., Seo, D.-J., Baeck, M.L., Hudlow, M.D., 1996. An intercomparison study of NEXRAD precipitation estimates. Water Resources Research 32 (7), 2035-2045.

Smith, M.B., Seo, D.-J., Koren, V.I., Reed, S.M., Zhang, Z., Duan, Q., Moreda, F., Cong, S., 2004. The distributed model intercomparison project (DMIP): motivation and experiment design. Journal of Hydrology 298, 4-26.

Smith, M.B., Koren, V., Zhang, Z., Zhang, Y., Reed, S.M., Cui, Z., Moreda, F., Cosgrove, B.A., Mizukami, N., Anderson, E.A., DIMP 2 Participants, 2012. Results of the DIMP 2 Oklahoma experiments. Journal of Hydrology 418-419, 17-48.

Smith, R.E., 1976. Approximations for vertical infiltration rate patterns. Transactions of the American Society of Agricultural Engineers 19 (3), 505-509.

Snyder, F.F., 1938. Synthetic unit-graphs. Transactions, American Geophysical Union 19, 447-454.

Snyder, J.A., 1987. Map projections – a working manual, Professional Paper 1395, US Geological Survey, Washington, D.C.

Soil Conservation Service (SCS), 1957, 1972. National Engineering Handbook, Section 4: Hydrology, Soil Conservation Service, Washington, D.C.

Spruill, C.A., Workman, S.R. Taraba, J.L., 2000. Simulation of daily and monthly streamflow discharge from small watersheds using SWAT model. Transactions of the American Society of Agricultural Engineers 43 (6), 1431-1439.

Steiner, M., Smith, J.A., Burges, S.J., Alonso, C.V., Darden, R.W., 1999. Effect of bias adjustment and gauge data quality control on radar rainfall estimation. Water Resources Research 35 (8), 2487-2503.

Tarboton, D.G., Bras, R.L., Rodriguez-Iturbe, I., 1991. On the extraction of channel networks from digital elevation data. Hydrological Processes 5, 81-100.

Tsoukalas, I., Kossieris, P., Efstratiadis, A., Makropoulos, C., 2016. Surrogate-enhanced evolutionary annealing simplex algorithm for effective and efficient optimization of water resources problems on a budget. Environmental Modelling & Software 77, 122-142.

TWRI (Texas Water Resources Institute), 2014. Soil and Water Assessment Tool, Input/Output Documentation (ver.2012, TR-439), 246-248.

U.S. Army Corps of Engineers, 1996a. A pilot application of weather radar-based runoff forecasting, Salt River Basin, MO (PR-31), Hydrologic Engineering Center, Davis, CA.

U.S. Army Corps of Engineers, 1996b. Runoff simulation using radar rainfall data (TP-155), Hydrologic Engineering Center, Davis, CA.

U.S. Army Corps of Engineers, 1996c. ModClark model development for the Muskingum River Basin, OH (PR-33), Hydrologic Engineering Center, Davis, CA.

U.S. Army Corps of Engineers, 1998. HEC-1 Flood Hydrograph Package, User's Manual (CPD-1A, Ver. 4.1), Hydrologic Engineering Center, Davis, CA.

U.S. Army Corps of Engineers, 2009. HEC-DSSVue HEC Data Storage System Visual Utility Engine, User's Manual (CPD-79, Ver. 2.0), Hydrologic Engineering Center, Davis, CA.

U.S. Army Corps of Engineers, 2010. Hydrologic Modeling System HEC-HMS, User's Manual (CPD-74A, Ver. 3.5), Hydrologic Engineering Center, Davis, CA.

U.S. Army Corps of Engineers, 2011. HEC-GridUtil Grid Utility Program Managing Gridded Data with HEC-DSS, User's Manual (CPD-89, Ver. 2.0), Hydrologic Engineering Center, Davis, CA.

U.S. Army Corps of Engineers, 2013. HEC-GeoHMS Geospatial Hydrologic Modeling Extension, User's Manual (CPD-77, Ver. 10.1), Hydrologic Engineering Center, Davis, CA.

U.S. Department of Agriculture, Natural Resources Conservation Service (USDA NRCS), 2010. National engineering handbook, Part 630, Washington, D.C.

Van Mullem, J.A., Woodward, D.E., Hawkins, R.H., Hjelmfelt, A.T., 2002. Runoff curve number method: beyond the handbook. In: Hydrologic Modeling for the 21st Century. 2nd Federal Interagency Hydrologic Modeling Conference, July 28 to August 1, Las Vegas, Nevada.

Veni, G., 2002. Revising the karst map of the United States. Journal of Cava and Karst Studies 64 (1), 45-50.

Vieux, B.E., 2004. Distributed hydrologic modeling using GIS (2nd edition), Kluwer Academic Publishers, Dordrecht, The Netherlands, 123-127.

Wang, X., Xie, H., Sharif, H., Zeitler, J., 2008. Validating NEXRAD MPE and Stage III precipitation products for uniform rainfall on the Upper Guadalupe River Basin of the Texas Hill Country. Journal of Hydrology 348, 73-86.

Water Resources Center (WRC), University of Minnesota, 2013. NRCS GIS Engineering Tools, ftp://ftp.lmic.state.mn.us/pub/data/ elevation/lidar/tools/NRCS_engineering

Welle, P.I., Woodward, D., 1986. Time of concentration. Hydrology Technical Note No. N4, USDA SCS, Washington, D.C.

Wilkerson, J.L., Merwade, V., 2010. Incorporating surface storage and slope to estimate Clark unit hydrographs for ungauged Indiana watersheds. J. Hydrol. Eng. 15 (11), 918-930.

Williams, J.R., LaSeur, W.V., 1976. Water yield model using SCS curve numbers. Journal of the hydraulics division 102 (HY9), 1241-1253.

Williams, J.R., Jones, C. A., Dyke, P.T., 1984. A modeling approach to determining the relationship between erosion and soil productivity. Transactions of the American Society of Agricultural Engineers 27 (1), 129-144.

Williams, J.R., Nicks, A.D., Arnold, J.G., 1985. Simulator for water resources in rural basins. Journal of Hydraulic Engineering 111 (6), 970-986.

Williams, J.R., Arnold, J.G., Srinivasan, R., 2000. The APEX model. BRC Report No. 00-06, Texas A & M Blackland Research and Extension Center, Temple, TX.

Williams, J.R., Kannan, N., Wang, X., Santhi, C., Arnold, J.G., 2012. Evolution of the SCS runoff curve number method and its application to continuous runoff simulation. Journal of Hydrologic Engineering 17 (11), 1121-1229.

Winchell, M., Gupta, H.V. Sorooshian, S., 1998. On the simulation of infiltration- and saturation-excess runoff using radar-based rainfall estimates: effects of algorithm uncertainty and pixel aggregation. Water Resources Research 34 (10), 2655-2670.

Woodward, D.E., Hawkins, R.H., Hjelmfelt, A.T., Van Mullem, J.A., Quan, Q.D., 2002. Curve number method: origins, applications and limitations. In: Hydrologic Modeling for the 21st Century. 2nd Federal Interagency Hydrologic Modeling Conference, July 28 to August 1, Las Vegas, Nevada.

Xie, Hongjie, Zhou, X., Vivoni, E.R., Hendrickx, J., Small, E.E., 2005. GIS-based NEXRAD Stage III precipitation database: automated approaches for data processing and visualization. Computers and Geosciences 31, 65-76.

Xie, Hongjie, Zhou, X., Hendrickx, J., Vivoni, E.R., Guan, H., Tian, Y.Q., Small, E.E., 2006. Evaluation of NEXRAD Stage III precipitation data over a semiarid region. Journal of the American Water Resources Association 41 (1), 237-256.

Xie, Hongjie, Zhang, X., Yu, B., Sharif, H., 2011. Performance evaluation of interpolation methods for incorporating rain gauge measurements into NEXRAD precipitation data: a case study in the Upper Guadalupe River Basin. Hydrological Processes 25, 3711-3720.

Xu, C.-Y., Singh, V.P., 2001. Evaluation and generalization of temperature-based methods for calculating evaporation. Hydrological Processes 15, 305-319.

Yen, B.C., 1991. Channel flow resistance: Centennial of Manning's formula, Water Resources Publications, Littleton, CO., 43-46.

Young, C.B., Bradley, A., Krajewski, W.F., Kruger, A., 2000. Evaluating NEXRAD multisensor precipitation estimates for operational hydrologic forecasting. Journal of Hydrometeorology 1, 241-254.

Young, R.A., Onstad, C.A., Bosch, D.D., Anderson, W.P., 1989. AGNPS: A nonpoint-source pollution model for evaluating agricultural watersheds. Journal of Soil and Water Conservation 44 (2), 168-173.

Zhang, X., Srinivasan, R., Zhao, K., Liew, M.V., 2009. Evaluation of global optimization algorithms for parameter calibration of a computationally intensive hydrologic model. Hydrological Processes 23, 430-441.

Zhang, X., Srinivasan, R., 2010. GIS-based spatial precipitation estimation using next generation radar and raingauge data. Environmental Modelling & Software 25, 1781-1788.

APPENDICES

Appendix A Statistical result (detail) comparisons of model calibration and validation for spatially distributed (Thiessen polygon) and averaged rainfall data simulation

Table A 1 Illinois River

Storm Events (#) [model]		Direct Runoff				Streamflow				
		E_{NS}	R^2	*PBIAS* (%)	Total (mm)	E_{NS}	R^2	*PBIAS* (%)	Peak flow (m^3/s) [time, hour]	Total (mm)
	Dist.[D1]	0.93	0.93	-0.03	46.2	0.93	0.93	-0.03	658.2 [66]	56.4
	Avg.[D2]	0.95	0.95	-0.09	46.2	0.95	0.95	-0.07	680.7 [66]	56.4
1	Diff.	-0.02	-0.02	0.06	-	-0.02	-0.02	0.04	-22.5 [-]	-
	Avg.[H]	0.86	0.86	0.08	46.2	0.86	0.86	0.06	592.2 [65]	56.4
	Diff.	0.07	0.07	-0.11	-	0.07	0.07	-0.09	66.0 [1]	-
	Dist.[D1]	0.84	0.85	-0.04	28.9	0.84	0.85	-0.03	487.9 [62]	34.1
	Avg.[D2]	0.80	0.82	-0.04	28.9	0.80	0.82	-0.03	475.5 [62]	34.1
2	Diff.	0.04	0.03	-	-	0.04	0.03	-	12.4 [-]	-
	Avg.[H]	0.64	0.66	0.12	28.9	0.64	0.66	0.10	434.3 [60]	34.1
	Diff.	0.20	0.19	-0.16	-	0.20	0.19	-0.13	53.6 [2]	-
	Dist.[D1]	0.79	0.79	0.08	5.6	0.78	0.79	0.00	138.8 [57]	14.6
	Avg.[D2]	0.76	0.77	0.05	5.6	0.75	0.76	-0.01	137.2 [57]	14.6
3	Diff.	0.03	0.02	0.03	-	0.03	0.03	0.01	1.6 [-]	-
	Avg.[H]	0.54	0.54	-0.11	5.6	0.52	0.52	-0.08	131.2 [56]	14.6
	Diff.	0.25	0.25	0.19	-	0.26	0.27	0.08	7.6 [1]	-
	Dist.[D1]	0.58	0.62	-0.10	6.4	0.58	0.62	-0.05	129.9 [86]	13.8
	Avg.[D2]	0.55	0.60	-0.15	6.4	0.55	0.59	-0.07	128.4 [86]	13.8
4	Diff.	0.03	0.02	0.05	-	0.03	0.03	0.02	1.5 [-]	-
	Avg.[H]	0.41	0.47	0.16	6.4	0.41	0.47	0.08	119.3 [84]	13.8
	Diff.	0.17	0.15	-0.26	-	0.17	0.15	-0.13	10.6 [2]	-
	Dist.[D1]	0.70	0.74	0.13	23.3	0.70	0.74	0.12	367.6 [68]	24.8
	Avg.[D2]	0.68	0.72	0.13	23.3	0.68	0.72	0.12	364.0 [68]	24.8
5	Diff.	0.02	0.02	-	-	0.02	0.02	-	3.6 [-]	-
	Avg.[H]	0.60	0.63	0.50	23.3	0.60	0.63	0.47	328.6 [69]	24.8
	Diff.	0.10	0.11	-0.37	-	0.10	0.11	-0.35	39.0 [-1]	-
	Dist.[D1]	0.79	0.82	0.01	30.0	0.79	0.82	0.01	369.8 [77]	33.9
	Avg.[D2]	0.75	0.80	0.01	30.0	0.75	0.80	0.01	368.6 [77]	33.9
6	Diff.	0.04	0.02	-	-	0.04	0.02	-	1.2 [-]	-
	Avg.[H]	0.32	0.47	0.13	30.0	0.32	0.47	0.11	348.5 [73]	33.9
	Diff.	0.47	0.35	-0.12	-	0.47	0.35	-0.10	21.3 [4]	-

Dist.- distributed; Avg. - averaged; [D1] and [D2] - Distributed-Clark; [H] - HEC-HMS; Diff. - differences from averaged output ('-' means 'reduction' in time to peak)

Statistics are for the period of model simulation (for direct runoff), not the total storm event duration.

Table A 2 Elk River

Storm Events (#) [model]		Direct Runoff				Streamflow				
		E_{NS}	R^2	*PBIAS* (%)	Total (mm)	E_{NS}	R^2	*PBIAS* (%)	Peak flow (m^3/s) [time, hour]	Total (mm)
	Dist.[D1]	0.84	0.84	-1.10	15.1	0.95	0.95	-0.31	836.5 [53]	54.3
	Avg.[D2]	0.84	0.84	-0.89	15.1	0.95	0.95	-0.25	835.9 [53]	54.3
1	Diff.	-	-	-0.21	-	-	-	-0.06	0.6 [-]	-
	Avg.[H]	0.88	0.89	-0.88	15.1	0.96	0.96	-0.24	800.2 [52]	54.3
	Diff.	-0.04	-0.05	-0.22	-	-0.01	-0.01	-0.07	36.3 [1]	-
	Dist.[D1]	0.81	0.81	-1.55	5.0	0.94	0.95	-0.37	225.6 [70]	21.2
	Avg.[D2]	0.83	0.83	-2.08	5.0	0.95	0.95	-0.50	229.3 [69]	21.2
2	Diff.	-0.02	-0.02	0.53	-	-0.01	-	0.13	-3.7 [1]	-
	Avg.[H]	0.88	0.88	-1.70	5.0	0.96	0.97	-0.41	236.1 [68]	21.2
	Diff.	-0.07	-0.07	0.15	-	-0.02	-0.02	0.04	-10.5 [2]	-
	Dist.[D1]	0.93	0.93	-0.31	12.9	0.97	0.97	-0.09	828.1 [26]	44.0
	Avg.[D2]	0.88	0.89	-0.41	12.9	0.95	0.96	-0.12	751.3 [26]	44.0
3	Diff.	0.05	0.04	0.10	-	0.02	0.01	0.03	76.8 [-]	-
	Avg.[H]	0.79	0.81	-0.23	12.9	0.92	0.93	-0.07	710.9 [30]	44.0
	Diff.	0.14	0.12	-0.08	-	0.05	0.04	-0.02	117.2 [-4]	-
	Dist.[D1]	0.86	0.89	-3.08	8.8	0.95	0.96	-0.78	569.1 [38]	35.7
	Avg.[D2]	0.91	0.91	-2.93	8.8	0.96	0.96	-0.74	502.1 [38]	35.7
4	Diff.	-0.05	-0.02	-0.15	-	-0.01	-	-0.04	67.0 [-]	-
	Avg.[H]	0.86	0.86	-2.58	8.8	0.95	0.95	-0.65	461.9 [44]	35.7
	Diff.	-	0.03	-0.50	-	-	0.01	-0.13	107.2 [-6]	-
	Dist.[D1]	0.71	0.71	-1.44	4.8	0.91	0.91	-0.32	245.9 [53]	22.1
	Avg.[D2]	0.96	0.97	-1.55	4.8	0.99	0.99	-0.34	253.2 [48]	22.1
5	Diff.	-0.25	-0.26	0.11	-	-0.08	-0.08	0.02	-7.3 [5]	-
	Avg.[H]	0.71	0.73	-0.86	4.8	0.91	0.93	-0.19	217.1 [53]	22.1
	Diff.	-	-0.02	-0.58	-	-	-0.02	-0.13	28.8 [-]	-
	Dist.[D1]	0.85	0.86	-1.38	2.7	0.95	0.96	-0.31	124.5 [51]	11.8
	Avg.[D2]	0.69	0.70	-1.08	2.7	0.89	0.91	-0.24	130.2 [54]	11.8
6	Diff.	0.16	0.16	-0.30	-	0.06	0.05	-0.07	-5.7 [-3]	-
	Avg.[H]	0.24	0.25	-0.62	2.7	0.74	0.75	-0.14	106.6 [60]	11.8
	Diff.	0.61	0.61	-0.76	-	0.21	0.21	-0.17	17.9 [-9]	-

Dist.- distributed; Avg. - averaged; [D1] and [D2] - Distributed-Clark; [H] - HEC-HMS; Diff. - differences from averaged output ('-' means 'reduction' in time to peak)

Statistics are for the period of model simulation (for direct runoff), not the total storm event duration.

Table A 3 Silver Creek

Storm Events (#) [model]		Direct Runoff				Streamflow				
		E_{NS}	R^2	*PBIAS* (%)	Total (mm)	E_{NS}	R^2	*PBIAS* (%)	Peak flow (m^3/s) [time, hour]	Total (mm)
1	Dist.[D1]	0.83	0.86	-0.67	10.1	0.96	0.97	-0.22	99.3 [57]	30.8
	Avg.[D2]	0.77	0.79	-0.47	10.1	0.94	0.96	-0.15	97.8 [57]	30.8
	Diff.	0.06	0.07	-0.20	-	0.02	0.01	-0.07	1.5 [-]	-
	Avg.[H]	0.86	0.90	0.02	10.1	0.96	0.97	0.00	101.1 [57]	30.8
	Diff.	-0.03	-0.04	-0.69	-	-	-	-0.22	-1.8 [-]	-
2	Dist.[D1]	0.88	0.89	-0.68	23.7	0.98	0.98	-0.20	220.1 [59]	79.9
	Avg.[D2]	0.88	0.89	-0.29	23.7	0.98	0.98	-0.09	219.7 [59]	79.9
	Diff.	-	-	-0.39	-	-	-	-0.11	0.4 [-]	-
	Avg.[H]	0.75	0.75	-0.09	23.7	0.95	0.95	-0.03	229.7 [55]	79.9
	Diff.	0.13	0.14	-0.59	-	0.03	0.03	-0.17	-9.6 [4]	-
3	Dist.[D1]	0.87	0.89	-0.78	16.4	0.97	0.97	-0.24	151.4 [53]	55.0
	Avg.[D2]	0.80	0.81	-0.84	16.4	0.96	0.96	-0.25	155.6 [48]	55.0
	Diff.	0.07	0.08	0.06	-	0.01	0.01	0.01	-4.2 [5]	-
	Avg.[H]	0.75	0.76	-0.69	16.4	0.95	0.95	-0.21	158.9 [48]	55.0
	Diff.	0.12	0.13	-0.09	-	0.02	0.02	-0.03	-7.5 [5]	-
4	Dist.[D1]	0.85	0.92	-0.06	11.9	0.96	0.97	-0.02	118.4 [39]	37.7
	Avg.[D2]	0.79	0.82	-0.13	11.9	0.95	0.95	-0.04	122.0 [39]	37.7
	Diff.	0.06	0.10	0.07	-	0.01	0.02	0.02	-3.6 [-]	-
	Avg.[H]	0.72	0.75	-0.17	11.9	0.93	0.93	-0.06	124.7 [38]	37.7
	Diff.	0.13	0.17	0.11	-	0.03	0.04	0.04	-6.3 [1]	-
5	Dist.[D1]	0.75	0.76	-0.39	14.4	0.94	0.94	-0.12	143.3 [47]	48.2
	Avg.[D2]	0.75	0.76	-0.39	14.4	0.94	0.94	-0.12	143.3 [47]	48.2
	Diff.	-	-	-	-	-	-	-	- [-]	-
	Avg.[H]	0.67	0.67	-0.42	14.4	0.92	0.92	-0.13	147.3 [47]	48.2
	Diff.	0.08	0.09	0.03	-	0.02	0.02	0.01	-4.0 [-]	-
6	Dist.[D1]	0.65	0.71	-0.38	6.4	0.88	0.88	-0.11	74.7 [36]	21.1
	Avg.[D2]	0.48	0.48	-0.43	6.4	0.82	0.82	-0.13	77.6 [35]	21.1
	Diff.	0.17	0.23	0.05	-	0.06	0.06	0.02	-2.9 [1]	-
	Avg.[H]	0.39	0.39	-0.10	6.4	0.79	0.80	-0.03	79.1 [35]	21.1
	Diff.	0.26	0.32	-0.28	-	0.09	0.08	-0.08	-4.4 [1]	-

Dist.- distributed; Avg. - averaged; [D1] and [D2] - Distributed-Clark; [H] - HEC-HMS; Diff. - differences from averaged output ('-' means 'reduction' in time to peak)

Statistics are for the period of model simulation (for direct runoff), not the total storm event duration.

Table A 4 Muscatatuck River

Storm Events (#) [model]		Direct Runoff				Streamflow				
		E_{NS}	R^2	*PBIAS* (%)	Total (mm)	E_{NS}	R^2	*PBIAS* (%)	Peak flow (m^3/s) [time, hour]	Total (mm)
1	Dist.[D1]	0.96	0.97	-1.30	27.8	0.98	0.99	-0.65	426.9 [32]	55.8
	Avg.[D2]	0.95	0.97	-1.38	27.8	0.98	0.99	-0.69	433.6 [33]	55.8
	Diff.	0.01	-	0.08	-	-	-	0.04	-6.7 [-1]	-
	Avg.[H]	0.97	0.97	-1.03	27.8	0.99	0.99	-0.51	408.2 [33]	55.8
	Diff.	-0.01	-	-0.27	-	-0.01	-	-0.14	18.7 [-1]	-
2	Dist.[D1]	0.91	0.92	-1.62	9.0	0.95	0.95	-0.83	133.8 [51]	17.5
	Avg.[D2]	0.86	0.90	-2.02	9.0	0.92	0.94	-1.04	139.2 [51]	17.5
	Diff.	0.05	0.02	0.40	-	0.03	0.01	0.21	-5.4 [-]	-
	Avg.[H]	0.92	0.93	-1.69	9.0	0.96	0.96	-0.87	127.1 [51]	17.5
	Diff.	-0.01	-0.01	0.07	-	-0.01	-0.01	0.04	6.7 [-]	-
3	Dist.[D1]	0.96	0.96	-4.72	41.1	0.98	0.98	-2.57	562.6 [52]	76.7
	Avg.[D2]	0.96	0.96	-4.75	41.1	0.98	0.98	-2.58	592.0 [51]	76.7
	Diff.	-	-	0.03	-	-	-	0.01	-29.4 [1]	-
	Avg.[H]	0.96	0.97	-4.39	41.1	0.98	0.98	-2.39	535.7 [51]	76.7
	Diff.	-	-0.01	-0.33	-	-	-	-0.18	26.9 [1]	-
4	Dist.[D1]	0.98	0.98	-0.09	11.7	0.99	0.99	-0.04	218.2 [26]	22.8
	Avg.[D2]	0.98	0.98	-0.13	11.7	0.99	0.99	-0.07	210.6 [27]	22.8
	Diff.	-	-	0.04	-	-	-	0.03	7.6 [-1]	-
	Avg.[H]	0.87	0.88	0.15	11.7	0.94	0.95	0.08	222.2 [28]	22.8
	Diff.	0.11	0.10	-0.24	-	0.05	0.04	-0.12	-4.0 [-2]	-
5	Dist.[D1]	0.98	0.98	-0.49	21.3	0.99	0.99	-0.24	364.5 [40]	42.5
	Avg.[D2]	0.97	0.97	-0.48	21.3	0.99	0.99	-0.24	368.7 [41]	42.5
	Diff.	0.01	0.01	-0.01	-	-	-	-	-4.2 [-1]	-
	Avg.[H]	0.98	0.98	-0.50	21.3	0.99	0.99	-0.25	345.0 [40]	42.5
	Diff.	-	-	0.01	-	-	-	0.01	19.5 [-]	-
6	Dist.[D1]	0.87	0.91	-0.25	13.1	0.95	0.95	-0.13	213.5 [28]	26.0
	Avg.[D2]	0.89	0.93	-0.15	13.1	0.95	0.96	-0.08	214.6 [28]	26.0
	Diff.	-0.02	-0.02	-0.10	-	-	-0.01	-0.05	-1.1 [-]	-
	Avg.[H]	0.80	0.83	0.04	13.1	0.92	0.92	0.02	192.5 [28]	26.0
	Diff.	0.07	0.08	-0.29	-	0.03	0.03	-0.15	21.0 [-]	-

Dist.- distributed; Avg. - averaged; [D1] and [D2] - Distributed-Clark; [H] - HEC-HMS; Diff. - differences from averaged output ('-' means 'reduction' in time to peak)

Statistics are for the period of model simulation (for direct runoff), not the total storm event duration.

Appendix B Forms Statistical result (detail) comparisons of model calibration and validation for spatially distributed (NEXRAD radar-based grid cell) and averaged rainfall data simulation

Table B 5 Illinois River

Storm Events (#) [model]		Direct Runoff				Streamflow				
		E_{NS}	R^2	*PBIAS* (%)	Total (mm)	E_{NS}	R^2	*PBIAS* (%)	Peak flow (m^3/s) [time, hour]	Total (mm)
1	Dist.[D1]	0.97	0.97	-0.01	46.2	0.97	0.97	-0.01	727.4 [65]	56.4
	Avg.[D2]	0.95	0.95	-0.09	46.2	0.95	0.95	-0.07	680.7 [66]	56.4
	Diff.	0.02	0.02	0.08	-	0.02	0.02	0.06	46.7 [-1]	-
	Avg.[D1a]	-	-	-	45.4	-	-	-	681.1 [67]	55.6
	Diff.	-	-	-	0.8	-	-	-	46.3 [-2]	0.8
2	Dist.[D1]	0.86	0.89	-0.18	28.9	0.86	0.89	-0.16	553.8 [65]	34.1
	Avg.[D2]	0.80	0.82	-0.04	28.9	0.80	0.82	-0.03	475.5 [62]	34.1
	Diff.	0.06	0.07	-0.14	-	0.06	0.07	-0.13	78.3 [3]	-
	Avg.[D1a]	-	-	-	27.4	-	-	-	438.0 [63]	32.6
	Diff.	-	-	-	1.5	-	-	-	115.8 [2]	1.5
3	Dist.[D1]	0.83	0.84	-0.07	5.6	0.82	0.83	-0.06	142.8 [55]	14.6
	Avg.[D2]	0.76	0.77	0.05	5.6	0.75	0.76	-0.01	137.2 [57]	14.6
	Diff.	0.07	0.07	-0.12	-	0.07	0.07	-0.05	5.6 [-2]	-
	Avg.[D1a]	-	-	-	5.3	-	-	-	127.0 [53]	14.3
	Diff.	-	-	-	0.3	-	-	-	15.8 [2]	0.3
4	Dist.[D1]	0.58	0.60	-0.12	6.4	0.58	0.60	-0.06	128.4 [87]	13.8
	Avg.[D2]	0.55	0.60	-0.15	6.4	0.55	0.59	-0.07	128.4 [86]	13.8
	Diff.	0.03	-	0.03	-	0.03	0.01	0.01	- [1]	-
	Avg.[D1a]	-	-	-	6.2	-	-	-	124.7 [86]	13.6
	Diff.	-	-	-	0.2	-	-	-	3.7 [1]	0.2
5	Dist.[D1]	0.70	0.73	0.08	23.3	0.70	0.73	0.08	353.3 [69]	24.8
	Avg.[D2]	0.68	0.72	0.13	23.3	0.68	0.72	0.12	364.0 [68]	24.8
	Diff.	0.02	0.01	-0.05	-	0.02	0.01	-0.04	-10.7 [1]	-
	Avg.[D1a]	-	-	-	23.0	-	-	-	356.8 [69]	24.5
	Diff.	-	-	-	0.3	-	-	-	-3.5 [-]	0.3
6	Dist.[D1]	0.79	0.82	-0.04	30.0	0.79	0.82	-0.03	369.8 [77]	33.9
	Avg.[D2]	0.75	0.80	0.01	30.0	0.75	0.80	0.01	368.6 [77]	33.9
	Diff.	0.04	0.02	-0.05	-	0.04	0.02	-0.04	1.2 [-]	-
	Avg.[D1a]	-	-	-	28.2	-	-	-	339.8 [76]	32.1
	Diff.	-	-	-	1.8	-	-	-	30.0 [1]	1.8

Dist. - distributed; Avg. - averaged; [D1], [D1a], and [D2] - Distributed-Clark; Diff. - differences from averaged output ('-' means 'reduction' in time to peak)

Statistics are for the period of model simulation (for direct runoff), not the total storm event duration.

Table B 6 Elk River

Storm Events (#) [model]	Direct Runoff				Streamflow				
	E_{NS}	R^2	*PBIAS* (%)	Total (mm)	E_{NS}	R^2	*PBIAS* (%)	Peak flow (m^3/s) [time, hour]	Total (mm)
Dist.[D1]	0.90	0.91	-0.55	15.1	0.97	0.97	-0.15	809.7 [52]	54.3
Avg.[D2]	0.84	0.84	-0.89	15.1	0.95	0.95	-0.25	835.9 [53]	54.3
1 Diff.	0.06	0.07	0.34	-	0.02	0.02	0.10	-26.2 [-1]	-
Avg.[D1a]	-	-	-	14.9	-	-	-	804.4 [52]	54.1
Diff.	-	-	-	0.2	-	-	-	5.3 [-]	0.2
Dist.[D1]	0.93	0.93	-1.89	5.0	0.98	0.98	-0.45	245.1 [70]	21.2
Avg.[D2]	0.83	0.83	-2.08	5.0	0.95	0.95	-0.50	229.3 [69]	21.2
2 Diff.	0.10	0.10	0.19	-	0.03	0.03	0.05	15.8 [1]	-
Avg.[D1a]	-	-	-	5.0	-	-	-	239.4 [69]	21.2
Diff.	-	-	-	-	-	-	-	5.7 [1]	-
Dist.[D1]	0.93	0.93	-0.41	12.9	0.97	0.97	-0.12	827.2 [25]	44.0
Avg.[D2]	0.88	0.89	-0.41	12.9	0.95	0.96	-0.12	751.3 [26]	44.0
3 Diff.	0.05	0.04	-	-	0.02	0.01	-	75.9 [-1]	-
Avg.[D1a]	-	-	-	11.5	-	-	-	700.5 [26]	42.6
Diff.	-	-	-	1.4	-	-	-	126.7 [-1]	1.4
Dist.[D1]	0.92	0.93	-2.25	8.8	0.97	0.98	-0.56	556.7 [39]	35.7
Avg.[D2]	0.91	0.91	-2.93	8.8	0.96	0.96	-0.74	502.1 [38]	35.7
4 Diff.	0.01	0.02	0.68	-	0.01	0.02	0.18	54.6 [1]	-
Avg.[D1a]	-	-	-	8.3	-	-	-	495.2 [38]	35.2
Diff.	-	-	-	0.5	-	-	-	61.5 [1]	0.5
Dist.[D1]	0.97	0.98	-1.85	4.8	0.99	0.99	-0.41	275.4 [48]	22.1
Avg.[D2]	0.96	0.97	-1.55	4.8	0.99	0.99	-0.34	253.2 [48]	22.1
5 Diff.	0.01	0.01	-0.30	-	-	-	-0.07	22.2 [-]	-
Avg.[D1a]	-	-	-	4.4	-	-	-	258.2 [49]	21.7
Diff.	-	-	-	0.4	-	-	-	17.2 [-1]	0.4
Dist.[D1]	0.78	0.78	5.39	2.7	0.93	0.93	1.21	134.1 [53]	11.8
Avg.[D2]	0.69	0.70	-1.08	2.7	0.89	0.91	-0.24	130.2 [54]	11.8
6 Diff.	0.09	0.08	6.47	-	0.04	0.02	1.45	3.9 [-1]	-
Avg.[D1a]	-	-	-	1.8	-	-	-	120.5 [54]	10.9
Diff.	-	-	-	0.9	-	-	-	13.6 [-1]	0.9

Dist. - distributed; Avg. - averaged; [D1], [D1a], and [D2] - Distributed-Clark; Diff. - differences from averaged output ('-' means 'reduction' in time to peak)

Statistics are for the period of model simulation (for direct runoff), not the total storm event duration.

Table B 7 Silver Creek

Storm Events (#) [model]	Direct Runoff				Streamflow				
	E_{NS}	R^2	*PBIAS* (%)	Total (mm)	E_{NS}	R^2	*PBIAS* (%)	Peak flow (m^3/s) [time, hour]	Total (mm)
Dist.[D1]	0.85	0.90	-0.09	10.1	0.96	0.97	-0.02	100.1 [57]	30.8
Avg.[D2]	0.77	0.79	-0.47	10.1	0.94	0.96	-0.15	97.8 [57]	30.8
1 Diff.	0.08	0.11	0.38	-	0.02	0.01	0.13	2.3 [-]	-
Avg.[D1a]	-	-	-	9.9	-	-	-	99.6 [57]	30.6
Diff.	-	-	-	0.2	-	-	-	0.5 [-]	0.2
Dist.[D1]	0.88	0.89	-0.49	23.7	0.98	0.98	-0.15	220.4 [59]	79.9
Avg.[D2]	0.88	0.89	-0.29	23.7	0.98	0.98	-0.09	219.7 [59]	79.9
2 Diff.	-	-	-0.20	-	-	-	-0.06	0.7 [-]	-
Avg.[D1a]	-	-	-	22.0	-	-	-	214.8 [61]	78.2
Diff.	-	-	-	1.7	-	-	-	5.6 [-2]	1.7
Dist.[D1]	0.88	0.89	-1.24	16.4	0.97	0.97	-0.37	151.3 [53]	55.0
Avg.[D2]	0.80	0.81	-0.84	16.4	0.96	0.96	-0.25	155.6 [48]	55.0
3 Diff.	0.08	0.08	-0.40	-	0.01	0.01	-0.12	-4.3 [5]	-
Avg.[D1a]	-	-	-	16.2	-	-	-	151.0 [53]	54.8
Diff.	-	-	-	0.2	-	-	-	1.3 [-]	0.2
Dist.[D1]	0.86	0.93	-0.50	11.9	0.96	0.97	-0.16	117.8 [40]	37.7
Avg.[D2]	0.79	0.82	-0.13	11.9	0.95	0.95	-0.04	122.0 [39]	37.7
4 Diff.	0.07	0.11	-0.37	-	0.01	0.02	-0.12	-4.2 [1]	-
Avg.[D1a]	-	-	-	10.9	-	-	-	115.6 [41]	36.7
Diff.	-	-	-	1.0	-	-	-	2.2 [-1]	1.0
Dist.[D1]	0.82	0.85	-0.35	14.4	0.96	0.96	-0.11	142.5 [48]	48.2
Avg.[D2]	0.75	0.76	-0.39	14.4	0.94	0.94	-0.12	143.3 [47]	48.2
5 Diff.	0.07	0.09	0.04	-	0.02	0.02	0.01	-0.8 [1]	-
Avg.[D1a]	-	-	-	13.7	-	-	-	141.1 [48]	47.5
Diff.	-	-	-	0.7	-	-	-	1.4 [-]	0.7
Dist.[D1]	0.66	0.75	-1.66	6.4	0.88	0.89	-0.50	73.9 [36]	21.1
Avg.[D2]	0.48	0.48	-0.43	6.4	0.82	0.82	-0.13	77.6 [35]	21.1
6 Diff.	0.18	0.27	-1.23	-	0.06	0.07	-0.37	-3.7 [1]	-
Avg.[D1a]	-	-	-	6.3	-	-	-	73.4 [36]	21.0
Diff.	-	-	-	0.1	-	-	-	0.5 [-]	0.1

Dist. - distributed; Avg. - averaged; [D1], [D1a], and [D2] - Distributed-Clark; Diff. - differences from averaged output ('-' means 'reduction' in time to peak)

Statistics are for the period of model simulation (for direct runoff), not the total storm event duration.

Table B 8 Muscatatuck River

Storm Events (#) [model]		Direct Runoff				Streamflow				
		E_{NS}	R^2	*PBIAS* (%)	Total (mm)	E_{NS}	R^2	*PBIAS* (%)	Peak flow (m^3/s) [time, hour]	Total (mm)
1	Dist.[D1]	0.74	0.95	37.71	17.1	0.90	0.98	18.80	295.9 [33]	45.1
	Avg.[D2]	0.95	0.97	-1.38	27.8	0.98	0.99	-0.69	433.6 [33]	55.8
	Diff.	-0.21	-0.02	39.09	-10.7	-0.08	-0.01	19.49	-137.7 [-]	-10.7
	Avg.[D1a]	-	-	-	17.1	-	-	-	296.4 [33]	45.1
	Diff.	-	-	-	-	-	-	-	-0.5 [-]	-
2	Dist.[D1]	0.82	0.87	-1.87	9.0	0.90	0.91	-0.97	137.8 [51]	17.5
	Avg.[D2]	0.86	0.90	-2.02	9.0	0.92	0.94	-1.04	139.2 [51]	17.5
	Diff.	-0.04	-0.03	0.15	-	-0.02	-0.03	0.07	-1.4 [-]	-
	Avg.[D1a]	-	-	-	8.9	-	-	-	139.0 [50]	17.4
	Diff.	-	-	-	0.1	-	-	-	-1.2 [1]	0.1
3	Dist.[D1]	0.73	0.97	36.80	24.8	0.85	0.96	20.05	401.9 [52]	60.4
	Avg.[D2]	0.96	0.96	-4.75	41.1	0.98	0.98	-2.58	592.0 [51]	76.7
	Diff.	-0.23	0.01	41.55	-16.3	-0.13	-0.02	22.63	-190.1 [1]	-16.3
	Avg.[D1a]	-	-	-	24.6	-	-	-	399.1 [52]	60.2
	Diff.	-	-	-	0.2	-	-	-	2.8 [-]	0.2
4	Dist.[D1]	0.97	0.97	0.00	11.7	0.99	0.99	0.00	199.3 [28]	22.8
	Avg.[D2]	0.98	0.98	-0.13	11.7	0.99	0.99	-0.07	210.6 [27]	22.8
	Diff.	-0.01	-0.01	0.13	-	-	-	0.07	-11.3 [1]	-
	Avg.[D1a]	-	-	-	10.9	-	-	-	201.3 [27]	22.0
	Diff.	-	-	-	0.8	-	-	-	-2.0 [1]	0.8
5	Dist.[D1]	0.99	0.99	-0.38	21.3	0.99	1.00	-0.19	359.3 [40]	42.5
	Avg.[D2]	0.97	0.97	-0.48	21.3	0.99	0.99	-0.24	368.7 [41]	42.5
	Diff.	0.02	0.02	0.10	-	-	0.01	0.05	-9.4 [-1]	-
	Avg.[D1a]	-	-	-	21.2	-	-	-	366.9 [39]	42.4
	Diff.	-	-	-	0.1	-	-	-	-7.6 [1]	0.1
6	Dist.[D1]	0.98	0.99	-0.15	13.1	0.99	1.00	-0.07	221.2 [31]	26.0
	Avg.[D2]	0.89	0.93	-0.15	13.1	0.95	0.96	-0.08	214.6 [28]	26.0
	Diff.	0.09	0.06	-	-	0.04	0.04	0.01	6.6 [3]	-
	Avg.[D1a]	-	-	-	12.6	-	-	-	218.5 [30]	25.5
	Diff.	-	-	-	0.5	-	-	-	2.7 [1]	0.5

Dist. - distributed; Avg. - averaged; [D1], [D1a], and [D2] - Distributed-Clark; Diff. - differences from averaged output ('-' means 'reduction' in time to peak)

Statistics are for the period of model simulation (for direct runoff), not the total storm event duration.

Appendix C Statistical results of intensive model calibration for spatially distributed and averaged rainfall data simulations to find reasonable and best matched simulated hydrographs

Table C 9 Illinois River (NEXRAD data)

Parameters	Statistics	Optimal value	Threshold (runoff precipitation)				
			50 mm	40 mm	30 mm	20 mm	10 mm
R_{low} 48.0 hour	Volume (m^3/sec)	17009.20	16990.06	16991.90	17004.05	17020.77	17037.44
	R^2	1.000	0.623	0.661	0.708	0.741	0.755
	E_{NS}	1.000	0.611	0.651	0.698	0.735	0.752
	RMSE (m^3/sec)	0.000	45.593	43.218	40.181	37.675	36.447
R_{low} 42.0 hour	Volume (m^3/sec)	17009.20	17012.28	17014.30	17023.73	17036.57	<u>17049.75*</u>
	R^2	1.000	0.637	0.671	0.713	0.744	<u>0.755</u>
	E_{NS}	1.000	0.627	0.662	0.705	0.738	<u>0.752</u>
	RMSE (m^3/sec)	0.000	44.689	42.523	39.719	37.462	<u>36.436</u>
R_{low} 36.0 hour	Volume (m^3/sec)	17009.20	17031.63	17033.56	17040.63	17049.76	17059.73
	R^2	1.000	0.653	0.682	0.720	0.746	0.754
	E_{NS}	1.000	0.644	0.674	0.713	0.741	0.752
	RMSE (m^3/sec)	0.000	43.636	41.724	39.203	37.242	36.445
R_{low} 30.0 hour	Volume (m^3/sec)	17009.20	17051.55	17053.15	17057.42	17062.97	17069.03
	R^2	1.000	0.671	0.695	0.727	0.748	0.754
	E_{NS}	1.000	0.664	0.689	0.721	0.744	0.751
	RMSE (m^3/sec)	0.000	42.415	40.810	38.634	37.029	36.486

Previously fixed parameter values - i 0.05 mm/hour; R_{high} 5.0 hour; λ 0.05; F_c 4.28 mm/day

*Underlined values are calibrated results

Table C 10 Illinois River (Gauged data)

Parameters	Statistics	Optimal value	Threshold (runoff precipitation)				
			50 mm	40 mm	30 mm	20 mm	10 mm
R_{low} 48.0 hour	Volume (m^3/sec)	17009.20	16910.39	16910.39	16910.04	17003.37	17008.00
	R^2	1.000	0.635	0.635	0.663	0.780	0.778
	E_{NS}	1.000	0.634	0.634	0.663	0.780	0.777
	RMSE (m^3/sec)	0.000	44.232	44.232	42.463	34.319	34.500
R_{low} 42.0 hour	Volume (m^3/sec)	17009.20	16952.58	16952.58	16952.35	17016.93	17019.35
	R^2	1.000	0.651	0.651	0.677	0.781	0.778
	E_{NS}	1.000	0.651	0.651	0.676	0.781	0.778
	RMSE (m^3/sec)	0.000	43.228	43.228	41.616	34.259	34.485
R_{low} 36.0 hour	Volume (m^3/sec)	17009.20	16988.52	16988.52	16988.38	17028.10	17028.99
	R^2	1.000	0.670	0.670	0.692	0.781	0.778
	E_{NS}	1.000	0.670	0.670	0.692	0.781	0.778
	RMSE (m^3/sec)	0.000	42.039	42.039	40.614	34.207	34.487
R_{low} 30.0 hour	Volume (m^3/sec)	17009.20	17016.06	17016.06	17016.00	<u>17036.28*</u>	17036.37
	R^2	1.000	0.692	0.692	0.710	<u>0.782</u>	0.777
	E_{NS}	1.000	0.691	0.691	0.709	<u>0.782</u>	0.777
	RMSE (m^3/sec)	0.000	40.630	40.630	39.434	<u>34.173</u>	34.516

Previously fixed parameter values - i 0.05 mm/hour; R_{high} 5.0 hour; λ 0.05; F_c 5.10 mm/day

*Underlined values are calibrated results

Table C 11 Elk River (NEXRAD data)

Parameters	Statistics	Optimal value	Threshold (runoff precipitation)				
			50 mm	40 mm	30 mm	20 mm	10 mm
R_{low} 48.0 hour	Volume (m^3/sec)	17739.27	17721.31	17724.62	17726.34	17731.94	17741.55
	R^2	1.000	0.727	0.766	0.779	0.801	0.791
	E_{NS}	1.000	0.717	0.758	0.775	0.800	0.791
	RMSE (m^3/sec)	0.000	38.292	35.430	34.118	32.217	32.952
R_{low} 42.0 hour	Volume (m^3/sec)	17739.27	17725.89	17729.04	17731.02	<u>17736.08*</u>	17745.31
	R^2	1.000	0.734	0.769	0.782	<u>0.801</u>	0.789
	E_{NS}	1.000	0.727	0.763	0.779	<u>0.800</u>	0.789
	RMSE (m^3/sec)	0.000	37.652	35.019	33.869	<u>32.207</u>	33.084
R_{low} 36.0 hour	Volume (m^3/sec)	17739.27	17734.88	17737.11	17739.15	17743.24	17751.10
	R^2	1.000	0.742	0.773	0.783	0.800	0.787
	E_{NS}	1.000	0.736	0.769	0.781	0.799	0.786
	RMSE (m^3/sec)	0.000	36.980	34.626	33.659	32.271	33.282
R_{low} 30.0 hour	Volume (m^3/sec)	17739.27	17747.56	17748.77	17750.00	17752.72	17757.89
	R^2	1.000	0.749	0.776	0.784	0.797	0.783
	E_{NS}	1.000	0.746	0.773	0.783	0.797	0.783
	RMSE (m^3/sec)	0.000	36.291	34.279	33.522	32.449	33.572

Previously fixed parameter values - i 0.52 mm/hour; R_{high} 7.0 hour; λ 0.05; F_c 2.30 mm/day

*Underlined values are calibrated results

Table C 12 Elk River (Gauged data)

Parameters	Statistics	Optimal value	Threshold (runoff precipitation)				
			50 mm	40 mm	30 mm	20 mm	10 mm
R_{low} 48.0 hour	Volume (m^3/sec)	17739.27	17728.72	17712.58	17741.44	17731.53	17729.37
	R^2	1.000	0.191	0.275	0.417	0.398	0.366
	E_{NS}	1.000	0.075	0.178	0.365	0.321	0.253
	RMSE (m^3/sec)	0.000	69.270	65.279	57.364	59.322	62.253
R_{low} 42.0 hour	Volume (m^3/sec)	17739.27	17745.26	17735.58	17753.60	17747.71	17745.90
	R^2	1.000	0.206	0.284	0.421	0.403	0.369
	E_{NS}	1.000	0.090	0.186	0.369	0.326	0.257
	RMSE (m^3/sec)	0.000	68.694	64.976	57.205	59.137	62.070
R_{low} 36.0 hour	Volume (m^3/sec)	17739.27	17757.57	17752.67	17762.31	17759.38	17758.13
	R^2	1.000	0.223	0.295	0.425	0.407	0.373
	E_{NS}	1.000	0.108	0.195	0.372	0.330	0.262
	RMSE (m^3/sec)	0.000	68.004	64.612	57.083	58.962	61.879
R_{low} 30.0 hour	Volume (m^3/sec)	17739.27	17765.62	17763.71	<u>17767.74*</u>	17766.64	17765.96
	R^2	1.000	0.244	0.308	<u>0.428</u>	0.410	0.377
	E_{NS}	1.000	0.130	0.206	<u>0.372</u>	0.333	0.266
	RMSE (m^3/sec)	0.000	67.152	64.162	<u>57.043</u>	58.827	61.686

Previously fixed parameter values - i 0.05 mm/hour; R_{high} 5.0 hour; λ 0.05; F_c 3.51 mm/day

*Underlined values are calibrated results

Table C 13 Silver Creek (NEXRAD data)

Parameters	Statistics	Optimal value	Threshold (runoff precipitation)				
			50 mm	40 mm	30 mm	20 mm	10 mm
R_{low} 24.0 hour	Volume (m^3/sec)	6560.53	6568.05	6567.93	6567.83	6567.83	6567.89
	R^2	1.000	0.638	0.637	0.641	0.648	0.652
	E_{NS}	1.000	0.627	0.625	0.627	0.633	0.636
	RMSE (m^3/sec)	0.000	10.394	10.426	10.394	10.304	10.274
R_{low} 20.0 hour	Volume (m^3/sec)	6560.53	6568.04	6568.04	6568.04	6568.04	6568.04*
	R^2	1.000	0.653	0.653	0.653	0.653	0.653
	E_{NS}	1.000	0.635	0.635	0.635	0.635	0.635
	RMSE (m^3/sec)	0.000	10.276	10.276	10.276	10.276	10.276

Previously fixed parameter values - i 17.50 mm/hour; R_{high} 20.0 hour; λ 0.05; F_c 2.06 mm/day

*Underlined values are calibrated results

Table C 14 Silver Creek (Gauged data)

Parameters	Statistics	Optimal value	Threshold (runoff precipitation)				
			50 mm	40 mm	30 mm	20 mm	10 mm
R_{low} 24.0 hour	Volume (m^3/sec)	6560.53	6562.41	6562.41*	6562.43	6562.43	6562.47
	R^2	1.000	0.466	0.470	0.473	0.473	0.477
	E_{NS}	1.000	0.415	0.416	0.411	0.408	0.407
	RMSE (m^3/sec)	0.000	13.013	13.009	13.062	13.096	13.105
R_{low} 20.0 hour	Volume (m^3/sec)	6560.53	6562.58	6562.58	6562.58	6562.58	6562.58
	R^2	1.000	0.479	0.479	0.479	0.479	0.479
	E_{NS}	1.000	0.409	0.409	0.409	0.409	0.409
	RMSE (m^3/sec)	0.000	13.088	13.088	13.088	13.088	13.088

Previously fixed parameter values - i 17.50 mm/hour; R_{high} 20.0 hour; λ 0.05; F_c 3.41 mm/day

*Underlined values are calibrated results

Table C 15 Muscatatuck River (NEXRAD data)

Parameters	Statistics	Optimal value	Threshold (runoff precipitation)				
			50 mm	40 mm	30 mm	20 mm	10 mm
R_{low} 30.0 hour	Volume (m^3/sec)	12529.54	12526.10	12527.13	12528.02	12533.09	12539.55
	R^2	1.000	0.495	0.498	0.497	0.511	0.522
	E_{NS}	1.000	0.468	0.432	0.399	0.392	0.375
	RMSE (m^3/sec)	0.000	23.048	23.813	24.487	24.626	24.977
R_{low} 24.0 hour	Volume (m^3/sec)	12529.54	<u>12540.05*</u>	12540.81	12541.50	12543.48	12538.37
	R^2	1.000	<u>0.509</u>	0.511	0.509	0.517	0.510
	E_{NS}	1.000	<u>0.470</u>	0.435	0.406	0.394	0.396
	RMSE (m^3/sec)	0.000	<u>23.004</u>	23.744	24.352	24.583	24.546
R_{low} 18.0 hour	Volume (m^3/sec)	12529.54	12544.26	12545.02	12545.50	12546.86	12548.50
	R^2	1.000	0.523	0.523	0.521	0.524	0.527
	E_{NS}	1.000	0.462	0.432	0.408	0.394	0.376
	RMSE (m^3/sec)	0.000	23.173	23.817	24.305	24.597	24.963
R_{low} 12.0 hour	Volume (m^3/sec)	12529.54	12545.27	12545.90	12546.31	12547.41	12548.90
	R^2	1.000	0.532	0.532	0.530	0.530	0.529
	E_{NS}	1.000	0.428	0.410	0.397	0.386	0.374
	RMSE (m^3/sec)	0.000	23.896	24.273	24.535	24.762	24.995

Previously fixed parameter values - i 2.25 mm/hour; R_{high} 7.5 hour; λ 0.05; F_c 1.53 mm/day

*Underlined values are calibrated results

Table C 16 Muscatatuck River (Gauged data)

Parameters	Statistics	Optimal value	Threshold (runoff precipitation)				
			50 mm	40 mm	30 mm	20 mm	10 mm
R_{low} 30.0 hour	Volume (m^3/sec)	12529.54	12559.35	12558.13	12554.89	12553.37	12553.52
	R^2	1.000	0.356	0.349	0.357	0.350	0.358
	E_{NS}	1.000	0.311	0.272	0.249	0.188	0.152
	RMSE (m^3/sec)	0.000	26.225	26.958	27.372	28.468	29.088
R_{low} 24.0 hour	Volume (m^3/sec)	12529.54	<u>12559.76*</u>	12559.43	12558.54	12557.94	12558.04
	R^2	1.000	<u>0.383</u>	0.360	0.366	0.358	0.363
	E_{NS}	1.000	<u>0.306</u>	0.271	0.250	0.193	0.159
	RMSE (m^3/sec)	0.000	<u>26.315</u>	26.970	27.360	28.375	28.977
R_{low} 18.0 hour	Volume (m^3/sec)	12529.54	12559.98	12559.93	12559.83	12559.73	12559.75
	R^2	1.000	0.377	0.372	0.376	0.368	0.369
	E_{NS}	1.000	0.290	0.262	0.245	0.198	0.167
	RMSE (m^3/sec)	0.000	26.609	27.128	27.455	28.297	28.825
R_{low} 12.0 hour	Volume (m^3/sec)	12529.54	12560.23	12560.22	12560.21	12560.18	12560.15
	R^2	1.000	0.384	0.382	0.383	0.378	0.378
	E_{NS}	1.000	0.248	0.233	0.222	0.196	0.178
	RMSE (m^3/sec)	0.000	27.395	27.667	27.857	28.325	28.641

Previously fixed parameter values - i 0.05 mm/hour; R_{high} 5.0 hour; λ 0.05; F_c 2.10 mm/day

*Underlined values are calibrated results

Appendix D DistributedClark_10.1 (ArcGIS 10.1 based Python Toolbox)

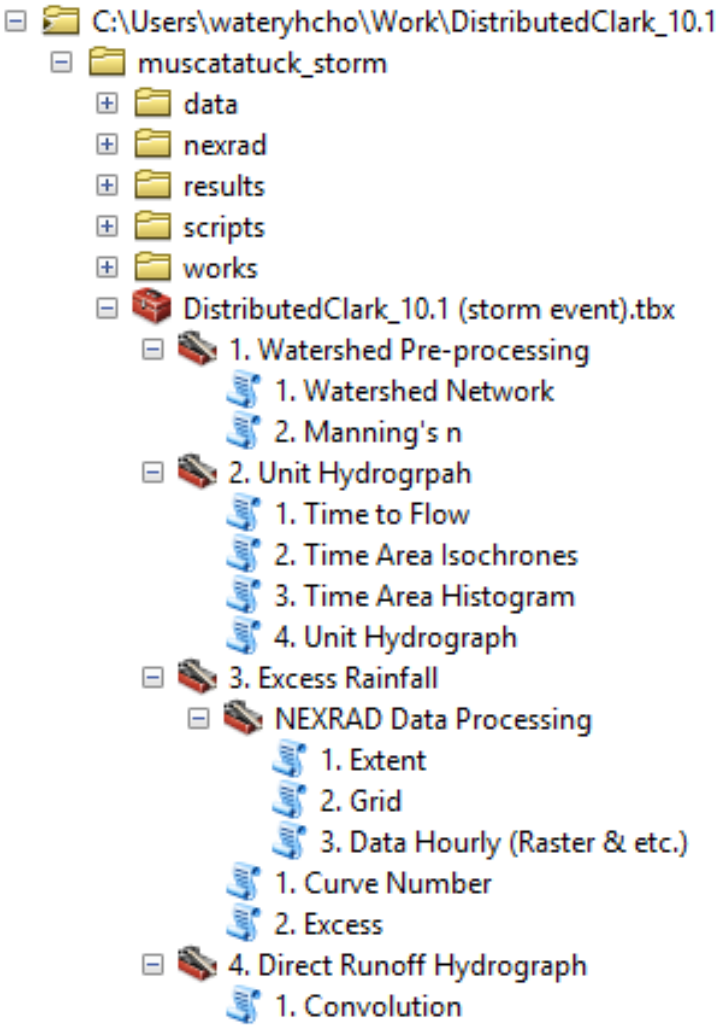

Figure D 1 DistributedClark_10.1 (storm event ver.)

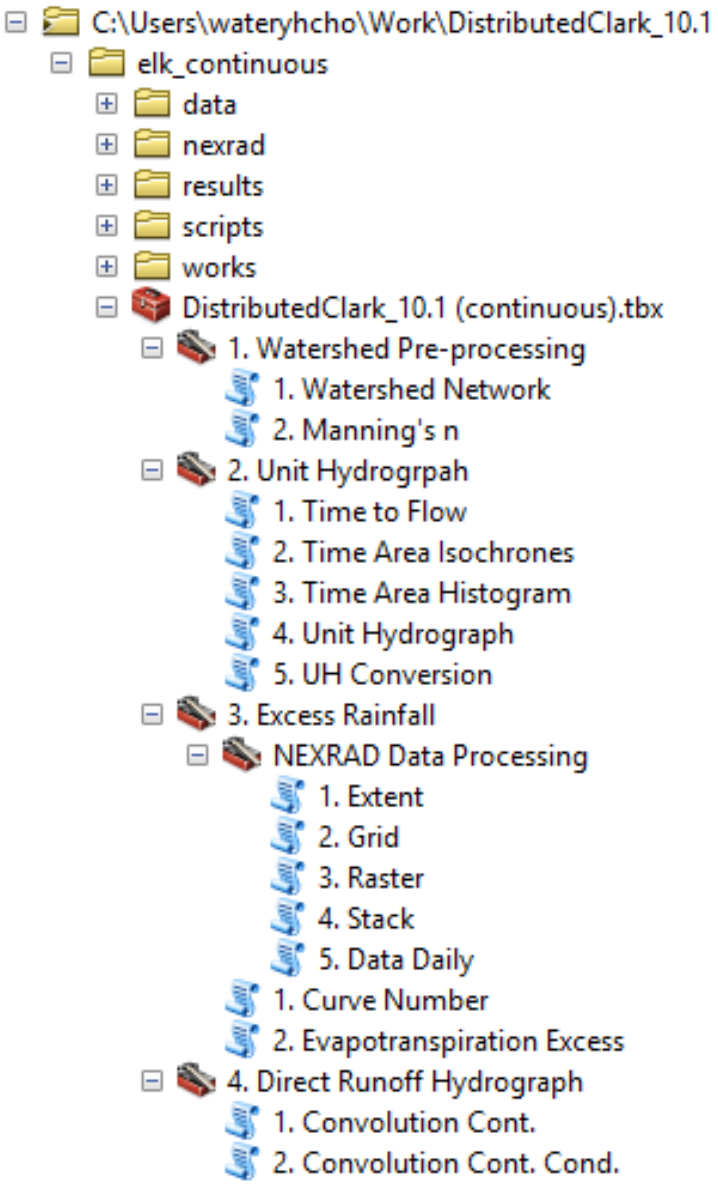

Figure D 2 DistributedClark_10.1 (continuous ver.)

VITA

VITA

Younghyun Cho was born in Cheongsong, the Republic of Korea (South Korea). He graduated with a Bachelor of Agriculture (B.Agri.) degree in Agricultural Civil Engineering from Kyungpook National University, Daegu, South Korea in 2001.

He received his Master of Science (M.Sc.) degree in Agricultural Engineering from Seoul National University, Seoul, South Korea in 2003. He has been working for K-water (Korea Water Resources Corporation) as a Civil Engineer in South Korea since 2003.

He joined the graduate program in Agricultural and Biological Engineering at Purdue University in August, 2013 and received Doctor of Philosophy (Ph.D.) degree in May, 2016.